



UNIVERSITEIT • STELLENBOSCH • UNIVERSITY
jou kennisvenoot • your knowledge partner

SEDIMENT TRANSPORT DYNAMICS IN SOUTH AFRICAN ESTUARIES

BY

Julia S Beck

Dissertation presented for the Degree of Doctor of Philosophy (Engineering)
at the University of Stellenbosch

Promoter: Prof GR BASSON

December 2005

Declaration

I, the undersigned, hereby declare that the work contained in this dissertation is my own original work and that I have not previously in its entirety or in part submitted it at any university for a degree.

Signature: _____

Date: _____

Summary

Estuaries are complex water bodies and differ considerably from fluvial river systems. In estuaries the flow reverses regularly due to the tidal currents and flow depths depend primarily on the tides and not the flow. An estuary has two sources of sediment: the river during floods and the ocean that supplies marine sediment through littoral drift which is transported by tidal currents into the estuary. Oversimplified models cannot be used to investigate the hydrodynamics and geomorphology of an estuary due to its complexity.

Sedimentation of South African estuaries has created several environmental and social problems. Sediment transport imbalances have been caused by changes in the river catchments such as increased sediment yields and flood peak attenuation due to dam construction. Historically floods used to flush estuaries to maintain the long-term sediment balance in the river-estuary system, but with reduced flood peaks, sediment transport capacities at the estuaries are reduced and flushing efficiency decreased, resulting in marine transport dominating in many estuaries.

Two-dimensional (horizontal, 2DH) numerical models have been found to be appropriate tools for studying hydro- and sediment dynamics in SA estuaries. The modelling shows that the sediment balance in the estuary relies on a delicate balance between dominant flood and ebb flows. Although the models performed very well, there are still additional processes to include such as time varying roughness changes and cohesive sediments. For long-term and long reach simulations, one-dimensional (or quasi-two-dimensional) models will also be required in future.

Mathematical modeling can be used to simulate the flushing of sediments during floods, but attempts should be made to calibrate these models when adequate field data become available in the future. The modelling has shown that floods play a very important part in estuarine sediment transport processes.

Physical modelling was undertaken of the breaching of an estuary mouth. The main aim was to illustrate the merits of breaching at higher water levels as well as to investigate the changes in the mouth during breaching. The data obtained from the experiments were used to calibrate and verify a mathematical model. Mathematical modelling of the breaching process at the Klein River estuary confirms what has been observed during numerous breachings in the field, i.e. that breaching at higher water levels and towards the southeast side is more effective.

Sediment transport by both waves and currents was investigated. It was found that with increasing wave and stream power, sediment transport rates would increase if both waves and currents travelled in the same direction. In contrast, it seems that with the current direction opposing that of the waves,

greater wave heights resulted in lower sediment transport rates. A new sediment transport equation, based on stream power, wave power, as well as sediment size was calibrated and verified, and compared to the well-known *Bijker* formula.

Samevatting

Strandmere is baie komplekse sisteme en verskil in 'n groot mate van riviersisteme. In strandmere verander die vloei-richting as gevolg van getystrome, en die vloei-dieptes word meer deur die getye bepaal as deur die rivier-vloei. 'n Strandmeer het twee bronne van sediment: die rivier tydens vloede en die see wat langsstrand vervoerde marinesediment met die getystrome invoer. Vereenvoudigde modelle kan nie gebruik word om die hidrodinamika en geomorfologie van 'n strandmeer te ondersoek nie, weens die kompleksiteit van strandmere.

Sedimentasie in Suid-Afrikaanse strandmere het 'n aantal omgewings- en sosiale probleme geskep. Sedimentvervoer wanbalans is deur verskillende veranderings in die rivieropvanggebiede veroorsaak, soos toenemende sedimentlewering en vloedpiekattenuasie as gevolg van damkonstruksie. In die verlede het rivier-vloede sediment uit strandmere gespoel en 'n langtermyn sedimentbalans is gehandhaaf in die rivier-strandmeer sisteem, maar met kleiner vloedpieke is sedimentvervoer vermoë in strandmere en daarmee die spoel-doeltreffendheid verminder, wat tot gevolg het dat marinesediment in baie strandmere oorheers.

Daar is gevind dat twee-dimensionele numeriese modelle gebruik kan word om die water- en sedimentdinamika in Suid-Afrikaanse strandmere te kan bestudeer. Die modellering wys dat die sedimentbalans in 'n strandmeer baie afhanklik is van die balans tussen dominante eb- en vloedgetystrome. Alhoewel die numeriese modelle goed werk, is daar bykomende prosesse wat ook rolle speel soos ruhede wat verander met tyd en kohesiewe sediment. Vir langtermyn en lang afstand simulaties moet een-dimensionele (of kwasi-twee-dimensionele) modelle in die toekoms gebruik word.

Numeriese modellering is geskik om die spoel van sediment tydens vloede te simuleer, maar dit is belangrik dat modelle gekalibreer word wanneer genoegsame velddata beskikbaar is. Die modellering wat hier uitgevoer is, het gewys dat vloede 'n baie belangrike rol speel in die sedimentvervoer prosesse in strandmere.

Fisiese modellering van die oopbreek van die mond van 'n strandmeer is uitgevoer. The hoofdoel was om te wys hoe belangrik dit is om op hoër watervlakke oop te breek asook om die veranderings in die mond tydens die oopbreek te ondersoek. Die data wat verkry is deur die fisiese model is gebruik om 'n wiskundige model te kalibreer en te verifieer. Die numeriese modellering van die oopbreek van die mond van die Kleinrivier het, soos ook in die veld gevind is, getoon dat die oopbreek by 'n hoër watervlak en teen die suidoostekant van die berm meer effektief is.

Sedimentvervoer deur golwe en strome is ondersoek. Daar is gevind dat met toenemende golf- en stroomdrywing die sedimentvervoer ook toeneem as die strome en golwe in dieselfde rigting is. In teenstelling daarmee is gevind dat wanneer die golwe in die teenoorgestelde rigting as die strome beweeg, toenemende golfhoogtes die tempo van sedimentvervoer verlaag. 'n Nuwe sedimentvervoer vergelyking, gebaseer op stroom- en golfdrywing, asook sedimentgrootte is gekalibreer en geverifieer en vergelyk met die bekende *Bijker* formule.

Acknowledgements

I would like to express my gratitude to the following persons and organisations:

- Prof. GR Basson for keeping me focused on my studies, your guidance and endless discussions and speculations on the subject.
- The Water Research Commission (WRC) for sponsorship of this research.
- Johan, Frank and Gerhard, thank you for putting so much effort into carrying out a large number of the mouth breaching experiments as part of your undergraduate thesis.
- Bo Christensen (DHI) for the basic crash course in MIKE21C, as well as all the little details that you normally don't find in the official manuals.
- Piet and Andre (CSIR, Stellenbosch), I knew precious little about estuaries when I started this research, but you have been instrumental in imparting some understanding on the nature of estuaries on me.
- US laboratory staff – Noel, Andreas and Ashley, thank you for your help in not only setting up the experiments, but also helping out with measurements when necessary.
- Onele Ngambi (Peninsula Technikon student) for your help with many of the laboratory experiments.
- My family for their unwavering support, even when it became obvious that this would take a lot longer than anticipated. Thank you for always being there for me when I needed you.

Table of Contents

DECLARATION	I
SUMMARY	II
SAMEVATTING	IV
ACKNOWLEDGEMENTS	VI
TABLE OF CONTENTS	VII
LIST OF FIGURES	XI
LIST OF TABLES.....	XVII
LIST OF SYMBOLS.....	XVIII
1. INTRODUCTION	1-1
1.1 AIMS	1-4
1.2 METHODOLOGY	1-4
2. PHYSICAL CHARACTERISTICS OF SOUTH AFRICAN ESTUARIES	2-1
2.1 TIDAL FLOW PATTERNS	2-1
2.1.1 <i>Tides (Open University, 1989)</i>	2-1
2.1.2 <i>Ebb and Flood Channels</i>	2-1
2.1.3 <i>Dominating Flows and the Effect on Sedimentation</i>	2-2
2.1.3.1 Tide-Dominated Estuaries.....	2-3
2.1.3.2 River-Dominated Estuaries	2-6
2.1.3.3 Wave-Dominated Estuaries.....	2-6
2.2 ORIGINS OF SEDIMENTS.....	2-6
2.3 SEDIMENTATION AREAS.....	2-7
2.4 MOUTH CLOSURE AND RELATED PROCESSES	2-7
2.4.1 <i>Equilibrium Conditions at Mouth</i>	2-7
2.4.2 <i>Mouth Closure</i>	2-10
3. SEDIMENTATION PROBLEMS AND IMPACTS ON ESTUARIES.....	3-1
3.1 NATURAL PROCESSES.....	3-1

3.1.1	<i>Flood Response</i>	3-1
3.2	HUMAN IMPACTS.....	3-3
3.2.1	<i>Local Developments</i>	3-4
3.2.2	<i>Catchment Developments</i>	3-11
3.2.3	<i>Coastal Developments</i>	3-15
3.3	SUMMARY.....	3-16
4.	SEDIMENT TRANSPORT PROCESSES	4-1
4.1	CRITICAL CONDITIONS FOR RE-ENTRAINMENT OF NON-COHESIVE SEDIMENT	4-1
4.2	BED ROUGHNESS	4-5
4.3	EXISTING SEDIMENT TRANSPORT FORMULAS	4-7
4.4	SEDIMENT TRANSPORT BY CURRENTS AND WAVES –STREAM AND WAVE POWER.....	4-14
4.4.1	<i>Stream Power</i>	4-14
4.4.2	<i>Wave Power</i>	4-17
4.4.2.1	Basic Definitions.....	4-17
4.4.2.2	Wave Energy.....	4-21
4.4.2.3	Wave Power	4-23
4.5	LABORATORY EXPERIMENTS	4-25
4.5.1	<i>Experimental Setup</i>	4-25
4.5.2	<i>Procedure</i>	4-28
4.5.3	<i>Discussion of Results</i>	4-30
4.6	CALIBRATION AND VERIFICATION OF A SEDIMENT TRANSPORT EQUATION IN TERMS OF STREAM AND WAVE POWER	4-37
4.6.1	<i>Calibration of Sediment Transport Equation with Waves and Currents Travelling in the same Direction</i>	4-37
4.6.2	<i>Calibration of Sediment Transport Equation with Waves and Currents Travelling in Opposing Directions</i>	4-40
4.6.3	<i>Verification</i>	4-41
4.6.4	<i>Comparison</i>	4-42
4.7	SUMMARY.....	4-43
5.	OPEN MOUTH STATE: SEDIMENT TRANSPORT DURING THE TIDAL CYCLE	5-1
5.1	INTRODUCTION.....	5-1
5.2	FIELD INVESTIGATIONS AT THE GOUKOU ESTUARY	5-1
5.2.1	<i>Field Data Analysis</i>	5-2

5.3	LONG-TERM COMPUTATIONAL MODELLING	5-4
5.3.1	<i>One-Dimensional Modelling of an Artificial Estuary</i>	5-6
5.3.1.1	Tidal Action	5-6
5.3.1.2	Combined Flood and Tidal Action.....	5-12
5.3.2	<i>Long-Term Simulations of Water Resources Impacts: Thukela River</i>	5-14
5.3.2.1	Fluvial Morphological Scenarios	5-15
5.3.2.2	Flood Routing	5-16
5.3.2.3	Thukela Estuary Model Set-Up.....	5-20
5.3.2.4	Simulation Results	5-23
5.3.2.5	Resetting Floods.....	5-27
5.3.2.6	Conclusions.....	5-29
5.4	SUMMARY.....	5-29
6.	CLOSED MOUTH STATE: MOUTH BREACHING AND FLUSHING EFFICIENCY.....	6-1
6.1	INTRODUCTION.....	6-1
6.2	EFFECTS OF REDUCTION IN RIVER FLOW ON MOUTH CLOSURES	6-1
6.3	FIELD INVESTIGATIONS	6-3
6.3.1	<i>Objectives</i>	6-3
6.3.2	<i>Fieldwork at Klein River</i>	6-3
6.3.3	<i>Fieldwork at Groot Brak River</i>	6-8
6.3.4	<i>Conclusions</i>	6-10
6.4	PHYSICAL MODELLING.....	6-11
6.4.1	<i>Objectives</i>	6-11
6.4.2	<i>Model Setup and Procedures</i>	6-12
6.4.3	<i>Results and Observations</i>	6-16
6.4.4	<i>Analysis of Results</i>	6-29
6.4.4.1	Equilibrium Mouth Geometry.....	6-31
6.4.4.2	Flushing Efficiency	6-35
6.4.5	<i>Conclusions</i>	6-40
6.5	COMPUTATIONAL MODELLING	6-41
6.5.1	<i>Background of Computational Model</i>	6-41
6.5.2	<i>Laboratory Model</i>	6-43
6.5.2.1	Model Setup	6-43
6.5.2.2	Calibration and Verification.....	6-43
6.5.3	<i>Klein River Estuary Model</i>	6-45
6.5.3.1	Model Setup and Calibration	6-45
6.5.3.2	Simulation Results	6-49

6.6	SUMMARY.....	6-56
7.	CONCLUSIONS AND RECOMMENDATIONS.....	7-1
7.1	CONCLUSIONS	7-1
7.2	RECOMMENDATIONS	7-3
8.	REFERENCES.....	8-1
	APPENDIX A.....	1
	APPENDIX B.....	1

List of Figures

FIGURE 2.1-1	FLOOD AND EBB CHANNELS AT SHINNECOCK INLET, USA (WALTON, 2002)	2-2
FIGURE 2.1-2	ESTUARY TYPES, BASED ON FLOW DOMINANCE	2-3
FIGURE 2.1-3	TIDAL ASYMMETRY (SCHUMANN, 2003)	2-4
FIGURE 2.4-1	COMPARISON OF MEASURED AND CALCULATED EQUILIBRIUM INLET CROSS-SECTIONAL AREA.....	2-9
FIGURE 2.4-2	CLOSURE MECHANISMS (RANASINGHE <i>ET AL</i> , 1999)	2-11
FIGURE 3.1-1	THUKELA RIVER MOUTH AFTER MAJOR FLOOD, SOUTH AFRICA.....	3-2
FIGURE 3.2-1	UULKRAALS RIVER MOUTH, SOUTH AFRICA (CROWTHER, 1988)	3-5
FIGURE 3.2-2	ROYAL ALFRED MARINA IN KOWIE ESTUARY, SOUTH AFRICA (SCHUMANN 2003)	3-6
FIGURE 3.2-3	LOCATION MAP OF BRISBANE RIVER ESTUARY, AUSTRALIA	3-7
FIGURE 3.2-4	BERG RIVER MOUTH BEFORE AND AFTER MOUTH WAS STABILIZED	3-8
FIGURE 3.2-5	DIFFERENT PERSPECTIVES OF ARTIFICIAL BREACHING AT GROOT BRAK ESTUARY, SOUTH AFRICA, IN 2001 (A AND C SHOW THE START OF BREACHING, B AND D SHOW THE FINAL BREACHING CHANNEL).....	3-9
FIGURE 3.2-6	AERIAL VIEW OF GROOT BRAK ESTUARY, SOUTH AFRICA (CLOSED MOUTH) ...	3-10
FIGURE 3.2-7	AERIAL VIEW OF KLEIN RIVER ESTUARY, SOUTH AFRICA	3-11
FIGURE 3.2-8	ARTIFICIAL BREACHING AT KLEIN RIVER ESTUARY, SOUTH AFRICA, IN 2001 ...	3-11
FIGURE 3.2-9	LOCATION MAP OF EBRO RIVER, SPAIN (GUILLÉN AND PALANQUES, 1992)	3-13
FIGURE 3.2-10	LOCATION MAP OF OUED MASSA, MOROCCO (FOX, WILBY AND MOORE, 2001).....	3-14
FIGURE 3.2-11	MURRAY RIVER MOUTH, AUSTRALIA, WITH AN INSET OF AN ALMOST CLOSED MOUTH	3-15
FIGURE 4.1-1	FORCES ACTING ON A SEDIMENT PARTICLE RESTING ON THE BED.....	4-2
FIGURE 4.1-2	SHIELDS' DIAGRAM (CHADWICK AND MORFETT, 1998).....	4-3
FIGURE 4.1-3	INCIPIENT MOTION CONDITIONS FOR COHESIONLESS SEDIMENT PARTICLES (ROOSEBOOM AND MÜLKE, 1982)	4-5
FIGURE 4.2-1	BED FORMS AT GROOT BRAK RIVER AFTER BREACHING IN 2001	4-6
FIGURE 4.3-1	COMPARISON BETWEEN THE <i>BIJKER</i> FORMULA AND EXPERIMENTAL DATA (SOURCE OF DATA LISTED AT THE TOP) (CAMENEN AND LARROUDÉ, 2003).....	4-12
FIGURE 4.3-2	COMPARISON BETWEEN THE <i>BAILLARD</i> FORMULA AND EXPERIMENTAL DATA (SOURCE OF DATA LISTED AT THE TOP) (CAMENEN AND LARROUDÉ, 2003).....	4-13

FIGURE 4.3-3	COMPARISON BETWEEN THE <i>DIBAJNIA AND WATANABE</i> FORMULA AND EXPERIMENTAL DATA (SOURCE OF DATA LISTED AT THE TOP) (CAMENEN AND LARROUDÉ, 2003).....	4-13
FIGURE 4.4-1	PROGRESSIVE WAVE - DEFINITION OF TERMS (USACE, 2002).....	4-19
FIGURE 4.4-2	CHARACTERISTICS OF WAVE GROUPS (USACE, 2002).....	4-20
FIGURE 4.4-3	DEFINITION SKETCH FOR THE DETERMINATION OF POTENTIAL ENERGY (AFTER DEAN AND DALRYMPLE, 1992).....	4-22
FIGURE 4.5-1	EXPERIMENTAL LAYOUT.....	4-25
FIGURE 4.5-2	LABORATORY SETUP.....	4-27
FIGURE 4.5-3	GRADING CURVE OF SEDIMENT USED IN EXPERIMENTS.....	4-28
FIGURE 4.5-4	MEASURED SEDIMENT LOADS DURING EXPERIMENTS WITH OR WITHOUT WAVES.....	4-32
FIGURE 4.5-5	RELATIONSHIP BETWEEN WAVE HEIGHT AND SEDIMENT LOAD.....	4-33
FIGURE 4.5-6	RELATIONSHIP BETWEEN CURRENT VELOCITY AND SEDIMENT LOAD.....	4-33
FIGURE 4.5-7	RELATIONSHIP BETWEEN STREAM POWER AND SEDIMENT LOAD.....	4-34
FIGURE 4.5-8	RELATIONSHIP BETWEEN WAVE POWER AND SEDIMENT LOAD.....	4-34
FIGURE 4.5-9	SEDIMENT MOVEMENT WITH OPPOSING WAVES AND CURRENTS.....	4-36
FIGURE 4.6-1	CALIBRATION OF NEW SEDIMENT TRANSPORT EQUATION (SISTERMANS' DATA – EQUATION 4.6-3).....	4-40
FIGURE 4.6-2	VERIFICATION OF NEW SEDIMENT TRANSPORT EQUATION.....	4-42
FIGURE 4.6-3	COMPARISON OF NEW SEDIMENT TRANSPORT EQUATION AND <i>BIJKER</i> FORMULA.....	4-43
FIGURE 5.2-1	AERIAL VIEW OF GOUKOU ESTUARY AND LOCATION OF CROSS-SECTION IN MARCH 2003.....	5-2
FIGURE 5.2-2	OBSERVED WATER LEVELS AT GOUKOU, MARCH 2003.....	5-3
FIGURE 5.2-3	MEASURED SEDIMENT CONCENTRATION AND CURRENT VELOCITIES (SPRING TIDE, JULY 2001).....	5-3
FIGURE 5.2-4	CUMULATIVE SEDIMENT TRANSPORT THROUGH CROSS-SECTION AT GOUKOU (MARCH 2003).....	5-4
FIGURE 5.3-1	ARTIFICIAL ESTUARY LAYOUT.....	5-6
FIGURE 5.3-2	SIMULATED WATER LEVELS IN THE ARTIFICIAL ESTUARY (A - OCEAN, B - MOUTH, C - UPPER ESTUARY).....	5-8
FIGURE 5.3-3	SIMULATED INITIAL AND FINAL BED LEVELS OF ARTIFICIAL ESTUARY UNDER TIDAL ACTION ONLY.....	5-9
FIGURE 5.3-4	SIMULATED BED LEVEL CHANGES OF ARTIFICIAL ESTUARY WITH TIME AT VARIOUS POSITIONS (IN PARENTHESES) ALONG THE ESTUARY. (10.1 KM IS IN THE	

	TRANSITION BETWEEN THE 80 AND 200 M WIDE CHANNELS, WHILE 14 KM IS JUST UPSTREAM OF THE TRANSITION TO THE OCEAN).....	5-9
FIGURE 5.3-5	FLOOD HYDROGRAPH.....	5-12
FIGURE 5.3-6	SIMULATED BED LEVEL BEFORE AND AFTER FLOOD (FLOOD PEAK = 2000 M ³ /S).....	5-13
FIGURE 5.3-7	THUKELA ESTUARY: SEDIMENT DEPOSITION DURING FLOOD (MAY 1976).....	5-14
FIGURE 5.3-8	AERIAL VIEW OF THUKELA ESTUARY (JULY 1985).....	5-15
FIGURE 5.3-9	THUKELA CATCHMENT LAYOUT (ADAPTED FROM ROWNTREE & WADESON, 1999)	5-16
FIGURE 5.3-10	PRE-DAM FLOWS AT PROPOSED JANA DAM SITE.....	5-17
FIGURE 5.3-11	POST-DAM FLOWS AT PROPOSED JANA DAM SITE.....	5-17
FIGURE 5.3-12	PRE-DAM FLOWS AT PROPOSED MIELIETUIN DAM SITE.....	5-18
FIGURE 5.3-13	POST-DAM FLOWS AT PROPOSED MIELIETUIN DAM SITE.....	5-18
FIGURE 5.3-14	PRE-DAM FLOWS AT THUKELA ESTUARY.....	5-19
FIGURE 5.3-15	POST-DAM FLOWS AT THUKELA ESTUARY.....	5-19
FIGURE 5.3-16	THUKELA ESTUARY.....	5-21
FIGURE 5.3-17	SEDIMENT LOAD-DISCHARGE RELATIONSHIP.....	5-22
FIGURE 5.3-18	THUKELA ESTUARY LONG SECTION UNDER NATURAL CONDITIONS (SCENARIO 0)....	5-24
FIGURE 5.3-19	SIMULATED LONG-TERM SEDIMENT BALANCE (ANNUAL SEDIMENT LOADS IN MILLION TON/A).....	5-24
FIGURE 5.3-20	THUKELA ESTUARY LONG SECTION UNDER PRESENT DAY CONDITIONS (SCENARIO 1).....	5-25
FIGURE 5.3-21	THUKELA ESTUARY LONG SECTION UNDER FUTURE CONDITIONS (SCENARIO 2).....	5-25
FIGURE 5.3-22	THUKELA ESTUARY LONG SECTION UNDER FUTURE CONDITIONS (SCENARIO 5).....	5-26
FIGURE 5.3-23	RESETTING FLOOD (1:50-YEAR) FOR SCENARIO 3.....	5-27
FIGURE 5.3-24	RESETTING FLOOD (1:50-YEAR) FOR SCENARIO 4.....	5-27
FIGURE 5.3-25	THUKELA ESTUARY LONG SECTION UNDER PRESENT DAY CONDITIONS WITH RESETTING FLOOD (SCENARIO 3).....	5-28
FIGURE 5.3-26	THUKELA ESTUARY LONG SECTION UNDER FUTURE CONDITIONS WITH RESETTING FLOOD (SCENARIO 4).....	5-28
FIGURE 6.3-1	START OF BREACHING AT KLEIN RIVER ESTUARY (SEPTEMBER 2001).....	6-4
FIGURE 6.3-2	DURING BREACHING AT KLEIN RIVER ESTUARY.....	6-5
FIGURE 6.3-3	ONE DAY AFTER BREACHING AT KLEIN RIVER ESTUARY.....	6-5
FIGURE 6.3-4	MEASURED WATER LEVELS DURING BREACHING OF THE KLEIN RIVER ESTUARY (SEPTEMBER 2001).....	6-6
FIGURE 6.3-5	CROSS-SECTIONS SHOWING TOPOGRAPHY BEFORE & AFTER BREACHING.....	6-7
FIGURE 6.3-6	MOUTH EXPANSION OVER TIME AT KLEIN ESTUARY DURING 2001 BREACHING ..	6-7

FIGURE 6.3-7	PHOTO SEQUENCE OF THE BREACHING OF GROOT BRAK RIVER, SOUTH AFRICA (SEPTEMBER 2001).....	6-8
FIGURE 6.3-8	ONE DAY AFTER BREACHING AT GROOT BRAK RIVER	6-9
FIGURE 6.3-9	WATER LEVELS DURING BREACHING AT GROOT BRAK RIVER (SEPTEMBER 2001)	6-10
FIGURE 6.3-10	MOUTH EXPANSION WITH TIME AT GROOT BRAK RIVER (SEPTEMBER 2001).....	6-10
FIGURE 6.4-1	EXPERIMENTAL LAYOUT.....	6-12
FIGURE 6.4-2	FLUME FOR FLUSHING EXPERIMENTS, UNIVERSITY OF STELLENBOSCH LABORATORY	6-13
FIGURE 6.4-3	INITIAL BERM (LOOKING UPSTREAM).....	6-15
FIGURE 6.4-4	INITIAL BERM (LOOKING DOWNSTREAM) WITH SUSPENDED GRID	6-15
FIGURE 6.4-5	RELATIONSHIP BETWEEN OBSERVED BREACHING PEAK DISCHARGE AND INITIAL WATER LEVEL IN THE ESTUARY AT KLEIN RIVER (BASED ON DATA FROM CSIR, 1999).....	6-16
FIGURE 6.4-6	PROGRESSION OF INLET CHANNEL WIDTH WITH TIME	6-16
FIGURE 6.4-7	HYDRAULIC CONTROL	6-18
FIGURE 6.4-8	POSITION OF HYDRAULIC CONTROL IN RELATION TO THE CREST OF THE BERM WITH TIME	6-18
FIGURE 6.4-9	WATER LEVEL CHANGES WITH TIME.....	6-19
FIGURE 6.4-10	INITIAL BATHYMETRY (A) FOR TESTS 1-7, 10, 14 (BERM HEIGHT 0.06 M) AND FINAL BATHYMETRY FOR TEST 1 (B)	6-20
FIGURE 6.4-11	FINAL BATHYMETRIES FOR TEST 2 (A) AND 3 (B).....	6-21
FIGURE 6.4-12	FINAL BATHYMETRIES FOR TEST 4 (A) AND 5 (B).....	6-22
FIGURE 6.4-13	FINAL BATHYMETRIES FOR TEST 6 (A) AND 7 (B).....	6-23
FIGURE 6.4-14	FINAL BATHYMETRIES FOR TEST 10.....	6-24
FIGURE 6.4-15	INITIAL BATHYMETRY (A) FOR TESTS 8, 11, 12 (BERM HEIGHT 0.04 M) AND FINAL BATHYMETRY FOR TEST 8 (B)	6-25
FIGURE 6.4-16	FINAL BATHYMETRIES FOR TEST 11 (A) AND 12 (B).....	6-26
FIGURE 6.4-17	INITIAL BATHYMETRY (A) FOR TEST 9 AND 13 (BERM HEIGHT 0.02 M) AND FINAL BATHYMETRY FOR TEST 9 (B)	6-27
FIGURE 6.4-18	FINAL BATHYMETRY FOR TEST 13	6-28
FIGURE 6.4-19	BED FORMS	6-29
FIGURE 6.4-20	RELATIONSHIP BETWEEN INITIAL WATER LEVEL AND MAXIMUM DISCHARGE FOR BOTH FIELD AND LABORATORY DATA.....	6-30
FIGURE 6.4-21	RELATIONSHIP BETWEEN OBSERVED BREACHING PEAK DISCHARGE AND INITIAL WATER LEVEL IN THE ESTUARY AT GROOT BRAK RIVER (DATA OBTAINED FROM CSIR, 2000)	6-31

FIGURE 6.4-22	RELATIONSHIP BETWEEN THE EQUILIBRIUM CHANNEL WIDTH OF THE FLUSHING CHANNEL AND THE DISCHARGE (PHYSICAL MODEL DATA).....	6-32
FIGURE 6.4-23	COMPARISON BETWEEN OBSERVED AND CALCULATED WIDTHS (EQUATION 6.4-2)	6-33
FIGURE 6.4-24	RELATIONSHIP BETWEEN THE EQUILIBRIUM CHANNEL DEPTH OF THE FLUSHING CHANNEL AND THE DISCHARGE	6-34
FIGURE 6.4-25	COMPARISON BETWEEN OBSERVED AND CALCULATED DEPTHS (EQUATION 6.4-7)...	6-34
FIGURE 6.4-26	RELATIONSHIP BETWEEN THE MAXIMUM DISCHARGE DURING FLUSHING AND THE POSITION OF THE CONTROL RELATIVE TO THE CREST OF THE BERM.....	6-36
FIGURE 6.4-27	RELATIONSHIP BETWEEN THE MAXIMUM DISCHARGE DURING FLUSHING AND THE LENGTH OF THE CONTROL	6-36
FIGURE 6.4-28	COMPARISON BETWEEN OBSERVED AND CALCULATED HYDRAULIC CONTROL POSITION (EQUATION 6.4-9).....	6-37
FIGURE 6.4-29	COMPARISON BETWEEN OBSERVED AND CALCULATED HYDRAULIC CONTROL LENGTH	6-37
FIGURE 6.4-30	RELATIONSHIP BETWEEN THE AVERAGE RATE OF EROSION AND THE MAXIMUM DISCHARGE DURING BREACHING	6-39
FIGURE 6.4-31	WIDTH CHANGES DURING TEST 9 WITH TIME.....	6-40
FIGURE 6.4-32	PROJECTED TIME TAKEN FOR WIDTH TO REACH 1.35 M IN RELATION TO THE MAXIMUM DISCHARGE	6-40
FIGURE 6.5-1	LABORATORY BATHYMETRY (VALUES IN M RELATIVE TO “MSL”)	6-43
FIGURE 6.5-2	ACTUAL (TOP) AND SIMULATED (BOTTOM) FINAL BED LEVELS OF TEST 3.....	6-44
FIGURE 6.5-3	ACTUAL (TOP) AND SIMULATED (BOTTOM) FINAL BED LEVELS OF TEST 7.....	6-45
FIGURE 6.5-4	KLEIN ESTUARY MODEL GRID.....	6-46
FIGURE 6.5-5	KLEIN ESTUARY BATHYMETRY (RELATIVE TO MEAN SEA LEVEL)	6-46
FIGURE 6.5-6	TIDAL WATER LEVELS SPECIFIED AT DOWNSTREAM BOUNDARY	6-47
FIGURE 6.5-7	SIMULATED BREACH AFTER 1 WEEK.....	6-48
FIGURE 6.5-8	VELOCITY DISTRIBUTION DURING EBB (A) AND FLOOD (B)	6-49
FIGURE 6.5-9	SCENARIO 3 - SIMULATED DISCHARGE AND WATER LEVEL	6-51
FIGURE 6.5-10	SCENARIO 4 - SIMULATED DISCHARGE AND WATER LEVEL	6-51
FIGURE 6.5-11	SCENARIO 1 - BREACHING CHANNEL TOWARDS THE SOUTH-EAST AFTER 7 DAYS (+2M MSL).....	6-52
FIGURE 6.5-12	SCENARIO 2 – BREACHING CHANNEL TOWARDS THE SOUTH-EAST AFTER 7 DAYS (+2.8 M MSL).....	6-52
FIGURE 6.5-13	SCENARIO 5 – BREACHING CHANNEL TOWARDS THE NORTH-WEST AFTER 7 DAYS....	6-53

FIGURE 6.5-14	SCENARIO 6 – BREACHING CHANNEL TOWARDS THE SOUTH-EAST AFTER 7 DAYS.....	6-53
FIGURE 6.5-15	SCENARIO 2 - EBB TIDE VELOCITY DISTRIBUTION.....	6-54
FIGURE 6.5-16	SCENARIO 2 - FLOOD TIDE VELOCITY DISTRIBUTION	6-54
FIGURE 6.5-17	SCENARIO 6 - EBB TIDE VELOCITY DISTRIBUTION.....	6-55
FIGURE 6.5-18	SCENARIO 6 - FLOOD TIDE VELOCITY DISTRIBUTION	6-55

List of Tables

TABLE 4.4-1	CLASSIFICATION OF WATER WAVES.....	4-18
TABLE 4.5-1	SUMMARY OF EXPERIMENTS.....	4-31
TABLE 4.6-1	RANGE OF PARAMETERS: SISTERMANS' DATA	4-37
TABLE 4.6-2	ACCURACY OF SEDIMENT TRANSPORT EQUATION 4.6-3 BASED ON CALIBRATION DATA	4-39
TABLE 4.6-3	ACCURACY OF EXISTING WAVE-CURRENT SEDIMENT TRANSPORT EQUATIONS (CAMENEN AND LARROUDÉ, 2003)	4-39
TABLE 4.6-4	ACCURACY OF SEDIMENT TRANSPORT EQUATION 4.6-3 BASED ON VERIFICATION DATA	4-41
TABLE 5.3-1	SIMULATED AVERAGE ANNUAL SEDIMENT LOADS (10^3 TON/A)	5-10
TABLE 5.3-2	AVERAGE SIMULATED VELOCITIES (M/S).....	5-11
TABLE 5.3-3	SIMULATED AVERAGE ANNUAL SEDIMENT LOADS (10^2 TON/A) – NEW SYSTEM..	5-12
TABLE 5.3-4	SIMULATED SEDIMENT LOADS DURING FLOOD (10^5 TON/A)	5-13
TABLE 5.3-5	PRE-DAM AND POST-DAM FLOOD PEAKS	5-20
TABLE 5.3-6	GRADED SEDIMENT (AS SIMULATED).....	5-21
TABLE 5.3-7	SEDIMENT YIELDS	5-22
TABLE 6.4-1	SUMMARY OF LABORATORY TESTS.....	6-17
TABLE 6.4-2	ACCURACY OF WIDTH AND DEPTH EQUATIONS	6-35
TABLE 6.4-3	ACCURACY OF REGRESSION EQUATIONS	6-38
TABLE 6.5-1	HYDRODYNAMIC AND MORPHOLOGICAL MODEL PARAMETERS - LABORATORY.	6-44
TABLE 6.5-2	HYDRODYNAMIC AND MORPHOLOGICAL MODEL PARAMETERS – KLEIN RIVER.	6-47
TABLE 6.5-3	SIMULATED MAXIMUM DISCHARGE	6-50
TABLE 6.5-4	KLEIN RIVER - SIMULATED VOLUMES OF SEDIMENT REMOVED FROM THE MOUTH AND UPSTREAM (M^3)	6-56

List of Symbols

Symbol	Description
δ_z^*/δ_n	Transverse bed slope
δ_z^*/δ_s	Longitudinal bed slope
α	Coefficient
δ	Angle between wave and current direction
ω	Angular frequency
ϕ	Friction angle of sediment
α_L	Longitudinal slope coefficient
β	Coefficient
γ	Specific weight of water
γ_s	Specific weight of sediment
ΔH_F	Difference in high tide levels in the sea and estuary
ΔH_L	Difference in low tide levels in the sea and estuary
ΔT_F	Lag between high tide in sea and estuary
ΔT_L	Lag between low tide in sea and estuary
ε_b	Bed load efficiency coefficient
ε_s	Suspended load efficiency coefficient
η	Water level elevation
θ	Wave phase
κ	Von Kármán constant
ρ	Specific density of water
ρ_s	Specific density of sediment
τ	Bottom shear stress
τ_c	Critical bottom shear stress
$\tau_{w,max}$	Wave-induced shear stress
ν	Kinematic viscosity
$\Psi_{cw(max)}$	Maximum Shields parameter due to wave-current interaction
Ω	Spring tidal prism
Ω'_c, Ω'_t	Amount of suspended sediment remaining from positive and negative half-cycles
Ω_c, Ω_t	Amount of sediment entrained and settled during half-periods T_{wc} and T_{wt} , respectively
ω_{cr}	Ripple diameter (<i>Dibajnia and Watanabe</i>)

Θ	Shields parameter
Θ_c	Critical Shields parameter
μ	Coefficient of viscosity
μ_c	Ripple parameter (<i>Bijker</i>)
$\tau_{b,wc}$	Bed shear stress due to waves and current
$\tau_{b,c}$	Bed shear stress due to current alone
ξ	Parameter due to wave-current interaction (<i>Bijker</i>)
dh/dt	Rate of water level rise
\vec{q}_s	Total sediment transport rate vector
\vec{u}	Velocity vector near bed
\bar{v}	Depth-averaged velocity
a	Transverse slope power (equation 6.5-1)
a	Wave amplitude
A	Amplitude of oscillations of water particles on sea bed
A	Wave parameter (<i>Bijker</i>)
a, b	Coefficients
A_1, A_2, A_3, A_4	Coefficients (Equation 4.6-1)
A_c	Cross-sectional area of an estuary mouth
$A_{c,min}$	Minimum inlet cross-sectional area
A_{dw}, B_{dw}	Coefficients (<i>Dibajnia and Watanabe</i>)
A_e	Water surface area of an estuary
A_{gr}	Coefficient (<i>Ackers and White</i>)
b	Mouth width
B	Equilibrium breaching channel width
B_w	Width of wave front
b_w	Inlet width
C	Chezy coefficient
C	Concentration
C	Wave celerity
c	Coefficient (<i>Ackers and White</i>)
$Cc50/Cc80$	Percentage of points with less than 50% or 20% error for “current only” data
C_D	Drag coefficient
C_e	Empirical constant (equation 2.5-3)
C_g	Wave group velocity
C_L	Lift coefficient

C_t	Total Sediment concentration
$Cw50/Cw80$	Percentage of points with less than 50% or 20% error for “wave-current” data
d	Sediment particle diameter
D	Flow depth
d_{50}	Median sediment diameter
dB	Rate of channel widening
dC	Rate of hydraulic control migration
d_{gr}	Particle size number (<i>Ackers and White</i>)
dH	Difference in water levels
E_k	Kinetic wave energy
E_p	Potential wave energy
f_c	Skin friction coefficient due to current
f_{ct}	Total friction coefficient due to current
f_{cw}	Friction coefficient due to wave-current interaction
F_D	Drag force
F_{gr}	Mobility number (<i>Ackers and White</i>)
F_L	Lift force
f_w	Wave friction factor
f_{wt}	Total friction coefficient due to waves
G	Transverse slope coefficient
G_{gr}	Sediment transport parameter (<i>Ackers and White</i>)
g_w	Weight of water per unit mass
h	Water depth
H	Wave height
H_0	Offshore wave height
h_e	Equilibrium scour depth
h_f	Friction losses
H_i	Initial water level
H_s	Significant wave height
I_1, I_2	Einstein integrals (<i>Bijker</i>)
k	Wave number
k_s	Bed roughness
L	Wave length
L	Distance between two measuring sections
L_0	Deep water wave length
L_{HC}	Length of hydraulic control

m	Exponent
M	Manning number (= $1/n$)
M_{tot}	Total annual littoral drift quantity
n	Horizontal coordinate in the transverse direction (MIKE 21C – equation 6.5-1)
n	Group velocity factor
n	Manning coefficient
n,m	Exponents (<i>Ackers and White</i>)
p	Pressure under wave
P_{HC}	Position of hydraulic control
P_s	Stream power
P_T	Tidal prism
P_w	Wave power
q	Discharge per unit width
Q	Discharge
$q(t)$	Bed load sediment transport
q_b	Bed load transport rate per unit width
q_e	Equilibrium maximum discharge per unit width in inlet channel
q_s	Sediment discharge per unit width
q_s	Suspended sediment transport rate (<i>Bijker</i>)
$q_{s,data}$	Experimental sediment discharge per unit width
$q_{s,num}$	Estimated sediment discharge per unit width
r	Bed roughness
R_{e*}	Reynolds number
R_T	Tidal range
s	Specific gravity of sediment
s	Horizontal coordinate along the streamline (MIKE 21C - equation 6.5-2)
S, S_f	Energy slope
S_0	Average bed slope
S_{bl}	Bed load
S_{cr}	Critical slope
S_n	Sediment transport across streamline
S_s	Sediment transport along streamlines
S_w	Average water surface slope
t	Time
T, T_c, T_t	Periods and half-periods of waves taking into account the effect of current
T, T_w	Wave period

$\tan \delta_s$	Bed shear direction change due to helical flow
T_T	Tidal period
U	Current velocity through the mouth
u	Horizontal velocity under wave
$u(t)$	Inlet channel velocity
$u(t)$	Instantaneous wave orbital velocity
u_*	Friction velocity
u_0	Maximum wave orbital velocity
u_c	Mean current velocity
U_c	Mean current velocity
$u_{cr}(t)$	Critical threshold velocity
U_m	Maximum horizontal velocity
U_{max}	Maximum velocity through inlet
u_{wc}, u_{wt}	Quadratic velocity (wave and current) over each half-period
v	Flow velocity
V	Volume flushed during breaching
v_c	Current only flow velocity
v_h	Horizontal component of local fluid velocity
v_p	Velocity in return pipe
v_v	Vertical component of local fluid velocity
W	Self weight
w	Settling velocity
X	Longitudinal distance
Y	Potential energy per unit weight above a certain datum
y_0	Distance above bed at which the velocity is mathematically = 0
z	Elevation
z	Suspension theory coefficient
z^*	Bed level at the centre point in the numerical scheme (MIKE 21C)

1. Introduction

The ecology of an estuary is closely related to its physical character, which is determined by the hydrodynamics, sediment dynamics and state of the river mouth. There is a need for an improved understanding of (and predictive capabilities regarding) the hydrodynamics and sediment dynamics in estuaries. Through the understanding of these processes and using predictive capabilities, ecologists could be provided with essential information on the physical behaviour of the system. This is also required for the effective implementation of new policies in estuaries, such as those related to the South African Water Act (No. 36 of 1998).

Estuaries are on the boundary between the coast and the catchment and as such they are not only affected by developments in the catchment but also any changes to the coastline, as well as any developments within the estuary itself. Changes in river catchments as a result of water resource developments such as the attenuation of flood peaks due to dam construction as well as changes in sediment yields have resulted in sediment transport imbalances, causing sedimentation problems in many South African estuaries. Whereas floods used to flush estuaries, thereby maintaining the sediment balance in the river/estuary system, reduced flood peaks have resulted in decreased sediment transport capacities and reduced flushing efficiency, leading to reduced quantities of river sediments reaching many estuaries. Eventually this could result in complete closure of the estuaries. However, estuaries are very dynamic, as are many coastal features such as beaches and coastal dunes, and as such it is not always possible to attribute all the sedimentation problems in estuaries to human impacts.

In order to determine to what extent coastal and catchment developments will affect the hydrodynamics and sediment dynamics in an estuary, it is firstly necessary to understand the underlying processes. Three factors play a crucial role in the hydrodynamic and sediment transport processes. The first is the river inflow. Studies have shown that reduced floods increase the sediment build-up in estuaries and can lead to closure of the mouth. Sufficient low flows on the other hand may be all that is needed to keep a mouth open for a certain period.

The second factor is the tidal action. During normal tidal action sediment moves in and out of the mouth, and depending on whether the estuary is ebb- or flood-dominated, there will be a net movement of sediment into or out of an estuary. Ebb- or flood-dominance is, however, not the only factor, as local wave conditions also play an important role in stirring up sediment in and around the mouth region. Wave action is generally much reduced inside an estuary, and it is therefore the tidal flows that are responsible for the movement of sediment inside an estuary, together with the river flows.

The third factor is the condition of the mouth. South African estuaries are small compared to many in other countries. This, together with the fact that due to the semi-arid climate of South Africa, local rivers experience long periods of low flows, means that many South African estuaries are cut-off periodically from the ocean as the mouths close. Studies have shown that a closed-mouth state can have far-reaching impacts on the estuarine ecology. The quality of the environment of these estuaries is largely determined by the frequency, duration and timing of open mouth conditions. Unfortunately estuaries are at present often closed more frequently and for longer periods than in the past and their environments have deteriorated. Open mouth conditions at large estuaries are mainly maintained by tidal flows. However, at smaller estuaries, it is commonly the river flows that keep mouths open. Reduced river flow is therefore the primary reason why many estuaries are closed more now than in the natural state.

The interaction of these three factors will ultimately determine the specific dynamics of an estuary, which means that it is very difficult to transfer the findings at one estuary to another. Every estuary would therefore have to be investigated individually as generalisation is difficult. In order to gain a better understanding of these estuarine hydrodynamics and sediment dynamics, it is necessary to first investigate the underlying processes.

The focus of this research was investigation of the sediment transport processes during both open and closed mouth conditions. During the open mouth state tidal flows move sediments in and out of the estuary. Waves play an important role in stirring up sediments which can then be transported by the tidal currents and during floods sediment is flushed out of the system into the sea. For the closed mouth state the time of breaching is very important in terms of sediment transport, as during the actual closed mouth period the only sediment transport taking place occurs at the head of the estuary where the river brings fluvial sediments into the system. During breaching it is not only important to establish a new link with the sea, but also to ensure that some of the sediment that has accumulated in the estuary is flushed out.

The sediment transport processes are similar to river/reservoir sediment transport processes, but modifications are needed to incorporate the effects of features typical of the coastal environment. For instance, during a tidal cycle a reversal in flow direction takes place and in addition the effect of waves has to be taken into consideration. Usually there is a phase where no or very little sediment transport takes place as the tide turns, because the flow velocities are very small, picking up again after the tide has turned. The effect of waves is usually taken into account by adjusting certain parameters (such as the bottom shear stress or friction coefficients) in traditional sediment transport formulations to account for the combined effect of currents and waves.

Wave-current interaction considerably complicates sediment transport predictions. That is why in many cases, existing sediment transport equations for currents have been modified to some degree to incorporate the effect of waves. However, wave action is generally thought to be much reduced inside an estuary and traditional current-related sediment transport equations are often applied. Then again, in a permanently open, or recently opened estuary, wave action, especially in the mouth region, may actually be quite significant under certain conditions, which means that traditional current-related sediment transport equations may not be able to describe the sediment transport in an estuary fully. For this reason, and given the difficulties associated with applying the existing sediment transport equations for wave-current interaction, there seems to be a need for a different approach to describe sediment transport under both waves and currents.

The concept of stream power has been used extensively to determine the sediment transport under currents alone. The concept of wave power has also been used to describe longshore and cross-shore sediment transport. Both stream and wave power concepts have yielded very good results over a large range of conditions, and it was therefore thought that by combining the two, it would be possible to describe sediment transport under both waves and currents. Laboratory experiments were carried out to determine the sediment transport capacity under waves and currents.

The ever-increasing reports of sedimentation problems in South African estuaries has led to calls for increased flushing of these estuaries and mouth breachings, both natural and mechanical, in order to remove the sediment. However, breachings have occurred at water levels in the estuary that were too low, with a negative effect on the flushing efficiency. A physical model study was therefore undertaken to investigate the mouth breaching process of an estuary in greater detail. The following aspects in particular were of interest:

- The effect of the height of the water level in the estuary when breaching occurs, as well as the effect of the sea water level on the flushing efficiency.
- Changes in the mouth geometry during breaching, the rate of erosion, as well as the final mouth geometry.
- Relationships to predict equilibrium scoured mouth geometry.

The data collected during these experiments were used to calibrate and verify a mathematical model in order to do a more extensive investigation than is possible with the physical model. Once calibrated, the mathematical model was used to model field conditions reliably.

The research performed for this dissertation was aimed mainly at gaining a better understanding of estuarine hydrodynamic and sediment transport processes by looking at various aspects of estuarine dynamics, and trying to improve some of the available tools to describe these processes.

1.1 Aims

The main objectives of this research were, based on the foregone discussion:

- Identification of typical sediment related problems and probable causes.
- Improved understanding of estuarine sediment dynamics.
- Hydraulic description of sediment transport processes through the estuary during the tidal cycle.
- Hydraulic description of flushing efficiency of estuaries during breaching.

1.2 Methodology

The proposed research focused on the hydraulic description of sediment transport processes through the estuaries during the tidal cycle as well as during mouth breachings.

This research consisted of the following components:

1. Short description of the basic physical characteristics of South African estuaries (Chapter 2).
2. A literature survey of sedimentation problems in estuaries and possible causes (Chapter 3).
3. Hydraulic description of estuarine sediment transport processes during the tidal cycle and the development of the stream and wave power approach to estuarine sediment transport (Chapter 4).
4. Field work to supplement existing data during a tidal cycle and long-term mathematical modelling of the hydrodynamics and sediment transport in open estuaries (Chapter 5).
5. Investigation into mechanical breaching and flushing efficiency by looking at water levels, timing, frequency and breach location by means of physical and mathematical modelling (Chapter 6).
Prediction of the mouth width and depth and assessment of the flushing efficiency.

The author carried out all the physical and mathematical modelling (as described in Chapters 4 to 6), was involved with some of the fieldwork (described in Chapter 5) and was responsible for all the subsequent analyses.

2. Physical Characteristics of South African Estuaries

This chapter discusses some of the physical characteristics of South African estuaries, such as the tidal flow patterns, origin of sediments and mouth closure.

2.1 Tidal Flow Patterns

2.1.1 Tides (Open University, 1989)

Tides result from the gravitational pull between the sun, moon and earth. The paths of the moon around the earth and the earth around the sun are both elliptical, so that the gravitational force of attraction pass through a maximum and minimum during each orbit. In addition the axis of the earth is inclined to the plane of its orbit around the sun. Therefore the gravitational tide-producing force at a given point on the earth varies in a complex, but predictable manner. Resulting tides occur approximately twice a day, i.e. they are semi-diurnal.

The tide-producing forces are not only responsible for ebb and flood flows, but they also produce *spring* and *neap* tides. Spring tides occur at new and full moon, when the interaction of the sun and moon produce the greatest tidal force, whereas neap tides occur at first and third quarter, when the sun's and moon's forces oppose each other.

Tidal amplitudes around the world vary considerable, and they are roughly classified as follows (Schuman, 2003):

- Microtidal: 0 to 2 m
- Mesotidal: 2 to 4m
- Macrotidal: > 4 m

Micro- and mesotidal ranges are usually found on open coasts, while macrotidal ranges are encountered in gulfs and embayments along coasts. Tides around South Africa are microtidal.

2.1.2 Ebb and Flood Channels

The main channel of many estuaries can be subdivided into two parts, the ebb and the flood channel (see Figure 2.1-1). According to Dyer (1997) the ebb channel forms when the tidal flats become exposed and the flow follows a meandering channel over the tidal flats. Flood flow can take a short-

cut across the banks and a secondary channel is thus formed. In this way the main channel can be divided in two branches, one in which the ebb currents dominate and one in which the flood currents dominate. The two channels often cross, and it is here where shoaling can take place. Sand is deposited in the flood-dominated channel during ebb tide and deposited in the ebb-dominated channel during flood tide. This occurs quite frequently as the flood and ebb channels usually cross several times. Ebb and flood channels are not always stable and tend to shift with time, so that shoaling could take place in several regions, often leading to the mistaken conclusion that the estuary is undergoing sedimentation.

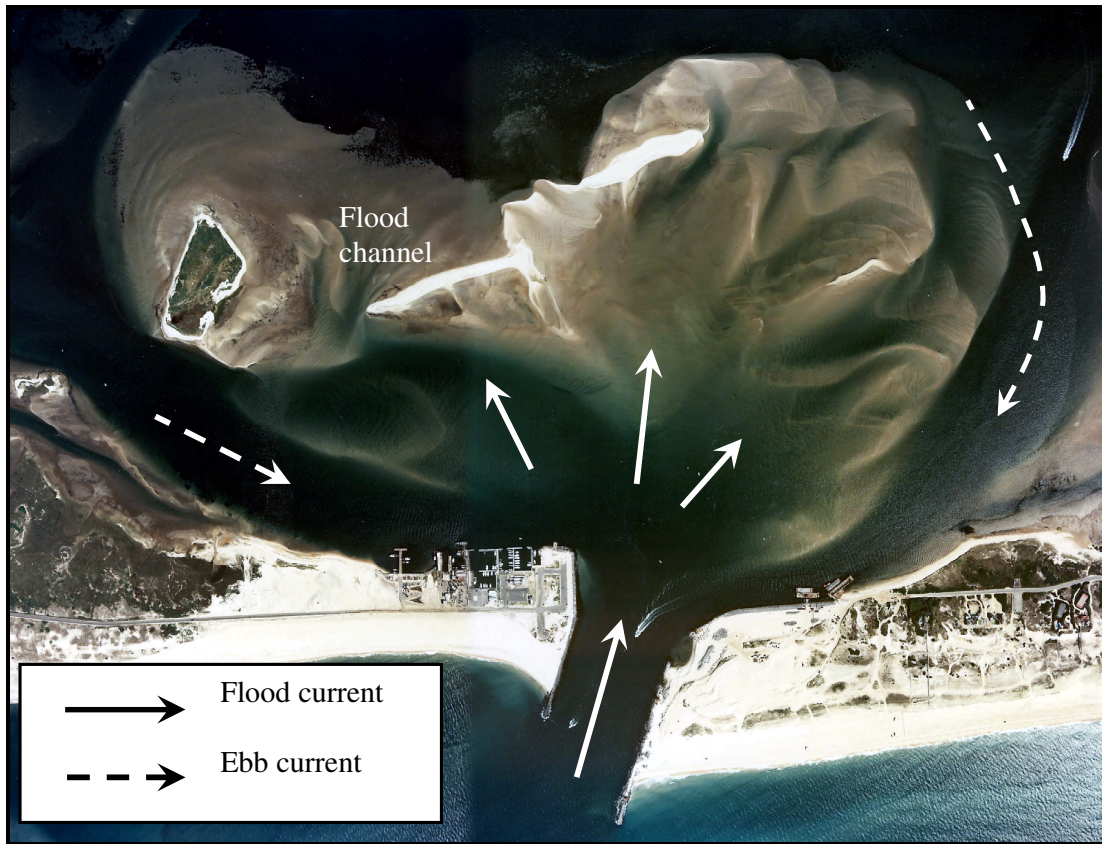


Figure 2.1-1 Flood and ebb channels at Shinnecock Inlet, USA (Walton, 2002)

2.1.3 Dominating Flows and the Effect on Sedimentation

Estuaries can be tide-, river- or wave-dominated, depending on the relative strength of the tidal flow, river flow and wave action. In tide-dominated estuaries the river flows are insignificant in comparison to the tidal flows, except during floods (i.e. Goukou and Berg Estuaries, South Africa). In river-dominated estuaries on the other hand, the tidal flows are minor compared to the river flows (i.e.

Mgeni, Great Fish and Orange Rivers, South Africa). Sedimentation is closely linked to the type of estuary (Figure 2.1-2).

Tide-dominated estuaries can be sub-divided into ebb- or flood-dominated estuaries. In ebb-dominated estuaries the ebb currents are stronger than the flood currents. The mouth characteristics and the presence of tidal flats determine whether ebb or flood currents are likely to dominate.

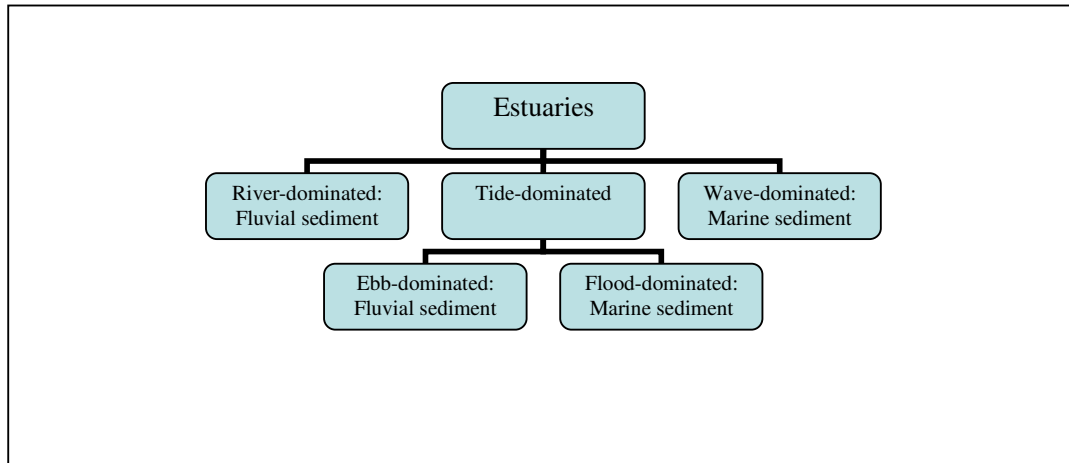


Figure 2.1-2 Estuary types, based on flow dominance

2.1.3.1 Tide-Dominated Estuaries

In tide-dominated estuaries, tidal asymmetry often occurs in the form of a temporal asymmetry in ebb and flood currents, i.e. the flood currents are higher than the ebb currents or vice versa (Walton, 2002). When the duration of the rising tide is shorter than the duration of the falling tide, the peak flood current is greater than the peak ebb current and the system is termed flood-dominant. If the duration of the falling tide is shorter than the duration of the rising tide, giving rise to higher peak ebb currents than flood currents, the system is referred to as ebb-dominant. Spatial asymmetries may also occur in the form of ebb and flood channels, discussed in Section 2.1.2. Some reasons for such asymmetries and their effect on sedimentation are discussed below.

According to Schuman, (2003), the constricted mouth of an estuary modifies the ocean waves as these move into and out of the estuary. As the water level rises and falls, the cross-sectional area of the mouth changes. At high tide the cross-sectional area of the mouth is generally quite large, allowing for a largely free exchange of water and the lag between high tide in the sea and the estuary (ΔT_F) is quite small, as is the difference in the high tide levels in the sea and estuary (ΔH_F). During ebb tide, on the other hand, the cross-sectional area of the inlet is much smaller and the drag resistance increases. The

lag between ebb tide in the sea and in the estuary (ΔT_L) is greater than for high tide, as is the difference in ebb tide levels, ΔH_L (see Figure 2.1-3). This means that the total time for the estuary to ebb is much longer than the time to flood, and the resulting ebb currents are lower than the flood currents.

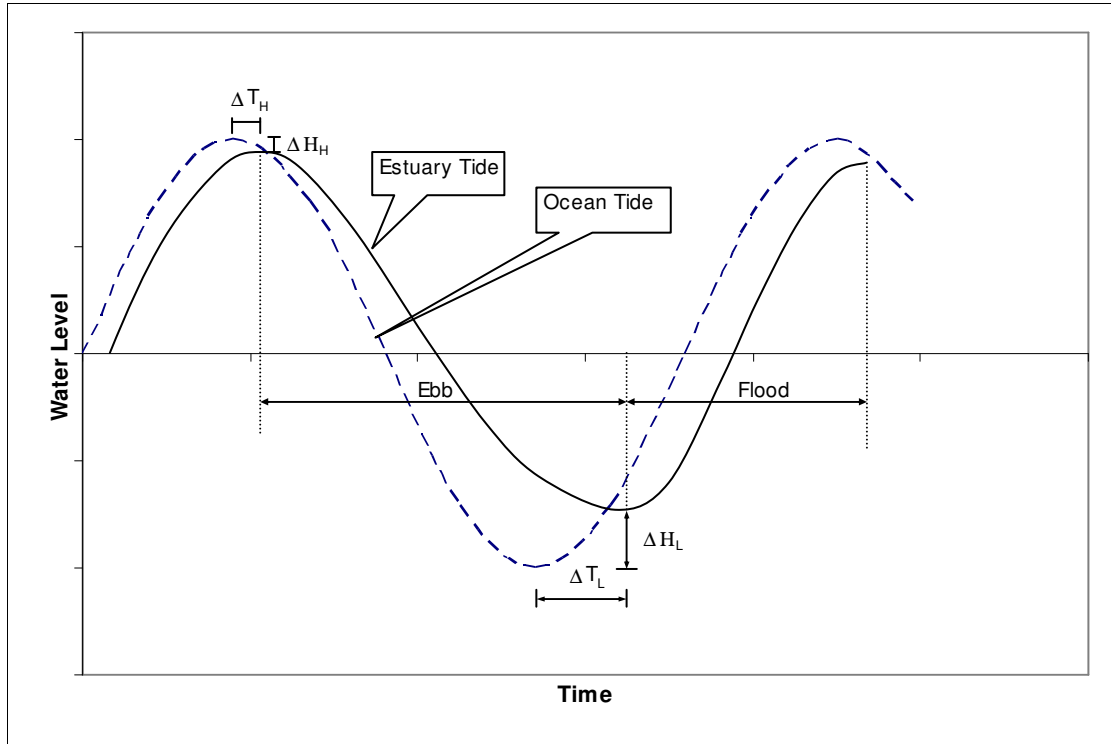


Figure 2.1-3 Tidal asymmetry (Schumann, 2003)

The cross-sectional area of the inlet is not the only factor determining whether an estuary will be ebb- or flood-dominated. It is an important one, but the estuarine geometry also plays a role. Fitzgerald and Nummedal (1983) and Walton (2002) tried to explain the ebb- or flood-dominance of a system in the following way: Considering an inlet with a cross-sectional area A_c , water surface area in the estuary A_e , mean current velocity through the mouth u and rate of water level rise in the estuary dh/dt . The principle of continuity can be applied as follows:

$$A_e \cdot \frac{dh}{dt} = A_c \cdot u \dots\dots\dots 2.1-1$$

This demonstrates that the rate of change in water level in the estuary is directly proportional to A_c/A_e . If the water surface area at ebb tide is much smaller than at high tide, due to the presence of large tidal flats that become exposed during ebb for example, then A_c/A_e is generally larger at low tide than at high tide, and for a given value of u , dh/dt will be greater at low tide than at high tide. The water

surface in the estuary adjusts more quickly to fluctuations in the ocean tide at low tide than at high tide, and the lag between ebb tide in the ocean and the estuary is therefore less than the lag at high tide. This also means that the flood phase generally lasts longer than the ebb phase, and since roughly the same volume of water has to move through the mouth during both ebb and flood phases, the flood currents are therefore smaller than the ebb currents. Estuaries with significant tidal flats are thus more likely to be ebb-dominated than those with limited tidal flats.

Walton (2002) cited several other factors that could also lead to tidal velocity asymmetry. Several studies have shown that inlets with deeper channels would be more likely to be ebb-dominant than shallow, rough bed channels, and that higher friction in the inlet channel could lead to a flood-dominant system.

Fry and Aubrey (1990) argued that tidal velocity asymmetries can cause a net sediment transport in or out of an estuary. They stated that bed load sediment transport (based on the Meyer-Peter Müller bedload formula) can be related to current velocity as follows:

$$q(t) \propto (u(t)^2 - u_{cr}(t)^2)^m \dots\dots\dots 2.1-2$$

- with $q(t)$ = bed load sediment transport
- $u(t)$ = inlet channel velocity
- $u_{cr}(t)$ = critical threshold velocity of sediment
- m = exponent ($\sim 3/2$)

The ratio of flood-to-ebb sediment transport is therefore:

$$\frac{\int_{flood} (u^2(t) - u_{cr}^2(t))^{3/2} dt}{\int_{ebb} (u^2(t) - u_{cr}^2(t))^{3/2} dt} \dots\dots\dots 2.1-3$$

In a flood-dominant system (i.e. higher flood currents, directed toward the estuary), the ratio of flood to ebb bedload sediment transport will be greater than 1 and as a consequence there will be a net influx of sediment into the estuary. In an ebb-dominant system (i.e. higher ebb currents, directed towards the sea), the ratio in equation 2.1-3 is less than 1 and the net sediment transport will be in the direction of the ocean. This means that in flood-dominant systems, marine sediment will likely dominate, while in ebb-dominant systems, marine sediment input is limited.

2.1.3.2 River-Dominated Estuaries

In river-dominated estuaries the river flows are much greater than the tidal flows and as such tidal action is limited. In the Mgeni Estuary, for example, the fluvial sediment extends to the barrier and marine deposition is restricted to the inlet area (Cooper, 1993).

According to Cooper (1993), mature, stable river-dominated estuaries in KwaZulu-Natal have cohesive banks, with moderately deep channels and small flood-tidal deltas, but no real ebb-tidal deltas, which are prevented from forming by wave-action. Many of the KwaZulu-Natal estuaries have very high river discharges as well as high catchment sediment yields. This means that substantial volumes of fluvial sediment are delivered to the estuaries, but these sediments were generally flushed out with regular flooding, except when the frequency and magnitude of the floods are reduced. While these river-dominated estuaries will probably not be threatened by marine sedimentation, fluvial sedimentation can be problematic.

2.1.3.3 Wave-Dominated Estuaries

Wave-dominated estuaries are largely subject to landward movement of sediment, or else to sand being by-passed around inlets (Hubbard *et al*, 1979). The dominant features are the flood tidal deltas, whereas ebb tidal deltas are small. The tidal range (i.e. tidal currents) has to be relatively small in relation to wave-induced currents for wave-dominance to occur.

It thus seems that flood- and wave- dominated estuaries will be more prone to marine sedimentation than ebb- or river-dominated estuaries. These on the other hand could experience a problem with sedimentation of fluvial origin, especially in river-dominated estuaries where catchment sediment yields are high.

2.2 Origins of Sediments

Sediments in estuaries can be fluvial, i.e. catchment derived, or from marine origin. Tide-dominated estuaries can be either flood- or ebb-dominated, depending on the relative strength of the ebb and flood currents. In flood-dominated estuaries the flood currents are stronger than the ebb currents and as such the marine sediments entering the mouths during flood tides cannot all be removed during ebb tides. Flood-dominated estuaries are therefore mainly characterised by sediments of marine origin. Many South African estuaries are flood-dominated and even under natural conditions marine sediments tend to accumulate in the estuaries, especially near the mouth. Ebb-dominated estuaries are

less likely to be dominated by marine sediments, as the ebb currents are stronger than the flood tide currents and are able to remove the marine sediments that are brought into the estuary during flood tides. This does not mean that ebb-dominated estuaries are characterised by fluvial sediments, because marine sediments do not only enter the estuaries during the tidal cycle, but also for example from surrounding areas by wind erosion, or during storms. It means that ebb-dominated estuaries are less likely to accumulate marine sediments. River-dominated estuaries are largely characterised by fluvial sediments. Estuaries that are dominated by marine sediments are the Keurbooms (Reddering, 1983) with less than 10% of the total volume of sediment influx being of fluvial origin, and Kromme Estuaries (Reddering and Esterhuysen, 1983) in South Africa, the Ems Estuary in the Netherlands (where almost 85% of sediments are of marine origin) and the Seine Estuary in France, with 75% of sediments consisting of marine mud, according to Guilcher (1967). Estuaries dominated by fluvial sediments include the Thukela in South Africa, the Loire in France, and the Vigo in Spain (Guilcher, 1967).

2.3 Sedimentation Areas

Sedimentation usually takes place in three different regions in an estuary (Schumann, 2003). At the tidal head, sediment accumulates because of the change in bed slope from the steeper river to the estuary. This accumulated sediment is mainly of fluvial origin.

At the mouth of the estuary marine sediment, diverted from the littoral drift accumulates on the flood tidal delta inside the estuary because of the decrease in the strength of tidal currents as they emerge from the narrow inlet into the wider estuary.

In between sedimentation at the head and at the mouth, sediment accumulation also occurs where tidal mixing between the fresh water from the catchment and the sea water takes place. The fine material carried by the fresh water flocculates and settles in the mixing zone, due to the difference in density of the two water bodies.

2.4 Mouth Closure and Related Processes

2.4.1 Equilibrium Conditions at Mouth

The size of the inlet depends to a large degree on the size of the system, and usually the greater the tidal prism, the greater the inlet opening. The inlet channel has to be able to accommodate the larger flows from a large tidal prism, and if the channel were too small, scouring would take place to increase

the cross-sectional area of the inlet. If the size of the tidal prism were to decrease, for example due to increased sedimentation in the estuary, the reduced tidal currents would not be able to keep all the sediment out of the mouth and the inlet would become smaller. Therefore, the larger the system, the larger the inlet area.

Seabergh *et al* (2001) have performed laboratory investigations to determine the equilibrium inlet area for tidal inlets under tidal action, without river inflow. Tide period, sediment size and wave conditions were varied to create different hydraulic conditions. They found, however, that there was no significant change in the inlet morphology for extremely different hydraulic conditions. The sides of the inlet remained parallel as the channel width increased to its equilibrium condition. With the addition of waves the oceanward part of the inlet channels widens and the narrowest part of the channel migrates landward. The equilibrium inlet area could be predicted with reasonable accuracy (see Figure 2.4-1) with the following tidal prism/minimum inlet cross-sectional area relationship:

$$A_{c,min} = \frac{\pi P_T}{T_T U_{max}} \dots\dots\dots 2.5-1$$

- where
- $A_{c,min}$ = minimum inlet cross-sectional area
 - P_T = tidal prism
 - T_T = tidal period
 - U_{max} = maximum velocity through inlet

Moreover, Seabergh *et al* (2001) have shown that equation 2.5-1 is valid for both laboratory and field data, although more accurate results are obtained for smaller inlets. They reasoned that this could be due to the fact that larger systems can have significant river inflows, which temporarily enlarge the inlet area. Thus the field data for larger inlets could have been obtained during periods in which the inlets were not in equilibrium, and thus the cross-sectional areas were larger than usual. It is important to note that equation 2.5-1 is based on the assumption that the tidal wavelength is much greater than the estuary length; a nearly sinusoidal estuary tide; and a channel cross-section that does not change appreciably during the tidal cycle. The fact that equation 2.5-1 gives good results for a wide range of data means that many inlets apparently fit those assumptions.

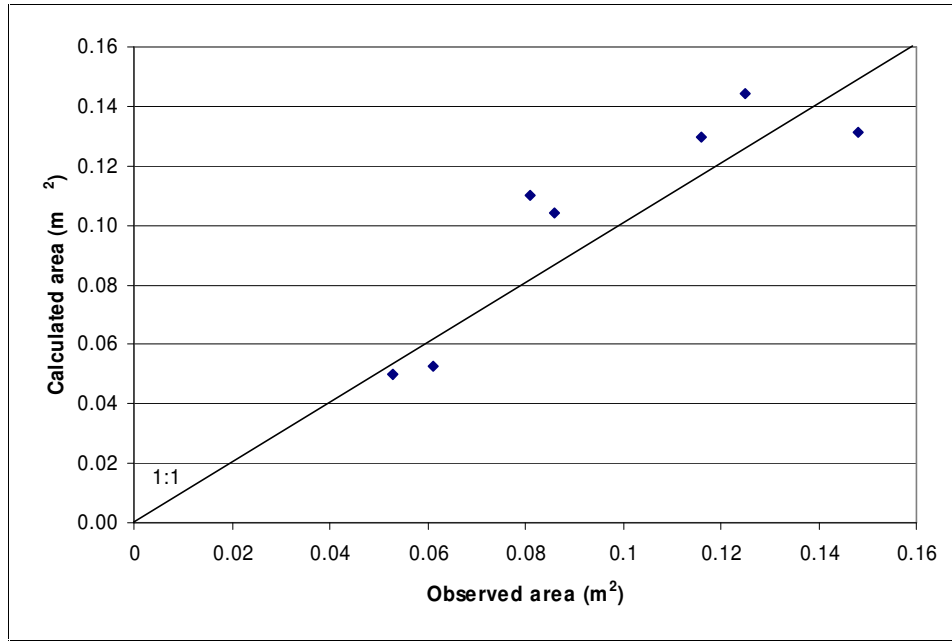


Figure 2.4-1 Comparison of measured and calculated equilibrium inlet cross-sectional area (Seabergh, *et al*, 2001)

Hughes (1999) has shown that there exists a simple relationship between the maximum discharge per unit width and the depth of scour at a certain location in the inlet channel. The equilibrium maximum discharge per unit width q_e is given by:

$$q_e = \bar{v}h \dots\dots\dots 2.5-2$$

where \bar{v} = depth-averaged velocity
 h = water depth

For a given equilibrium maximum discharge per unit width, the equilibrium scour depth h_e (relative to the tide level at maximum discharge) is given by:

$$h_e = \frac{C_e q_e^{8/9}}{[g(s-1)]^{1/9} d_{50}^{1/3}} \dots\dots\dots 2.5-3$$

where d_{50} = median grain diameter
 $s = \rho_s/\rho_w$ = specific gravity of sediment
 C_e = empirical constant (= 0.234 for Hughes' data)

Application of equation 2.5-3 should, however, be limited to inlets where the scour appears to be caused by the maximum discharge. Equation 2.5-3 also does not account for scour due to wave action.

2.4.2 Mouth Closure

Usually an inlet is maintained in a state of dynamic equilibrium through the interaction of several processes. Dynamic, because floods and storms can have a significant impact on the estuarine morphology, but under normal circumstances the estuary will return to its 'equilibrium' state. The two biggest factors governing inlet processes, and therefore also the closure of the mouth, are the wave height and tidal range. Higher waves tend to be responsible for mouth closure, especially during storms, and as such estuaries on wave-sheltered coasts tend to have permanently open mouths. A higher tidal range on the other hand tends to keep the mouth open, and estuaries with larger tidal prisms (dependent on the tidal range) tend to be permanently open.

Ranasinghe *et al.* (1999) explained two different mechanisms of inlet closure of small estuaries on micro-tidal, wave-dominated coasts with strong seasonal variations in river discharge, such as those in Australia and South Africa.

a) Mechanism 1: interaction between inlet current and longshore current.

The tidal inlet disrupts the longshore current and with it the longshore sediment transport. A shoal will form updrift of the inlet, because sediment deposits as the ebb current is reduced when it is diverted by the longshore current. If the river and tidal flows are strong enough to remove the sediment that is deposited in the mouth, the shoal will not grow and the inlet will remain open. However, if the inlet currents decrease, such as during months of low river flows, the shoal may grow and eventually block the inlet (see Figure 2.4-2).

b) Mechanism 2: interaction between inlet current and onshore sediment transport

Under stormy conditions, sand eroded from the beach and surf zone is carried offshore and stored. When the storms subside, the stored sand will be transported onshore. If the ebb flow is strong (i.e. due to high river flows or large tidal ranges) the onshore transport will be disrupted. If the ebb flows are however weak, the continuous onshore transport can cause closure of the inlet.

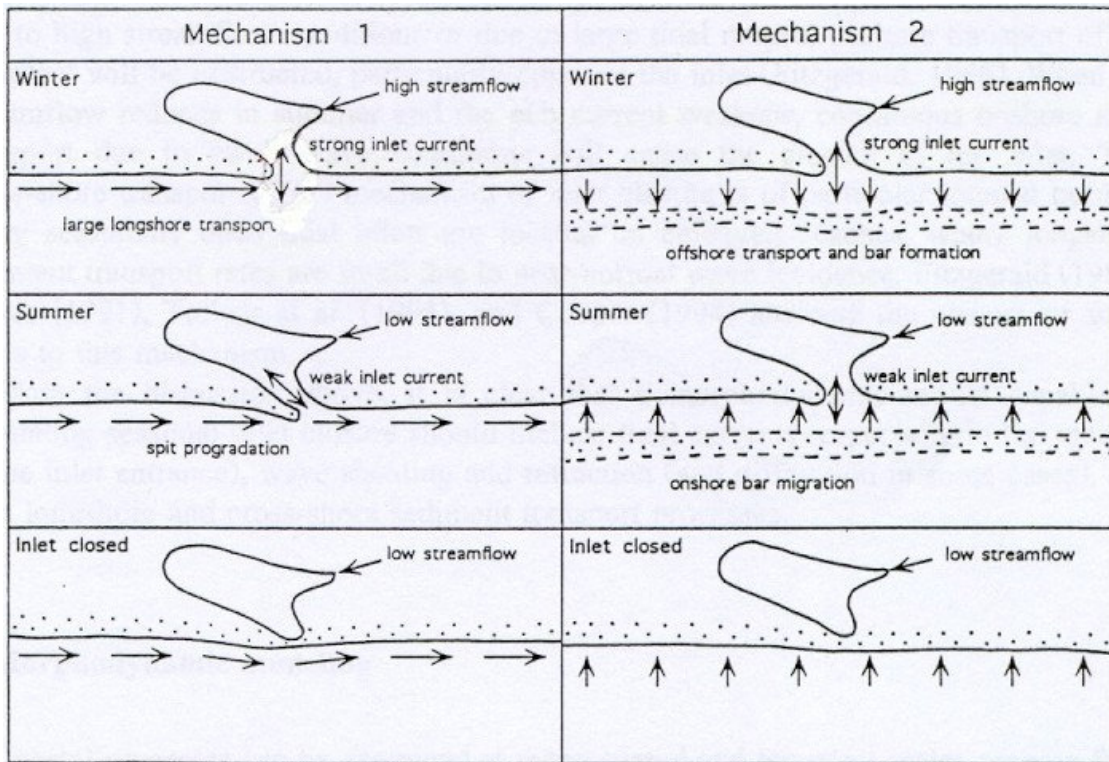


Figure 2.4-2 Closure mechanisms (Ranasinghe *et al*, 1999)

O'Brien (1976) presented the following theory to predict the closure of inlets. It is based on the relative power of the tidal prism to the wave power of the coast.

$$\frac{P_T \cdot R_T}{g_w \cdot b_w \cdot T \cdot T_T \cdot H_0^2} = \frac{\text{Tidal prism power}}{\text{Wave power}} \dots\dots\dots 2.5-4$$

- with
- P_T = tidal prism
 - R_T = tidal range
 - g_w = weight of water per unit mass
 - b_w = inlet width
 - T = wave period
 - T_T = tidal period
 - H_0 = offshore wave height

The larger the tidal prism power in relation to the wave power, the more stable the inlet and vice versa. This theory, however, ignores the effect of a strong streamflow, which can be significant in some estuaries.

Bruun and Gerritsen (Bruun, 1978) established a similar stability criterion for tidal inlets in 1960, with Ω/M_{tot} (Ω = spring tidal prism, M_{tot} = total annual littoral drift quantity). For large values of Ω/M_{tot} , the inlet will be very stable, whereas small ratios predict unstable inlets. They argued that there are several forces acting on a tidal inlet, such as the tidal flow causing sediment transport, littoral transport carrying material alongshore to the entrance and wave energy from the ocean. In order to maintain an open inlet these forces have to balance to ensure that the sediment deposited in the mouth by the littoral drift currents, is flushed out by the tidal currents. Bruun (1978) stressed that this criterion is actually not applicable to estuaries, because the fresh water inflow is ignored. However, many South African estuaries are not considered true estuaries in the classical definition, because they are subject to periods of very low river flows as well as periods of closed mouth conditions. On the other hand, South African estuaries are very small compared to other estuaries around the world, and the cross-shore dynamics play a much greater role than the longshore drift, and as such the Ω/M_{tot} criterion is not really applicable to South African estuaries.

3. Sedimentation Problems and Impacts on Estuaries

Estuaries are on the boundary between coasts and catchments and as such they are not only affected by developments in the catchments but also changes to the coastline, as well as developments within the estuaries themselves. However, as estuaries are very dynamic, as are many coastal features such as beaches and coastal dunes, it is not always possible to attribute all the sedimentation problems in estuaries to human impacts. This chapter serves to point out some of the more common developments affecting estuarine sediment dynamics, with case studies from South Africa and elsewhere in the world.

3.1 Natural Processes

Some estuaries in South Africa are not fully mature (Reddering, 1988), and as such they may not have attained their equilibrium state, such as the Knysna Estuary (Schumann, 2003), and therefore perceived sedimentation is actually part of a natural process.

A study on the sedimentation in the Bushmans Estuary in the Eastern Cape (Reddering and Esterhuysen, 1981) has shown that the reported shoaling in the estuary is part of a natural process, the interaction between ebb- and flood-dominated channels causing the shoaling.

Storms and major floods also cause a shift in the natural balance. During storms it is possible for the inlet to close if the combined river and tidal flows are not sufficient for keeping the mouth open. Temporarily blocked mouths are common features in many South African estuaries, but many estuaries are now blocked for longer periods than in the past.

3.1.1 Flood Response

During major floods large amounts of sediment are scoured from an estuary, but as a flood recedes, sediment carried by the flood from the catchment may be deposited in the estuary. It usually takes only a few months after a major flood for the estuary to revert back to its previous state.

In September 1987 a large flood, with a calculated recurrence interval of 120 years and estimated flood peak of about 10 000 m³/s, occurred in the Mgeni River estuary on the east coast of South Africa (Cooper, 1993). The seaward barrier, the vegetated island in midstream and the southern bank were eroded from the estuary and high suspended sediment concentrations (up to 5700 mg/ℓ) were measured 3 km from the mouth, whilst sediment accumulation was noticed in the upper reaches. In

total about $1.8 \times 10^6 \text{ m}^3$ of sediment was eroded from the estuary, although the flood impact was controlled to some degree by the rock outcrops on the northern bank. A month later the barrier started to re-emerge and by October of 1988 it had completely recovered. In the eight months following the flood the channel underwent rapid accretion and within 21 months of the flood, $1.36 \times 10^6 \text{ m}^3$ of sediment was deposited in the estuary. Stabilization of the intertidal bars and supratidal accretion in the two years after the flood, seem to follow the same pattern as that which, over a 50-year period, transformed the estuary to its stable (1986) morphology.

The flood peaks of the Thukela River are high and therefore the estuarine system is very dynamic with rapid changes in the estuarine morphology from time to time. During falling stages of flood hydrographs sediment deposition has been observed in the river mouth, but this sediment is later scoured by the south to north long-shore currents. Typically during low flow conditions ($< 10 \text{ m}^3/\text{s}$) numerous sandbanks are exposed in the main channel (Figure 3.1-1).



Figure 3.1-1 Thukela River mouth after major flood, South Africa

The Richmond River estuary on the northern New South Wales coast, Australia, due to its small capacity in contrast to its freshwater inputs, can be subjected to significant morphological changes during floods (Hossein, Eyre and McConchie, 2001). During minor floods net sedimentation occurs in the estuary, as the tidal flows interfere with the flood currents. During larger floods all the eroded catchment sediment is flushed from the estuary. Sediment was even scoured in the upper estuary. In

contrast the Rappahannock Estuary on the east coast of the United States manages to trap almost 90% of all flood-borne sediment because the freshwater inflow is not large enough.

Tide-dominated estuaries (e.g. Nahoon, Sundays and the Mtamvuna, South Africa) and river-dominated estuaries (e.g. Mgeni, Mvoti and Orange, South Africa) recover differently from major floods. In tide-dominated estuaries erosion is usually confined to the lower reaches and cohesive sediments and deeper waters tend to reduce erosion in the upper reaches. In the Nahoon Estuary, for example, it was found (Reddering and Esterhuysen, 1985) that about 78% of the sediment scoured from the estuary during a flood in 1985 came from the lower reaches. The same trend was observed in the Mtamvuna Estuary on the KwaZulu-Natal coast, where flood impacts in the estuary were mainly restricted to erosion in the berm area, unlike the usually river-dominated estuaries in KwaZulu-Natal. It is thought that the Mtamvuna Estuary represents a transitional phase between the river-dominated estuaries and the wave-dominated estuaries on the south-east coast (Cooper, 1993). In river-dominated estuaries, on the other hand, there is no such variation, and erosion or deposition occurs throughout the river channel.

In both tide- and river-dominated estuaries the berm erosion is accompanied by deposition of an ephemeral delta and the barrier is reformed by landward transport of sediment under wave action (Cooper, 2002). However, river-dominated estuaries operate as conduits for fluvial sediments and the ephemeral delta consists of both fluvial sediment from the catchment and former barrier sediments, and there is therefore a surplus of sediment which has to be dispersed. The reworking of the large sediment influxes during major floods could take decades. In tide-dominated estuaries on the other hand, only the former barrier and tidal delta sediments have to be reworked into the barrier and tidal deltas, which usually takes place over several years.

3.2 Human Impacts

Floods and storms are natural phenomena that affect the estuarine dynamics, but many other factors occur through human intervention. The impacts of these can take many years to become obvious, whereas others have an almost immediate effect on the estuary. There are three areas in which developments can affect the normal functioning of the estuary. These are local disturbances, i.e. in and around the estuary, upstream developments in the catchment and coastal developments.

Local developments/activities:

- Stabilization of the mouth
- Channel training, through structures such as bridges, groynes and embankments

- Dredging
- Mouth breachings

Catchment developments:

- Construction of dams
- Interbasin water transfers and water abstraction
- Change in land use
- Deforestation

Coastal developments/activities:

- Dumping of dredged soil
- Stabilization of coastline

3.2.1 Local Developments

Estuaries are very attractive environments that many people view as ideal places for leisure activities or as places to develop industrial or port sites. Very few estuaries are, however, large enough to be used as harbours in South Africa, for example Richards Bay and Durban, and these have to be kept open by artificial means. Inevitably some developments have occurred in many estuaries that will affect the natural sediment dynamics of these estuaries. Developments that can affect the natural dynamics of an estuary include bridges, marinas, groynes, dredging and mouth stabilizations to name but a few.

i) Bridges: Many bridges are not wide enough to allow larger floods to pass through unhindered, with the result that flows become concentrated and also the natural meandering tendency of a river channel becomes restricted, which could lead to local scour.

In 1973 a 220 m long road bridge was built over the Uilkraals River estuary about 800 m upstream of the mouth (Crowther, 1988). The bridge opening is only 100 m wide and the embankment on the eastern side is 120 m long (see Figure 3.2-1). This has forced the river and tidal flows to concentrate on the western side. As a result, sand has been building up in an open area downstream of the bridge, due to the sheltering effect of the embankment during floods, and is being stabilized by vegetation. The sand build-up downstream of the embankment can also be attributed to the fact that windblown sediment is prevented from moving into the estuary by the embankment. The main channel on the other hand has been eroded due to increased velocity as the flow is forced through the limited bridge opening and the migration of the main channel has been curbed to some degree.

ii) Groynes: Groynes operate by deflecting the flow and as such can cause large-scale eddying and consequent energy loss, which could lead to severe sediment deposition (as well as erosion).

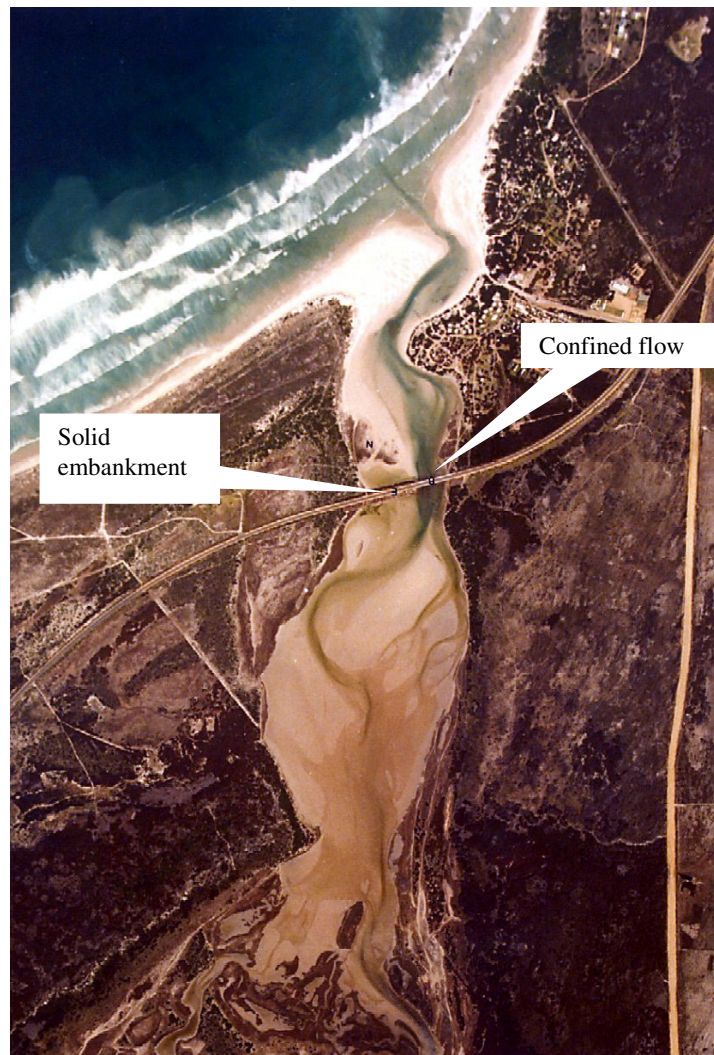


Figure 3.2-1 Uilkraals River mouth, South Africa (Crowther, 1988)

iii) Marinas: Marinas can also affect the natural flow pattern, usually by diverting part of the flow, which causes sedimentation in the main channel. The Kowie Estuary was modified extensively over the years (Schumann and Gray, 1998). During the early 19th century a harbour was built and later the main channel was straightened and breakwaters were built at the mouth. However, it was the building of the Royal Alfred Marina (Figure 3.2-2) in the late 1980s that caused a definite change in the sedimentation pattern in the estuary. A large part of the flow passes through the marina canals, built parallel to the main channel, causing a decrease in velocity in the estuary at the downstream marina entrance during flood tide. During ebb tide a significant part of the flow again passes through the marina and the currents in the estuary are therefore not strong enough to resuspend the material which

has been deposited at the entrance. It is thought that if the total ebb tidal flow would again pass through the estuary, the currents would be enough to flush the accumulated sediments out. This could be achieved by closing off the upstream marina entrance during ebb tides for a number of days.

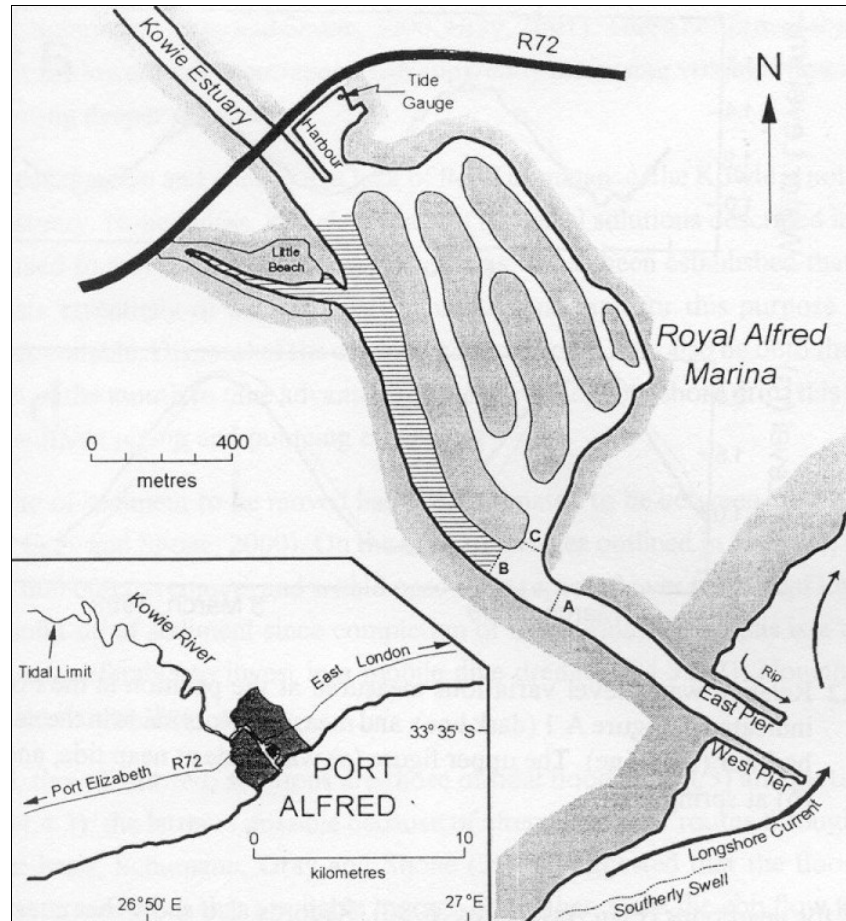
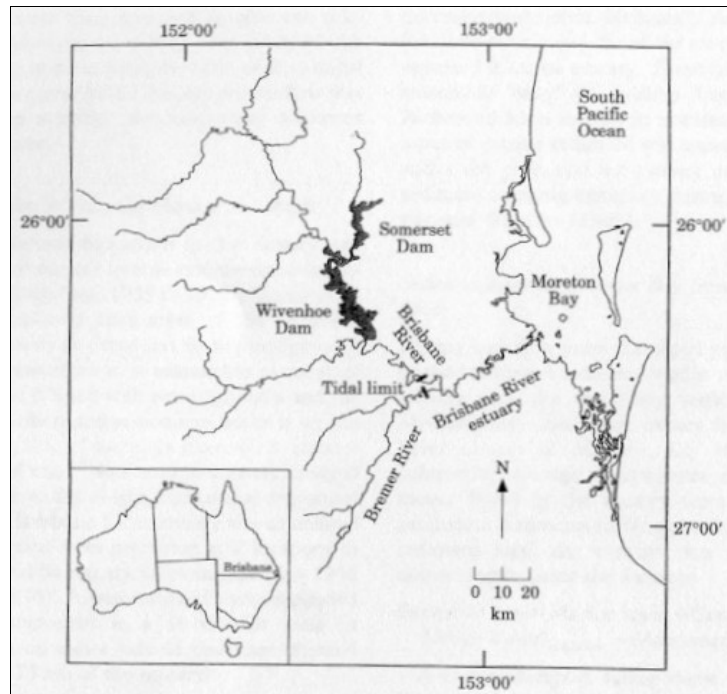


Figure 3.2-2 Royal Alfred Marina in Kowie Estuary, South Africa (Schumann 2003)

iv) Dredging: Dredging can significantly affect the sediment dynamics in estuaries. A dredged channel can completely modify the tidal flow, tidal prism, ebb and flood channels, and the intertidal profile. The sediments which are suspended during the operation can be deposited on the intertidal flats. The increased depth after dredging causes a reduction in the velocities, which means that the flushing ability of the estuary is reduced. The subtropical Brisbane River estuary (Figure 3.2-3) on the south-east coast of Queensland, Australia, has been subjected to dredging for decades and as such traps a greater proportion of flood-borne sediment than other similar estuaries (Eyre, Hossein and McKee, 1998). At present the estuary needs $2200 \times 10^6 \text{ m}^3$ of freshwater flow to scour. During a 1:20-year flood in 1996 only 79% of the flood-borne sediment was flushed from the estuary. In contrast, in the subtropical Richmond River estuary (northern New South Wales coast, Australia), 100% of the flood-borne sediment was removed during a 1:5-year flood.



**Figure 3.2-3 Location map of Brisbane River estuary, Australia
(Eyre, Hossein and McKee, 1998)**

The lower reach of the Berg River estuary on the west coast of South Africa, close to the towns of Velddrif and Laaipelek, has been dredged since the mid 1950's, mainly to accommodate the larger fishing boats from Laaipelek and Velddrif, as well as to ensure that the vessels of the fishing fleets operating in St Helena Bay could use the estuary as a shelter (Van Wyk, 1983). However, dredging had increased the water flow and the old mouth region (a new mouth was constructed in 1966) had sanded up completely within two years after construction of the new mouth.

v) Mouth stabilization: The decision to stabilize the mouth of the Berg River estuary (Figure 3.2-4) was made because of the perceived sedimentation in the estuary. Initial investigations into the stabilization of the mouth revealed bed rock at relatively shallow depths in and around the mouth. Local sandbanks were constantly being shifted around on the rocky bottom by wave and tidal currents. Various factors were taken into account in deciding on a design for the stabilized inlet, such as the wind and sediment dynamics. In the end it was decided to build a new inlet at the opposite end of the berm, with breakwaters to streamline the river flow and also to prevent the inlet from silting up. A navigation channel was to be constructed at the same level as the inlet channel, extending as far upstream as the fully laden fishing boats would travel. However, the navigation channel silted up rapidly and maintenance dredging has been necessary ever since. The wider than planned inlet together with wave refraction from the breakwaters has increased erosion of the south bank opposite the inlet at rates of about 4 m per year (Van Wyk, 1983).



Figure 3.2-4 Berg River mouth before and after mouth was stabilized

The Seekoei Estuary in the Eastern Cape, South Africa, has undergone considerable change as a result of developments within the estuary. Firstly the inlet was artificially shifted to make way for a swimming pool complex. After that a causeway was built across the estuary connecting the communities on opposite sides of the estuary. As a result excessive sediment built-up occurred in the lower estuary due to wind-deposited sand and sand from the longshore drift transported into the lower estuary. The part of the estuary upstream of the causeway was being taken over by fluvial sediment and in time the upper part could become a freshwater reservoir (Esterhuysen, 1982).

vi) Artificial breaching: Many South African estuaries are temporarily closed, more so now than in the past. Numerous developments have taken place on the floodplains of many South African estuaries and the mouths were artificially opened to prevent flooding of these developments. The main

problem is that a significant number of these developments were built at low levels and the water levels at which breachings have taken place are much lower (under +2 m MSL) than under natural conditions (between +2.5 and +3 m MSL). The effect has been that the estuaries do not flush properly and the mouths stay open for shorter periods.

The mouth of the Great Brak Estuary, South Africa, has been artificially breached a few times a year over the last decade (Figure 3.2-5 and Figure 3.2-6). In the early 1990s the water levels at which breachings took place were below +1.6 m MSL, but in more recent years the water levels have been as high as +2 m MSL. The result is that more sediment is now flushed out during breaching than earlier (CSIR, 2000).

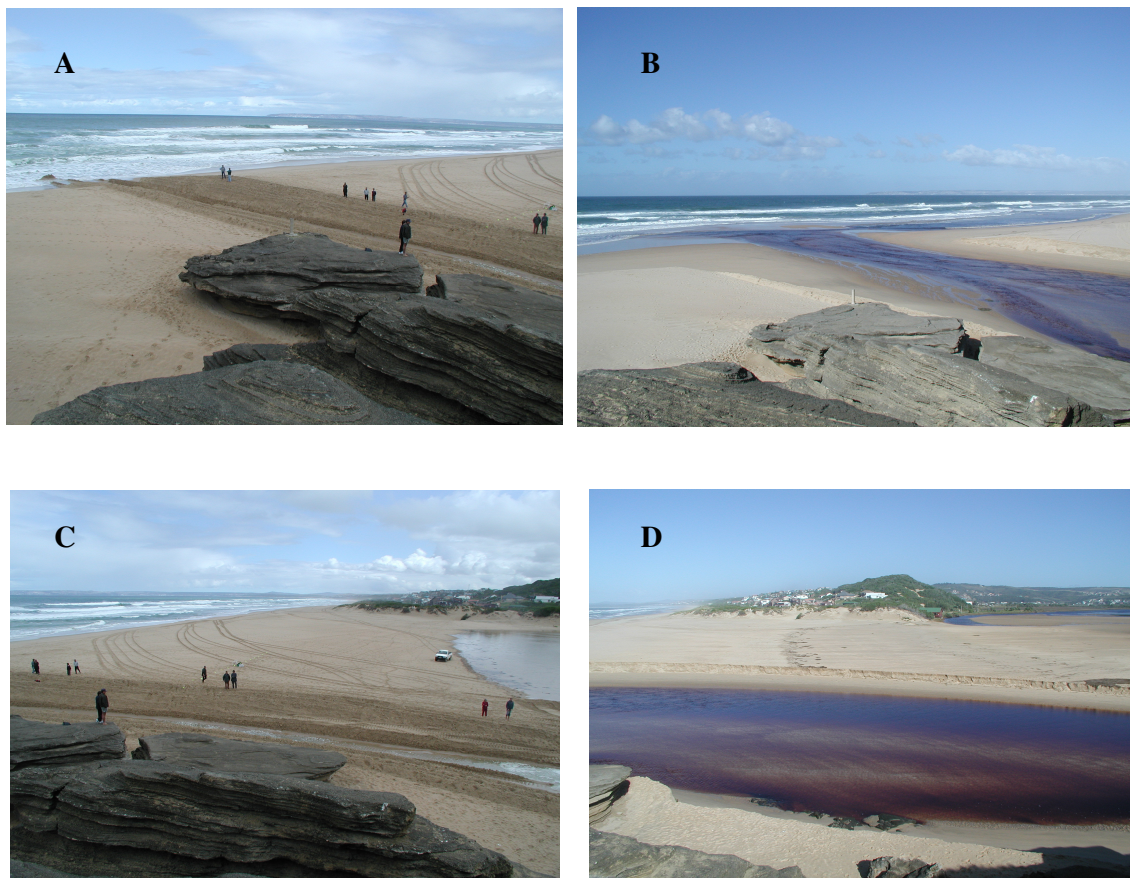


Figure 3.2-5 Different perspectives of artificial breaching at Groot Brak Estuary, South Africa, in 2001 (A and C show the start of breaching, B and D show the final breaching channel)



Figure 3.2-6 Aerial view of Groot Brak Estuary, South Africa (closed mouth)

Artificial breaching has also taken place at the Klein River estuary near Hermanus, South Africa (Figure 3.2-7 and Figure 3.2-8). Natural breaching would take place at +3 m MSL (CSIR, 1999), but the mouth has been artificially breached at levels as low as +1.81 m MSL. The benefit of breaching at higher water levels in the Klein can be seen from maximum discharges observed in the mouth during breaching. These can be over 400 m³/s at water levels above +2.6 m MSL, which is in the order of a 1:50-year flood in the Klein River.



Figure 3.2-7 Aerial view of Klein River estuary, South Africa



Figure 3.2-8 Artificial breaching at Klein River estuary, South Africa, in 2001

3.2.2 Catchment Developments

Water resource developments in the catchment, such as dams and abstraction works cause a reduction in streamflow. Dams have the added effect that the natural variability inherent in the streamflow pattern of semi-arid countries such as South Africa is reduced. This leads to reduced sediment transport capacity and also reduced flushing efficiency especially in river-dominated estuaries. Tidal

deltas can thus grow, which restrict the tidal inlets. As the tidal inlet becomes restricted the normal tidal flows may not be able to keep the mouth open.

It is not only the dams with large reservoirs that will have an impact on an estuary, but a number of small dams can be equally detrimental. This is because both low flows and major floods are important for the normal functioning of an estuary. The low flows tend to keep the mouth open and floods tend to flush sediment out of the estuary. While the smaller dams may not have a significant effect on the larger floods, they can remove most of the baseflow from the system.

When the river flow is reduced, sediment tends to accumulate for a longer time and the volume might become too large to flush out during a single flood. It also starts to consolidate, which makes it much more difficult to erode, especially in the case of cohesive sediments. This confirms how important smaller floods are, as these would be able to prevent too much sediment from accumulating in the estuary, thereby also reducing the consolidation time of the sediments in the estuary.

Together with reduced river flows, dams also tend to trap most of the sediments coming from their catchments. The sediment-free water has a higher erosive capacity, and combined with the reduced streamflow, the net effect usually is that less fluvial sediment tends to reach an estuary. On the other hand significant changes in land use, overgrazing and deforestation could have the opposite effect in that the total sediment yield from the catchment could increase with time, which could cause fluvial sedimentation in an estuary.

The effects of future developments in the catchment have been investigated in detail for the Thukela Estuarine Reserve Determination (see Chapter 6), and it was found that the building of two new dams higher up in the catchment would not have a severe effect at first, as the combination of reduced streamflow and sediment yield prevents significant scouring or aggradation in the river mouth. However, an increase in the sediment yield could cause serious aggradation in the estuary resulting in a shorter estuary.

The Impofu Dam just 4 km upstream of the Kromme River estuary, South Africa, has a capacity of $105 \times 10^6 \text{ m}^3$, which is approximately equal to the mean annual runoff (MAR) of the Kromme River (Reddering, 1988). It is therefore apparent that very little river flow reaches the estuary. In fact in 1983, shortly after the construction of the dam, while still relatively empty, a flood completely filled the dam and little discharge reached the estuary. This means that a water volume of about $105 \times 10^6 \text{ m}^3$ was lost to the estuary, and as a result the flood tidal delta was left almost intact (Reddering, 1988).

The catchment of the Breede River in the Western Cape, South Africa, contains several dams, the largest of which is the Theewaterskloof Dam on a tributary, the Sonderend River. Historical records show extensive mudflats (of fluvial origin) had been present in the flood delta until at least the 1950s, but by the end of the 1970s these mudflats had been largely inundated by marine sand, probably due to the combined effect of reduced river flows and reduced fluvial sediment (De Villiers, 1988).

Many dams and reservoirs were built on the Ebro River (Figure 3.2-9), Spain, during the 20th century (Guillén and Palanques, 1992). The mean discharge had decreased from 590 m³/s to 430 m³/s by the late 1980s. During the same period the annual sediment load had decreased by more than 99%. The combined effects of low annual rainfall and reduced mean water discharge through the estuary in the late 1980s have allowed significant amounts of mud to accumulate in the estuary, although the associated sediment discharge was also low (two large dams about 100 km from the mouth trap almost 75% of the sediment load). During higher river flows this mud is resuspended, but the underlying sand cannot be transported. The drastic reduction in sediment transport has led to a sediment deficit in the delta, which is causing erosion of some reaches of the coastline (Ibáñez, Prat and Canicio, 1996).

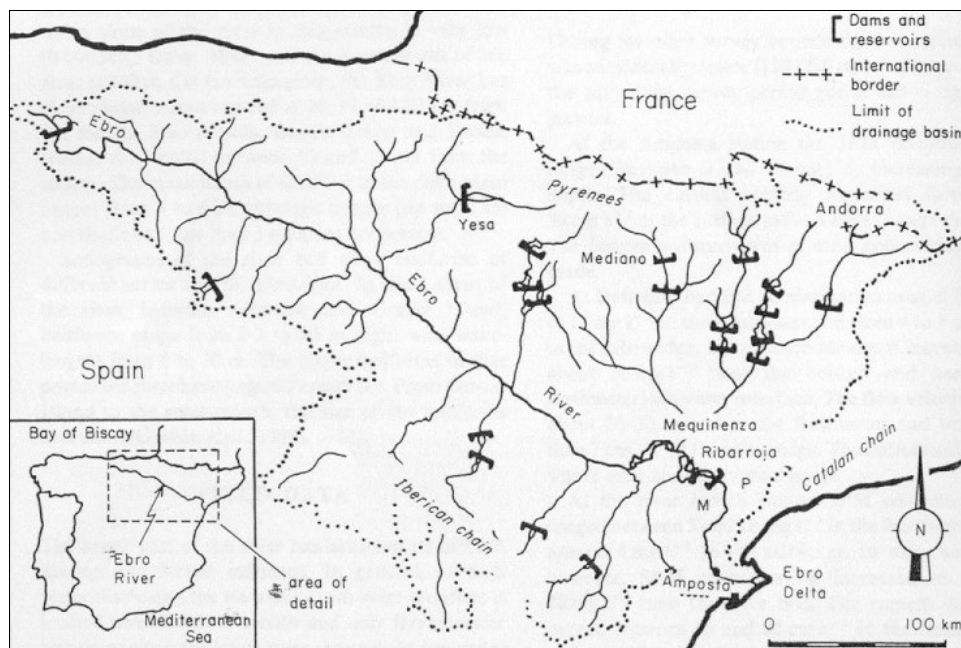


Figure 3.2-9 Location map of Ebro River, Spain (Guillén and Palanques, 1992)

The river flows to the Oued Massa Estuary in southern Morocco (Figure 3.2-10) have been regulated since 1974 by a barrage and all but the largest flows are retained (Fox, Wilby and Moore, 2001). Since then the estuary has been closed for about 50% of the time compared to 15-20% during the pre-dam period. The first significant spills in 1988/89 were insufficient to cause breaching, but two years later 35 x 10⁶ m³ of water were released, and this time breaching of the barrier took place. The mouth stayed

open until 1996, when a second spill of $89 \times 10^6 \text{ m}^3$ re-established a strong connection with the sea. It was found that it would probably take between 20 and 60 months for the mouth to close again after a major flood, and that it would take discharges of between 19 and $35 \times 10^6 \text{ m}^3$ to open the mouth.

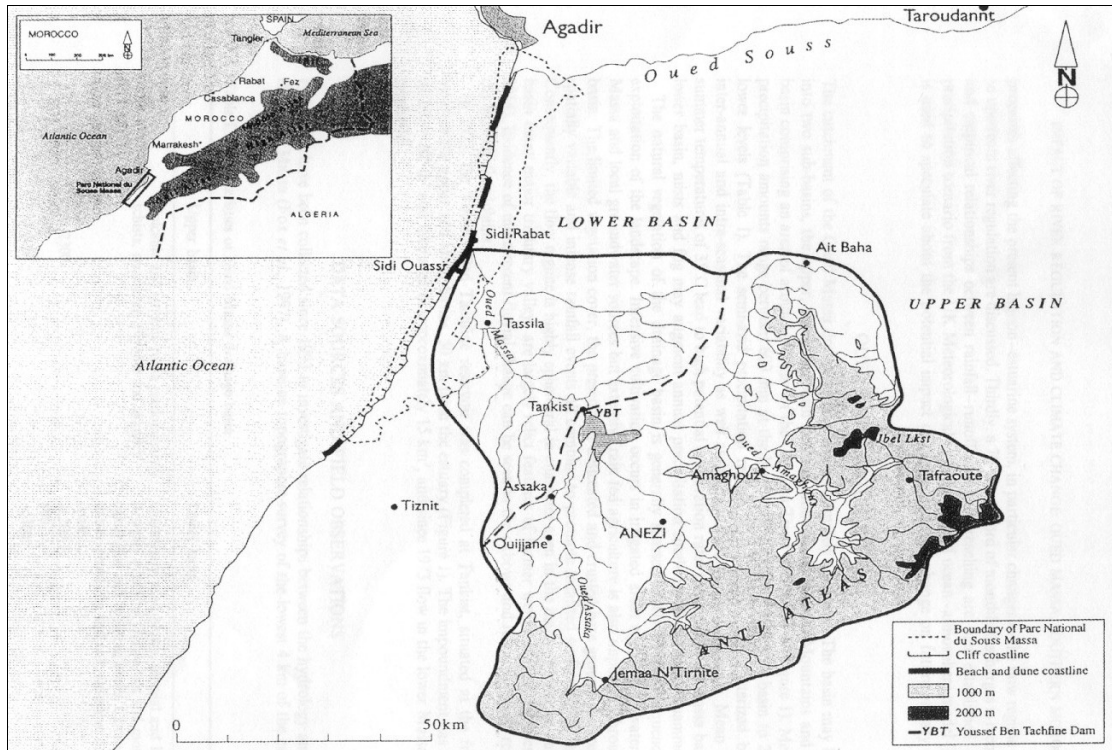


Figure 3.2-10 Location map of Oued Massa, Morocco (Fox, Wilby and Moore, 2001)

In the catchment of the Groot Brak Estuary, the Wolwedans Dam was built in the early 1990s just 2 km upstream of the estuary. Although the mean annual runoff (MAR) was already reduced from the natural MAR at the time the dam was built, the MAR will be even further reduced when the dam meets its full demand. Therefore $1 \times 10^6 \text{ m}^3$ is reserved annually for release to the estuary (Huizinga, 1994). It was found that by using the water to breach the mouth at higher levels, more sediment is flushed out during breachings and that the state of sedimentation in the lower estuary is similar to what it was before the dam was built (Schumann, 2003).

Several barrages had been built on the lower Murray River, Australia, by 1940, reducing the tidal prism by 85% and reducing the rate and size of river flows through the estuary (Harvey, 1996). In fact there have been many periods of no river flow when the barrages have been closed consecutively for 100 days or more. Coastal processes have been dominant at the mouth ever since, resulting in the accretion and stabilization of a flood-tidal delta and the accumulation of a new flood-tidal delta (Figure 3.2-11). In 1981 an artificial channel had to be excavated to re-open the mouth. A first attempt

to open the mouth was not successful, but the second channel in a different location managed to re-open the mouth, but also caused rapid erosion of the adjacent peninsula. The restriction to flow by the barrages has also been responsible for rapid deposition of mud (4.5 mm per year) in the lower reaches over the past 60 years (Bourman and Barnett, 1995).



Figure 3.2-11 Murray River mouth, Australia, with an inset of an almost closed mouth

The flow needed to maintain open mouth conditions depends on several factors. Estuaries on coasts sheltered from direct wave action tend to need smaller flows than those on wave-exposed coast, as closure is mainly wave-induced. The size of the estuaries is also a factor, because the larger estuaries generally have larger tidal prisms and therefore greater flows through the mouth. The Groot Brak Estuary needs only about $0.5 \text{ m}^3/\text{s}$ to keep it open during neap tides, and it stays open during spring tides (CSIR, 2000). The Mgeni Estuary near Durban on the other hand, closes even at spring tide and with a flow of $10 \text{ m}^3/\text{s}$. In the case of the Groot Brak Estuary, it sometimes only takes a minor release from the Wolwedans Dam to keep the mouth open.

3.2.3 Coastal Developments

The longshore transport of sediment plays an important role in estuarine sediment dynamics. Any changes tend to affect an estuary, although the extent will be different for each estuary. If dredged soil for example is dumped on the shoreline the sediment could be transported to other estuaries down-drift. In

the same manner, if the coastline is stabilised in some way, the sediment transported by the longshore current is reduced, and as such erosion could occur at other places on the coastline. During the tidal cycle a certain amount of sediment is moved into the estuary by the flood currents, if the available sediment however is reduced it could lead to erosion of the area around the mouth. In the same way, the return of dredged soil to the estuary could cause accretion in the mouth area.

3.3 Summary

This chapter serves to highlight some of the impacts on estuaries related to sedimentation. There are of course numerous factors affecting our estuaries, but as pointed out, not all of them are the result of human impacts. Floods and storms can have a devastating effect on the estuarine system, but this forms part of the dynamic nature of estuaries. Sedimentation related to human impacts is mainly the result of catchment developments, such as dams, and local developments or activities such as dredging and structures built around an estuary. The human impacts have been quite substantial in some estuaries such as the Seekoei Estuary, while in others it is difficult to ascertain to what degree the perceived sedimentation problems are natural and how much is the result of human impacts. It is therefore important to understand the natural sedimentation processes first, before attempting to offer solutions to sedimentation problems.

4. Sediment Transport Processes

The sediment transport in an estuary is similar to the sediment transport in rivers, except that during the tidal cycle a reversal in flow direction takes place and the effect of waves has to be taken into consideration. Usually there is a time where no or very little sediment transport takes place as the tide turns, because the flow velocities are very small, picking up again after the tide has turned. The effect of waves is usually taken into account by adjusting certain parameters (such as the bottom shear stress or friction coefficients) in traditional sediment transport formulas to account for the combined effect of currents and waves. Some of the existing sediment transport formulas and the development of a new sediment transport formula based on stream and wave power are discussed in this chapter.

4.1 Critical Conditions for Re-Entrainment of Non-Cohesive Sediment

The forces acting on a grain on the bottom in steady uni-directional flow are depicted in Figure 4.1-1 (Chadwick and Morfett, 1998):

$$\text{The drag force } F_D = \frac{1}{2} \rho \cdot C_D \frac{\pi d^2}{4} (\alpha \cdot u_*^2) \dots\dots\dots 4.1-1$$

$$\text{The lift force } F_L = \frac{1}{2} \rho \cdot C_L \frac{\pi d^2}{4} (\alpha \cdot u_*^2) \dots\dots\dots 4.1-2$$

$$\text{The self weight } W = (\rho_s - \rho)g \frac{\pi d^3}{6} \dots\dots\dots 4.1-3$$

where C_D = drag coefficient

C_L = lift coefficient

d = sediment grain diameter

α = coefficient

u_* = friction velocity

The shear stress at the interface τ_0 is the sum of forces on the individual particles. At the start of movement the shear stress at the interface $\tau_0 = \tau_c$ (critical shear stress). From this the Shields parameter θ can be derived:

$$\theta = \frac{u_*^2}{(s-1)gd} = \frac{\tau}{\rho(s-1)gd} \dots\dots\dots 4.1-4$$

where s = specific gravity of sediment

τ = bottom shear stress

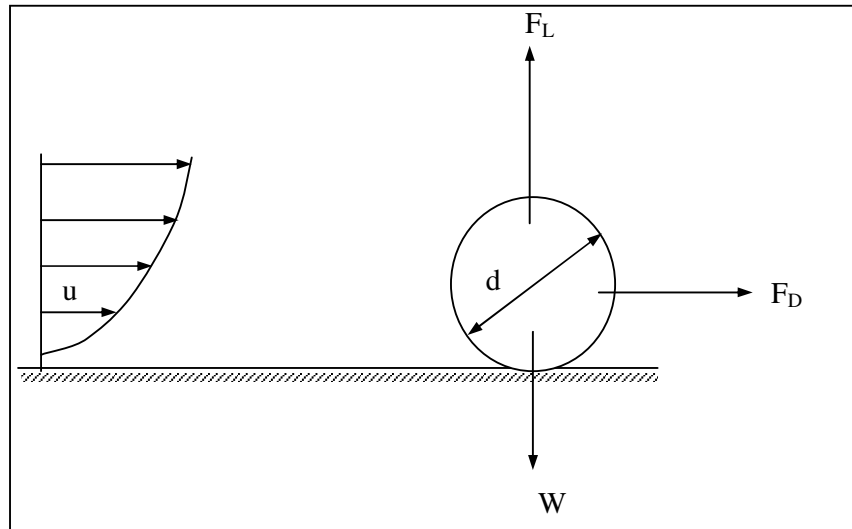


Figure 4.1-1 Forces acting on a sediment particle resting on the bed

Now it is possible to define different conditions when sediment particles will start to move:

$$\theta > \theta_c \quad \text{or} \quad \tau > \tau_c \dots\dots\dots 4.1-5$$

where θ_c = critical Shields parameter = $\frac{\tau_c}{(\rho_s - \rho)gd}$

τ_c = critical bottom shear stress

The critical Shields parameter can be determined from the Shields diagram in Figure 4.1-2, as a function of the grain Reynolds number $Re_* (= \rho u_* d / \mu)$.

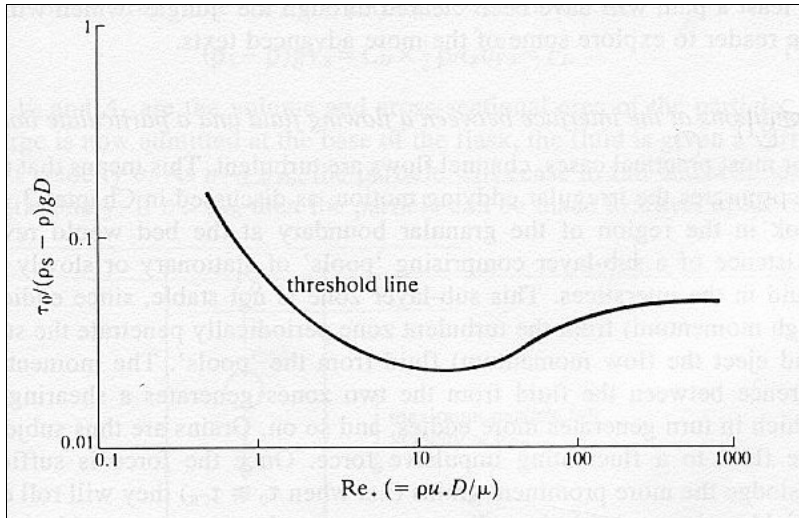


Figure 4.1-2 Shields' diagram (Chadwick and Morfett, 1998)

In the coastal environment sediment transport is as a result of both currents and waves. The Shields criterion for currents alone can be adjusted for wave-current interaction (Bruun, 1972), by replacing the current-induced bottom shear stress with the wave-induced shear stress τ_w :

$$\tau_{w,max} = \frac{1}{2} \rho f_w U_m^2 \dots\dots\dots 4.1-6$$

where U_m = maximum horizontal velocity (m/s) = $A \frac{2\pi}{T}$

$$f_w = \text{wave friction coefficient} = 5.5 \left[\frac{k_s}{A} \right]^{0.2} - 6.3$$

$$A = \text{amplitude of oscillation of water particles on sea bed} = \frac{H}{2} \cdot \frac{1}{\sinh\left(\frac{2\pi \cdot h}{L}\right)}$$

k_s = bed roughness

H = wave height

L = wave length

T = wave period

h = water depth

Although the Shields criterion is still widely used, Rooseboom and Mülke (1982) have shown that incipient motion can be described more comprehensively in terms of stream power.

The unit stream power (per unit volume) required to suspend a particle with mass density ρ_s and settling velocity w is equal to

$$(\rho_s - \rho)g w \dots\dots\dots 4.1-7$$

In rough turbulent flow, the unit stream power applied in maintaining motion along a plane bed, is proportional to

$$\frac{\rho g S D \sqrt{g D S}}{d} \dots\dots\dots 4.1-8$$

where S = energy slope
 D = flow depth

Particles will be entrained when the power required to suspend particles becomes less than the power required to maintain motion.

$$(\rho_s - \rho)g w \propto \frac{\rho g S D \sqrt{g D S}}{d} \dots\dots\dots 4.1-9$$

By manipulating equation 4.1-9, the condition of incipient motion under rough turbulent flow conditions is given by

$$\frac{\sqrt{g D S}}{w} = constant \dots\dots\dots 4.1-10$$

Similarly, in smooth turbulent and laminar flow, the applied unit stream power equals to

$$\frac{(\rho g D S)^2}{\rho \nu} \dots\dots\dots 4.1-11$$

where ν = kinematic viscosity

And for values of $\frac{\sqrt{g D S} \cdot d}{\nu} < 13$, the incipient motion criteria has been calibrated as follows

$$\frac{\sqrt{gDS}}{w} = \frac{1.6}{\frac{\sqrt{gDS} \cdot d}{\nu}} \dots\dots\dots 4.1-12$$

This criterion is illustrated in Figure 4.1-3.

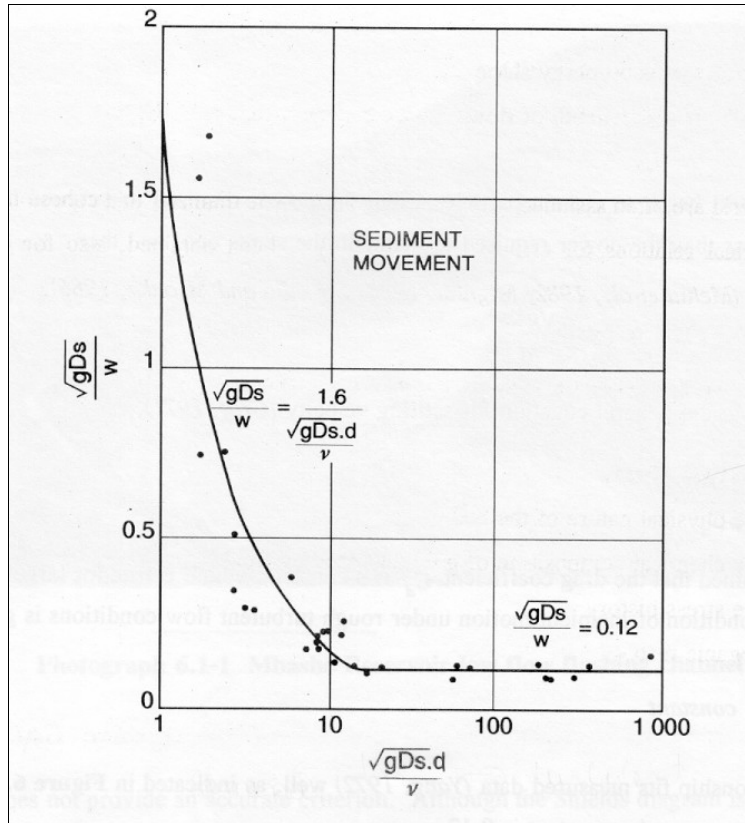


Figure 4.1-3 Incipient motion conditions for cohesionless sediment particles (Rooseboom and Mülke, 1982)

Cohesive sediment did not form part of the scope of work of the research, but is important in many estuaries. A critical shear stress is usually used to describe a rate of erosion of the cohesive bed. It is important to note that with a cohesive fraction (silt and clay) of as low as 7% in the bed, the bed will react as cohesive.

4.2 Bed Roughness

The prediction of the bed roughness and possible changes in roughness is very important, since bed roughness determines friction losses and depth of flow for a given discharge, as well as the sediment transport capacity. As discovered during the field investigation the bed forms can be very significant

(see Figure 4.2-1). The calculation of the flow resistance is quite complex, since a large part of the flow resistance is caused by form drag on the bed forms, the configuration of which is determined by the flow and sediment transport. As the flow increases, the bed forms will change from small scale ripples to dunes, which are generally the most important bed forms in the subcritical flow regime. As the flow increases further a transitional phase is reached, in which all bed forms are washed away, and a flat bed emerges. In the supercritical flow regime antidunes occur. The second part of the flow resistance is skin friction, dependent on the size of the sediment particles.



Figure 4.2-1 Bed forms at Groot Brak River after breaching in 2001

Flow resistance is often expressed in the form of the Manning n or the Chezy C coefficient, or in terms of the absolute roughness k_s . Many mathematical models use either the Manning or Chezy value in their resistance formulation. The focus of the many attempts at developing a universal flow resistance formulation has usually been on alluvial rivers (e.g. Karim (1995 and 1999) and Rooseboom and Le Grange (2000)), but less research has been carried out on the flow resistance in the coastal environment (Houwman and Van Rijn (1999)). Predicting the flow resistance reliably in the coastal environment is problematic because of the oscillating current and waves. During the flood tide for example, the bed forms develop in the direction of the tide, i.e. the shorter, steeper side of the dunes is on the downstream side. As the tide changes to ebb, it takes a certain amount of time before the bed forms change to face in the opposite direction. This depends largely on the strength of the currents. It

can take a while before the currents are strong enough to transport sediment, and thus affect the formation of bed forms.

The wave-current interaction influences both the flow profile and sediment transport. In the wave boundary layer the shear stress and turbulence is the result of both currents and waves, but in the region above the wave boundary layer the current is subjected to a shear stress that is affected by the shear stress in the boundary layer. The result is that the shear stress experienced by the current above the wave boundary layer is different from a current only situation. This process can be schematized by an apparent roughness value experienced by the flow above the wave boundary layer (Houwman and Van Rijn (1999)). Houwman and Van Rijn have carried out investigations on several apparent and physical roughness models, and have found that the apparent roughness may be as much as 100 times greater than the physical roughness, however, the results are very sensitive to the choice of a model.

4.3 Existing Sediment Transport Formulas

Sediment transport in estuaries is the result of the interaction of both currents and waves, which is especially important in the mouth region, since inside the estuary wave action is generally rapidly reduced. A short summary of some of the existing sediment transport formulas for currents only as well as wave-current interaction follows.

a) Ackers and White (1973) – current only

One of the most well known sediment transport formulas is the Ackers and White equation. It is based on Bagnold's (1966) stream power concept, and it is represented by three dimensionless numbers, G_{gr} (sediment transport parameter), F_{gr} (mobility number) and d_{gr} (particle size number).

$$G_{gr} = \frac{q_s D}{qd} \left(\frac{u_*}{v} \right)^n = c \left(\frac{F_{gr}}{A_{gr}} - 1 \right)^m \dots\dots\dots 4.3-1$$

where c , n , m and A_{gr} are coefficients.

q_s = sediment discharge per unit width

q = discharge per unit width

v = flow velocity

$$F_{gr} = \frac{u_*^n}{\sqrt{gd(\rho_s/\rho - 1)}} \left(\frac{v}{\sqrt{32 \log(10 D/d)}} \right)^{1-n} \dots\dots\dots 4.3-2$$

$$d_{gr} = d \left(\frac{g(\rho_s/\rho - 1)}{v^2} \right)^{1/3} \dots\dots\dots 4.3-3$$

The values for c , n , m and A_{gr} are as follows:

For coarse sediment ($d_{gr} > 60$): $n = 0$; $m = 1.78$; $A_{gr} = 0.17$ and $c = 0.025$

For smaller sizes ($1 < d_{gr} < 60$): $n = 1 - 0.56 \log(d_{gr}) \dots\dots\dots 4.3-4$

$$m = 1.67 + 6.83/d_{gr} \dots\dots\dots 4.3-5$$

$$A_{gr} = 0.14 + 0.23 / \sqrt{d_{gr}} \dots\dots\dots 4.3-6$$

$$\log c = 2.79 \log(d_{gr}) - 0.98 (\log(d_{gr}))^2 - 3.46 \dots\dots\dots 4.3-7$$

b) Engelund and Hansen (1967) – current only

Another well-known sediment transport formula is the Engelund and Hansen formula.

$$\frac{2gDS}{v^2} \phi = 0.1\theta^{5/2} \dots\dots\dots 4.3-8$$

where $\phi = \frac{q_s}{\sqrt{(s-1)gd^3}} \dots\dots\dots 4.3-9$

and $\theta = \frac{\rho g DS}{(\gamma_s - \gamma)d} \dots\dots\dots 4.3-10$

and γ_s = specific weight of sediment
 γ = specific weight of water

c) Bijker (1971) – waves and current

One of the first and most well-known sediment transport formulas for wave-current interaction is the Bijker formula. It is based on the Frijlink formula (1952) for currents alone, with a modification of the bed shear stress for waves and currents. It is valid for both breaking and non-breaking waves (Bayram *et al*, 2001), and the bed load and suspended are calculated separately.

The bed load transport rate ($m^3/s.m$) is given by Camenen *et al* (2003) as:

$$q_b = A \cdot d_{50} \cdot \sqrt{\frac{\mu_c \cdot \tau_c}{\rho}} \cdot e^{\left[\frac{-0.27 \cdot (s-1) d_{50} \cdot \rho \cdot g}{\mu \tau_{b,cw}} \right]} \dots\dots\dots 4.3-11$$

with A = wave parameter (1.0 for non-breaking waves and 5.0 for breaking waves)

d_{50} = median grain diameter

$\tau_{b,c}$ = bed shear stress due to current alone

ρ = water density

s = relative sediment density

$$\mu_c = \text{ripple parameter} = \left(\frac{f_{ct}}{f_c} \right)^{3/2}$$

f_{ct} = total friction coefficient due to current

f_c = skin friction coefficient due to current

$$\tau_{b,wc} = \text{bed shear stress due to waves and current} = \tau_{b,c} \cdot \left[1 + 0.5 \cdot \left(\frac{\xi \cdot u_o}{u_c} \right)^2 \right]$$

$$\xi = \sqrt{\frac{f_{wt}}{f_{ct}}}$$

u_o = maximum wave orbital velocity

u_c = mean current velocity

f_{wt} = total friction coefficient due to waves

The suspended load transport rate is given as a function of the bed load transport rate:

$$q_s = 1.83 \cdot q_b \cdot \left[I_1 \cdot \ln\left(\frac{33h}{r} \right) + I_2 \right] \dots\dots\dots 4.3-12$$

with I_1, I_2 = Einstein integrals

r = bed roughness

h = water depth

$$I_1 = 0.216 \cdot \frac{B^{z-1}}{(1-B)^z} \cdot \int_B^1 \left(\frac{1-C}{C} \right)^z \cdot dC \dots\dots\dots 4.3-13$$

$$I_2 = 0.216 \cdot \frac{B^{z-1}}{(1-B)^z} \cdot \int_B^1 \left(\frac{1-C}{C} \right)^z \cdot \ln(C) \cdot dC \dots\dots\dots 4.3-14$$

$B = r/h$

$C = z/h$

$$z = \frac{w}{\kappa \cdot u_*}$$

w = settling velocity

κ = Von Kármán constant

u_* = shear velocity

d) Bailard (1981) – waves and current

Another sediment transport formula for wave-current interaction is the Bailard formula, based on Bagnold’s stream power approach, modified for oscillatory flow. The total sediment transport rate vector is given as (Camenen *et al*, 2003):

$$\vec{q}_s = \frac{0.5 \cdot f_{cw}}{g(s-1)} \left[\frac{\epsilon_b}{\tan \phi} \cdot \langle |\vec{u}|^2 \vec{u} \rangle + \frac{\epsilon_s}{w} \langle |\vec{u}|^3 \vec{u} \rangle \right] \dots\dots\dots 4.3-15$$

with f_{cw} = friction coefficient due to wave-current interaction

ϵ_b, ϵ_s = bed load and suspended load efficiency coefficients (generally 0.1 and 0.02, respectively)

ϕ = friction angle of sediment

\vec{u} = velocity vector near the bed

$\langle \rangle$ = average over several periods of waves

One drawback of this formula is the estimation of the friction coefficient due to wave-current interaction, as Bailard did not specify any expression for this friction factor.

e) Dibajnia and Watanabe (1992) – waves and current

A more recent sediment transport relationship is that by Dibajnia and Watanabe, which breaks down the sediment transport into two half-cycles due to the presence of waves. During the first half-cycle the sediment moves in the same direction as the waves, whereas in the second half-cycle sediment movement is opposed to the wave direction. The volumetric load is then:

$$q_s = A_{dw} \cdot w \cdot d_{50} \cdot \frac{\bar{\Gamma}}{\Gamma} \cdot \Gamma^{B_{dw}} \dots\dots\dots 4.3-16$$

with $A_{dw} = 0.001$

$$B_{dw} = 0.55$$

$$\bar{\Gamma} = \frac{T_c \cdot \bar{u}_c (\Omega_c^3 + \Omega_t^3) + T_t \cdot \bar{u}_t (\Omega_t^3 + \Omega_c^3)}{(u_{wc} + u_{wt})T} \dots\dots\dots 4.3-17$$

with T, T_c, T_t = period and half-periods of wave taking into account the effect of current
 Ω_c, Ω_t = amount of sediment entrained and settled during the half-period T_c and T_t ,
 respectively
 Ω_c', Ω_t' = amount of suspended sediment remaining from positive and negative half-cycle,
 respectively
 u_{wc}, u_{wt} = quadratic velocity (wave and current) over each half-period, where

$$u_{wj}^2 = \frac{2}{T_{wj}} \int_t^{t+T_{wj}} u^2(t) dt + 2 \cdot U_c^2 \sin^2 \delta \dots\dots\dots 4.3-18$$

where j can be c or t .

$$u(t) = U_c \cdot \cos \delta + u_w(t)$$

$u(t)$ = instantaneous wave orbital velocity
 δ = angle between wave direction and current direction

If $\omega_j \leq \omega_{cr}$ then $\Omega_j = \omega_j \cdot \frac{2wT_j}{d_{50}}$
 and $\Omega_j' = 0$

If $\omega_j > \omega_{cr}$ then $\Omega_j = \frac{2wT_j}{d_{50}} \dots\dots\dots 4.3-19$
 and $\Omega_j' = (w_j - 1) \frac{2wT_j}{d_{50}}$

with $\omega_j = \frac{u_{wj}^2}{2 \cdot (s-1) \cdot g \cdot w \cdot T_j} \dots\dots\dots 4.3-20$

where j can be c or t and ω_{cr} is a ripple parameter:

$$\begin{aligned}
 \omega_{cr} &= 0.03 && \text{if } \Psi_{cw(max)} \leq 0.2 \\
 &= 1 - 0.97 \left(1 - \left(\frac{\Psi_{cw(max)} - 0.2}{0.4} \right)^2 \right)^{0.5} && \text{if } 0.2 < \Psi_{cw(max)} < 0.6 \dots\dots\dots 4.3-21 \\
 &= 1 && \text{if } 0.6 < \Psi_{cw(max)}
 \end{aligned}$$

with $\Psi_{cw(max)}$ = maximum Shields parameter due to wave-current interaction

Camenen and Larroudé (2003) have compared several sediment transport formulas for the coastal environment, including those of Bijker, Bailard and Dibajnia and Watanabe. The data which they used came from several different sources, including data for currents only and wave-current interaction. They have shown that, as is the case for many other sediment transport formulas, these equations yield good results only for the limited range of data on which they were calibrated. However, over a large range of data, all the formulas give similar results, except for Bijker’s formula, which Camenen and Larroudé found was unsuitable for a large range of certain parameters.

In Figure 4.3-1 to Figure 4.3-3 the experimental data $q_{s,data}$ is plotted together with the calculated data from the three sediment transport models, $q_{s,num}$. The two dashed lines indicate the region where the estimated data is between 0.5 and 2 times the experimental data. The percentage of points with less than 50% and 20% error is also computed for “current only” and “wave-current” data (i.e. Cc50, Cc80, Cw50, Cw80, respectively).

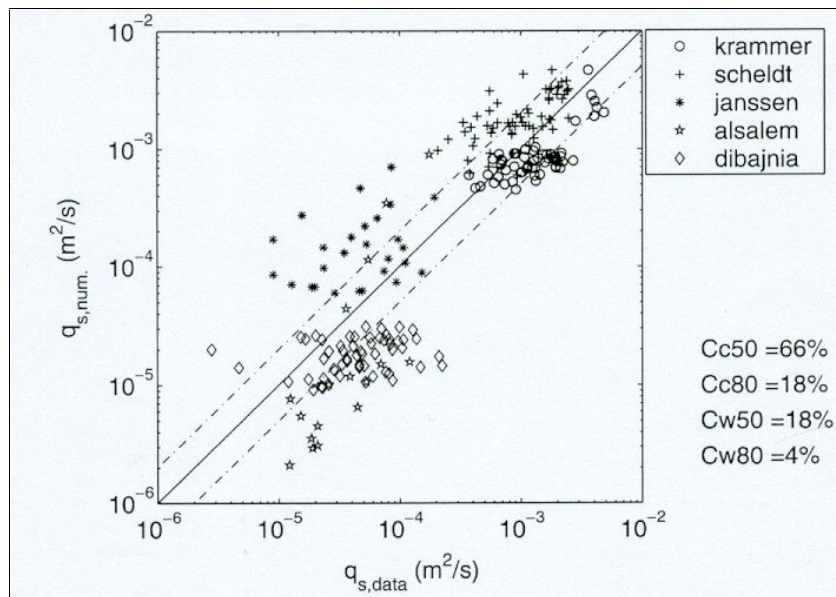


Figure 4.3-1 Comparison between the *Bijker* formula and experimental data (source of data listed at the top) (Camenen and Larroudé, 2003)

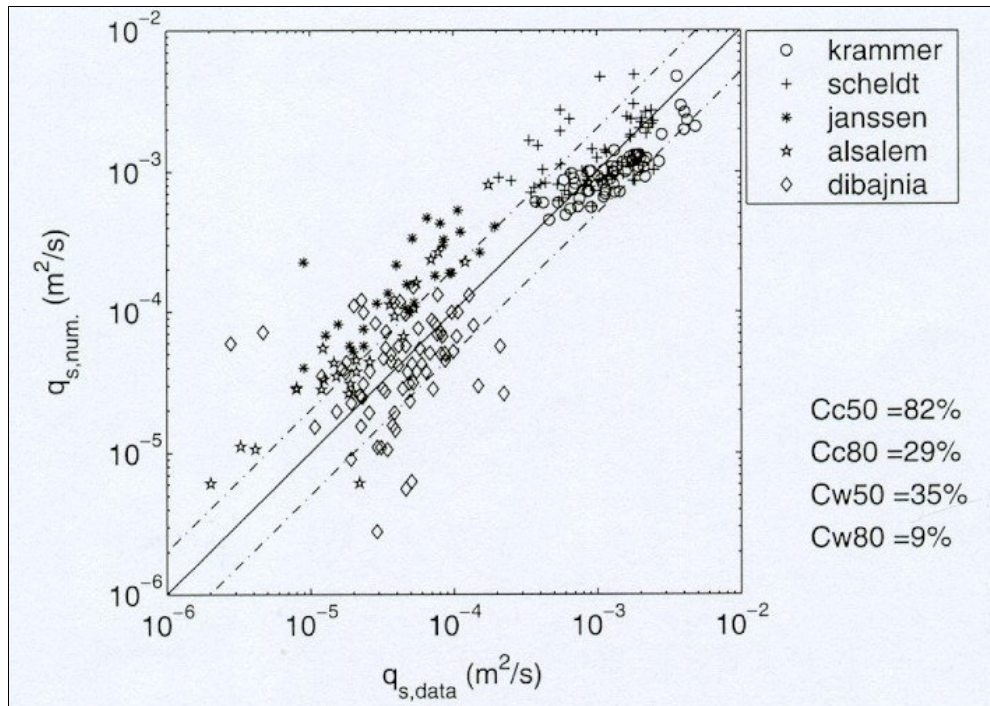


Figure 4.3-2 Comparison between the *Bailard* formula and experimental data (source of data listed at the top) (Camenen and Larroudé, 2003)

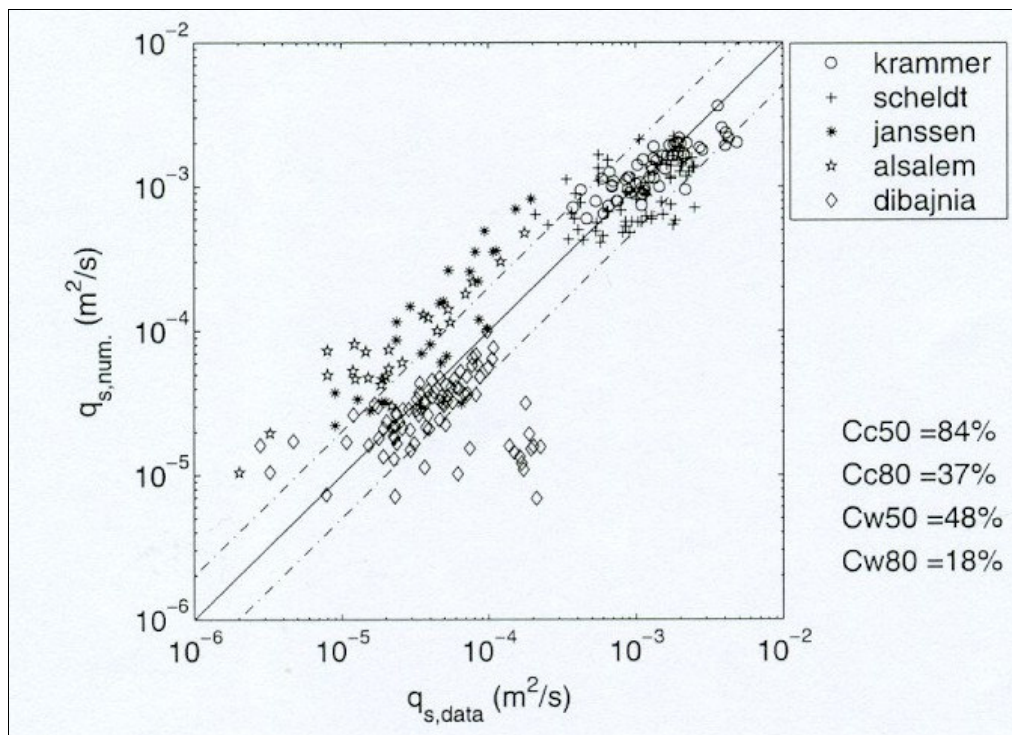


Figure 4.3-3 Comparison between the *Dibajnia and Watanabe* formula and experimental data (source of data listed at the top) (Camenen and Larroudé, 2003)

As can be seen from the above discussion, wave-current interaction considerably complicates the sediment transport predictions. The formulas for current-related sediment transport predictions are much easier to apply than those for wave-current interaction. That is why in many cases, the existing sediment transport equations have been modified to some minor degree (see, for example, Bayram, *et al.*, 2001) to incorporate the effect of waves and currents. However, wave action is generally thought to be much reduced inside an estuary and traditional current-related sediment transport equations are often applied. Then again, in a permanently open or recently opened estuary, wave action, especially in the mouth region, may actually be quite significant under certain conditions, which means that by relying on traditional current-related sediment transport equations, sediment transport in an estuary may not be fully described. For this reason, as well as the above-mentioned difficulties associated with applying the existing sediment transport equations for wave-current interaction, there seems to be a need for a different approach to describing the sediment transport under both waves and currents.

4.4 Sediment Transport by Currents and Waves –Stream and Wave Power

The concept of stream power has been used extensively to determine sediment transport by currents alone. The concept of wave power has been used to describe sediment transport in the coastal environment, specifically longshore sediment transport. However, the author could find no evidence that the sediment transport under the combined effect of waves and currents has been described in terms of wave and stream power. Both stream and wave power concepts have yielded very good results over a large range of conditions, and it was therefore thought that by combining the two, it would be possible to describe the sediment transport under both waves and currents.

4.4.1 Stream Power

The concept of stream power has been used in various forms to determine the sediment transport, such as Bagnold (1966), Rooseboom (1992) and Yang (1972).

Bagnold used the stream power per unit bed area to relate the rate of energy dissipation used in transporting sediment particles to the sediment transport capacity, with two separate components for bedload and suspended load.

Rooseboom's theory (1992) is based on the principle of conservation of power, i.e. that the average amount of power applied must equal the average amount of power which becomes available. The sediment transporting capacity per unit width can thus be expressed in terms of flow parameters:

$$q_s = \int_{y_0}^D C v \, dy \dots\dots\dots 4.4-1$$

with $C \propto \left(\tau \frac{dv}{dy} \right)^z$

$\tau \frac{dv}{dy}$ = applied power

τ = bed shear stress

$\frac{dv}{dy}$ = velocity gradient

C = sediment concentration

v = velocity

D = flow depth

y_0 = distance above the bed at which velocity is mathematically = 0

$z = \frac{w}{\kappa \sqrt{gDS}}$ = suspension theory coefficient

w = particle settling velocity

κ = Von Kármán coefficient

Equation 4.4-1 after integration leads to an equation of the form:

$$\log\left(\frac{q_s}{q}\right) = \alpha \log(\bar{v}S) + \beta \dots\dots\dots 4.4-2$$

with α, β = coefficients

\bar{v} = average velocity

Yang (1972) defined the unit stream power as the rate of potential energy expenditure per unit weight of water:

$$\frac{dY}{dt} = \frac{dX}{dt} \frac{dY}{DX} = vS \dots\dots\dots 4.4-3$$

where Y = potential energy per unit weight above a certain datum

X = longitudinal distance

t = time

vS = unit stream power

Yang argued that since the sediment transport is related to the strength of the turbulent flow conditions, the rate of total sediment transport rate or concentration should be directly related to the unit stream power. The basic form of Yang's unit stream power equation is:

$$\log(C_t) = \alpha + \beta \log(vS - vS_{cr}) \dots\dots\dots 4.4-4$$

where C_t = total sediment concentration
 α, β = coefficients
 vS_{cr} = critical unit stream power

Yang found that both α and β are dependent on the water depth and that β is also dependent on the particle size. In 1973 Yang sought to improve on Equation 4.4-4 through dimensional analysis. He found the following:

$$C_t = \Phi \left(\frac{vS}{w} - \frac{v_{cr}S}{w}, \frac{U_*}{w}, \frac{wd}{\nu} \right) \dots\dots\dots 4.4-5$$

where U_* = shear velocity = \sqrt{gDS}
 ν = kinematic viscosity
 d = particle size

The basic form of Equation 4.4-5 is very similar to Equation 4.4-4:

$$\log(C_t) = \alpha + \beta \log \left(\frac{vS}{w} - \frac{v_{cr}S}{w} \right) \dots\dots\dots 4.4-6$$

where α, β = coefficients
 $\frac{vS}{w}, \frac{v_{cr}S}{w}$ = dimensionless unit stream power and critical unit stream power, respectively

When the concentrations are more than 100 ppm the dimensionless critical unit stream power is relatively small in relation to the value of the unit stream power and the $\left(\frac{v_{cr}S}{w} \right)$ term can be excluded (Yang and Molinas, 1982).

$$\log(C_t) = \alpha + \beta \log\left(\frac{vS}{w}\right) \dots\dots\dots 4.4-7$$

As can be seen equations 4.4-2 and 4.4-7 are very similar, and both have been successfully used to describe the sediment transport in rivers under currents only conditions. Therefore the unit stream power seems to be a good indicator for the total sediment transporting capacity in a stream.

4.4.2 Wave Power

A significant amount of wave energy is dissipated in the nearshore region and on beaches. Wave energy forms beaches; sorts bottom sediments on the shore face; transports bottom materials onshore, offshore and alongshore; and exerts forces upon coastal structures. Wave power has been used to describe sediment transport in the coastal environment, specifically longshore sediment transport (CEM, 2004). Deepwater wave energy was first related to the rate of littoral sand transport by a Danish engineer in the late 1930s. Several other formulas were developed and further refined in time, with the most well-known formula, called the CERC formula, being incorporated into the 1966 coastal design manual by the US Army Corps of Engineers. Even Bagnold, who linked stream power to sediment transport in rivers as mentioned in the previous section, carried out some research on longshore sediment transport rates. Before the concept of wave power is discussed in more detail, some basic definitions are given first.

4.4.2.1 Basic Definitions

The simplest wave theory is the first-order, small-amplitude or Airy theory, which is applicable to many engineering problems and is usually called linear theory. The following definitions and derivations are taken from the Coastal Engineering Manual (USACE, 2002) and Dean and Dalrymple (1992).

A progressive wave may be represented by the variables x (spatial) and t (temporal) or their phase, defined as:

$$\theta = kx - \omega t \quad (0 < \theta < 2\pi) \dots\dots\dots 4.4-8$$

with $k = \text{wave number} = 2\pi/L$
 $\omega = \text{angular frequency} = 2\pi/T$

Figure 4.4-1 shows the parameters that define a simple, progressive wave as it passes a fixed point in the ocean. A simple, periodic wave over a horizontal bottom may be completely characterised by the wave height H , wavelength L and water depth h . The height from the trough to the still water level (SWL) and the height from the crest to SWL are both equal to the wave amplitude a . The wave period T is the time interval between the passage of two successive crests or troughs at a given point. The wave celerity C is the speed at which a wave propagates:

$$C = \frac{L}{T} \dots\dots\dots 4.4-9$$

where $L = \frac{gT^2}{2\pi} \tanh(kh) \dots\dots\dots 4.4-10$

Waves are classified as in Table 4.4-1, based on the relative depth criterion h/L . In deep water (parameters identified with the subscript 0 , i.e. L_0 or C_0), wave characteristics are virtually independent of the water depth, whereas in shallow water the wave celerity is dependent only on the water depth.

Table 4.4-1 Classification of water waves

Classification	h/L	$\tanh(kh)$	C	C_g
Deep water	$1/2$ to ∞	≈ 1	$\frac{gT}{2\pi}$	$\frac{1}{2} \frac{L_0}{T}^*$
Transitional	$1/20$ to $1/2$	$\tanh(kh)$	$\frac{gT}{2\pi} \tanh\left(\frac{2\pi h}{L}\right)$	$\frac{1}{2} \frac{L}{T} \left[1 + \frac{4\pi h / L}{\sinh(4\pi h / L)} \right]$
Shallow water	0 to $1/20$	$\approx kh$	\sqrt{gh}	\sqrt{gh}

*: $L_0 = \text{deep water wave length} = \frac{gT^2}{2\pi}$

The symbol η is used to describe the displacement of the water surface relative to SWL as a function of x and t . Assuming a sinusoidal wave profile:

$$\eta = a \cos(kx - \omega t) = \frac{H}{2} \cos\left(\frac{2\pi x}{L} - \frac{2\pi t}{T}\right) = a \cos \theta \dots\dots\dots 4.4-11$$

The so-called group velocity is another important parameter, which is the speed at which wave energy travels. This group velocity is generally not equal to the phase velocity of individual waves (USACE, 2002). For waves propagating in deep or transitional water, the group velocity will be less than the phase velocity.

The group velocity can be derived by looking at the propagation of a group of waves. If there are two sinusoidal wave trains (Figure 4.4-2) moving in the same direction at slightly different wavelengths (L_1, L_2) and periods (T_1, T_2) they are superimposed as:

$$\eta = \eta_1 + \eta_2 = \frac{H}{2} \cos\left(\frac{2\pi x}{L_1} - \frac{2\pi t}{T_1}\right) + \frac{H}{2} \cos\left(\frac{2\pi x}{L_2} - \frac{2\pi t}{T_2}\right) = \frac{H}{2} \cos(k_1 x - \omega_1 t) \cos(k_2 x - \omega_2 t) \dots \dots \dots 4.4-12$$

where:

$$k_1 = k - \frac{\Delta k}{2}; \quad \omega_1 = \omega - \frac{\Delta \omega}{2}$$

$$k_2 = k + \frac{\Delta k}{2}; \quad \omega_2 = \omega + \frac{\Delta \omega}{2}$$

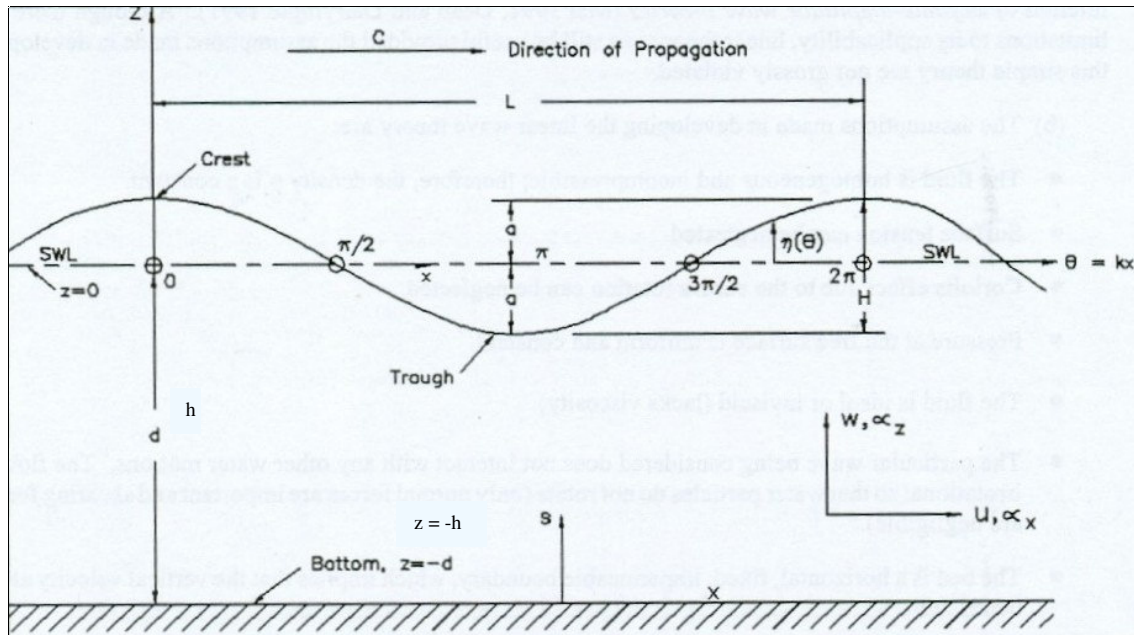


Figure 4.4-1 Progressive wave - definition of terms (USACE, 2002)

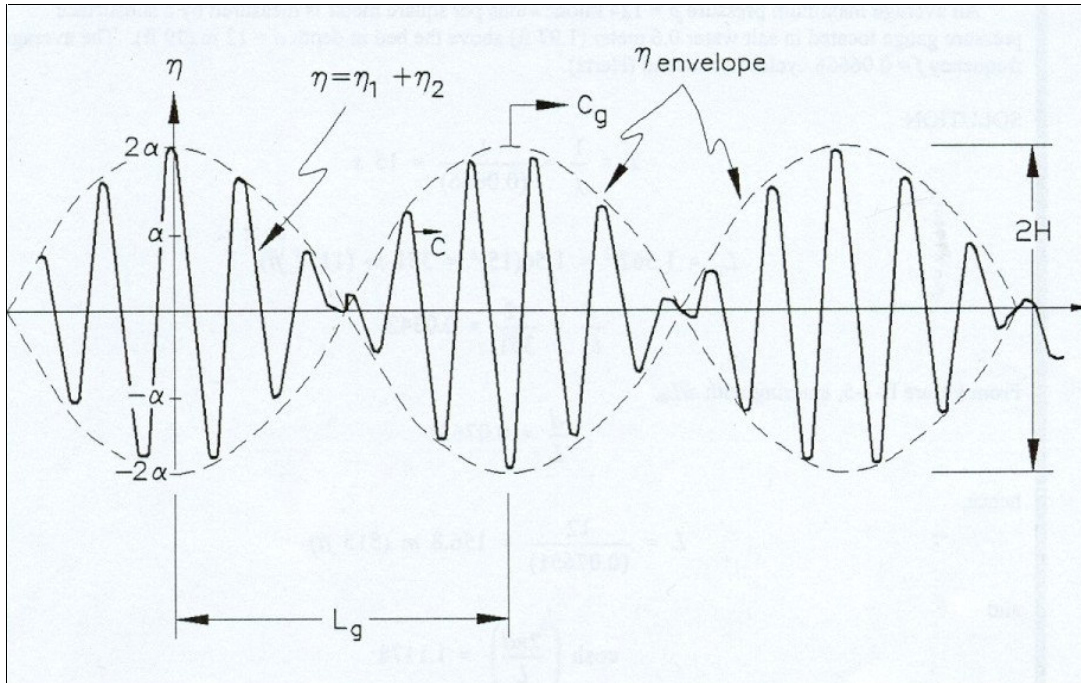


Figure 4.4-2 Characteristics of wave groups (USACE, 2002)

For simplicity the wave heights of the two components have been assumed equal. Since the wavelengths have been assumed slightly different, for some values of x at a given time the two components will be in phase and the wave height observed to be $2H$. At other times the two components will be completely out of phase and the resultant wave height will be zero. Using trigonometric identities equation 4.4-12 can be re-written as:

$$\eta = H \cos\left(\frac{1}{2}((k_1 + k_2)x - (\omega_1 + \omega_2)t)\right) \cos\left(\frac{1}{2}((k_1 - k_2)x - (\omega_1 - \omega_2)t)\right)$$

$$\eta = H \cos(kx - \omega t) \cos\left(\frac{1}{2} \Delta k \left(x - \frac{\Delta \omega}{\Delta k} t\right)\right) \dots\dots\dots 4.4-13$$

This shows that while the wave forms travel with a velocity $C=T/L$, the whole group propagates at a speed of $\Delta\omega / \Delta k$, which is called the group velocity C_g .

The wave groups as they become large (i.e. L_1 approaches L_2 and therefore $\Delta k \rightarrow 0$) have a limiting group velocity of $C_g = d\omega / dk$, which can be evaluated as follows:

$$\omega^2 = gk \tanh(kh) \dots\dots\dots 4.4-14$$

$$2\omega \frac{d\omega}{dk} = g \tanh(kh) + gkh \operatorname{sech}^2(kh) \dots\dots\dots 4.4-15$$

$$\frac{d\omega}{dk} = \frac{(g \tanh(kh) + gkh \operatorname{sech}^2(kh))\omega}{2gk \tanh(kh)} = \frac{1}{2} \frac{\omega}{k} \left(1 + \frac{2kh}{\sinh(2kh)} \right) = nC \dots\dots\dots 4.4-16$$

where $n = \frac{1}{2} \left(1 + \frac{2kh}{\sinh(2kh)} \right) \dots\dots\dots 4.4-17$

and therefore $C_g = nC \dots\dots\dots 4.4-18$

The group velocities for deep and shallow water are listed in Table 4.4-1.

4.4.2.2 Wave Energy

The total energy of a wave system consists of both kinetic and potential energy. The kinetic energy is due to water particle velocities associated with wave motion. The kinetic energy of a small volume of fluid with a mass dm is:

$$d(\bar{E}_k) = dm \frac{v_h^2 + v_v^2}{2} = \rho dx dz \frac{v_h^2 + v_v^2}{2} \dots\dots\dots 4.4-19$$

The average kinetic energy per unit surface area \bar{E}_k is obtained by integrating equation 4.4-19:

$$\bar{E}_k = \frac{1}{L} \int_x^{x+L} \int_{-h}^{\eta} \rho \frac{v_h^2 + v_v^2}{2} dz dx \dots\dots\dots 4.4-20$$

with $v_h = \frac{H}{2} \frac{gT_w}{L} \frac{\cosh[2\pi(z+h)/L]}{\cosh[2\pi h/L]} \cos \theta =$ horizontal component of the local fluid velocity

$$v_v = \frac{H}{2} \frac{gT_w}{L} \frac{\sinh[2\pi(z+h)/L]}{\cosh[2\pi h/L]} \sin \theta =$$
 vertical component of the local fluid velocity

Equation 4.4-20 yields:

$$\bar{E}_k = \frac{1}{16} \rho g H^2 \dots\dots\dots 4.4-21$$

Potential energy results from the displacement of a mass from equilibrium against a gravitational field. The potential energy of a small column of fluid \bar{E}_p , as shown in Figure 4.4-3, with a mass dm relative to the bottom is:

$$d(\bar{E}_p) = dm \, g z \dots\dots\dots 4.4-22$$

with $z = \text{height of the centre of gravity of the mass} = \frac{h + \eta}{2}$

$$dm = \rho(h + \eta) dx$$

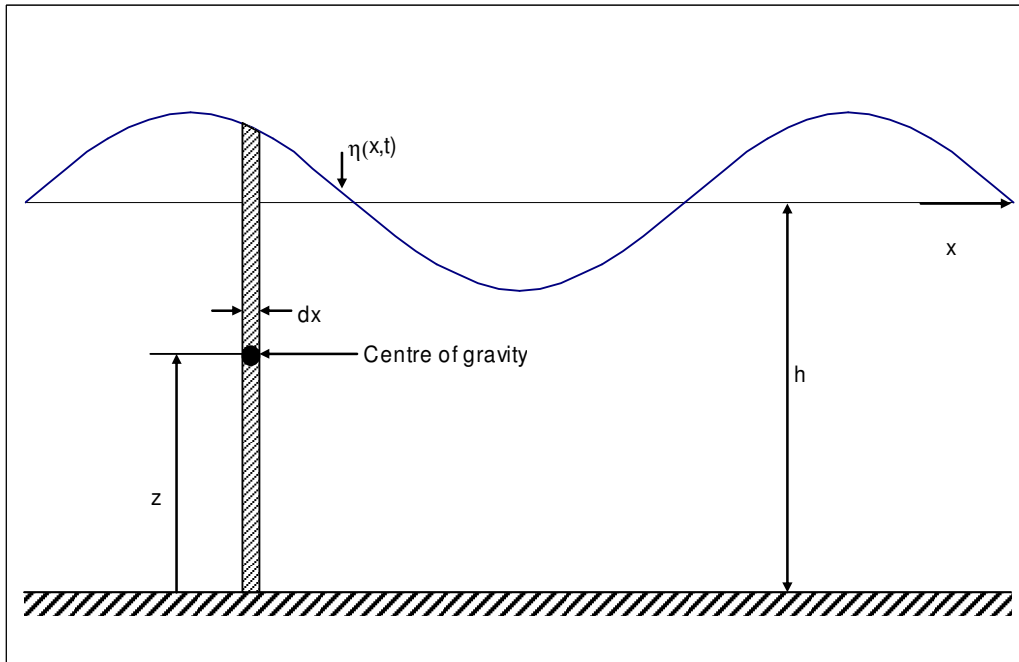


**Figure 4.4-3 Definition sketch for the determination of potential energy
(after Dean and Dalrymple, 1992)**

Integration of equation 4.4-22 over one wavelength gives the total potential energy of the water column averaged over one wave length:

$$(\bar{E}_p)_{total} = \frac{1}{L} \int d(\bar{E}_p) dx = \frac{1}{L} \int_x^{x+L} \rho g \frac{(\eta + h)^2}{2} dx \dots\dots\dots 4.4-23$$

Equation 4.4-23 yields:

$$(\bar{E}_p)_{total} = \frac{1}{16} \rho g H^2 + \rho g \frac{h^2}{2} \dots\dots\dots 4.4-24$$

The potential energy due to the waves alone is the difference between the total potential energy and that without waves present:

$$(\bar{E}_p)_{waves} = (\bar{E}_p)_{total} - (\bar{E}_p)_{without\ waves} = \frac{1}{16} \rho g H^2 \dots\dots\dots 4.4-25$$

The total wave energy E in per unit surface area is the sum of the kinetic and potential energy which is given by:

$$E = \bar{E}_k + \bar{E}_p = \frac{1}{16} \rho g H^2 + \frac{1}{16} \rho g H^2 = \frac{1}{8} \rho g H^2 \dots\dots\dots 4.4-26$$

The total wave energy per unit width of wave front is therefore:

$$E_T = \frac{1}{8} \rho g H^2 L \dots\dots\dots 4.4-27$$

4.4.2.3 Wave Power

Water waves transmit energy as they travel to and break on the shore. Assuming that linear theory holds, the rate at which energy is transmitted in the direction of wave propagation across a vertical plane perpendicular to the direction of wave advance is (USACE, 2002):

$$P = \frac{1}{T_w} \int_t^{t+T_w} \int_{-h}^{\eta} p u \, dz \, dt \dots\dots\dots 4.4-28$$

where p = pressure under wave
 u = horizontal velocity under wave

Equation 4.4-28, upon integration, yields:

$$P = \left(\frac{1}{8} \rho g H^2 \right) \frac{L}{T} \left[\frac{1}{2} \left(1 + \frac{4\pi h/L}{\sinh(4\pi h/L)} \right) \right] = EnC \dots\dots\dots 4.4-29$$

where nC , the group velocity, is the speed at which the energy is transmitted. Since $L/T = C$:

$$P = \left(\frac{1}{8} \rho g H^2 \right) \frac{gT}{2\pi} \tanh \left(\frac{2\pi h}{L} \right) \left[\frac{1}{2} \left(1 + \frac{4\pi h/L}{\sinh(4\pi h/L)} \right) \right] \dots\dots\dots 4.4-30$$

The total power [W/m] per unit width of wave front is therefore:

$$P = \frac{\rho g^2 H^2 T}{32\pi} \tanh \left(\frac{2\pi h}{L} \right) \left(1 + \frac{4\pi h/L}{\sinh(4\pi h/L)} \right) \dots\dots\dots 4.4-31$$

For deep water conditions (the subscript 0 denotes deep water conditions) $C_0 = gT/2\pi$ and $n_0 = 1/2$

as $\frac{4\pi h/L}{\sinh(4\pi h/L)} \approx 0$ and equation 4.4-31 becomes:

$$P_0 = \frac{\rho g^2 H^2 T L}{32\pi} = \frac{\rho g^2 H^2 T^3}{64\pi^2} \dots\dots\dots 4.4-32$$

which presents the total wave power in deep water in [W].

For shallow water conditions $C = L/T = \sqrt{gh}$ and $n \approx 1$ as $\sinh(4\pi h/L) \approx 4\pi h/L$ and equation 4.4-31 becomes:

$$P = \frac{\rho g H^2 L^2}{8T} = \frac{\rho g H^2 \sqrt{gh} L}{8} \dots\dots\dots 4.4-33$$

which presents the total wave power in shallow water in [W].

The unit wave power [W/m³] in shallow water then becomes:

$$P_w = \frac{\rho g H^2 \sqrt{gh} \cdot L}{8 \cdot (B_w h L)} \dots\dots\dots 4.4-34$$

where B_w is the width of the wave front.

For transitional conditions equation 4.4-31 should be used.

4.5 Laboratory Experiments

The objective of the experiments was to obtain hydraulic and sediment transport data under non-breaking waves and currents to determine the effect of the wave-current interaction on the sediment transport characteristics and to supplement data obtained from other sources. The data obtained were used to calibrate a new sediment transport equation for wave-current conditions.

4.5.1 Experimental Setup

The experiments were carried out in the Hydraulics Laboratory of the University of Stellenbosch in a re-circulating flume (0.25 m wide, 0.4 m deep and 7.5 m long) and return pipe (\varnothing 75 mm) system as shown in Figure 4.5-1 and Figure 4.5-2. The flow rate could be varied by adjusting the variable speed pump. A flow deflector was placed over the inflow pipe to ensure that the incoming current would have as little impact on the generated waves as possible. Small-scale dolosse were placed at the opposite end of the flume to the wave generator to reduce wave reflection. The sampling point for suspended sediments was located on the return pipe to ensure that sediment and water were completely mixed. The setup could easily be changed so that the flow direction would be opposite to the direction in which the waves were travelling.

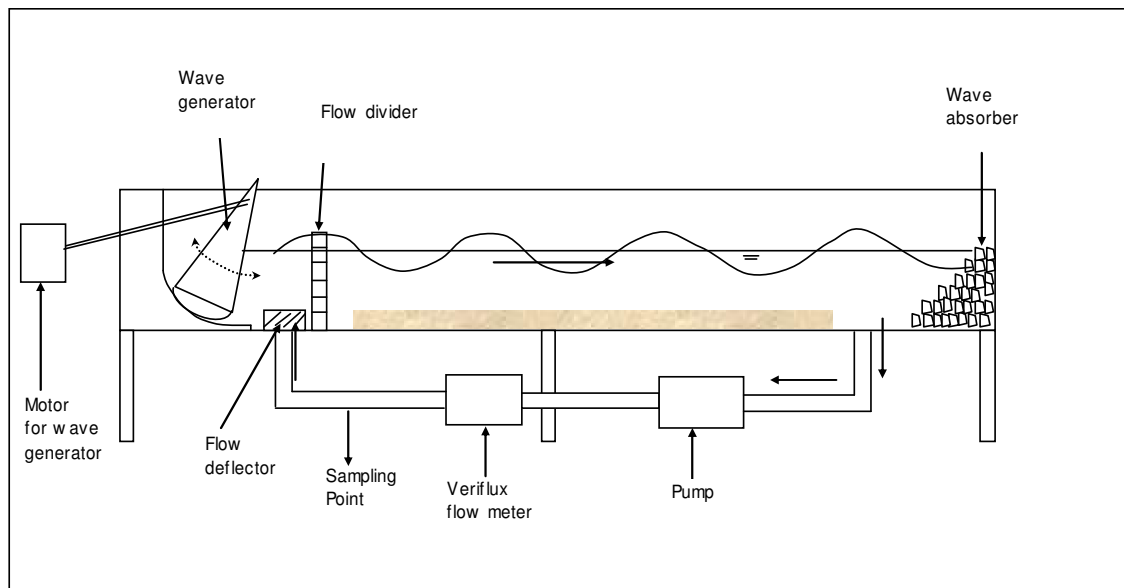


Figure 4.5-1 Experimental layout

Velocities were determined with the use of an electromagnetic VERIFLUX VAC 0.075 kW flow meter installed on the return pipe. The readings from the electromagnetic flow meter were converted to flow velocities as follows:

$$v_p = \frac{a \cdot b}{10} \dots\dots\dots 4.5-1$$

where a, b = readings from the converter

v_p = velocity in return pipe

Water level variations were measured at intervals along the length of the test section to determine wave characteristics such as wave height, period and length. Water depths and bed levels were also measured at regular intervals.

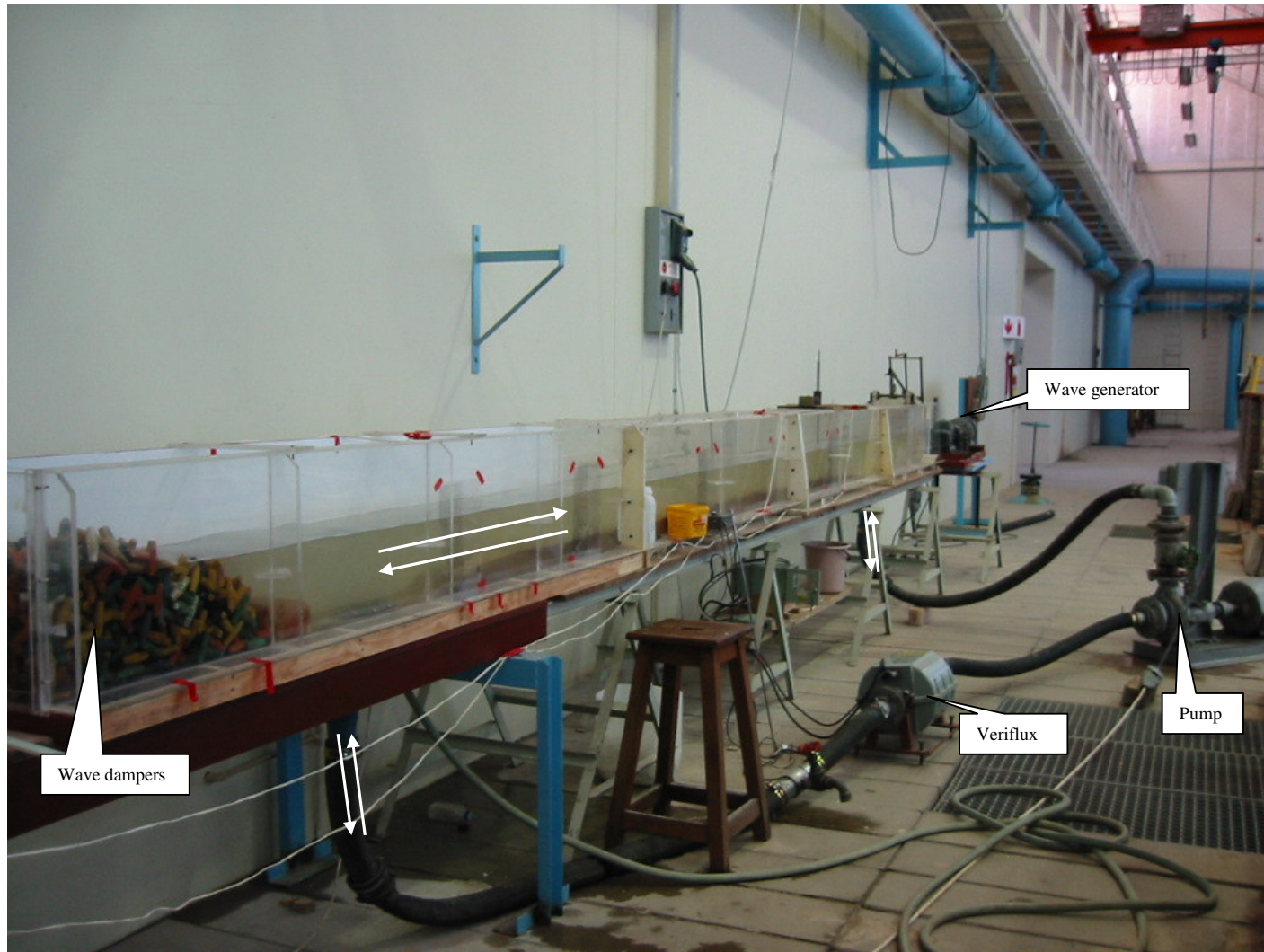


Figure 4.5-2 Laboratory setup

A 100 mm thick layer of sand was placed along the test section of the flume. The sediment used, was fine sand with a median diameter (d_{50}) of 0.15 mm (see Figure 4.5-3 for a grading curve).

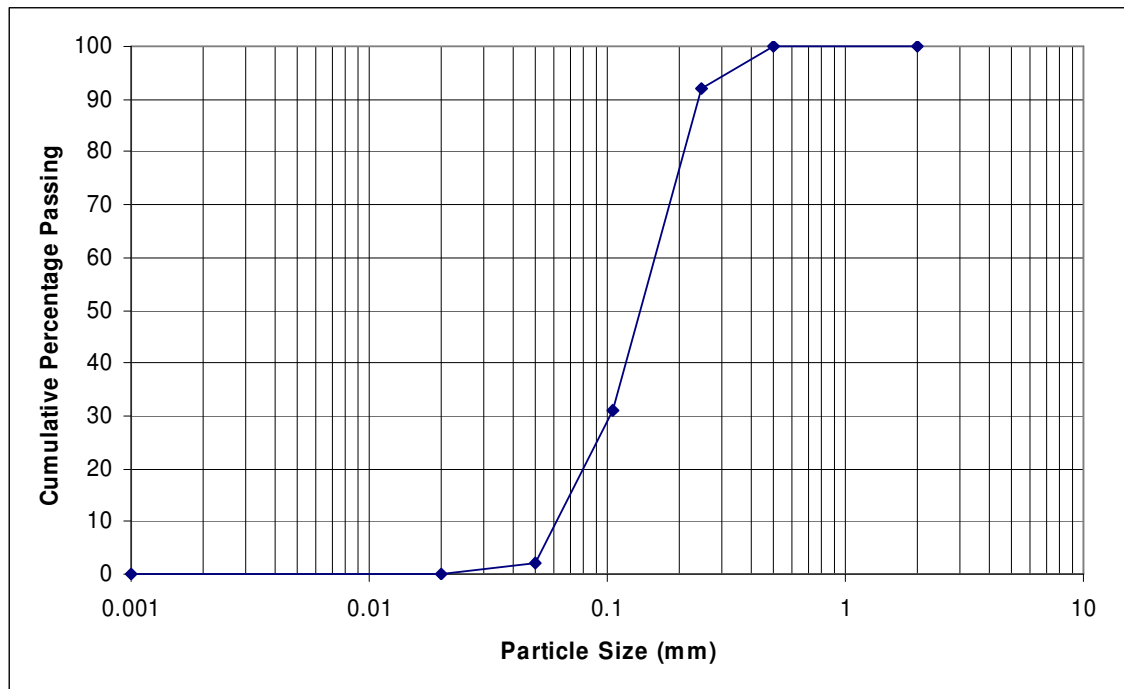


Figure 4.5-3 Grading curve of sediment used in experiments

4.5.2 Procedure

Prior to each test a 100 mm layer of sand was placed along the test section of the flume. The flume was then filled with water to a certain depth (approximately 0.15 m), after which the pump was turned on and measurements were taken to determine all applicable parameters for the current only conditions. After that the wave generator was switched on and once the flow and waves had become stable, the experiment was run for up to one hour until the bedforms had stabilised and some form of equilibrium had been obtained, with measurements taken at the end of each run. Only non-breaking waves were generated.

The following data were measured during all test runs:

- Average depth of flow h
- Current only flow velocity v_c
- Wave height H
- Wave period T
- Suspended-sediment concentrations C

The water surface and bed level were measured at 1 m intervals along a 5 m test section, which was chosen to exclude all entrance and exit influences. The flow depth was determined from the difference between the water surface and bed levels, and the discharge was obtained from the velocity meter, which had been installed in the pipe:

$$Q = A_p v_p \dots\dots\dots 4.5-2$$

where Q = discharge

v_p = velocity in return pipe

A_p = cross-sectional area of pipe

Suspended-sediment samples were taken at the end of each run.

The wave characteristics were determined from continuous data collected by three electromagnetic probes, placed at 1 m intervals along the test section, measuring the water level variations at 1 second intervals throughout each test run. From the measured data the following variables were computed:

- Average energy slope S_f :

The energy slope was determined from the energy equation:

$$z_1 + h_1 + \frac{v_1^2}{2g} - z_2 - h_2 - \frac{v_2^2}{2g} = h_f \dots\dots\dots 4.5-3$$

$$S_f = \frac{h_f}{L} \dots\dots\dots 4.5-4$$

where z_1, z_2 = elevation above arbitrary datum

h_1, h_2 = flow depths

v_1, v_2 = mean flow velocities

h_f = friction losses between two sections

L = distance between two sections

- Particle settling velocity w (For $0.1 < d_{50} < 1$ mm (Zanke, 1977)):

$$w = 10 \frac{v}{d_{50}} \left(\sqrt{1 + \frac{0.01(s-1)gd_{50}^3}{v^2}} - 1 \right) \dots\dots\dots 4.5-5$$

- Wave power P_w , based on equation 4.4-33, since the experiments were carried out in shallow water [W/m^3]:

$$P_w = \frac{\rho g H^2 \sqrt{gh} \cdot L}{8 \cdot (BhL)} \dots\dots\dots 4.5-6$$

where B is the flume width.

- Stream power P_s [W/m^3]:

$$P_s = \rho g v_c S_f \dots\dots\dots 4.5-7$$

4.5.3 Discussion of Results

A summary of the experiments carried out is given in Table 4.5-1. Altogether 35 different combinations of currents and waves were tested. The experiments were started at a particular current speed and between one and three different wave patterns were run for each current speed. The test series were started with a very low current speed, which was increased by a small margin after different wave patterns were tested. Out of the 35 tests, eight were performed with the current direction opposite to the wave direction. Further results are listed in Appendix A. It should be pointed out that it was sometimes difficult to determine the wave heights and energy slope precisely because of water surface fluctuations. These errors can have a significant effect on the results because of the small scale of the experimental setup.

Table 4.5-1 Summary of experiments

Test Series	Test No	Current velocity [m/s]	Flow depth [m]	Wave height [m]	Wave period [s]	Stream power [W/m ³]	Wave power [W/m ³]	q _s [10 ⁶ m ² /s]
1	1A-1	0.13	0.11	0.06	3.1	0.004	142.9	0.83
2	1B-1	0.13	0.13	0.04	3.4	0.107	72.5	1.21
3	1C-1	0.17	0.11	0.05	4.3	0.360	101.6	1.85
4	2A-1	0.12	0.15	0.04	3.1	0.039	66.2	0.94
	2A-2	0.12	0.15	0.07	2.9	0.039	178.5	0.94
	2A-3	0.12	0.15	0.08	3.1	0.039	194.9	1.98
5	3A-1	0.17	0.15	0.07	2.7	0.051	178.7	2.18
	3A-2	0.18	0.15	0.06	2.6	0.078	128.7	2.16
	3A-3	0.18	0.15	0.07	2.4	0.105	220.9	2.53
6	4A-1	0.18	0.15	0.05	2.7	0.020	83.7	1.23
	4A-2	0.18	0.15	0.05	2.2	0.020	115.4	1.44
7	5A-1	0.23	0.15	0.05	2.2	0.115	98.5	1.62
	5B-1	0.23	0.15	0.07	2.3	0.105	216.8	2.35
	5B-2	0.25	0.14	0.07	2.5	0.113	206.5	2.28
	5B-3	0.27	0.13	0.06	3.0	0.120	138.0	2.89
8	6A-1	0.23	0.15	0.05	2.0	0.353	94.6	2.55
	6A-2	0.24	0.15	0.06	2.0	0.303	120.3	3.08
	6A-3	0.24	0.15	0.05	2.5	0.250	96.5	3.83
9	7A-1	0.28	0.15	0.06	2.5	0.417	132.3	3.56
	7A-2	0.29	0.15	0.07	2.5	0.357	165.4	6.35
	7A-3	0.29	0.15	0.06	2.8	0.295	163.6	7.12
10	8A-1	0.38	0.15	0.06	2.7	0.232	149.3	12.59
	8A-2	0.31	0.15	0.06	2.5	0.325	147.4	4.84
	8A-3	0.31	0.15	0.06	2.3	0.415	162.3	7.18
11	9A-1	0.32	0.16	0.06	2.3	0.449	140.1	6.49
	9A-2	0.33	0.15	0.06	3.0	0.391	128.3	10.53
	9A-3	0.34	0.15	0.07	2.4	0.329	213.7	6.35
12	10B-1*	0.15	0.16	0.09	2.4	0.005	308.9	0.83
	10B-2*	0.15	0.16	0.08	2.7	0.114	261.5	1.01
13	11B-1*	0.19	0.15	0.07	2.8	0.097	176.7	2.32
	11B-2*	0.19	0.15	0.09	2.7	0.125	291.1	4.67
14	12A-1*	0.25	0.15	0.07	2.7	0.055	172.8	10.90
	12A-2*	0.26	0.14	0.08	2.7	0.307	229.8	13.48
15	13A-1*	0.31	0.14	0.08	3.0	0.097	242.8	8.22
	13A-2*	0.30	0.15	0.06	3.0	0.213	138.5	3.88

*: Opposing current

The most apparent observation from the experiments was that the sediment transport rate increased dramatically as soon as waves were superimposed on the current. The blue line in Figure 4.5-4 connects those test runs that were carried out without waves. The red squares represent the test runs with both waves and currents. It can be seen that for a certain series of tests with more or less the same current velocity, higher sediment transport rates were obtained with different wave patterns. The wave action lifts sediment particles from the bed, which can then be transported by the current. Without any

current the sediment particles were returned to where they were lifted from the bed by the orbital motion of the waves.

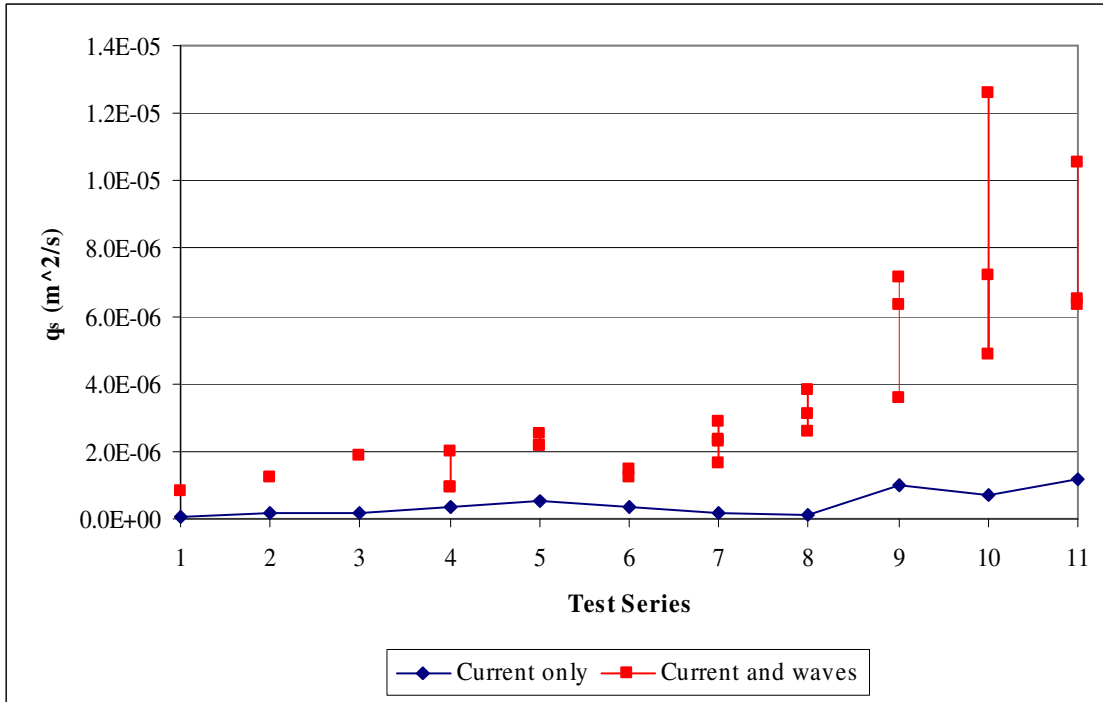


Figure 4.5-4 Measured sediment loads during experiments with or without waves

Another interesting observation was that with greater wave heights the sediment transport rates would increase (Figure 4.5-5). This is to be expected since most other parameters such as fluid velocity and wave power, are directly proportional to the wave height. The same trend could be observed with increasing current velocities (Figure 4.5-6). Since wave power is mainly dependent on wave height, and stream power on flow velocity, it follows that with both increasing stream and wave power the sediment transport rates increase as well. This trend can be seen in Figure 4.5-7 and Figure 4.5-8.

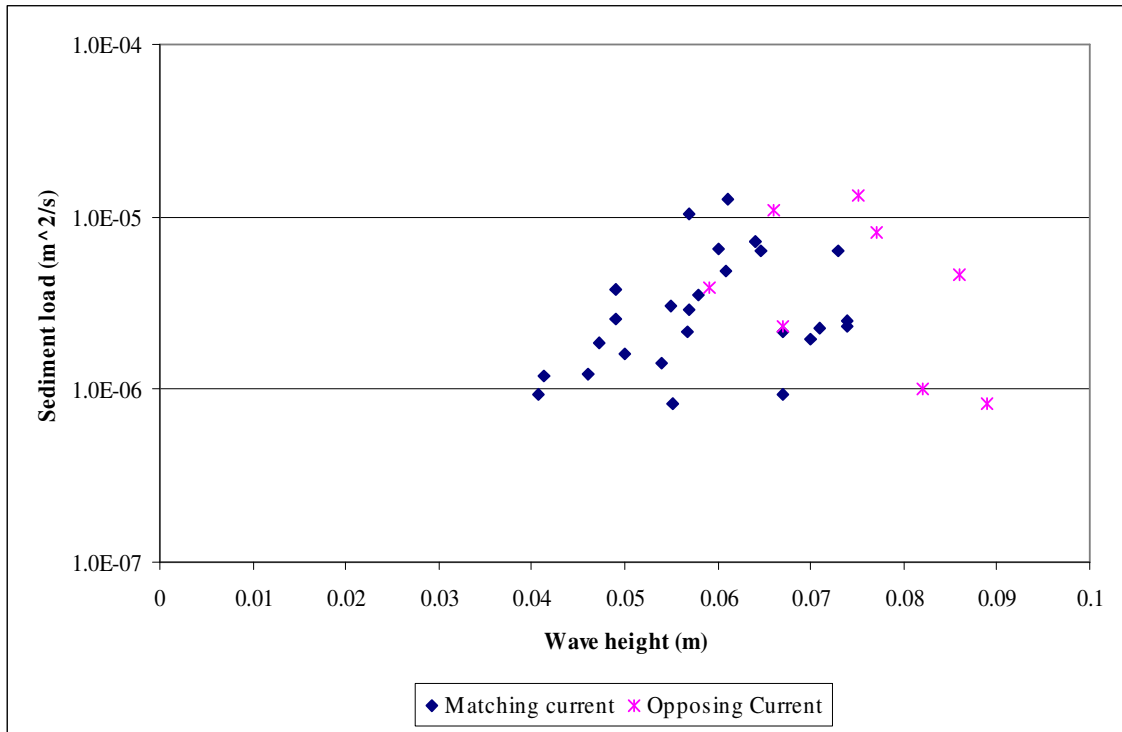


Figure 4.5-5 Relationship between wave height and sediment load

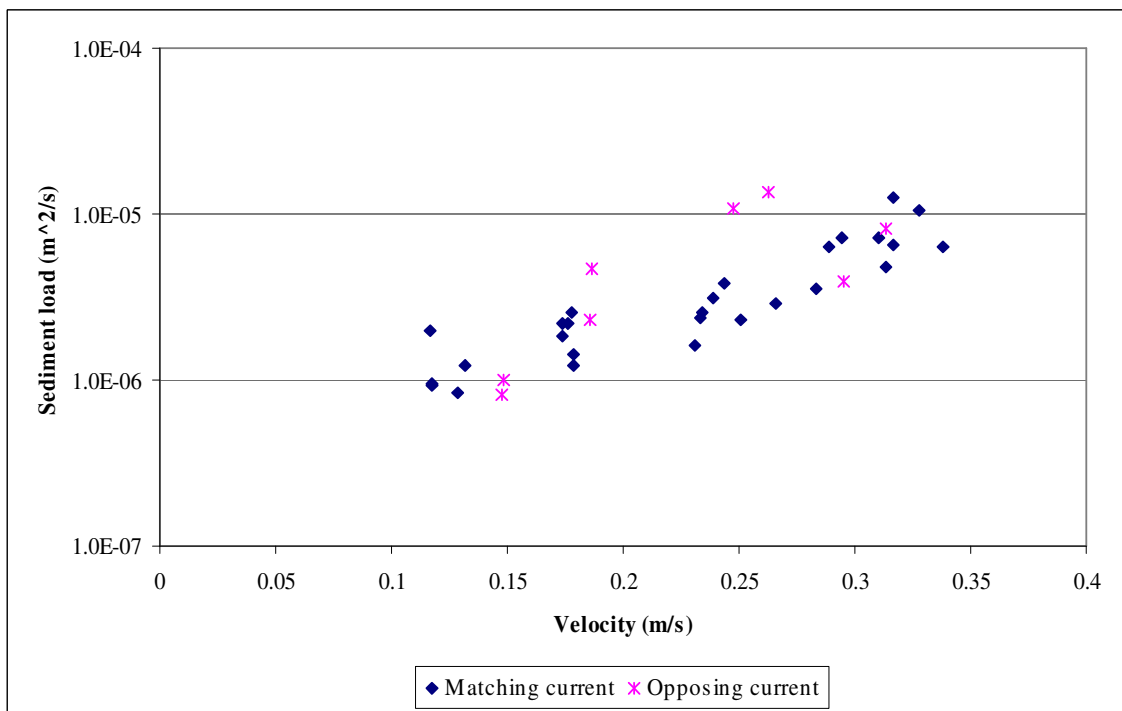


Figure 4.5-6 Relationship between current velocity and sediment load

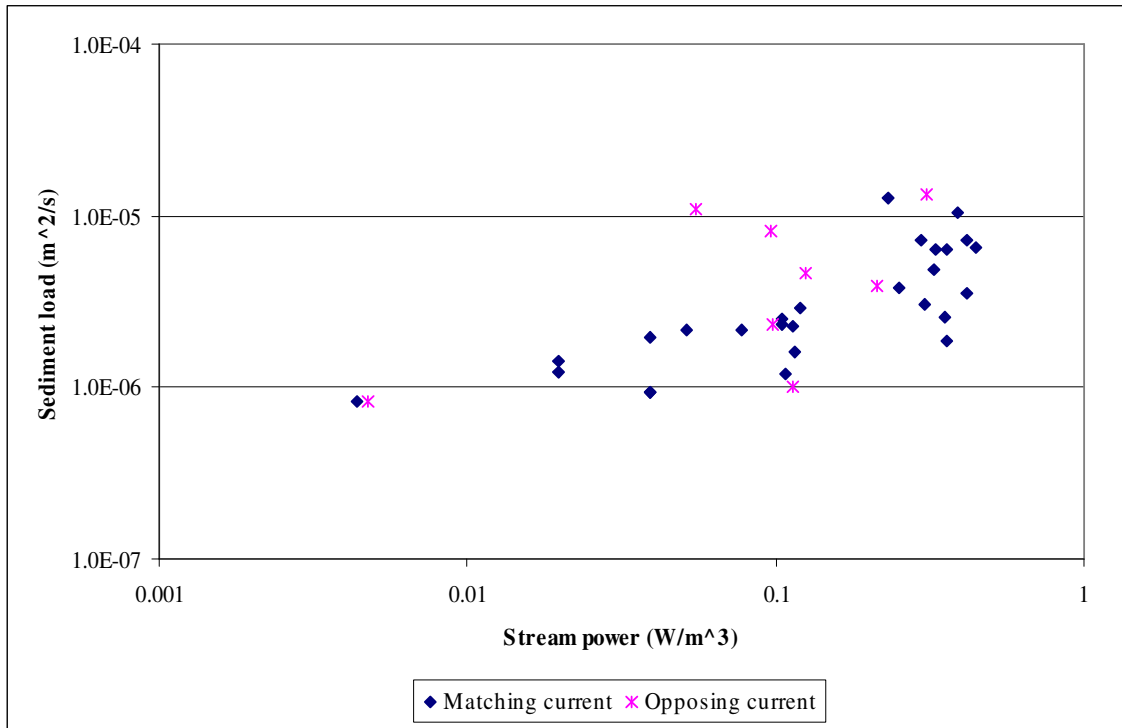


Figure 4.5-7 Relationship between stream power and sediment load

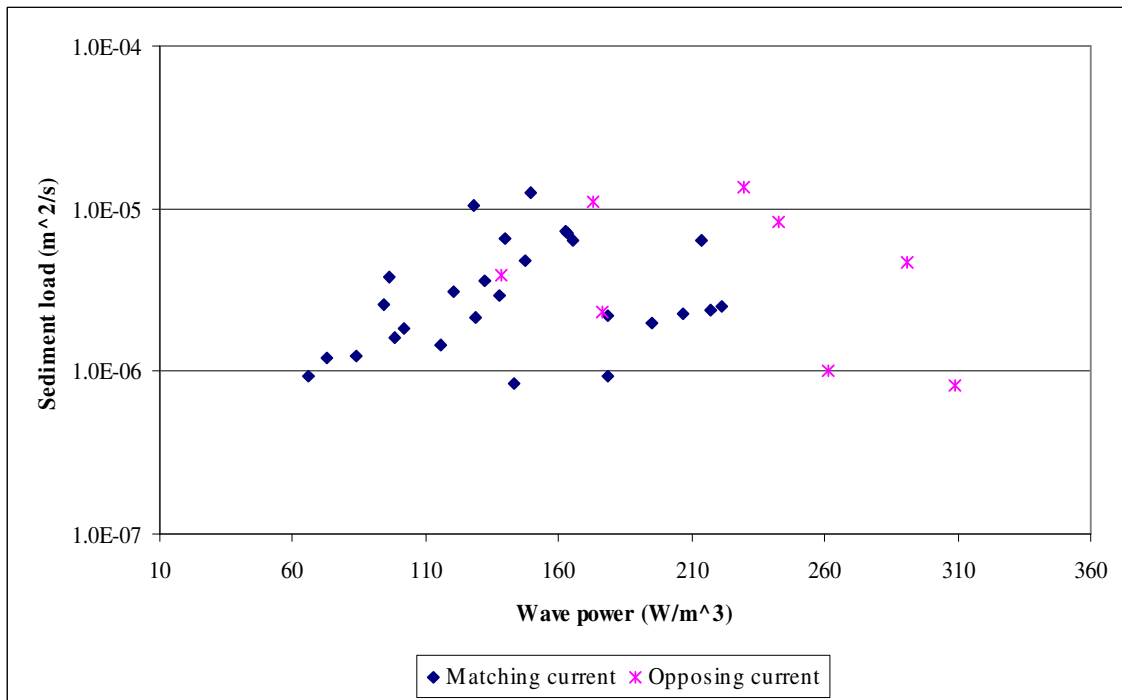


Figure 4.5-8 Relationship between wave power and sediment load

The correlation between current velocities and sediment transport rates is much better than between wave heights and sediment transport rates. The reason for this could be that the wave action only facilitates sediment transport rates by suspending sediment, but it is actually the currents that are mainly responsible for the sediment being transported downstream. For this reason the threshold at which sediment can actually be transported also very much depends on the sediment transport capacity of the current alone. If the sediment transport capacity of the current is very low, for example when the flow velocities are low, then even significant wave action will not result in increased sediment transport, because the current cannot transport the sediment that is entrained by the waves.

Another important observation was that the wave power is always much greater than the stream power. This is in part due to the magnitude of currents and waves selected for these experiments. Stronger currents or smaller waves would have reduced the difference between the wave and stream power, although not by much. The wave power has to be quite high to be able to entrain sediment particles into the water column then to be transported by the current. The current in this case does not have to be that strong, but just powerful enough to transport the particles. Without waves, the flow would have had to be much stronger to result in the same sediment transport rates. On average it was found that without the waves the sediment transport rates were five times lower for the same current speed than with the waves.

The results from the eight opposing current experiments show very similar results with regard to current velocities and stream power (see Figure 4.5-6 and Figure 4.5-7). However, it seems that with increasing wave heights the sediment transport rates decrease (see Figure 4.5-5). The reason for this is that with increasing wave heights the sediment that is lifted from the bed through the wave action is transported a short distance upstream against the current (see Figure 4.5-9 – B/C). If the current is not significant enough the sediment is moved back only a short distance towards the point where it was first picked up (see Figure 4.5-9 – D/E). By this time another wave arrives, moving sediment upstream again. If the current is strong, a sediment particle will actually be carried much further downstream than the point from which it was first picked up by the wave. The distance that the sediment effectively moves, and therefore the effective transport rates are very much dependent on the current velocities.

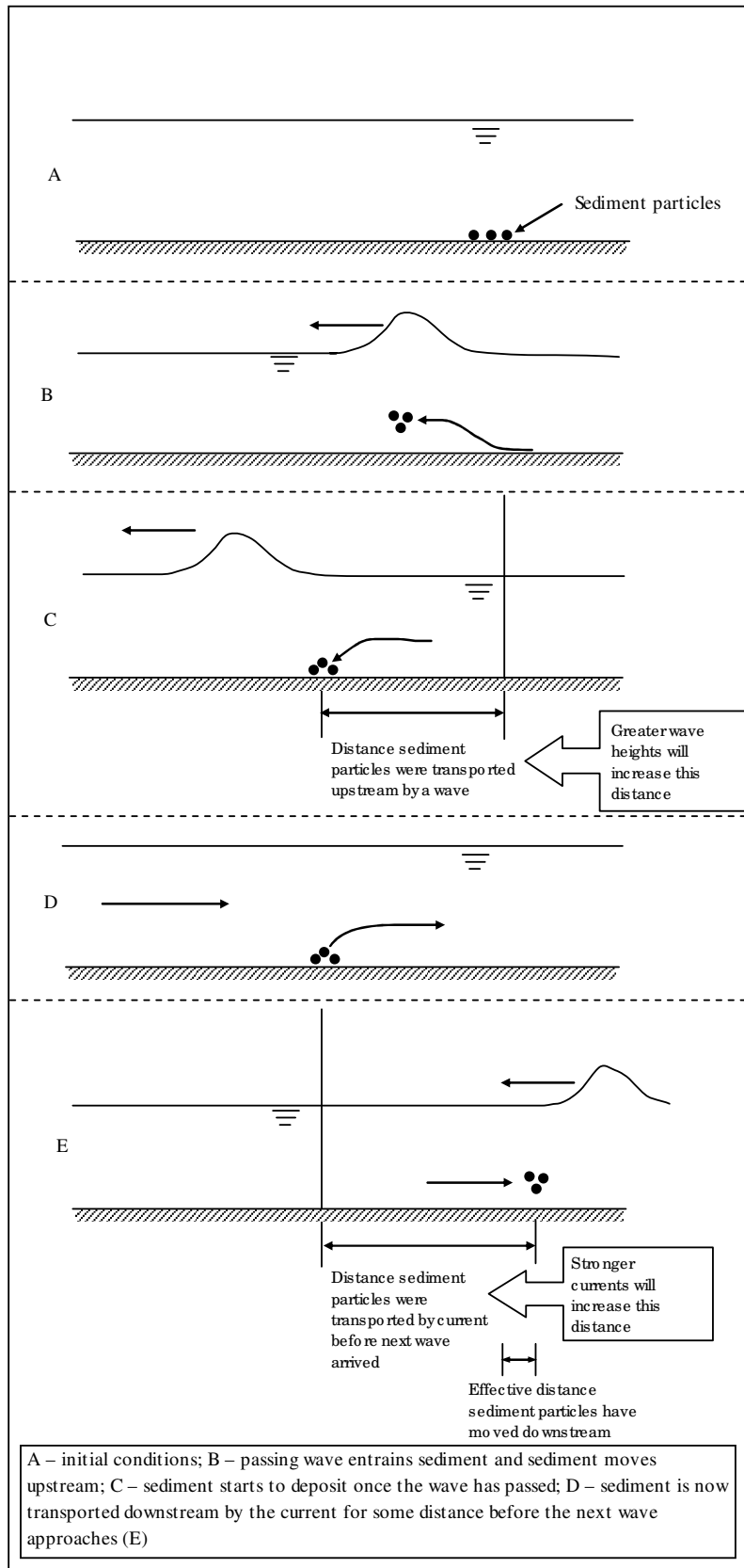


Figure 4.5-9 Sediment movement with opposing waves and currents

4.6 Calibration and Verification of a Sediment Transport Equation in Terms of Stream and Wave Power

4.6.1 Calibration of Sediment Transport Equation with Waves and Currents Travelling in the same Direction

In addition to the data obtained from my own experiments, data from one other researcher (Sistermanns, 2002) were also used for the calibration process. Although a number of studies have been carried out to determine sediment transport under waves or currents, a limited number have dealt with wave-current interaction. One data set, compiled by Sistermanns (2002), was used to supplement the data that were obtained from my experiments. Sistermanns' experiments were carried out to determine the effect of various parameters such as wave height, period and current velocity on the velocity profiles, as well as the effect of grading of sediments on these velocity profiles. The ranges of parameters in the relevant data are listed in Table 4.6-1. For the calibration process only Sistermanns' data was used, as the set was more extensive than that obtained during my experiments. These experiments were only carried out for currents and waves travelling in the same direction. Since the data obtained from my experiments are limited, only one new sediment transport equation for matching wave and current directions could be developed, although an attempt was made to develop one for opposing waves and currents as well.

Table 4.6-1 Range of parameters: Sistermanns' data

Parameter	Range
H_s [m]	0.12 – 0.20
T [s]	2.5 – 2.8
h [m]	0.49 – 0.55
u_c [m/s]	0.2 – 0.36
d_{50} [mm]	0.15 – 0.29
q_s [m ² /s]	$1.8 \times 10^{-6} - 1.4 \times 10^{-5}$
No of data points	36

Arguing that the sediment transport rate under waves and currents would be a result of the combination of wave and stream power, the proposed sediment transport equation would consist of two terms:

$$q_s = \Phi \left(\left(\frac{\rho g H^2}{8} \cdot \sqrt{gh} / (Bh) \right) ; (\rho g v S) \right) \dots\dots\dots 4.6-1$$

In addition to the stream and wave power the median sediment size was also included, since the type of sediment (i.e. silt, clay or sand) has a definite effect on sediment transport rates, as has been found in other sediment transport studies, e.g. Beck and Basson (2003):

$$q_s = \Phi \left(\left(\frac{\rho g H^2}{8} \cdot \sqrt{gh} / (Bh) \right); (\rho g v S), d_{50} \right) \dots\dots\dots 4.6-2$$

with the following regression format:

$$\log q_s = \left(A_1 \cdot \log \left(\frac{\rho g H^2}{8} \cdot \sqrt{gh} / (Bh) \right) + A_2 \cdot \log(\rho g v S) + A_3 \cdot \log(d_{50}) + A_4 \right) \dots\dots\dots 4.6-3$$

with $A_{1,2,3}$ regression coefficients and A_4 a regression constant.

Re-arranging equation 4.6-3 yields an equation with the following format, which was calibrated using Systersmans' data for waves and currents travelling in the same direction:

$$q_s = 10^{A_4} \cdot \left(\frac{\rho g H^2}{8} \cdot \sqrt{gh} / (Bh) \right)^{A_1} \cdot (\rho g v S)^{A_2} \cdot (d_{50})^{A_3} \dots\dots\dots 4.6-4$$

where A_1 is a constant, A_2, A_3, A_4 are coefficients and B is the flume width.

The calibrated sediment transport equation has a correlation coefficient of 0.66 and is shown in Figure 4.6-1:

$$q_s = 1.77 \cdot 10^{-3} \cdot \left(\frac{\rho g H^2}{8} \cdot \sqrt{gh} / (Bh) \right)^{0.565} \cdot (\rho g v S)^{0.713} \cdot (d_{50})^{0.87} \dots\dots\dots 4.6-5$$

where d_{50} [m].

Equation 4.6-5 is applicable to non-breaking shallow water waves, with currents and waves travelling in the same direction. The criteria for shallow water waves are given in Table 4.4-1.

The correlation coefficient is not high, which could be due to the difficulties in accurately measuring wave heights and energy slopes as mentioned in Section 4.5.3. The accuracy of equation 4.6-5,

however, is fairly good, as shown in Table 4.6-2, with more than 90% of the predicted values varying by no more than a factor of 2.

Table 4.6-2 Accuracy of sediment transport equation 4.6-5 based on calibration data

Equation	$0.83 < \frac{q_{s,calc}}{q_{s,obs}} < 1.2$	$0.67 < \frac{q_{s,calc}}{q_{s,obs}} < 1.5$	$0.5 < \frac{q_{s,calc}}{q_{s,obs}} < 2$
4.6-5	36%	72%	94%

If we compare the accuracy of the new sediment transport equation with those of existing sediment transport equations such as *Bijker* and *Bailard* as listed in Table 4.6-3, we can see these have much lower accuracies. This is an indication of how difficult it is to accurately describe sediment transport under wave and current conditions, and also that the wave and stream power concept seems to yield better results than some of the existing wave-current sediment transport equations.

It should be pointed out that the new sediment transport equation is based on a very small data set with very low sediment transport rates, and it remains to be seen whether the equation will yield good results for higher sediment transport rates.

Table 4.6-3 Accuracy of existing wave-current sediment transport equations (Camenen and Larroudé, 2003)

Equation	Less than 20% error	Less than 50% error
<i>Bijker</i>	4%	18%
<i>Bailard</i>	9%	35%
<i>Dibajnia & Watanabe</i>	18%	48%

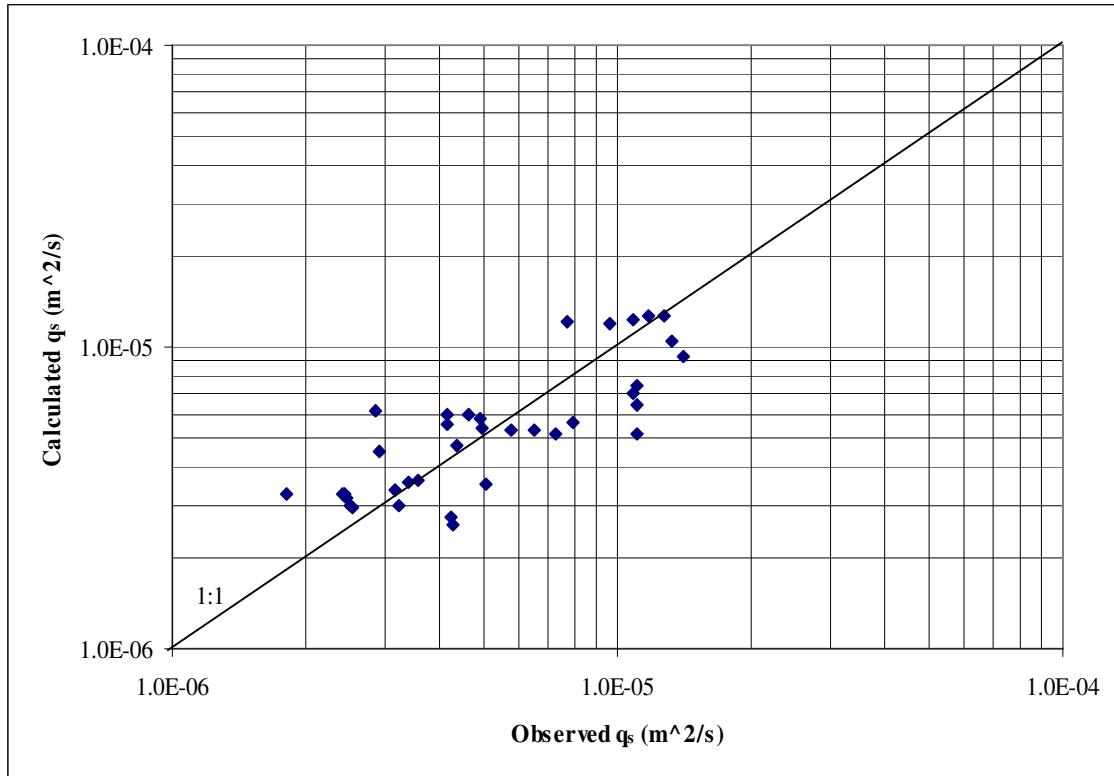


Figure 4.6-1 Calibration of new sediment transport equation (Sisternans’ data – equation 4.6-5)

4.6.2 Calibration of Sediment Transport Equation with Waves and Currents Travelling in Opposing Directions

The situation where waves and currents travel in opposite directions occurs frequently in the estuarine environment, for example when onshore wind-generated waves occur during the falling tide, when the ebb-currents direct flow towards the sea. An attempt was thus also made to calibrate a new sediment transport equation for opposing wave and current conditions. It has to be noted that very little data was obtained on these conditions from experiments that were carried out and that no verification data could be obtained.

The form of this new equation is similar to equation 4.6-4, i.e:

$$q_s = A_1 \cdot \left(\frac{\rho g H^2}{8} \cdot \sqrt{gh} l(Bh) \right)^{A_2} \cdot (\rho g v S)^{A_3} \dots\dots\dots 4.6-6$$

The median sediment diameter term was not included in equation 4.6-6, since the few experiments that were carried out under these conditions all had the same sediment grading, and as such the median sediment diameter term is meaningless. Would the calibration have been carried out with a different data set, which would include different sediment types, the term should of course have been included.

The calibration yielded the following equation:

$$q_s = 1.14 \cdot 10^{-4} \cdot \left(\frac{\rho g H^2}{8} \cdot \sqrt{gh} / (Bh) \right)^{-0.433} \cdot (\rho g v S)^{0.429} \dots\dots\dots 4.6-7$$

It is interesting to note that the wave power exponent here becomes negative, indicating that with increasing wave power (opposing the stream power) the sediment transport rates will decrease. The same principle could be observed during the experiments that were carried out. The correlation coefficient is very low, and as such equation 4.6-7 is not particularly meaningful, except to indicate that wave and stream power might also be useful in describing the sediment transport under opposing wave and current conditions, given more in-depth research and data on these conditions.

4.6.3 Verification

The data for waves and currents travelling in the same direction obtained from my experiments were used for verification purposes. As with the calibration process the accuracy of the new sediment transport equation was expressed in terms of its ability to predict data within certain accuracy ranges. Table 4.6-4 shows the accuracy ranges for equation 4.6-5, based on the verification data. The accuracy is fairly good with more than 80% of the predicted values varying by no more than a factor of 2. From Figure 4.6-2 it can also be seen that the two data sets show the same trend.

Table 4.6-4 Accuracy of sediment transport equation 4.6-5 based on verification data

Equation	$0.83 < \frac{q_{s,calc}}{q_{s,obs}} < 1.2$	$0.67 < \frac{q_{s,calc}}{q_{s,obs}} < 1.5$	$0.5 < \frac{q_{s,calc}}{q_{s,obs}} < 2$
4.6-5	33%	56%	85%

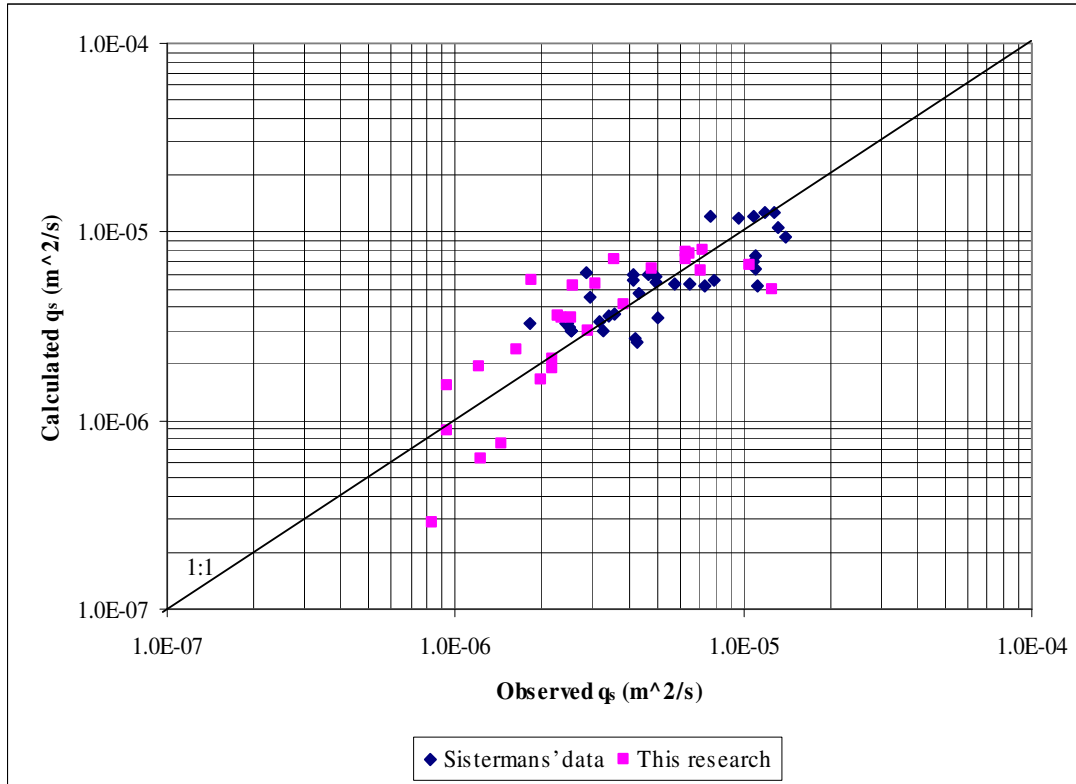


Figure 4.6-2 Verification of new sediment transport equation

4.6.4 Comparison

To examine the applicability of the proposed wave and stream power equation, it was compared to one of the most widely used sediment transport equation for wave-current interaction, the *Bijker* formula (see Section 4.3). The data used for this comparison, were once again Sistermans' data. It can be seen from Figure 4.6-3 that the *Bijker* formula yields sediment transport rates that are much too high. The problem with applying the *Bijker* formula is that it involves a rather complicated series of equations and also a considerable amount of information, as can be seen from Section 4.3. Therefore, although the *Bijker* formula is theoretically sound, it is difficult to accurately obtain all the data required, which could lead to inaccurate results. Equation 4.6-5 on the other hand is much more straightforward.

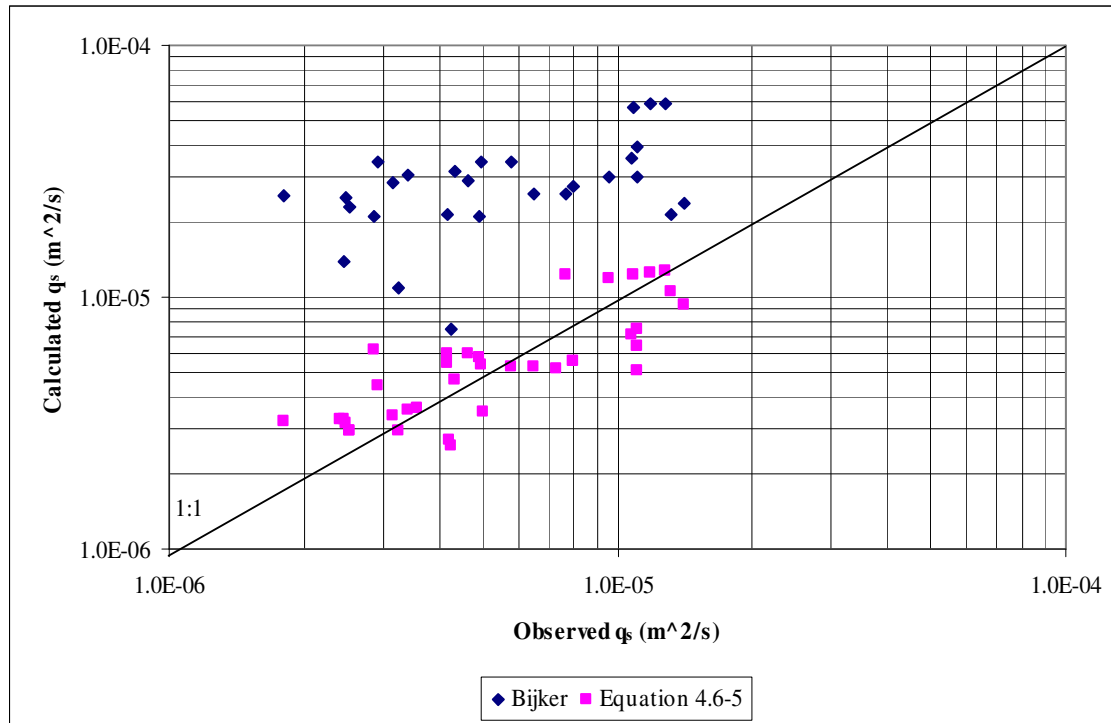


Figure 4.6-3 Comparison of new sediment transport equation and *Bijker* formula

4.7 Summary

Sediment transport under both waves and currents was investigated. It was found that with increasing wave heights (i.e. wave power) and increasing current velocities (i.e. stream power), sediment transport rates increase as well as is also the case when both waves and currents travel in the same direction. In contrast with the current direction opposing the waves, greater wave heights resulted in lower sediment transport rates. A sediment transport equation, based on stream power, wave power, as well as sediment size for waves and currents travelling in the same direction was calibrated and verified, and compared to the well-known *Bijker* formula. The results show that the new sediment transport equation is straightforward and gives better results than the *Bijker* formula for the data used.

An attempt was also made to calibrate a sediment transport equation for opposing wave and current conditions, indicating that with increasing opposing wave power the sediment transport rates will actually decrease. However, more research and data is needed on these conditions.

5. Open Mouth State: Sediment Transport during the Tidal Cycle

5.1 Introduction

As a result of flow reversal during the tidal cycle, sediment is transported in and out of the estuary, but since the ebb and flood tidal flows are rarely equal in magnitude, there is a nett movement of sediment into or out of the estuary. Other factors such as the local wave climate and certain estuary characteristics also play a role in this process. An important objective of this research was to determine under which circumstances sediment would enter the estuary. Field investigations and mathematical modelling were carried out to investigate this process.

5.2 Field Investigations at the Goukou Estuary

The Goukou River estuary was chosen, because it was considered to be representative of typical South African estuaries in which upstream sedimentation is perceived to be a problem, and for its typical open mouth conditions.

After an initial field investigation in July 2001, another joint field exercise by the University of Stellenbosch and the CSIR was conducted at the Goukou River estuary in March 2003. The purpose of the field exercise was mainly to obtain sediment transport related data through one cycle from neap tide to spring tide. The instruments were deployed during the neap tide and one week later, during spring tide, extensive field measurements were taken.

The instruments that were deployed were two electromagnetic current meters and a self-contained OBS (Optical Backscatter Sensor), mounted on tripods. The heart of the OBS monitor is an optical sensor for measuring turbidity and suspended solids concentrations by detecting infrared radiation scattered from suspended matter. The OBS actually contained three sensors, each set at a different gain, in order to ensure that the whole spectrum of suspended sediment concentrations could be measured. Two electronic water level recorders were also installed for one week, with one in the harbour and one on a jetty between the mouth and the DWAF water level recorder.

Field measurements were carried out at one cross-section (between the DWAF water level recorder and the mouth, see Figure 5.2-1) during the spring tide, which included:

- Point measurements of flow velocity (by means of a propeller current meter) at 20, 60 and 80% of the depth
- Water samples (in-situ horizontal grab sampler), at various depths over the cross-section and at the location of the instruments
- Bed sediment samples and grain size distribution analyses
- Survey of the cross-section as well as the area around the mouth of the estuary



Figure 5.2-1 Aerial view of Goukou estuary and location of cross-section in March 2003

5.2.1 Field Data Analysis

Figure 5.2-2 indicates water levels measured in Still Bay Harbour at the small jetty as well as the DWAF recorder (a bit further upstream) in the Goukou River estuary. The cut-off at the turn of the ebb-tide in the estuary (as a result of the mouth dimensions) is clearly observed.

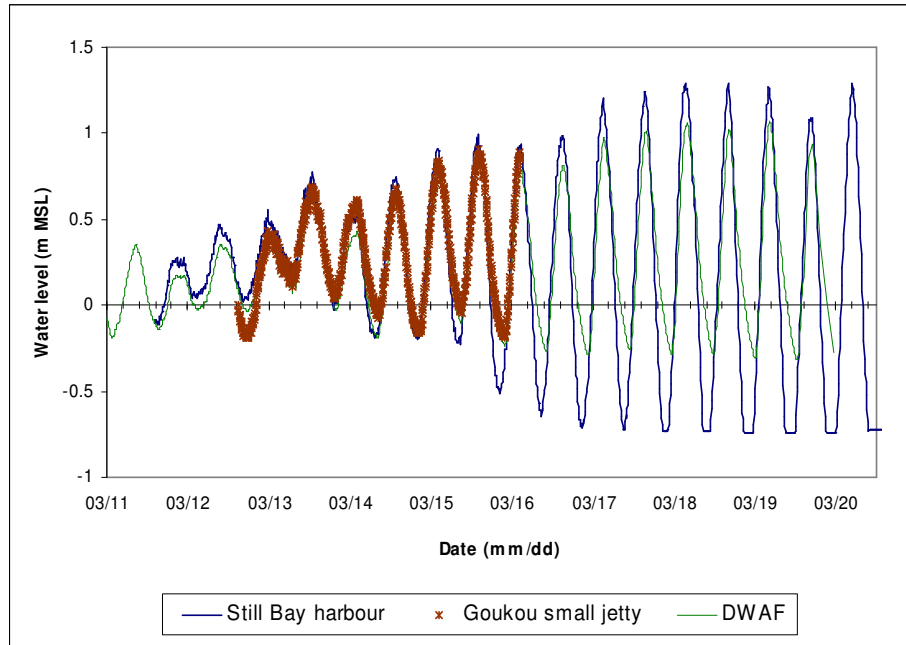


Figure 5.2-2 Observed water levels at Goukou, March 2003

Figure 5.2-3 shows the response of the fixed OBS (indication of suspended sediment concentration) with measured current velocities. The figure shows that velocities and sediment concentration peaks are higher for incoming tides than for outgoing tides. They also show that the duration of the outgoing tides is longer. According to the theories discussed in Chapter 2, the Goukou Estuary would be classified as flood-dominant, indicating that sediments of marine origin are likely to dominate.

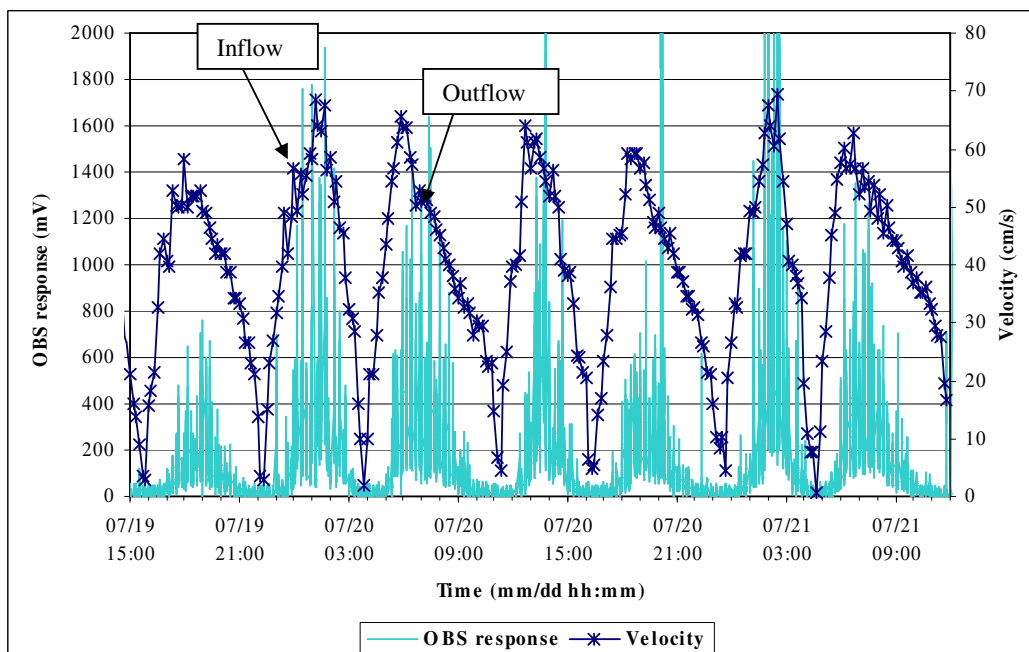


Figure 5.2-3 Measured sediment concentration and current velocities (Spring tide, July 2001)

The OBS measurements were converted to suspended sediment concentrations by means of calibrations done by the CSIR (Beck *et al*, 2004). The suspended sediment concentrations and average velocities throughout the cross-section were used to calculate total sediment transport through the cross-section. The total sediment transport over several tidal cycles during spring tide of July 2001 showed net sediment transport in the upstream direction. The same trend was observed over a 7-day neap to spring tidal cycle in March 2003. While this is not absolute proof that marine sediment is moving up into the estuary, as the net sediment transport is relatively small (in the order of 50 m³ over three spring tidal cycles, and 30 m³ during the 7-day neap to spring tidal cycle) and only measured at a certain cross-section, it does, however, strongly indicate that there is an influx of marine sediment.

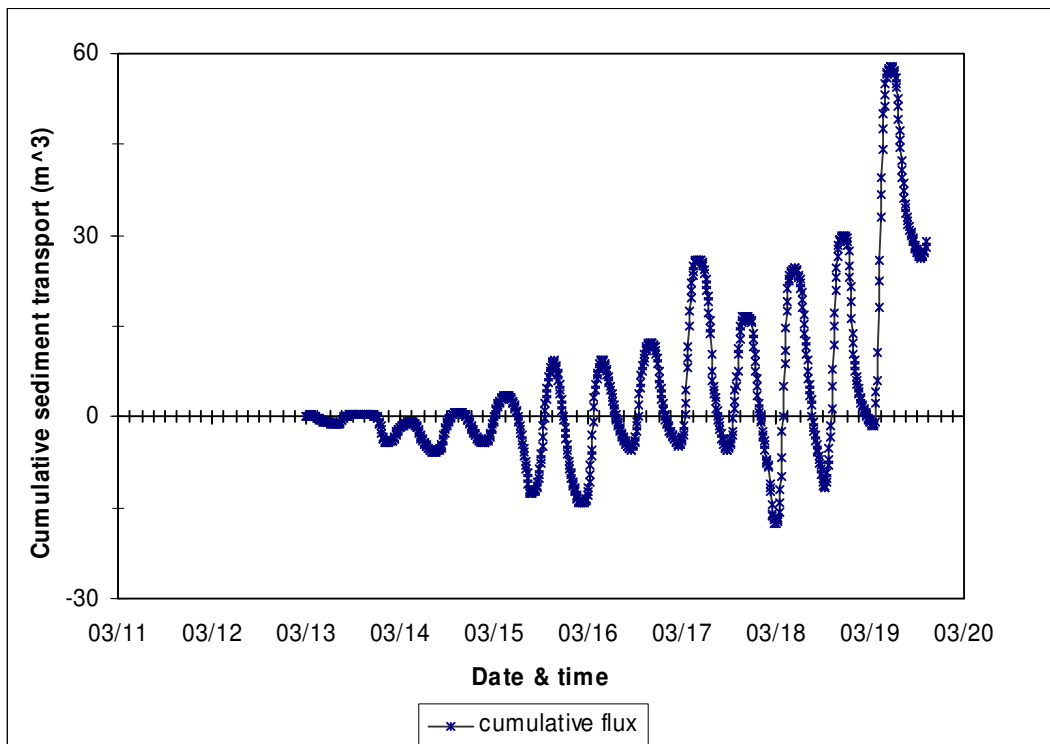


Figure 5.2-4 Cumulative sediment transport through cross-section at Goukou (March 2003) (Beck *et al*, 2004)

5.3 Long-Term Computational Modelling

Mathematical modelling of estuarine hydrodynamics and sediment transport is very complex due to the interaction between the coastal (such as waves and tides) and river processes (such as floods). Local conditions also differ from one estuary to the next. For example one estuary may be small and be located on a wave-sheltered part of the coast, with a permanently open mouth, whereas another could have a very large area, but be subject to high wave conditions. The hydrodynamics, especially

towards the mouth, and the sediment transport patterns will be very different. An important aspect of this research was to investigate sediment movement in and out of the estuary during normal tidal action and it was therefore decided to use a one-dimensional mathematical model of a simplified artificial estuary to investigate this aspect. In the next section the effects of floods and the possible impact of dams on the estuarine morphology of the Thukela River are discussed.

The one-dimensional computational modelling of both the simplified artificial estuary as well as the Thukela River Estuary was performed with MIKE 11 of the Danish Hydraulics Institute (DHI, 2001). The one-dimensional (1D) model, rather than the two-dimensional (2D) model was used to investigate the long-term effects of tidal action and floods, since it is usually impractical to do long-term simulations with a 2D model due to the considerable computational power required by the 2D model.

The following two modules of the river-modelling component of MIKE 11 were used for the simulations:

- Hydrodynamic (HD)
- Non-cohesive sediment transport and morphology (NST)

The overview given here is a short summary of the general descriptions of aspects of the MIKE 11 modelling system, as given in the MIKE 11 Reference Manual (DHI, 2001).

a) Hydrodynamic Module

The MIKE 11 hydrodynamic (HD) module uses an implicit, finite difference scheme for the computation of unsteady flows in rivers and estuaries, based on the St Venant equations representing conservation of mass and momentum. The model can describe both subcritical and supercritical flow conditions through a numerical scheme which adapts according to the local flow conditions (in time and space), and modules are incorporated that describe flow over hydraulic structures. The model can be applied to looped networks and quasi two-dimensional flow simulation on flood plains. The HD module has a dynamic wave approach, which uses the full momentum equation.

b) Non-Cohesive Sediment Transport Module

The non-cohesive sediment transport (NST) module can be run in two modes: explicit and morphological. In the explicit mode output is required from the HD module in both time and space, but no feedback occurs from the NST module to the HD module. The explicit mode is useful when significant morphological changes are unlikely to occur. In the morphological mode sediment transport is calculated together with the HD module and feedback is given from the NST module to the HD module. The feedback is achieved through the solution of the sediment continuity equation and

through updating of the bed resistance and sediment transport. The morphological model updates either the whole cross-section or only a part of it (generally the part representing the river channel).

Traditional sediment transport equations such as Ackers and White, and Engelund and Hansen are incorporated in the MIKE 11 model for non-cohesive sediment transport. All of these can be run with a single representative particle size or a number of particle sizes.

5.3.1 One-Dimensional Modelling of an Artificial Estuary

5.3.1.1 Tidal Action

The artificial bathymetry that was used for the model (Figure 5.3-1), had a relatively shallow, narrow channel of approximately 80 m wide and 1.5 m deep, stretching from the mouth upstream for about 4 km. Thereafter a wider and deeper channel can be found of approximately 200 m wide and 5 m deep, stretching approximately 10 km further upstream. On the “ocean” side the estuary stretches 2 km offshore, with a 1:20 sea floor slope.

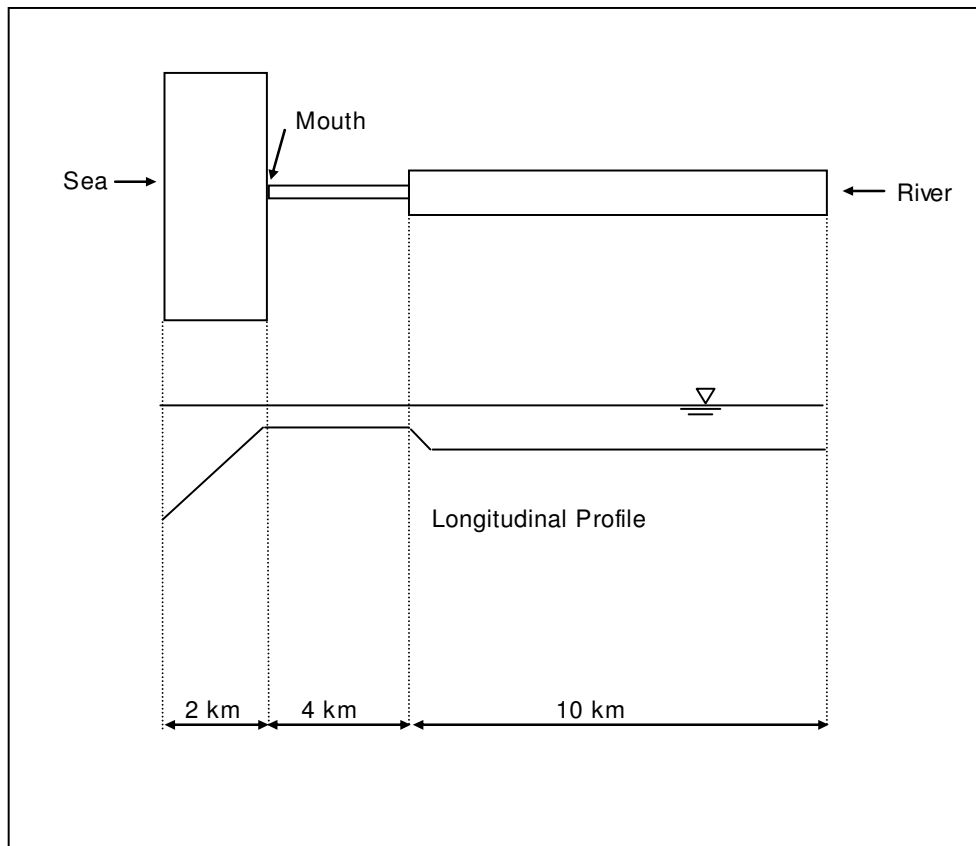


Figure 5.3-1 Artificial estuary layout

The effects of tidal action over an eight-and-a-half year period (2000/01 to 2008/06) on the sediment movement were investigated. The Van Rijn sediment transport model was used for both suspended and bed load transport. The wave action was not taken into account. Two initial sediment fractions in the bed sediment were specified ($d_1 = 0.2$ mm and $d_2 = 0.35$ mm), with 70% of d_1 and 30% of d_2 .

At the upstream boundary a constant river inflow of $10 \text{ m}^3/\text{s}$ was specified. At the downstream boundary a water level time-series was specified, based on a simulated spring-neap cycle (with correct amplitudes and periods). The same two-week tidal cycle was repeated over the eight-year period.

Model Results

The tidal action significantly decreases landward of the mouth (see Figure 5.3-2), although it is mainly the low tide water levels that are affected. The high tide water level remains unchanged, but the low tide levels decrease from about 0.6 m below mean sea level (MSL) during spring tide in the ocean to 0 m MSL in the upper estuary. This is due to the narrow, shallow channel at the mouth, which prevents the water in the estuary draining below 0 m MSL.

Sedimentation was confined to the 80 m narrow inlet channel (see Figure 5.3-3). Maximum erosion occurred just inside the mouth (1.9 m), and maximum deposition (1.8 m) occurred just upstream of the narrow inlet channel, as a result of the sudden widening of the channel from 80 to 200 m (as can be seen from Figure 5.3-4). Deposition also took place just downstream of the mouth, as a result of the sudden widening of the cross-section from the narrow inlet to the open sea. The erosion started at the seaward end of the narrow channel and progressed upstream from there. From Figure 5.3-4 it can be seen that the rate of erosion slows down over most of the narrow channel, and after an initial period of deposition at the upstream end of the channel, the sediment at that point is being eroded again.

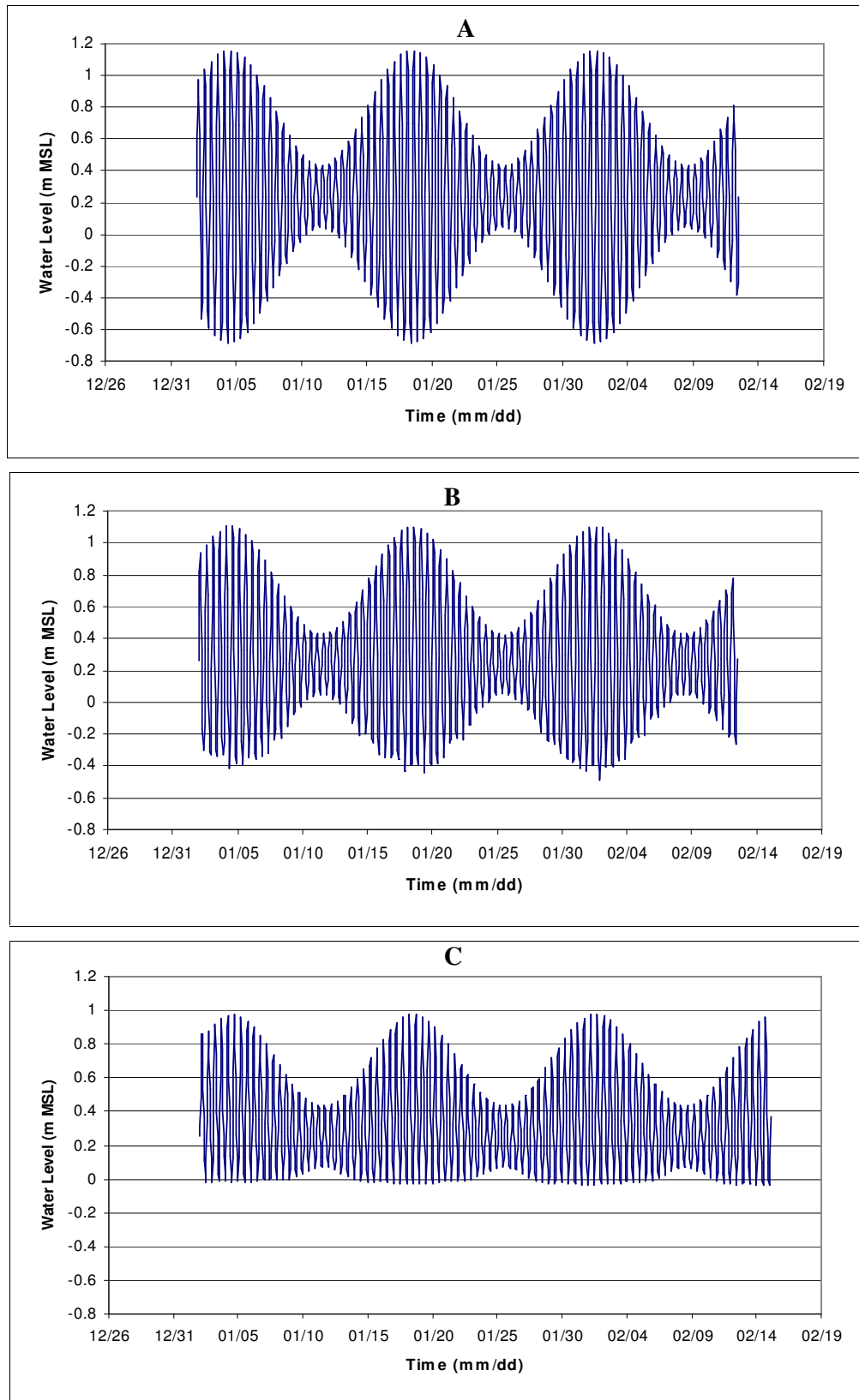


Figure 5.3-2 Simulated water levels in the artificial estuary (A - ocean, B - mouth, C - upper estuary)

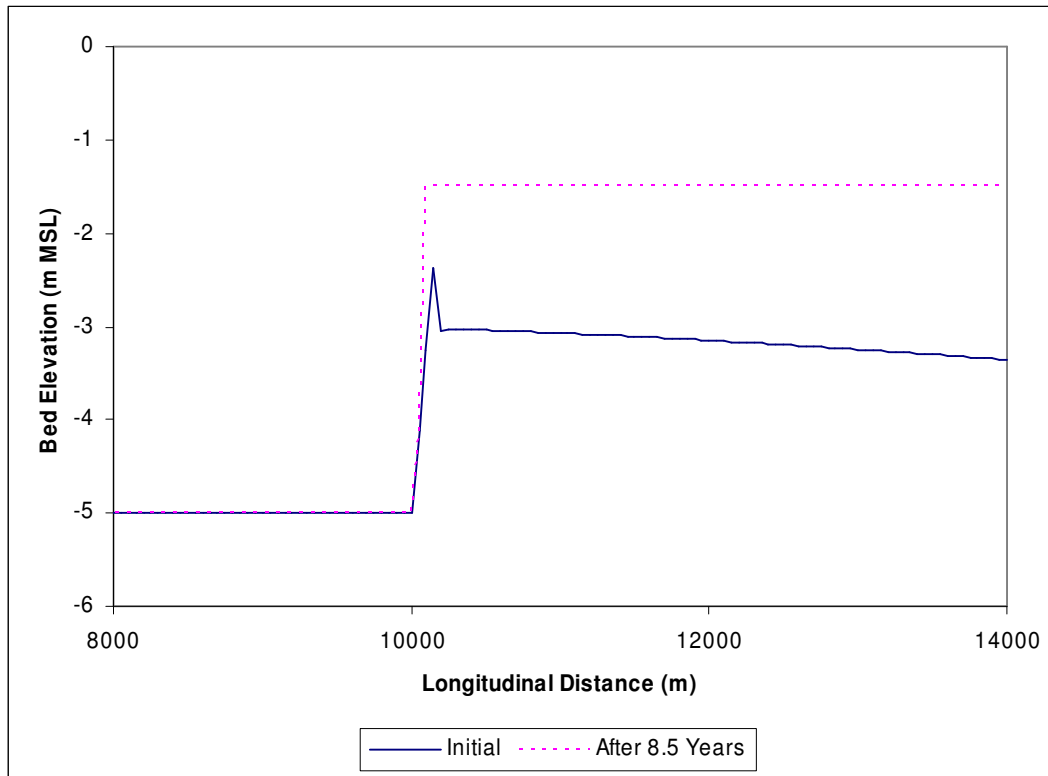


Figure 5.3-3 Simulated initial and final bed levels of artificial estuary under tidal action only

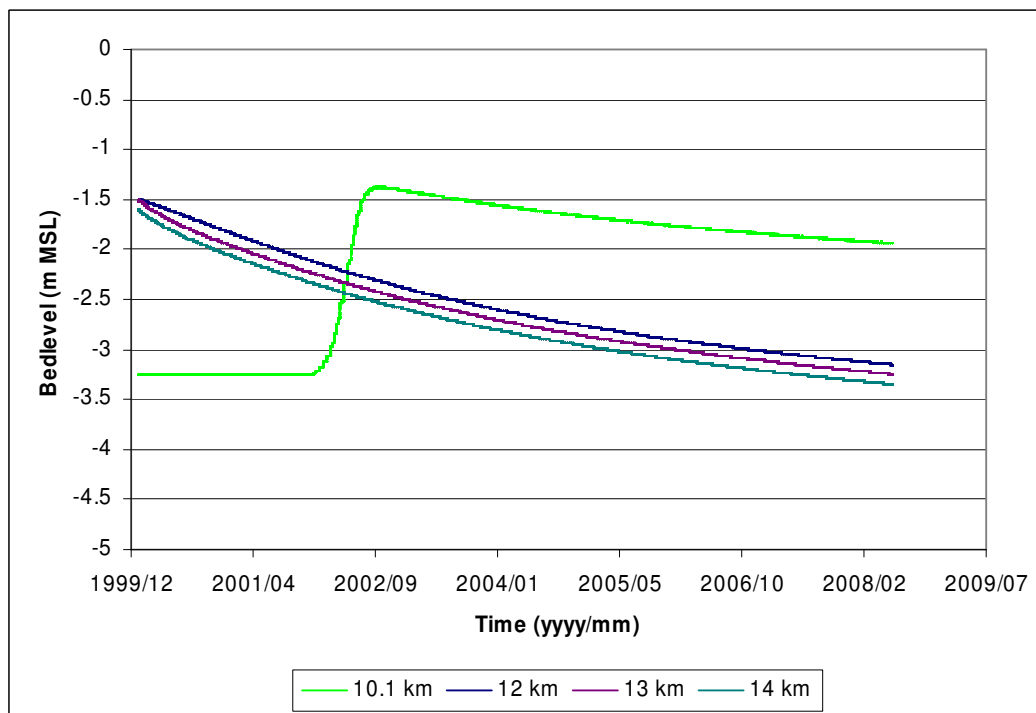


Figure 5.3-4 Simulated bed level changes of artificial estuary with time at various positions (in parentheses) along the estuary. (10.1 km is in the transition between the 80 and 200 m wide channels, while 14 km is just upstream of the transition to the ocean)

Overall it was found that more sediment is transported into the estuary during flood tide than out of the estuary during ebb tide in the upper part of the channel (see 11 and 12 km in Table 5.3-1).

However, the reverse is true for the lower part. Table 5.3-2 gives the average annual sediment loads over the simulation period. For the channel downstream of chainage 12 km, almost twice as much sediment is transported out of the estuary than into it, however, most of the outgoing sediment transport takes place during the first half of the simulation period and the transport reduces towards the end. For the upper part of the channel, more sediment is transported into the estuary, especially during the second half of the simulation. This reversal occurs after about three years into the simulation, at the same time that the erosion starts at chainage 10 km. It seems that the system is far from being in a stable state and therefore many changes occur, especially in the beginning.

On average more than 50% more sediment is transported out of the lower estuary under tidal action, than is transported into the estuary. The reason for that can be seen in Table 5.3-2. The flood tide velocities in the upper part of the narrow channel are always greater than the ebb velocities, and the sediment transport is therefore also greater during flood tide than ebb tide. The reverse is true for the lower part of the narrow channel. The one exception to this trend is that the flood tide velocities in the lower part of the channel are greater for the second half of the simulations than the ebb velocities. The reason for this is that there are other factors influencing the sediment transport. In this case sediment transport will only take place if the velocities are greater than 0.36 m/s, and the period of time that the ebb velocity magnitudes are above 0.36 m/s is greater than the period of time that the flood tide velocity magnitudes are above 0.36 m/s. Therefore, although the average flood tide velocities are greater, the period of time over which they are actually capable of moving sediment is shorter than for the ebb tide, and the total outgoing sediment transport is therefore greater.

Table 5.3-1 Simulated average annual sediment loads (10³ ton/a)

Location	10.1 km	11 km	12 km	13 km	14 km
In ¹	-35.6 (72 %)	-70.9 (62 %)	-59.3 (51 %)	-48.8 (40 %)	-21.7 (28 %)
Out	13.7	42.8	57.4	74.7	55.6
In ²	-26.6 (73 %)	-76.8 (61 %)	-61 (47 %)	-47.2 (33 %)	-25.6 (22 %)
Out	9.6	48.9	69.4	94.6	90
In ³	-43.7 (71 %)	-63.4 (64 %)	-56.2 (56 %)	-49.3 (48 %)	-17.2 (46 %)
Out	17.5	35.8	44.1	53	19.8

¹ Average over 8.5 year period (Values in parentheses indicate percentage of total sediment transport into estuary)

² Average over first 4 years

³ Average over last 4.5 years

Table 5.3-2 Average simulated velocities (m/s)

Location	10.1 km	11 km	12 km	13 km	14 km
Flood	-0.32	-0.49	-0.48	-0.47	-0.41
Ebb	0.28	0.45	0.47	0.48	0.43
Flood	-0.26	-0.5	-0.49	-0.47	-0.42
Ebb	0.24	0.49	0.5	0.51	0.48
Flood	-0.37	-0.47	-0.47	-0.47	-0.39
Ebb	0.32	0.42	0.43	0.44	0.37

The cross-sections in the numerical model were spaced at 50 m intervals. The fact that sediment deposition occurred only at the cross-section just upstream of the 80 m wide channel in the transition zone, indicates that sediment could at best move 50 m upstream into the estuary during the 8.5 year simulation period, which is about 6 m/year.

It is obvious that this particular system is not in equilibrium, and much of the sediment is locally re-distributed. There is no clear indication that the sediment transport is predominantly ebb or flood dominated. According to the theories stated in Chapter 2, the estuary should be flood-dominated, and in the upper part this is the case, as the velocities during the rising tide are always larger than the velocities during the falling tide. In Chapter 2 the main reasons why an estuary should be flood dominated are given as:

- No significant variation in the water surface area in the estuary during the tidal cycle and
- shorter flood durations (i.e. higher flood velocities) and longer ebb durations.

Because this particular system still seems to be trying to establish its equilibrium, it was decided to set up a different topography, which was thought to be already in equilibrium. This new topography was much the same as the old one, except for an initial bed level of -3 m MSL in the 80 m wide channel. Also the 200 m wide upstream channel was reduced to a width of 80 m, because the sudden transition from 200 to 80 m resulted in too much sediment being re-distributed in that area. After the same 8.5 year simulation period the bed level had dropped by only 0.15 m on the seaward side, and 0.3 m deposition occurred at the upstream end of the inlet channel. The simulated sediment loads are an order of magnitude smaller than those listed in Table 5.3-1, as can be seen in Table 5.3-3. There is almost no change in the sediment loads between the first half of the simulations and the second half. The ebb velocities are always greater than the flood velocities, and that trend is reflected in the larger sediment loads during the falling tide than the rising tide. This system is much more stable than the previously discussed system, and is clearly ebb-dominated.

Table 5.3-3 Simulated average annual sediment loads (10^2 ton/a) – new system

Location	10.1 km	12 km	14 km
In	0	-5.4 (39 %)	-14 (35 %)
Out	0	8.6	26
In	0	-5.5 (39 %)	-15 (35 %)
Out	0	8.7	28
In	0	-5.3 (38 %)	-13 (34 %)
Out	0	8.6	25

5.3.1.2 Combined Flood and Tidal Action

For simulations of flood conditions, a 36-hour flood with a 2000 m³/s peak was used in conjunction with the normal tidal action for the original estuary topography.

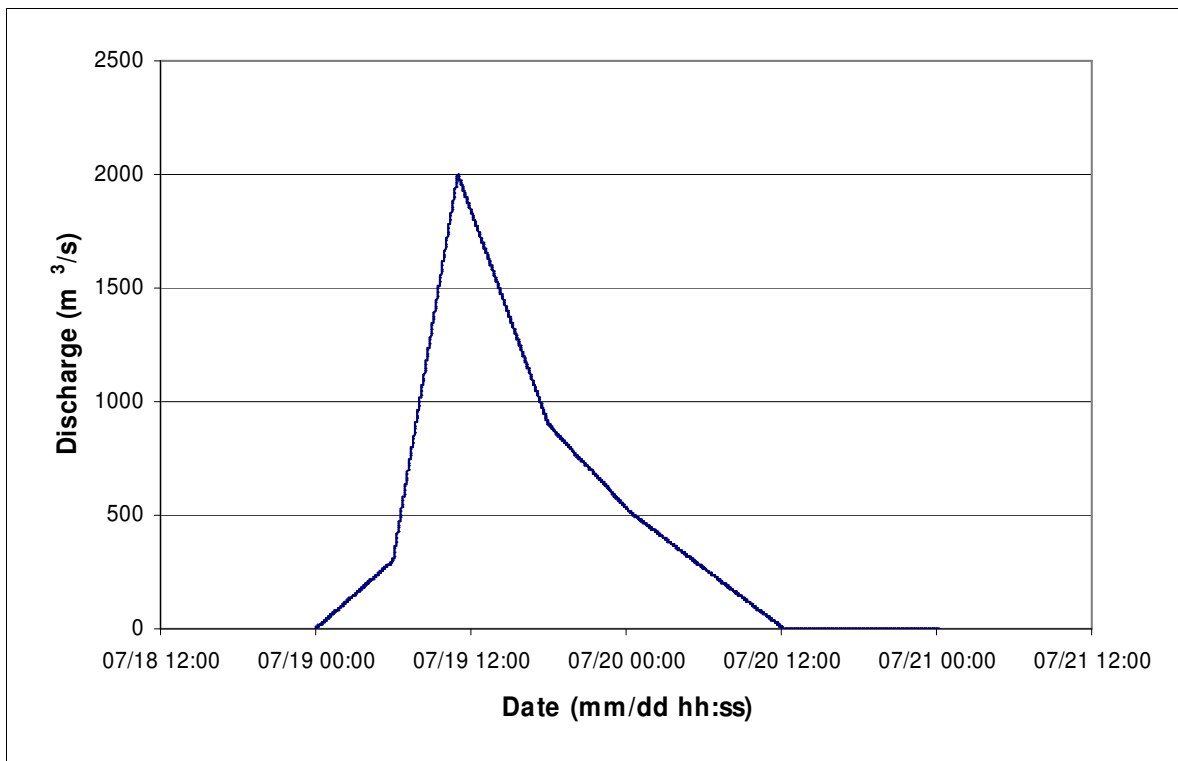


Figure 5.3-5 Flood hydrograph

Model Results

During a 36-hour flood about 10 times more sediment is removed from the artificial estuary than during a year with normal tidal action. Erosion was again confined to the narrow inlet channel (see Figure 5.3-6) and the flood managed to erode the inlet channel to almost the same level as the upper estuary. Deposition only occurred seaward of the mouth, but it was substantial and could at some point block the mouth to such an extent that it could close completely, unless the sediment can be dispersed by the subsequent tidal action. This just shows how important a flood of this magnitude is, as it obviously has the potential to bring about major geomorphological changes in the estuary.

Table 5.3-4 Simulated sediment loads during flood (10^5 ton/a)

Location	10 km	12 km	13.4 km
Sediment load	1.33	6.23	18.4

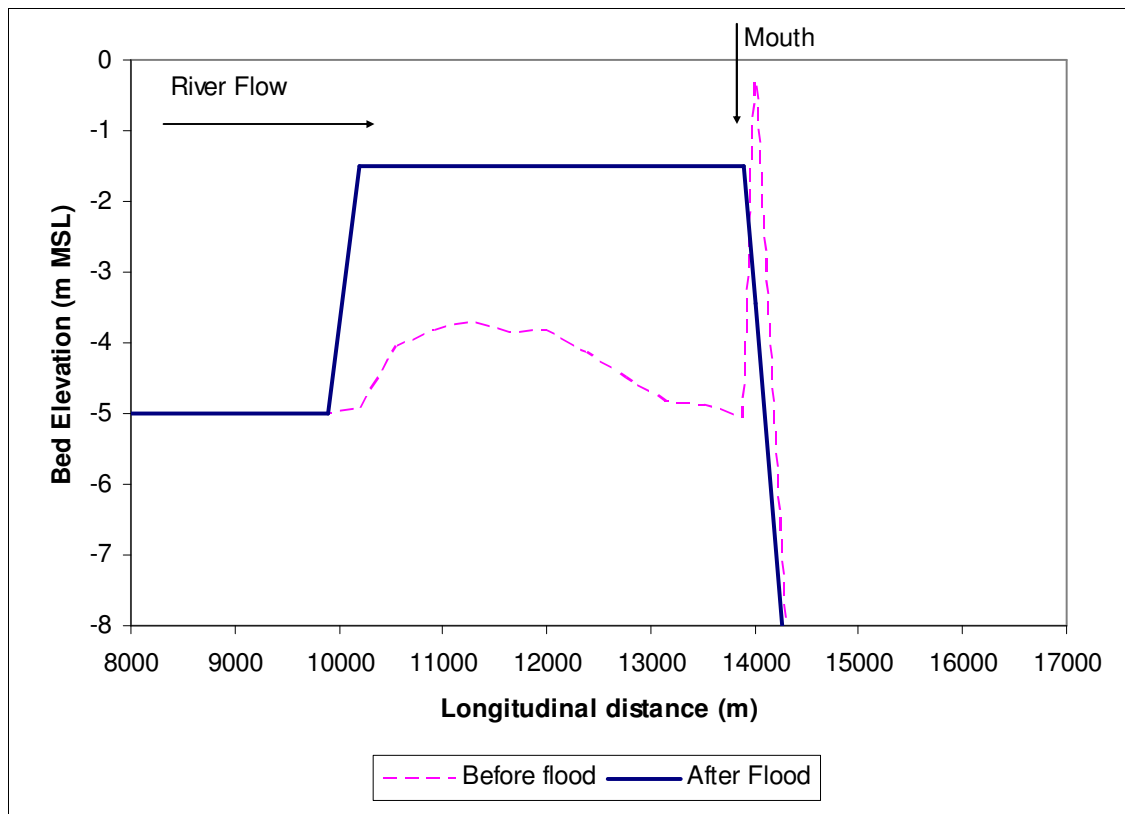


Figure 5.3-6 Simulated bed level before and after flood (flood peak = $2000 \text{ m}^3/\text{s}$)

5.3.2 Long-Term Simulations of Water Resources Impacts: Thukela River

In the previous section the long-term tidal simulations of an artificial estuary were discussed and the importance of floods for the sediment transport dynamics of the estuary was pointed out. This section discusses the Thukela Estuary, which is dominated by river flows, and where the sediment dynamics with proposed future dams have been assessed. The sediment dynamics of the Thukela Estuary were assessed as part of the Environmental Reserve Determination of the estuary (Taljaard *et al*, 2002). The Thukela Estuary is located on the sub tropical east coast of South Africa. The catchment area of the Thukela River at the estuary is large in size at 29100 km². The estuary is river dominated and therefore small. The Thukela River is relatively steep and has a high sediment transport capacity with a mean annual sediment yield (present day) of about 9.3 million ton.

The estuary is dominated by floods in the river and is relatively shallow and short (5 km in length). During low flow conditions (<10 m³/s) the river meanders through several sand banks in the main channel. The Thukela River flood peaks are high and therefore the system is very dynamic with rapid changes in the river morphology from time to time. During falling stages of flood hydrographs sediment deposition has been observed in the river mouth (Figure 5.3-7), but this sediment is later scoured by the south to north long-shore currents. A typical morphological picture of the estuary is shown in Figure 5.3-8.

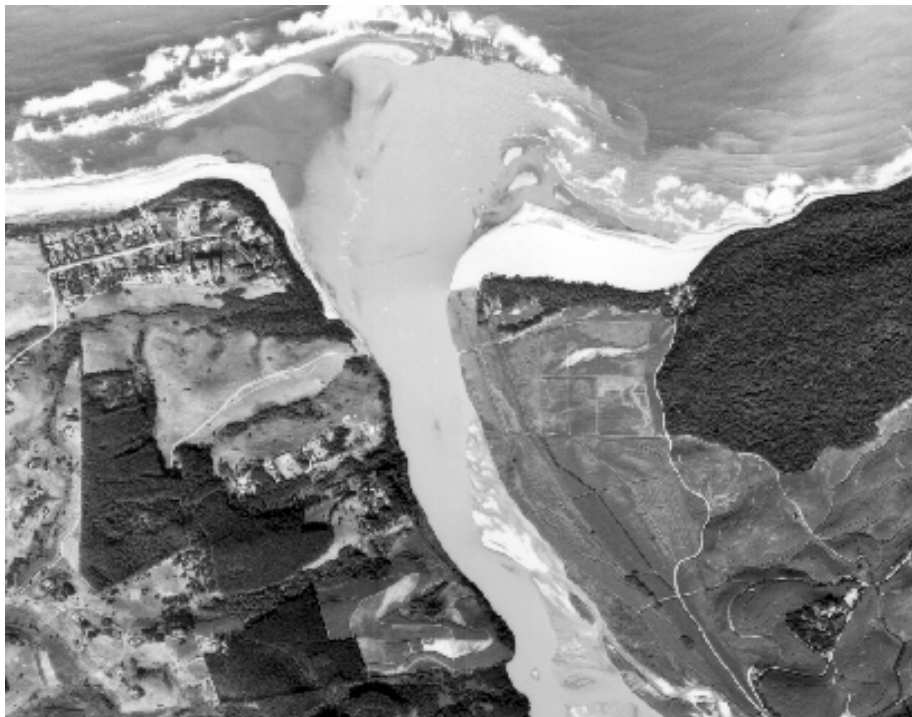


Figure 5.3-7 Thukela Estuary: sediment deposition during flood (May 1976)



Figure 5.3-8 Aerial view of Thukela Estuary (July 1985)

Several large dams have been constructed in the catchment such as Woodstock, Spioenkop, Chelmsford, Zaaihoek and Wagendrift. These dams would trap most of the sediment yield in their respective catchments and would also attenuate floods. The impact of these dams on the estuary would however be minimal, since they are located high up in the catchment.

Land use changes and overgrazing to date have probably caused a significant increase in the sediment yield, but the sediment yield under natural conditions longer than say 300 years ago is difficult to quantify. Any further development in the catchment, which could lead to an increase in the sediment yield, could cause significant changes to the Thukela Estuary fluvial morphology.

5.3.2.1 *Fluvial Morphological Scenarios*

In order to assess how the sediment dynamics of the Thukela Estuary might change with further catchment development, mathematical modelling of the hydraulics and morphology of the Thukela Estuary was carried out. Six scenarios were selected:

- Scenario 0: natural conditions (sediment yield of 200 ton/km².a)
- Scenario 1: present day
- Scenario 2: full demand placed on proposed dams, with environmental flow releases (worst case in terms of floods)
- Scenario 3: scenario 1 including a resetting flood
- Scenario 4: scenario 2 including a resetting flood
- Scenario 5: scenario 2 with a higher sediment yield of 600 ton/km².a

The 15-year period used for the simulations was a combination of flows from 1962 to 1967, and 1990 to 2000. This was done since it yielded the longest continuous and representative flow series from observed flow records (break point data).

5.3.2.2 Flood Routing

Before any estuary simulations could be performed the flows from the proposed dam sites had to be routed to the estuary, since both the proposed Jana Dam (Thukela River) and the Mielietuin Dam (Bushmans River) are situated relatively high in the catchment, with Jana Dam approximately 270 km from the estuary as shown in Figure 5.3-9.

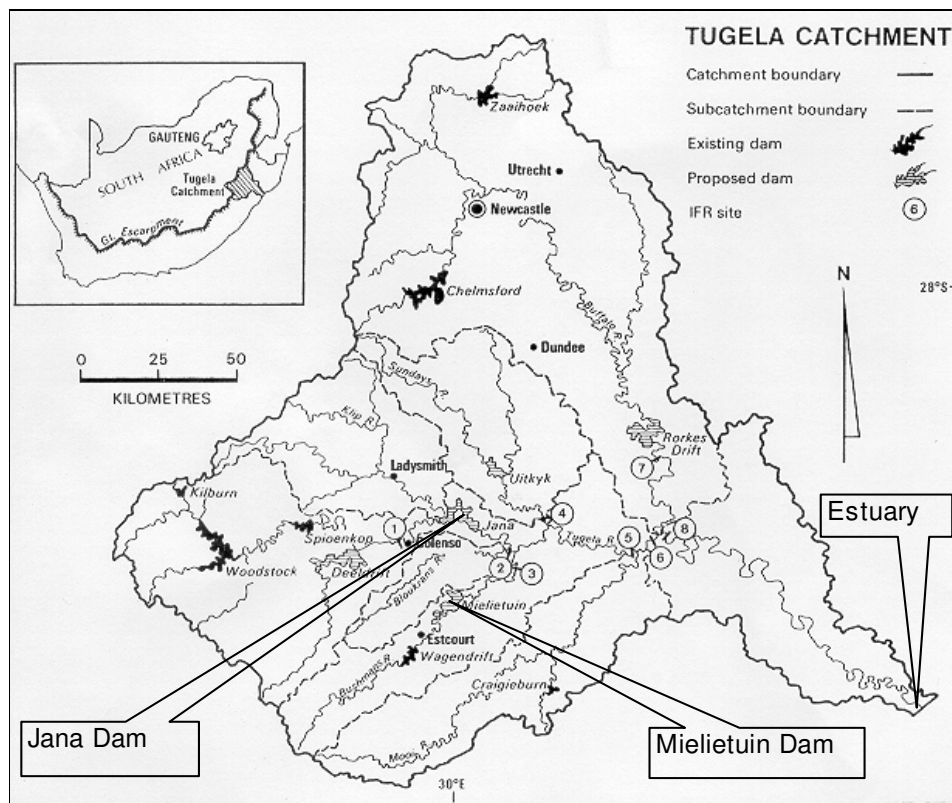


Figure 5.3-9 Thukela catchment layout (Adapted from Rowntree & Wadeson, 1999)

The pre-dam flows at the proposed Jana Dam and Mielietuin Dam sites, as well as the post-dam flows are shown in Figure 5.3-10 to Figure 5.3-13. The pre-dam and post-dam flows at the estuary are shown in Figure 5.3-14 and Figure 5.3-15.

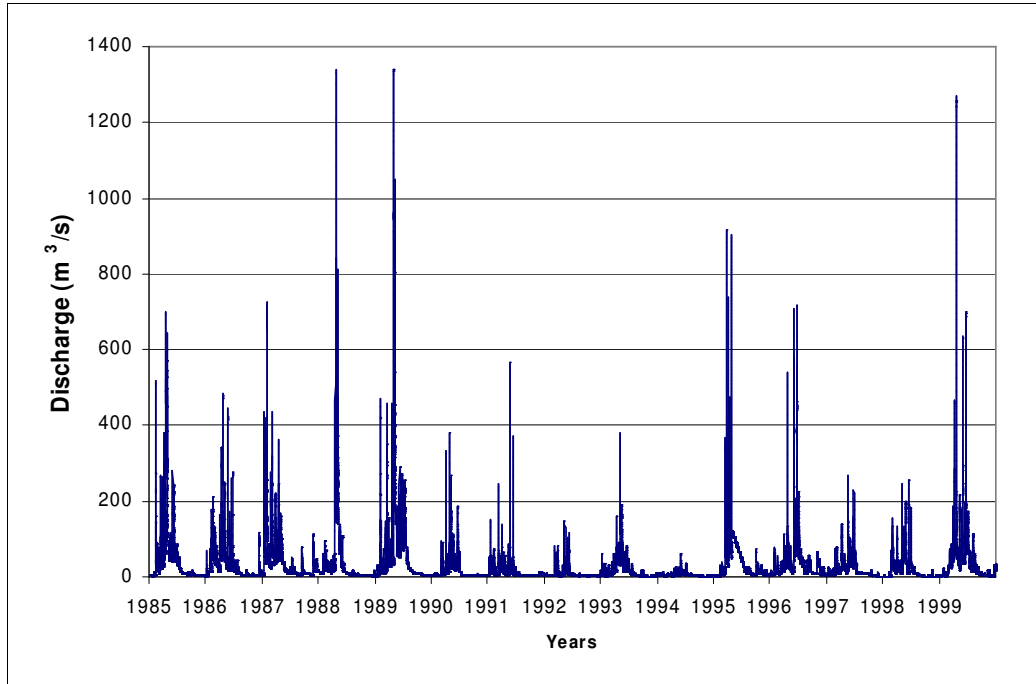


Figure 5.3-10 Pre-dam flows at proposed Jana Dam site

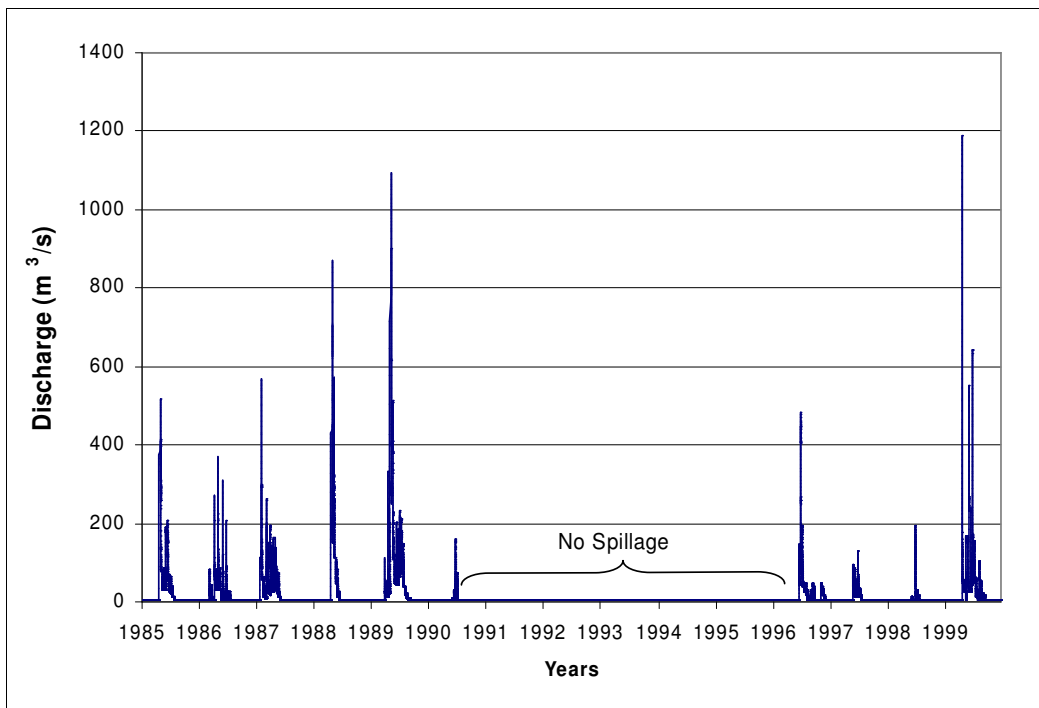


Figure 5.3-11 Post-dam flows at proposed Jana Dam site

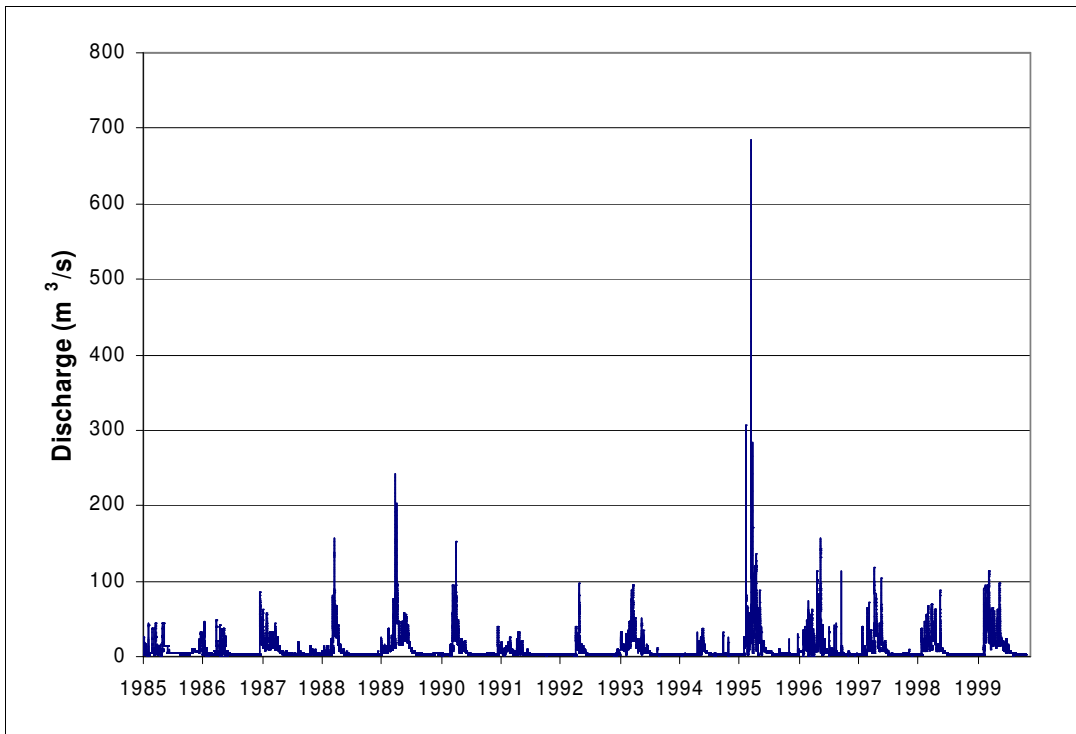


Figure 5.3-12 Pre-dam flows at proposed Mielietuin Dam site

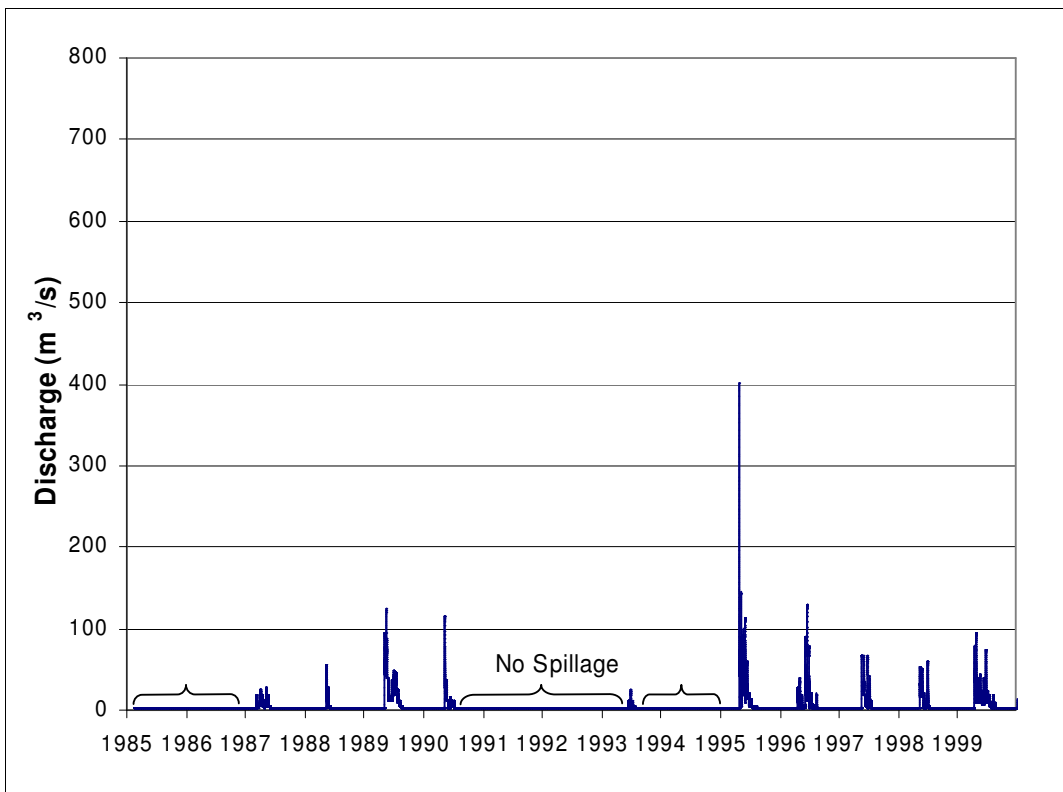


Figure 5.3-13 Post-dam flows at proposed Mielietuin Dam site

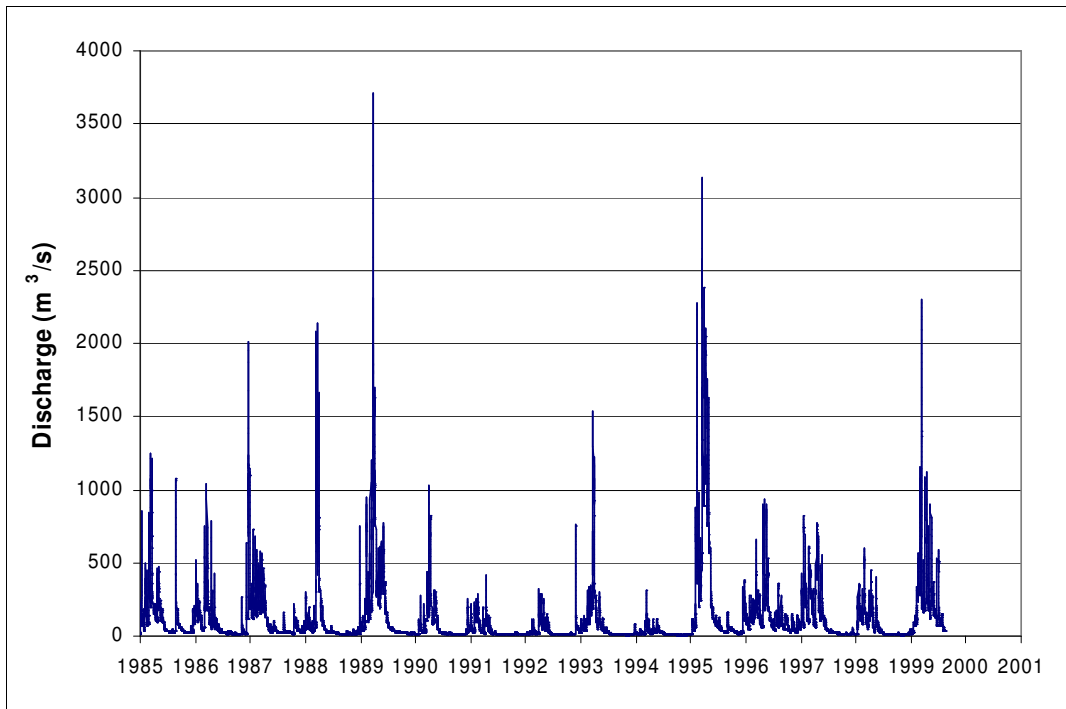


Figure 5.3-14 Pre-dam flows at Thukela Estuary

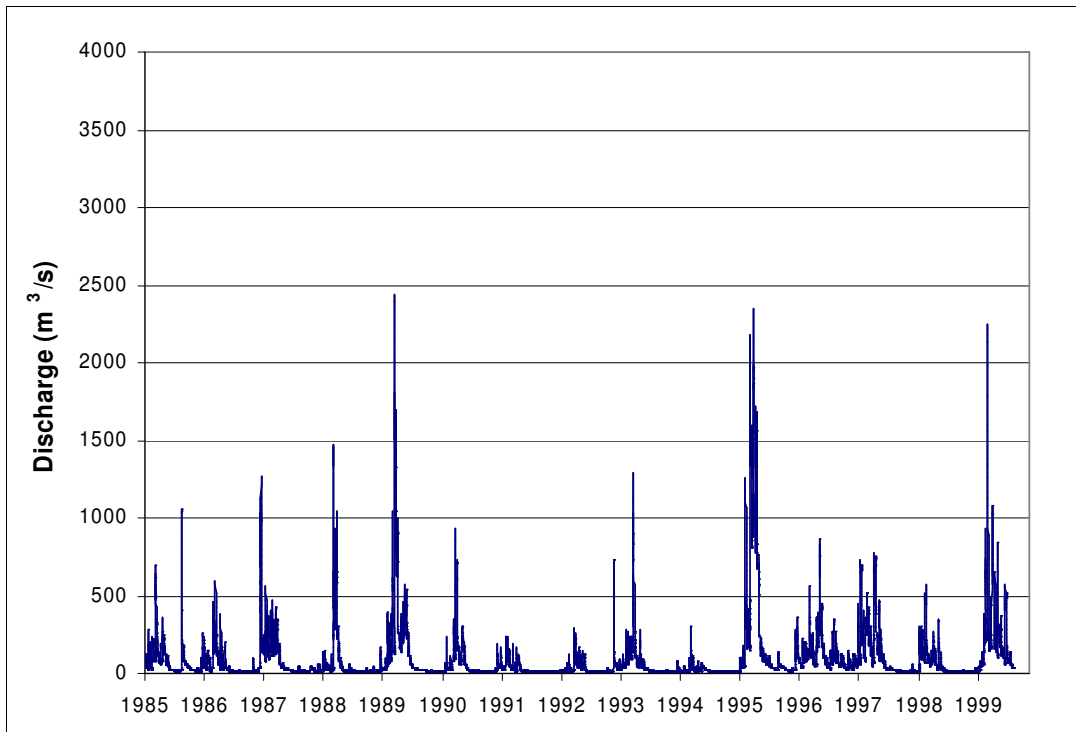


Figure 5.3-15 Post-dam flows at Thukela Estuary

As can be seen from these figures, the dams do not have a very dramatic effect on the flows at the estuary, because they are located relatively far up in the catchment and the incremental downstream

catchment area comprises more than 50% of the total catchment. Immediately downstream of both dams, however, many years would see no flood spillage, which will have to be rectified by the release of freshets and floods down the river.

The present day, as well as post-dam recurrence interval flood peaks, are indicated in Table 5.3-5. The present day recurrence interval flood peaks were determined based on statistical analysis of the complete flow record at gauging station V5H002 (39 years). The post-dam flood peaks were determined by adjusting the pre-dam flood peaks (based on the complete flow record) by a factor based on the reduction in flood peaks during the 15 years simulated as a result of the dam developments.

Table 5.3-5 Pre-dam and Post-dam flood peaks

Recurrence interval (Years)	Present day flood peaks (m³/s)	Post-dam flood peaks (m³/s)
2	1000	850
10	4500	3600
20	6800	5400
50	11000	8700

5.3.2.3 Thukela Estuary Model Set-Up

With the generated flow sequences for different scenarios available the model for the estuary could be set up. Cross-sections were obtained from a survey done by the Department of Water Affairs and Forestry (DWAF) in 1996. The cross-sections were spaced between 200 and 500 m apart (closer at the mouth). The model extends from the John Ross Bridge to the estuary mouth over 13 km. The Manning n-value was taken as 0.042 for the main channel and 0.055 for the more densely vegetated higher ground (see Figure 5.3-16), as obtained from calibrations done in 1990 (Basson and Rooseboom, 1990).

Two sediment fractions ($d_1 = 0.035$ mm and $d_2 = 0.22$ mm) were specified in the bed material (see Table 5.3-6). The first fraction represents the median particle size of bed samples taken in 1990 at the N2-bridge (Basson and Rooseboom, 1990). Fine sediment deposition occurs at the banks in reed beds. Finer material is generally present in the suspended load, which is not always present in the bed since the suspended load generally moves right through the system. It was found that about 50% of the suspended load consists of sediment finer than 0.22 mm, which was represented by fraction 2 during the simulations.



Figure 5.3-16 Thukela Estuary

Table 5.3-6 Graded sediment (as simulated)

	Fraction 1: 0.035 mm	Fraction 2: 0.22 mm
Bed material	5%	95%
Suspended load	50%	50%

The above-mentioned flow sequence together with a time series of sediment loads were introduced at the upstream boundary of the model. The sediment loads were determined with the aid of a sediment load–discharge rating curve obtained from suspended sediment samples taken between 1971 and 1984 at the gauging station V5H002. There was seasonal variability in the suspended sediment samples, with higher concentrations observed at the beginning of the rainy season. For this reason a different rating curve was used between September and December than that for the rest of the year as indicated in Figure 5.3-17.

There is a high variability (between 184 and 559 ton/km².a) in the sediment yields for different parts of the Thukela system found in the literature (Dollar, 2001), but only those applicable at the estuary are shown in Table 5.3-7.

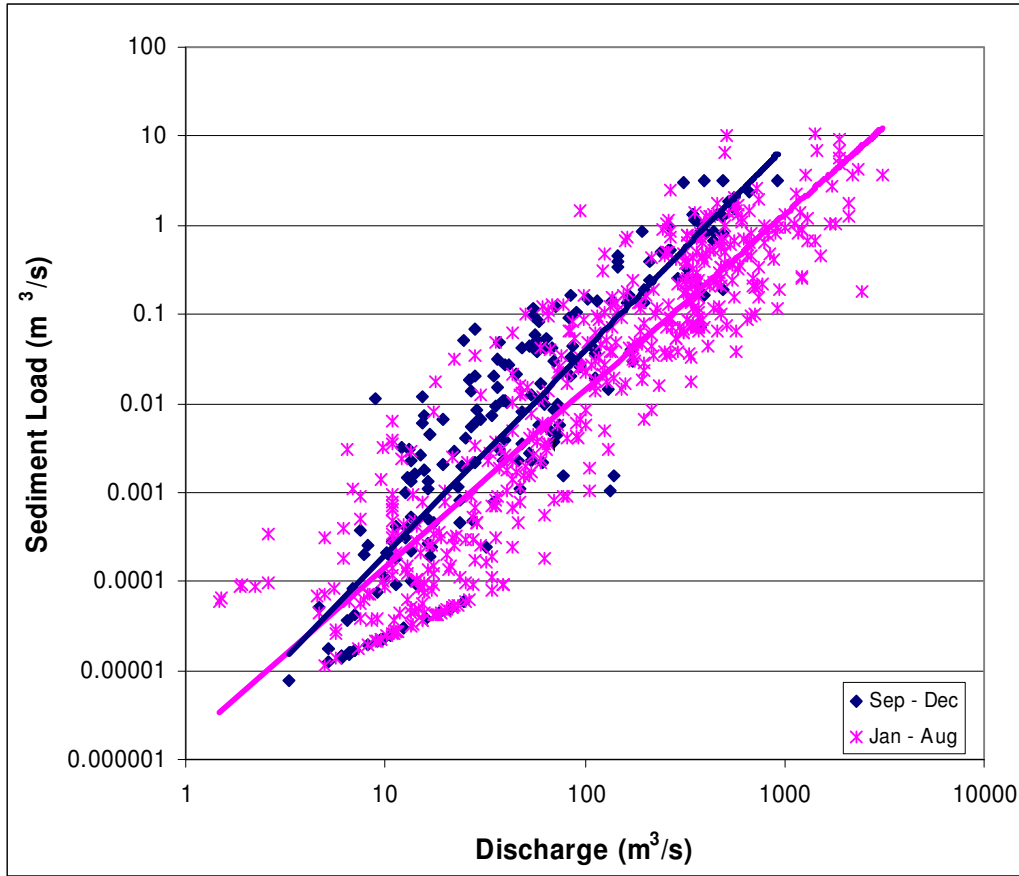


Figure 5.3-17 Sediment load-discharge relationship

Table 5.3-7 Sediment yields

Reference (Dollar, 2001)	Place	Catchment area (km ²)	Yield (ton/km ² .a)
Orme (1974)	Thukela	29046	375
Dingle & Scrutton (1974)	Thukela	29046	427
Flemming & Hay (1983)	Thukela	29046	386
Goodlad (1986)	Thukela	29046	406
Nicholson (1983)	Thukela	29046	390*

*: Average value

The average sediment yield for the lower Thukela obtained from those quoted in Dollar (2001) is about 400 ton/km².a. The sediment yield obtained from the suspended sediment samples is similar at 395 ton/km².a (including 25% for non-uniformity and bed load). A maximum sediment yield of 571 ton/km².a was found by Rooseboom (1992), but this was obtained from samples taken at Colenso, high up in the catchment, which generally has a higher yield than further downstream, and the period was also relatively wet (1950 – 1958). A sediment yield of 400 ton/km².a was adopted. For scenario 5

the sediment yield was increased to 600 ton/km².a, which could occur if increased areas of the catchment come under cultivation as well as with overgrazing.

Due to the fact that the planned reservoirs will trap most of the incoming sediment, the sediment loads also had to be adjusted for scenario 2, because the mean annual sediment load will reduce by up to 27% if all the sediment is trapped in the reservoirs.

The downstream boundary of the model represented a time series of tidal water levels based on tidal constituents at Richards Bay. No sediment input was specified at the downstream boundary since it was assumed that most of the sediment from the ocean would be scoured around the mouth of the estuary, which is included in the model, and that the sediment availability from the ocean is not limited.

The changing geometry of the mouth was not incorporated in the model because it was found that most of the time tidal action dominates the downstream water level, and only at flows of more than 300 m³/s does the river flow begin to dominate, at which stage the mouth should be completely open. Also, should the mouth close, it will not affect the sediment transport in the estuary, since the flows at that stage are very low and the mouth also does not stay closed for long periods.

The simulations were carried out with the one-dimensional MIKE 11 model, whereby the sediment transport and hydrodynamics (fully hydrodynamic) are coupled at each time step, with one minute time steps for the hydrodynamics and two minute time steps for the sediment transport calculations.

5.3.2.4 *Simulation Results*

The current sediment yield of the Thukela River is quite high, at more than 9 million ton/a at the estuary. Under natural conditions the estuary was reported to have been much longer and small boats were able to travel inland for at least 8 km. The flood peak reduction from natural to present day conditions is estimated at 8 percent mainly due to dam development. If the natural sediment yield was 50 % of the current sediment yield of 400 t/km².a, the simulations of the estuary sediment dynamics show that the estuary would have been 8.5 km in length (at 1.2 m above mean sea level taken as high spring tide), almost double its current length (Figure 5.3-18). The length is therefore very sensitive to the sediment yield.

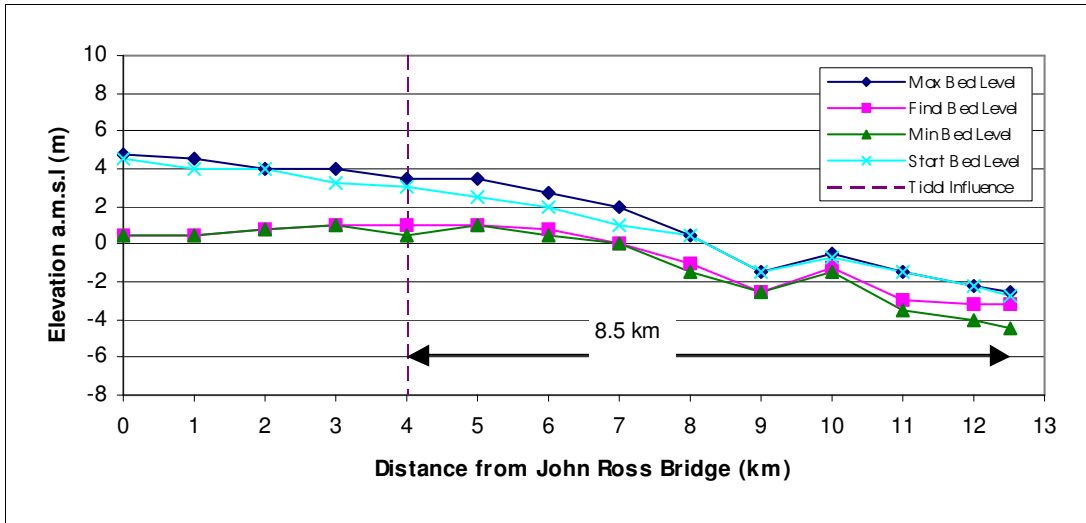


Figure 5.3-18 Thukela Estuary long section under natural conditions (Scenario 0)

The simulations of the present day scenario show very high sediment loads being transported through the estuary (see Figure 5.3-19), although there is a slight decrease in the annual sediment loads towards the mouth. This is probably due to the decreasing velocities as the river enters the estuary, and sediment being deposited. From the bed levels shown in Figure 5.3-20, the same trend can be observed, as some deposition occurs up to 6 km from the mouth. The estuary, however, is in dynamic equilibrium, with the bed levels changing constantly throughout the simulation period (maximum and minimum values are indicated in Figure 5.3-20).

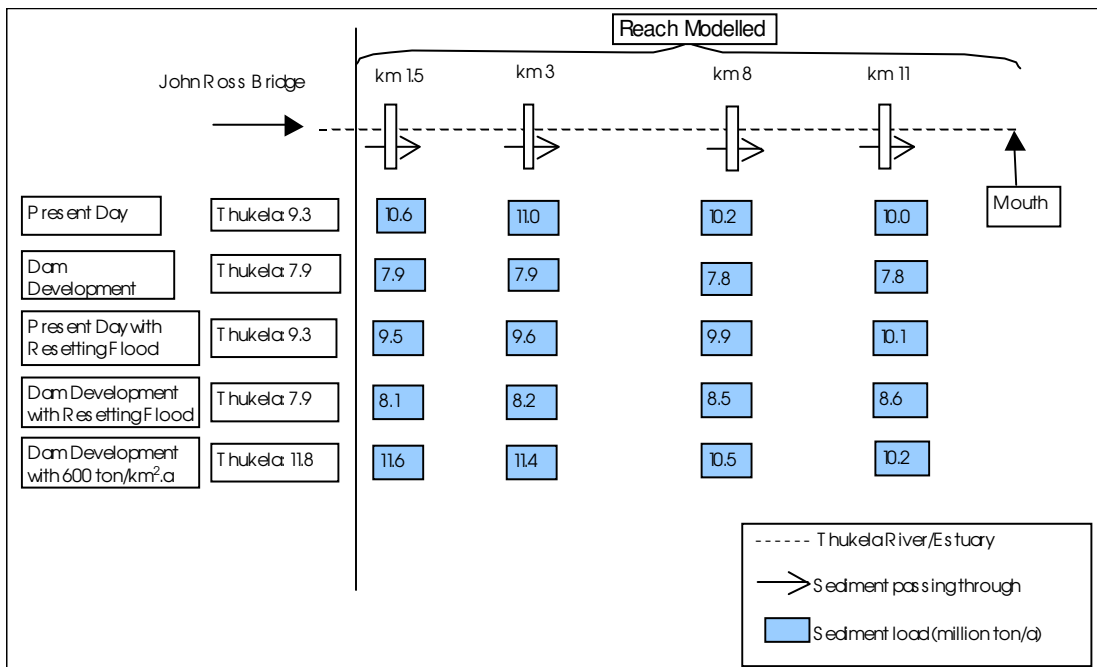


Figure 5.3-19 Simulated long-term sediment balance (Annual sediment loads in million ton/a)

With the Jana and Mielietuin Dams completed the incoming sediment load will of course be reduced, as mentioned before. The effect becomes evident when looking at the simulated annual sediment loads in Figure 5.3-19, which are also reduced by about 36% from the sediment loads under present day conditions. The combination of reduced incoming sediment and flood peaks is the reason why there is no evidence of severe scour or aggradation in the estuary (see Figure 5.3-21). The range (i.e. maximum and minimum) within which the bed level seems to move is also narrower than for the present day scenario. However, this could indicate that a further reduction in streamflow due to further catchment development could lead to aggradation in the estuary, especially if the sediment yield should increase due to changing land use.

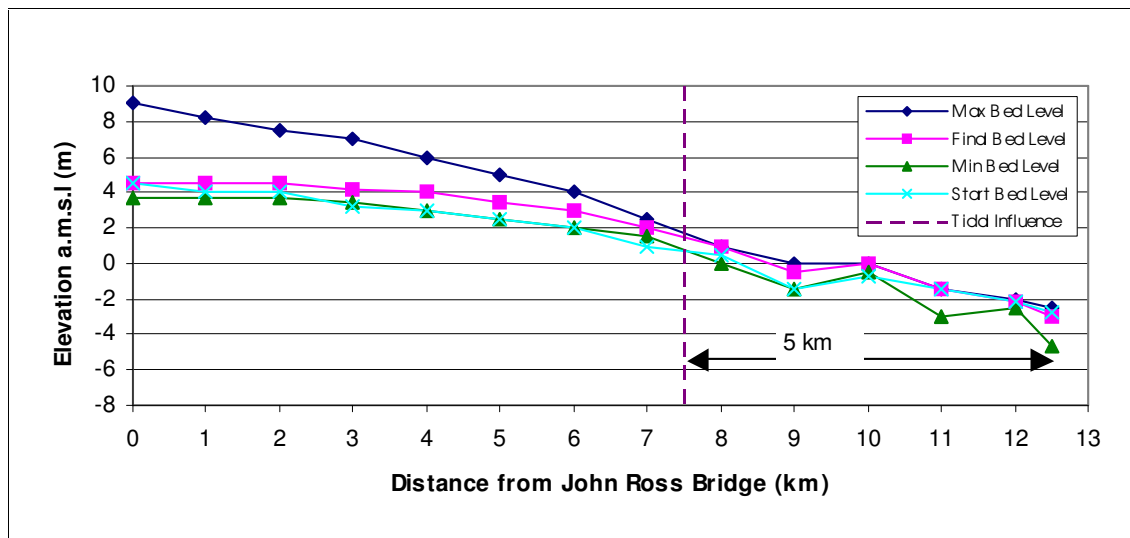


Figure 5.3-20 Thukela Estuary long section under present day conditions (Scenario 1)

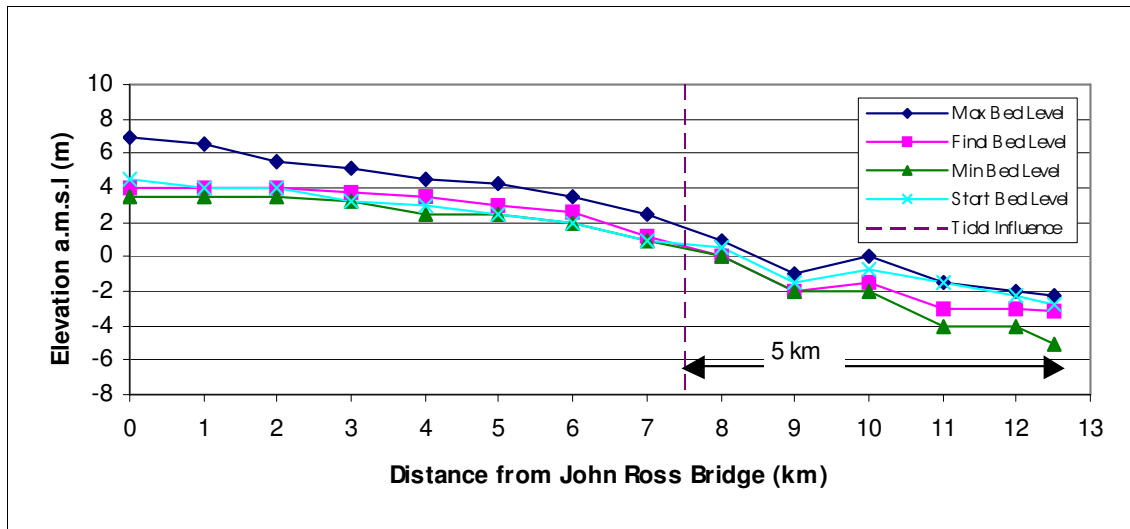


Figure 5.3-21 Thukela Estuary long section under future conditions (Scenario 2)

Simulations of scenario 5 have indicated aggradation of up to 2 m. This means that the estuary becomes somewhat shorter (at a stage only 3.5 km long), but aggradation is confined mainly to the river and the estuary itself will not become much shallower (see Figure 5.3-22 for details). Figure 5.3-19 also shows that the annual sediment loads have decreased by more than 1 million tons at the estuary, indicating that sediment has deposited upstream in the river.

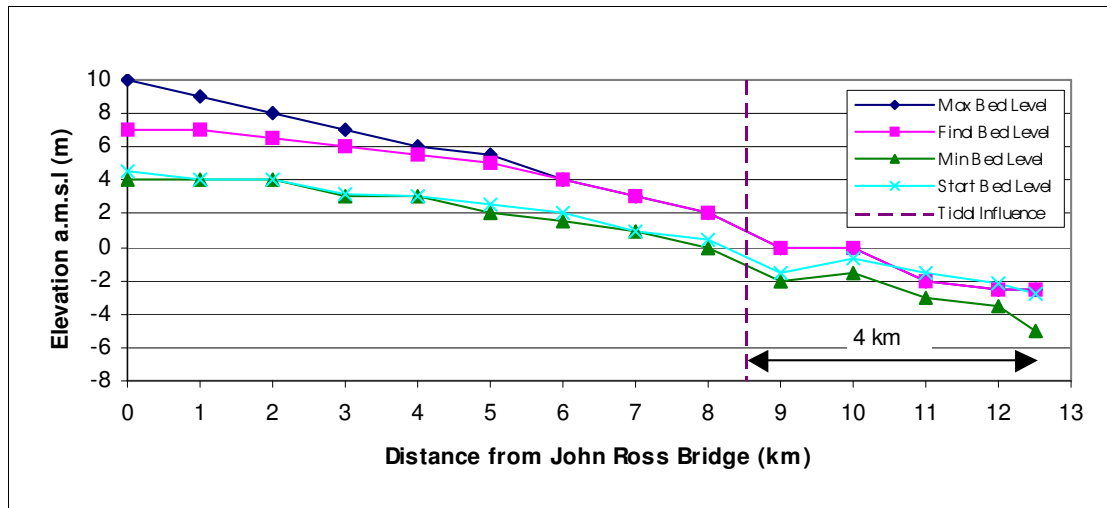


Figure 5.3-22 Thukela Estuary long section under future conditions (Scenario 5)

The length of the estuary (about 5.5 km) does not change very much, varying between 5 and 6 km, for the present day scenario. The same is true for the post-dam scenario (average length 5 km), which is a result of the fact that no dramatic scouring or aggradation takes place for both scenarios.

As mentioned, cohesive sediments were found in the estuary and the simulations have shown that the proportion of fraction 1 could increase dramatically between flood events, but would decrease again during a flood. Under the present day scenario fraction 1 would on average build up from 5 to 60% in the bed, and during the post-dam scenario to about 40%. The amount of cohesive sediment might therefore decrease as a result of dam developments, but there will still be large quantities present. The system is, however, very dynamic and the mean percentage of cohesive sediment in the bed may be as low as 5%. All this is only applicable to the estuary and more than 7 km from the mouth the percentage of cohesive sediment will remain between 5 and 10%.

As a result of the reduction in flood peaks the estuary could become narrower. Based on regime equations developed during a current Water Research Commission study (Beck and Basson, 2003) the estuary could become narrower by about 11% (from present state) and therefore the cross-section width could reduce to around 445 m.

5.3.2.5 Resetting Floods

Since the largest flood during the simulation period is only about a 1:10-year flood, it was important also to investigate what the effect of a large resetting flood, such as the 1:50-year flood, could be on the estuary. These floods are generally not affected to a great degree by dams, but Jana Dam will have a large storage capacity and therefore the flood peak could be reduced. The resetting flood was included in the simulations for both scenarios, right at the start of the 15-year simulation period. The resetting floods for the two scenarios and the corresponding sediment concentrations are indicated in Figure 5.3-23 and Figure 5.3-24.

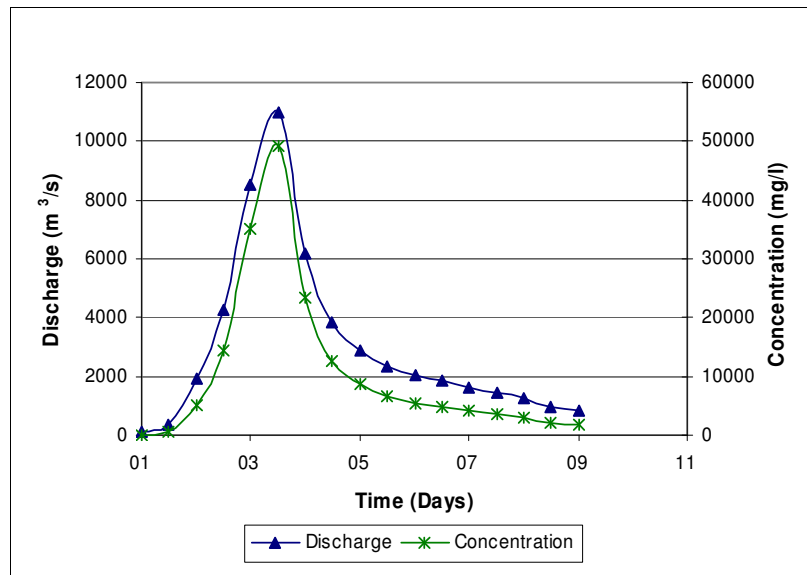


Figure 5.3-23 Resetting flood (1:50-year) for scenario 3

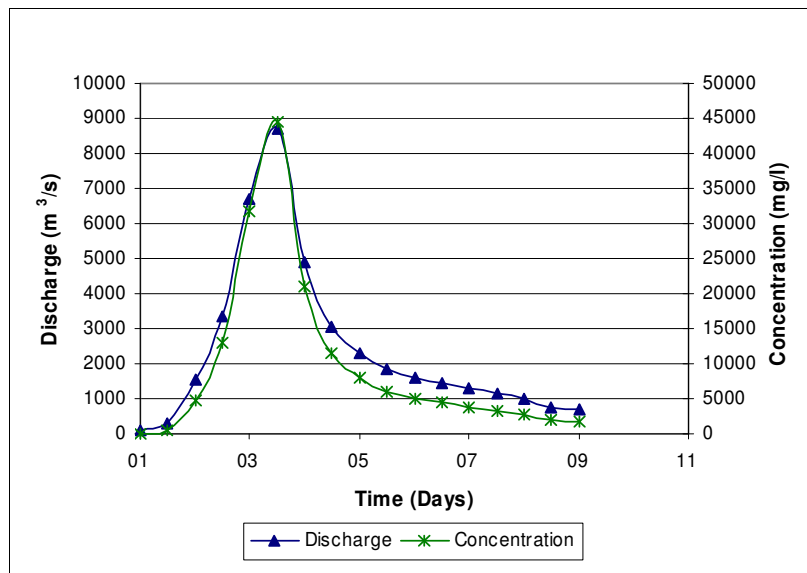


Figure 5.3-24 Resetting flood (1:50-year) for scenario 4

The surprising result was that for both scenarios some aggradation actually takes place immediately after the flood in the upper part of the simulated reach, but severe scouring was observed in the estuary itself closer to the mouth (see Figure 5.3-25 and Figure 5.3-26). The overall effect was that the bed slope increased dramatically during the flood, but returned to normal fairly quickly. It took only a few months to remove most of the sediment, and because the resetting flood carries so much sediment, less sediment is available for the rest of the time and therefore eventually the bed level ends up lower than at the start of the simulations. The fact is that these floods can have a major effect on both the Thukela River and the estuary, but it seems as though the estuary is able to recover to a certain degree.

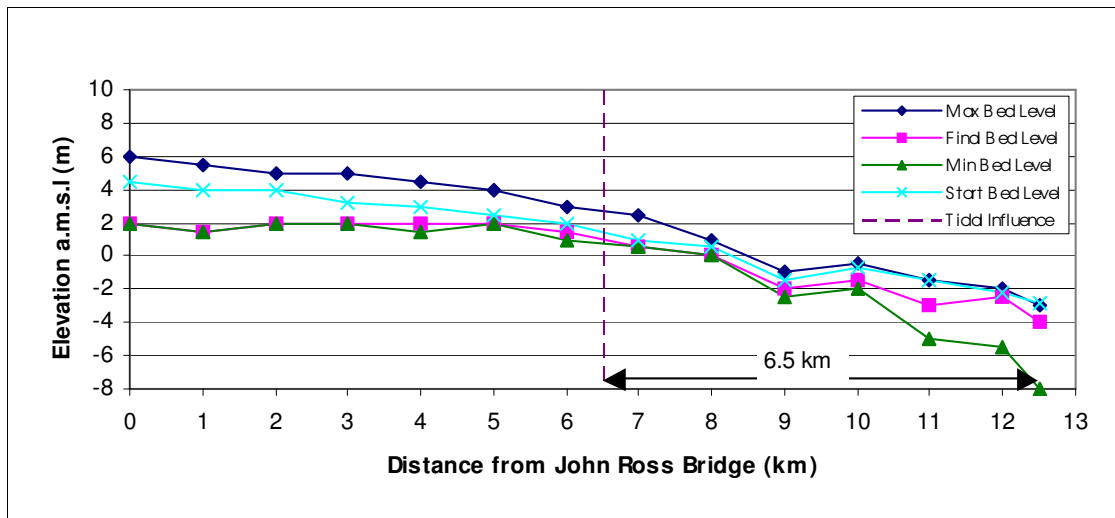


Figure 5.3-25 Thukela Estuary long section under present day conditions with resetting flood (Scenario 3)

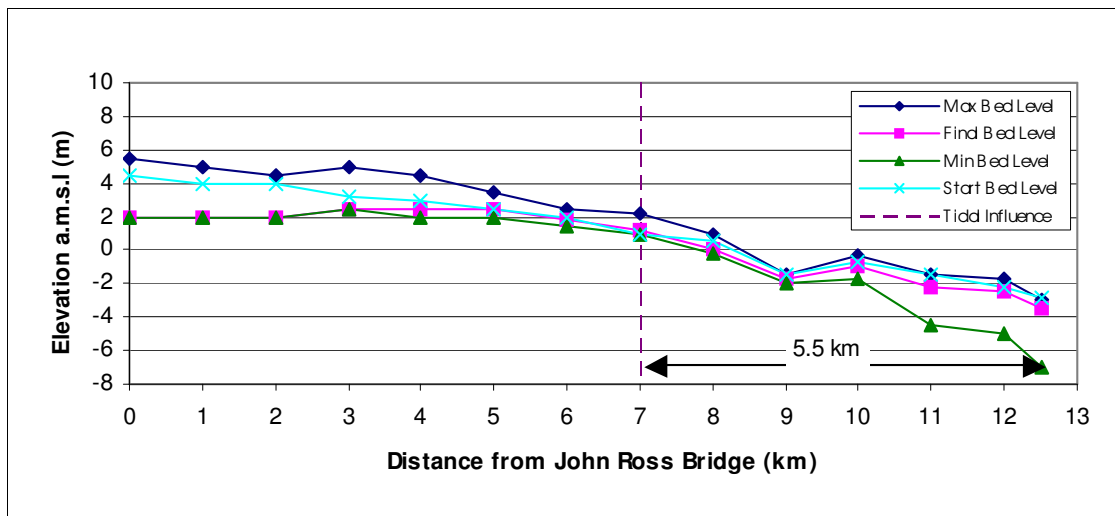


Figure 5.3-26 Thukela Estuary long section under future conditions with resetting flood (Scenario 4)

5.3.2.6 Conclusions

The key findings are:

- A number of large dams have been constructed high up in the catchment. Their effects on floods and sediment dynamics at the estuary are, however, minimal. The decrease in flood peaks at the estuary from natural to present day condition is estimated at 8%, while from present day to post-dam conditions the average peak discharge decreases a further 19%.
- The estuary sediment dynamics are in dynamic equilibrium under present day conditions. Simulations for the post-dam (worst case) scenario also indicate dynamic equilibrium of the fluvial morphology similar to present day conditions.
- The typical present-day (pre-dam) estuary length is 5.5 km, while the future post-dam length will be 5 km.
- Flood attenuation, caused by the proposed dams, will decrease the estuary width by about 11% from present state, equivalent to 55 m on a 500 m wide cross-section.
- If the sediment yield from the catchment increases in future, it would shorten the estuary which will become shallower.
- The role of the large resetting floods is important in scouring the river mouth, especially previously deposited cohesive sediments. Regular floods are therefore required to limit possible consolidation of cohesive sediment.

5.4 Summary

The objective was to investigate the slow rate of sedimentation due to tidal flows and also the flushing effects of large floods. An integrated approach of selected field measurement techniques combined with appropriate modelling techniques was thought to be the most efficient route to achieve this. In the long-term it is not affordable to do extensive field measurements at many SA estuaries. Thus, limited key field data should be collected and, using this as input, use can be made of mathematical models to simulate estuarine sediment dynamics and to predict the consequences of changes in the system or impacts of management actions.

The modelling shows that the sediment balance in the estuary relies on a delicate balance between dominant flood and ebb tide flows. It is therefore not correct to simply conclude that sedimentation occurs upstream due to the stronger flood tide since the cross-sections and durations of flow differ during the two tidal phases.

One-dimensional, long-term modelling also proved that it is very difficult to ascertain whether net sediment movement is upstream or downstream. Several factors seem to play an important role, such as the general characteristics of the estuary and whether the estuary is in a stable state. What became obvious from the modelling is that floods play a very important part in estuarine sediment transport processes. Large floods are capable of removing vast amounts of sediment from an estuary and are necessary to keep the upstream ingress of marine sediment and the accumulation of catchment sediment in check. However, these floods have to occur on a regular basis, or at least smaller floods have to occur between large magnitude flood events, otherwise the sediments, especially the cohesive sediments, will have time to consolidate. This means that it will be difficult to remove these sediments.

6. Closed Mouth State: Mouth Breaching and Flushing Efficiency

6.1 Introduction

Many estuaries in South Africa are only open to the sea intermittently. The environmental quality of these estuaries is determined largely by the frequency, duration and timing of open mouth conditions. Unfortunately they are at present often closed more frequently and for longer periods than in the past and their environments have deteriorated.

Open mouth conditions in large estuaries are mainly maintained by tidal flows. However, in smaller estuaries, it is commonly the river flow that keeps mouths open. Reduced river flow is therefore the primary reason why estuaries are closed more now than in their former natural states.

The ever-increasing reports of sedimentation problems in South African estuaries lead to calls for increased flushing of these estuaries and mouth breachings, both natural and mechanical, in order to remove the sediments. However, breachings have occurred at water levels in the estuary that are too low, which have a negative effect on the flushing efficiency.

The harmful effects of artificial mouth breachings at water levels lower than those at which natural breachings would occur, have already been discussed in an earlier chapter and later in this report the results of investigation to quantify these effects will be presented.

Before attempting to investigate the mouth breaching process of estuaries it is important firstly to understand which factors play a role in:

- determining the size of the mouth,
- keeping the mouth open, and
- closure of the mouth.

6.2 Effects of Reduction in River Flow on Mouth Closures

The ecological health of small, temporarily open estuaries strongly depends on the frequency and duration of mouth closures. Reliable data on open-mouth conditions in the past is not available for many estuaries, but it is perceived that many small estuaries are now closed for much longer periods than in the past.

Open-mouth conditions at small estuaries are principally maintained by river flow and especially by base flow. A reduction in minimum base flow therefore commonly results in an increase in closed mouth conditions.

Some estuaries, which were naturally open for most of the time, have now, because of reduced river flows, changed into estuaries that are commonly closed. The Seekoei Estuary is such an example. There are no major dams in the catchment of the Seekoei River, but many small farm dams are present. These dams normally do not affect high flows in the river, but they have almost completely cut off the low flows. As a result, the occurrence and duration of open mouth conditions has been reduced drastically, seriously affecting the ecological conditions in the estuary.

In many rivers base flow has also been drastically reduced because of evapo-transpiration by alien vegetation in the catchment and especially along the river beds. Removal of alien vegetation, as part of the working for water programme, can lead to an increase in base flow, and can therefore also result in an increase in open mouth conditions for some estuaries.

The base-flow required to keep an estuary mouth open is different for each estuary. The extent to which the mouth is protected against direct wave action is a controlling factor. The Umgeni Estuary near Durban, for example, closes even at spring tide and at a river flow of $10 \text{ m}^3/\text{s}$, whereas the Great Brak Estuary normally stays open without river flow at spring tide, and a flow of about $0.5 \text{ m}^3/\text{s}$ often keeps it open over neap tide (CSIR, 2000).

Another important aspect is the size of the estuary. The larger the estuary, the more the mouth is kept open by tidal flows.

The flow required to maintain an open mouth in an estuary, because of the importance of an open mouth for the ecological conditions, forms a crucial component of the environmental flow requirements of temporarily open estuaries. It therefore also needs to be included in the determination of the environmental reserve for these estuaries according to the National Water Act (No 36 of 1998).

In general, no simple relationship exists between river flow and mouth conditions, because of the specific flow requirements for each estuary to keep it open. Daily data on mouth openings and closures and continuous river flow data need to be collected to determine this relationship for each estuary. Continuous water level recordings normally automatically provide information regarding mouth openings and closures and it is therefore strongly recommended that water level recorders be installed in all the important temporarily open estuaries in South Africa.

6.3 Field Investigations

6.3.1 Objectives

Field investigations during breaching were carried out at Klein River and Groot Brak River as part of a recent WRC project (Beck *et al*, 2004) to investigate the mouth breaching processes in greater detail. The data collected during these field investigations were mainly used to calibrate and verify mathematical or physical models. The following aspects in particular were of interest:

- The effect of the height of the water level in the estuary when breaching occurs (as well as possibly the effect of the sea water level), which will influence the flushing efficiency.
- Changes in the mouth geometry during breaching.
- The final mouth geometry.
- Possible flushing/removal of sediments upstream of the mouth resulting from mouth breachings.

6.3.2 Fieldwork at Klein River

Fieldwork at the Klein River Estuary was conducted from 28/09/2001 to 29/09/2001 during neap tide. Measurements during the breaching included:

- Water levels in the estuary (see Figure 6.3-4).
- Water levels and flow measurements in the river (at the DWAF gauging station).
- Cross-section survey before and after breaching (see Figure 6.3-5).
- Mouth scouring over time (see Figure 6.3-6).

The berm between the estuary and the sea was breached by excavating a relatively small channel through the berm. The channel geometry initially changed very slowly, becoming first deeper then wider, with greater changes starting to take place after a few hours. After the width had begun to stabilise, the point of hydraulic control migrated upstream and the channel became longer. Water levels in the estuary remained relatively stable for the first few hours, and therefore the total volume only decreased slightly over this period. In consequence, the erosion potential also remained high (until major changes had occurred), since the energy gradient and the velocities were high. Once the channel had significantly adjusted its depth, the energy gradient gradually decreased. As the channel deepened the banks caved in occasionally. However, the greatest width changes took place after the equilibrium depth was reached. By increasing the width and depth and reducing the energy slope, the sediment transport capacity of the channel was eventually reduced until little further erosion could take place. The relationship between the final depth and the discharge is undetermined, as it is very

difficult to determine the depth during or just after high outflows occur. Both mobile and stationary bedforms appeared to be fairly large and distinct at certain times. Due mainly to the long duration of the breaching process, differences in water levels upstream (i.e. in the estuary) and downstream of the mouth (i.e. in the sea) are of lesser importance. It is likely that even if a wide section of the berm is overtopped, as could sometimes happen during a natural breaching event, at first a smaller/narrower channel will probably form.

Figure 6.3-1 to Figure 6.3-3 illustrates the mouth opening process at the Klein River Estuary.



Figure 6.3-1 Start of breaching at Klein River Estuary (September 2001)



Figure 6.3-2 During breaching at Klein River Estuary



Figure 6.3-3 One day after breaching at Klein River Estuary

From Figure 6.3-4 it can be seen that for about 6 hours after breaching, the water levels in the estuary remained virtually constant. The levels then dropped rapidly during the following 5 hours. At about 12 hours after the breaching, the effect of the sea tide was already discernable inside the estuary mouth. During the next day (29 September), the water levels within the estuary gradually dropped until they were close to the levels determined by tidal levels in the sea. Obviously, the water levels closer to the mouth responded much quicker than the levels further upstream (inland) in the estuary.

From Figure 6.3-5 it can be seen that the lowest point in the berm crest was at an elevation of about +2.5 m MSL. The top width of the final mouth opening was close to 300 m, while the width at MSL eventually reached about 150 m. The bottom of the final mouth section could not be surveyed, but from the available survey data, it appears that the bottom was at an elevation of between about -1 to -2 m MSL after most of the floodwater had drained from the estuary. The maximum depth of scouring during the flood could of course have been deeper.

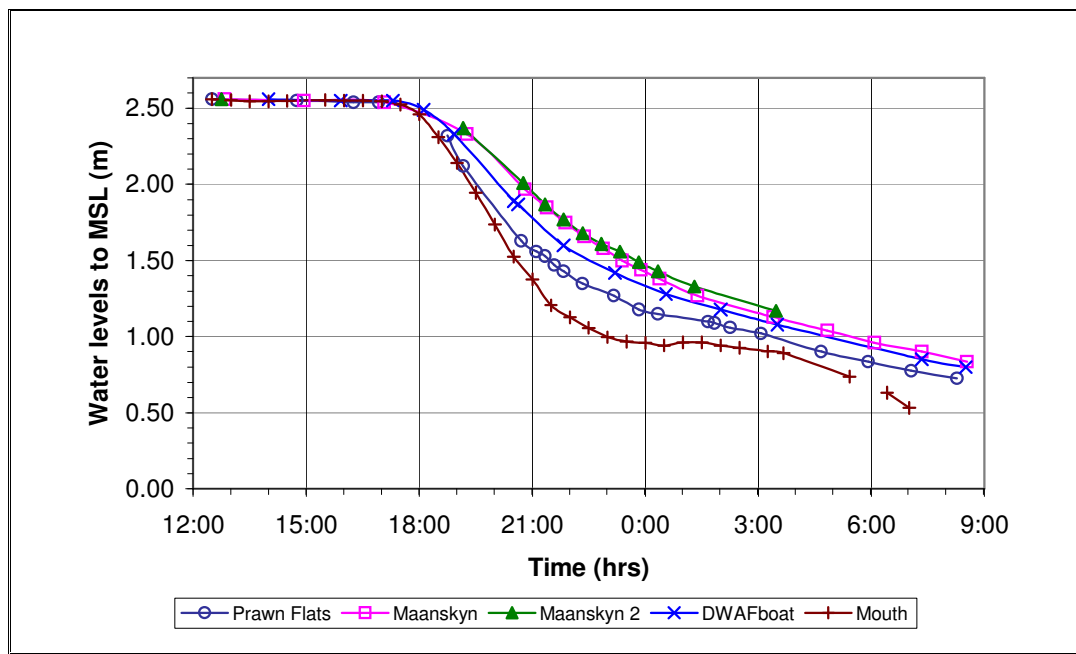


Figure 6.3-4 Measured water levels during breaching of the Klein River Estuary (September 2001)

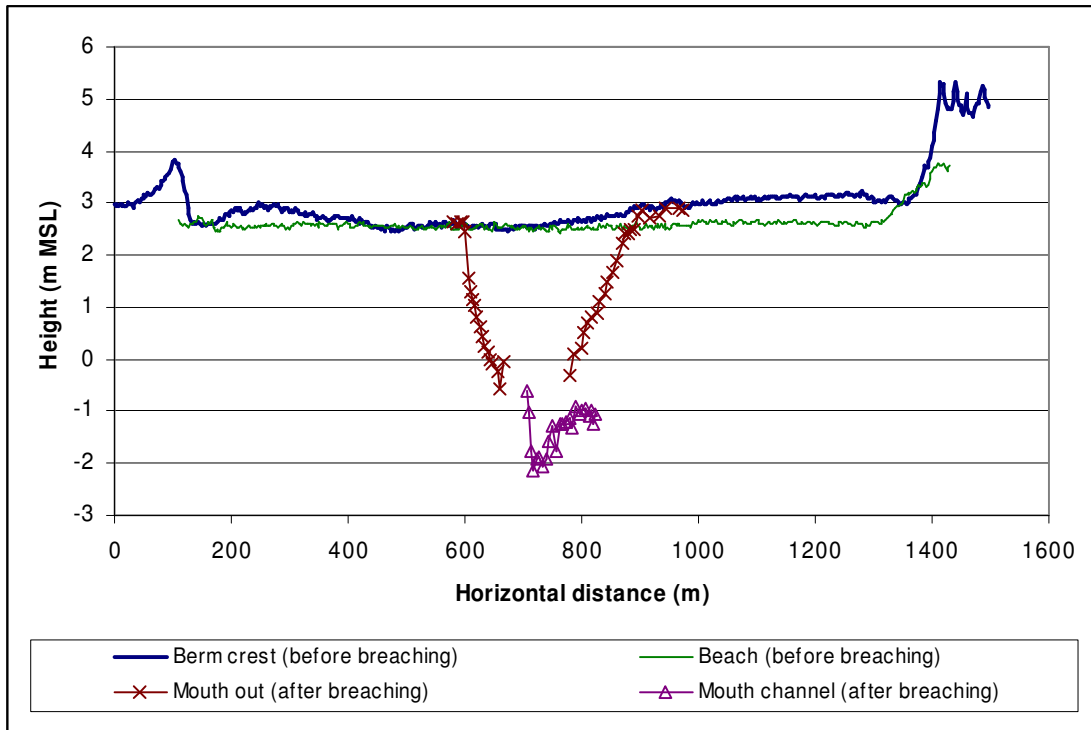


Figure 6.3-5 Cross-sections showing topography before & after breaching

For 4 hours after the initial mouth breaching, the mouth width slowly expanded, at a gradually increasing expansion rate. During about the next 3 hours there was a large increase in the mouth expansion rate and the highest rate of lateral erosion was attained. Thereafter the mouth expansion rate gradually decreased, becoming quite low about 14 hours after the breaching (see Figure 6.3-6).

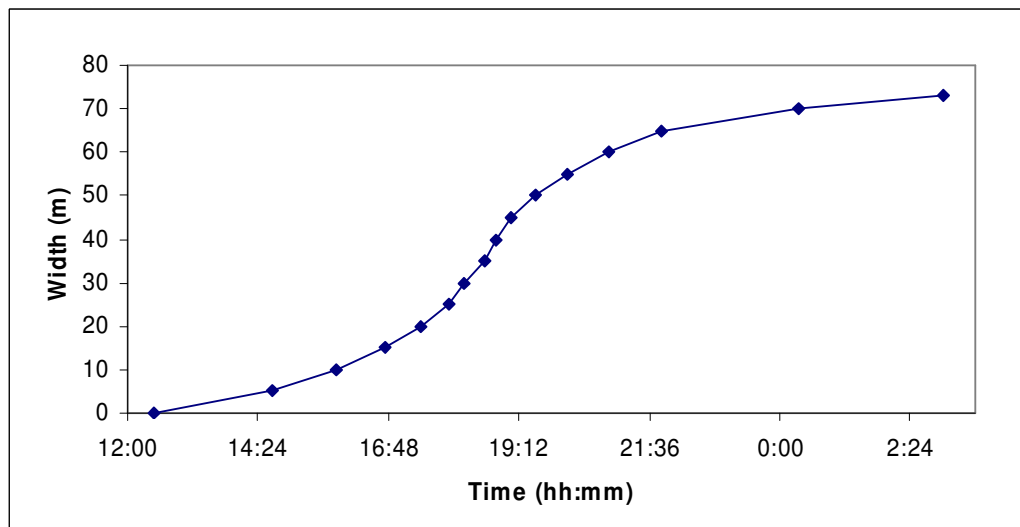


Figure 6.3-6 Mouth expansion over time at Klein Estuary during 2001 breaching

6.3.3 Fieldwork at Groot Brak River

The fieldwork at the Groot Brak River Estuary was conducted from 13/09/2001 to 15/09/2001 during neap tide (see Figure 6.3-7 and Figure 6.3-8). Some of the measurements included:

- Water levels in the estuary during the breaching.
- Water levels and flow measurements in the river (at the DWAF gauging station).
- Mouth scouring over time.



Figure 6.3-7 Photo sequence of the breaching of Groot Brak River, South Africa (September 2001)



Figure 6.3-8 One day after breaching at Groot Brak River

Water levels in the estuary were recorded by means of three graduated staffs as well as from a continuous DWAF recorder located on a train bridge across the estuary (number K2H004). The rate at which water levels dropped in the estuary, gradually increased from the initial breaching for 3 hours thereafter. From then onwards, water levels dropped rapidly for the next 4 hours (see Figure 6.3-9).

Figure 6.3-10 clearly shows a slow rate of scouring after breaching took place, then acceleration as the mouth expands and the scouring increases due to an increase in the flow rate through the mouth. The scouring rate then decelerates as the flow rate decreases and scouring capacity decreases.

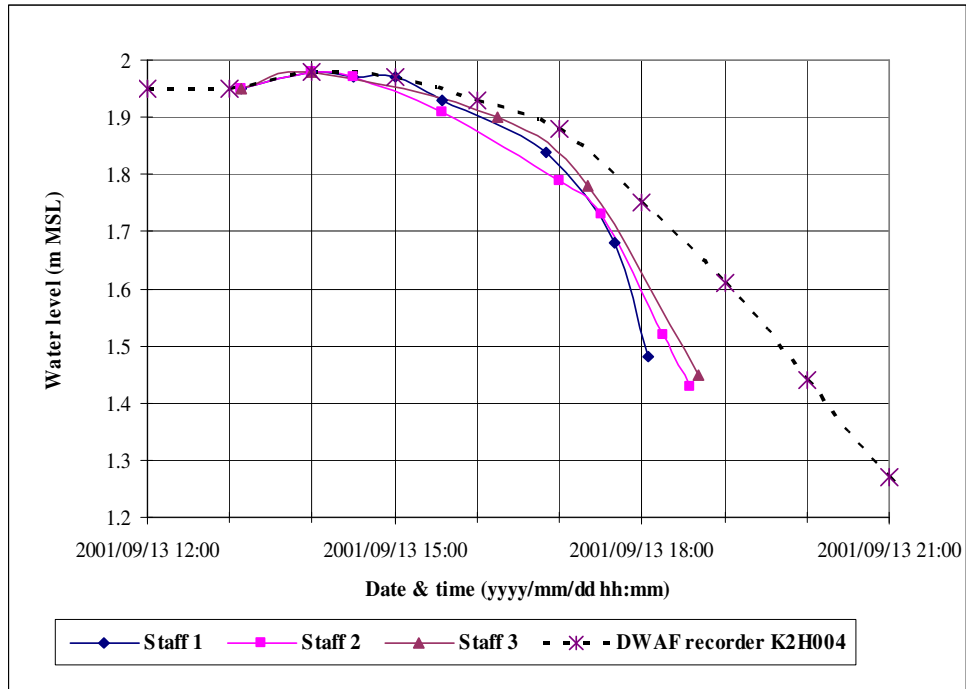


Figure 6.3-9 Water levels during breaching at Groot Brak River (September 2001)

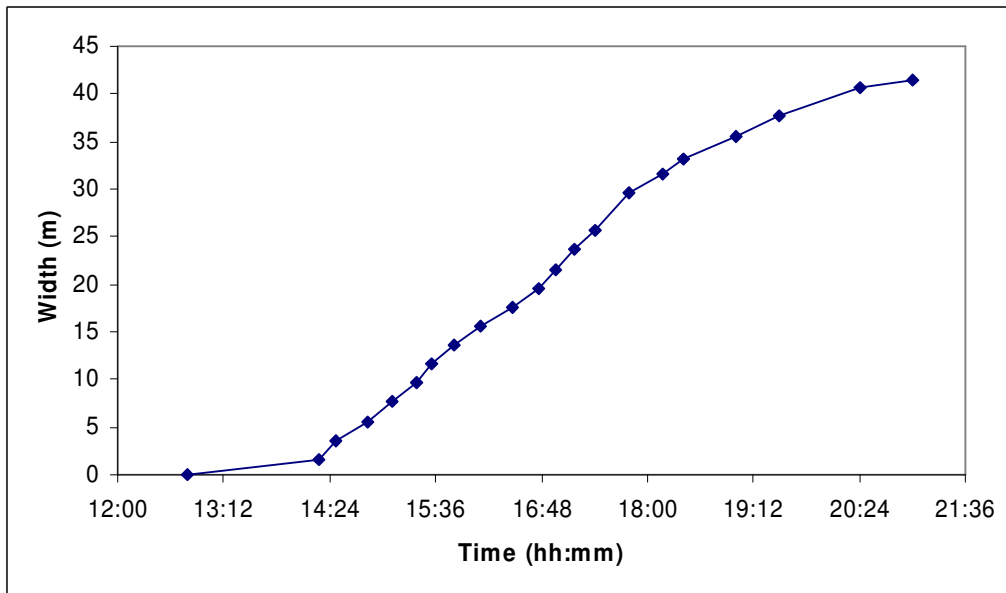


Figure 6.3-10 Mouth expansion with time at Groot Brak River (September 2001)

6.3.4 Conclusions

The field data obtained from the Klein River shows that due to its larger size, coupled with the significantly larger amount of sediment to be flushed, it takes much longer for flushing to become

effective than for the Groot Brak River. The volume of the Groot Brak Estuary is much smaller and as such the water levels drop faster when breached, whilst the volume of sediment to be flushed is also much less than at the Klein River. Also, a channel is usually excavated at the mouth of the Groot Brak River prior to breaching which facilitates the breaching process. From Figure 6.3-4 and Figure 6.3-9 it can be seen that it took about four hours before the water levels started dropping at the Klein River, whereas it only took one hour at the Groot Brak River. The time it took for the breaching itself was much longer (more than 10 hours) at the Klein River than at the Groot Brak River (8 hours). The long duration could create a problem, as the tide that moves into the estuary could disrupt the breaching process. From Figure 6.3-4 it can be seen that at the mouth the water level could not drop for a few hours whilst the tide pushed into the estuary. At the Klein River this does not pose much of a problem, as the discharge through the mouth during breaching is quite high ($> 100 \text{ m}^3/\text{s}$), which is much higher than the normal tidal flow. However, in a smaller system such as the Groot Brak Estuary, the incoming tidal flows could prevent the mouth from properly being flushed open. For this reason it is important not only to get the timing of the breaching right (as to prevent the tide from interfering with the breaching) but also to make sure that the initial, excavated flushing channel is sufficiently large. If the initial channel is too small, it will take some time and also a certain volume of water to flush the channel open before an efficient flushing discharge can develop.

More detailed investigations into the effect of the initial water level at the start of breaching, as well as the mouth geometry during breaching were investigated with the aid of a physical model (Section 6.4), and later with a mathematical model (Section 6.5).

6.4 Physical Modelling

6.4.1 Objectives

The ever-increasing reports of sedimentation problems in South African estuaries have led to calls for increased flushing of these estuaries and mouth breachings, both natural and mechanical, in order to remove the sediment. However, many breachings have occurred low water levels in the estuaries, which were too low, which had a negative effect on the flushing efficiency.

A physical model study was undertaken to investigate the mouth breaching process of an estuary in greater detail. The following aspects were of particular interest:

- The effect of the height of the water level in the estuary when breaching occurs, as well as the effect of the sea water level, which will influence the flushing efficiency.

- The changes in the mouth geometry during breaching, the rate of erosion, as well as the final mouth geometry.
- Relationships to predict the equilibrium scoured mouth geometry.

The data collected during these experiments were used to calibrate and verify a mathematical model (see Section 6.5.2) in order to do a more thorough investigation than possible with the physical model, and once calibrated such a mathematical model was used with reliability to model field conditions (Section 6.5.3).

6.4.2 Model Setup and Procedures

The model was loosely based on the Klein River estuary at Hermanus in terms of the average slopes of the berm, the berm height and the discharges observed during breaching. The scale of the model was approximately 1:50, constructed in a flume 2 m wide by 18 m long in the Hydraulics Laboratory of the University of Stellenbosch (Figure 6.4-1 and Figure 6.4-2). The average slope of the berm upstream (land side) was 1:100 (V:H) and the downstream (ocean side) slope 1:20. Berm levels of between 1 and 3 m MSL were used and the berm sediment had a median diameter (d_{50}) of 0.15 mm. The inflow and outflow were measured with 90° V-notch weirs. Water levels upstream and downstream were recorded continuously with probes and data were logged on a computer. A video camera was installed above the flume to record each experiment and a grid (250 x 250 mm) was suspended a short distance above the water surface in order to determine the rate and direction in which the flushing channel was formed.

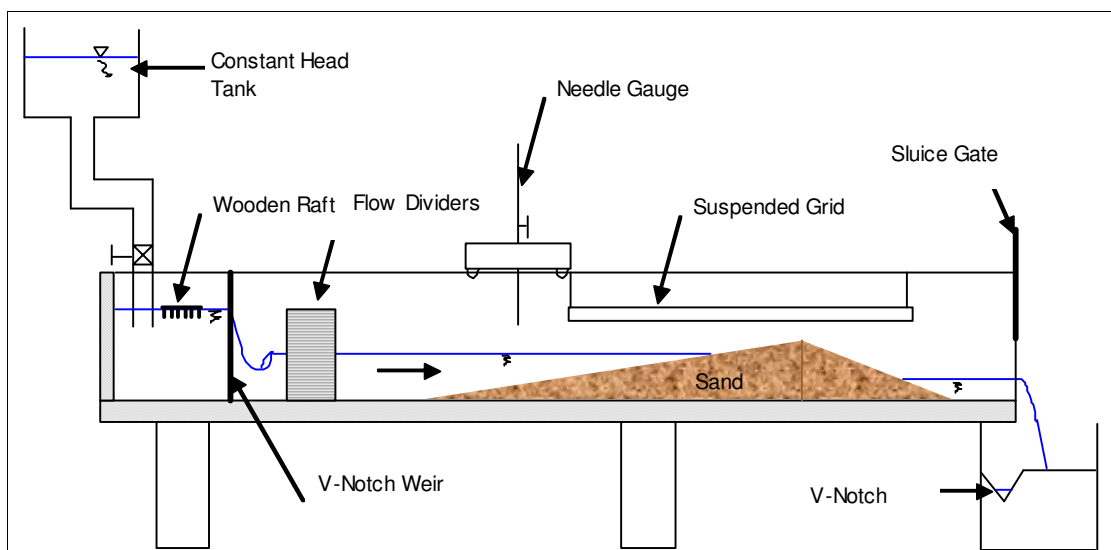


Figure 6.4-1 Experimental layout

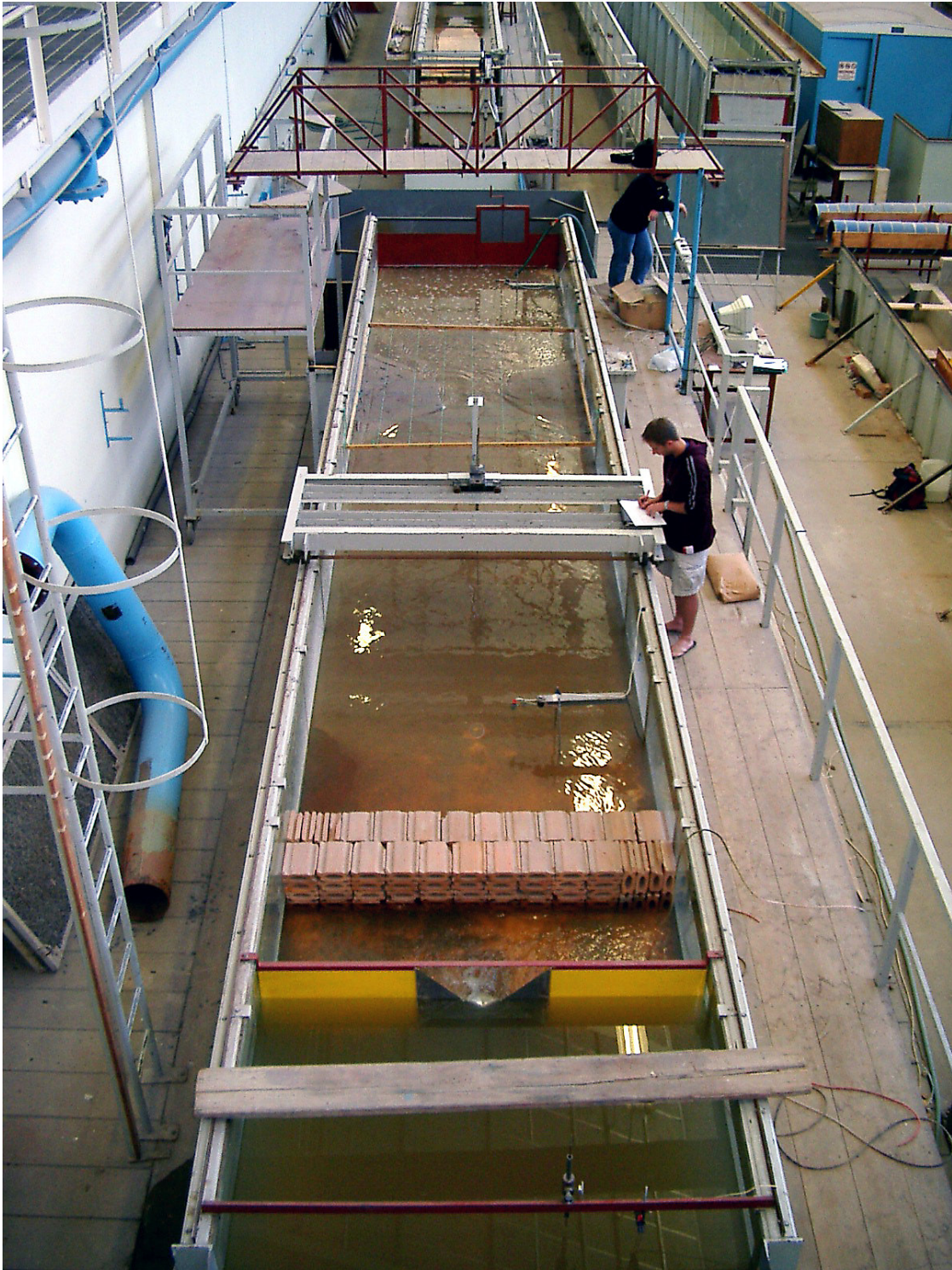


Figure 6.4-2 Flume for flushing experiments, University of Stellenbosch laboratory

The procedure was as follows:

- Sand was placed in the flume at a pre-determined berm height and slope (see Figure 6.4-3 and Figure 6.4-4). All measurements were taken relative to a pre-determined and fixed level, representing “mean sea level” in the setup.
- Water was then pumped in up to a certain level downstream, representing the mean water level in the sea and kept constant throughout the experiment. This is not completely correct since the level changes with the tides, but the flushing channel forms very quickly in the field and the water level would not change much during that time.
- The upstream water level was then slowly raised until it just started overtopping the berm at the lowest point of the berm. The lowest point was always in the middle of the berm, so that widening of the inlet channel could occur without being affected by the flume’s side walls. As the mouth (berm) was flushed open the inflow was increased up to a certain predetermined discharge after which the inflow was kept constant. Initially it was thought to keep the upstream water level constant, but as the mouth opens the water level drops dramatically and the inflow would have to be increased significantly to keep the water level constant, which is not realistic. For the Klein River Estuary (CSIR, 1999) a definite relationship was found between the water level at which breachings have taken place in the field and the maximum discharge observed (Figure 6.4-5). Therefore, in order to simulate breaching of the mouth at a certain upstream water level, the inflow was raised to the discharge corresponding to that water level, and held constant until equilibrium was established.
- The experiment was run until equilibrium scour conditions had been reached, i.e. the width, depth, and the position of the upstream hydraulic control remained unchanged.
- Water surface and bed profiles were measured throughout the duration of the experiment with a needle gauge. Surface velocities were measured by timing the movement of small wooden floats.

Thirteen experiments were carried out with:

- maximum discharges varying between 2 and 30 ℓ/s (35 – 530 m^3/s in prototype),
- upstream water levels varying between 0 and 0.06 m (+3 m MSL in prototype) above “mean sea level” in the model, and
- downstream water levels varying between 0 and 0.03 m (+1.5 m MSL in prototype) above “mean sea level” in the model.

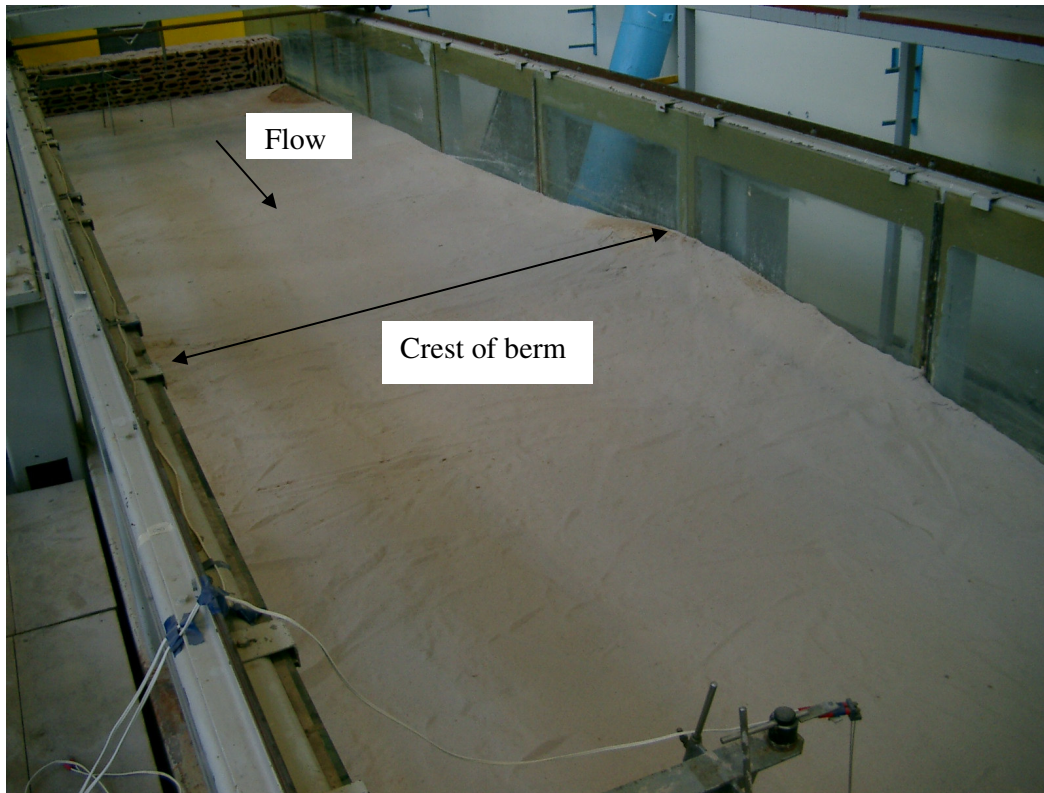


Figure 6.4-3 Initial berm (looking upstream)

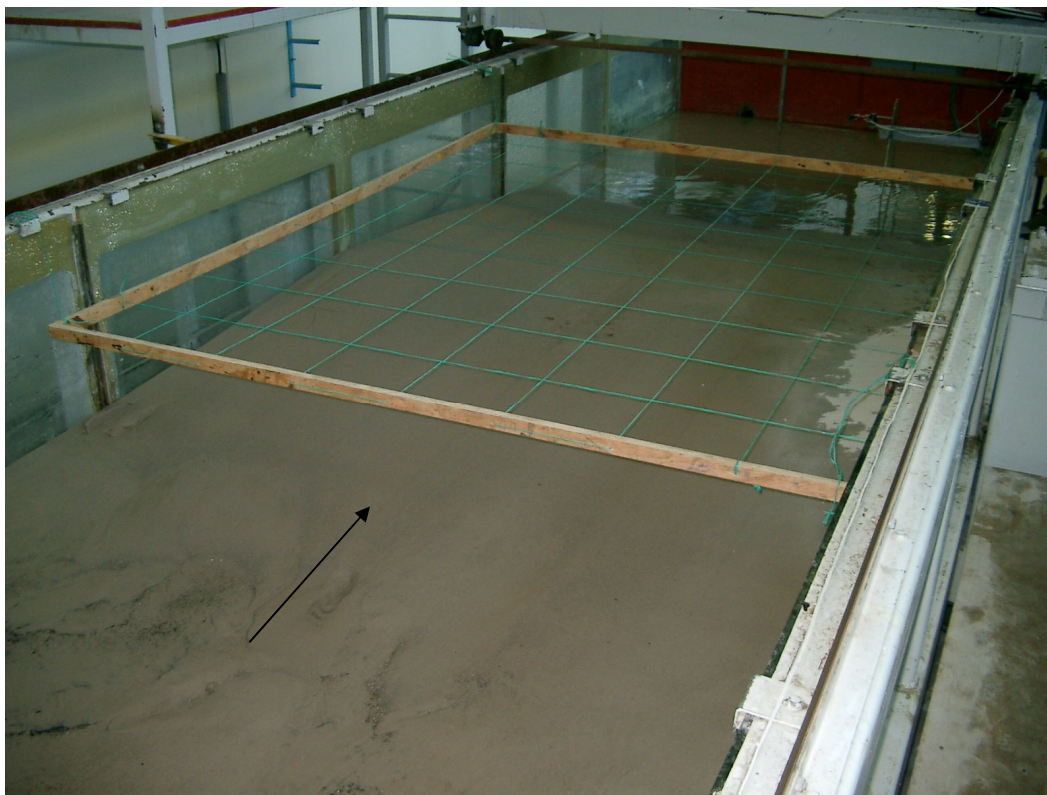


Figure 6.4-4 Initial berm (looking downstream) with suspended grid

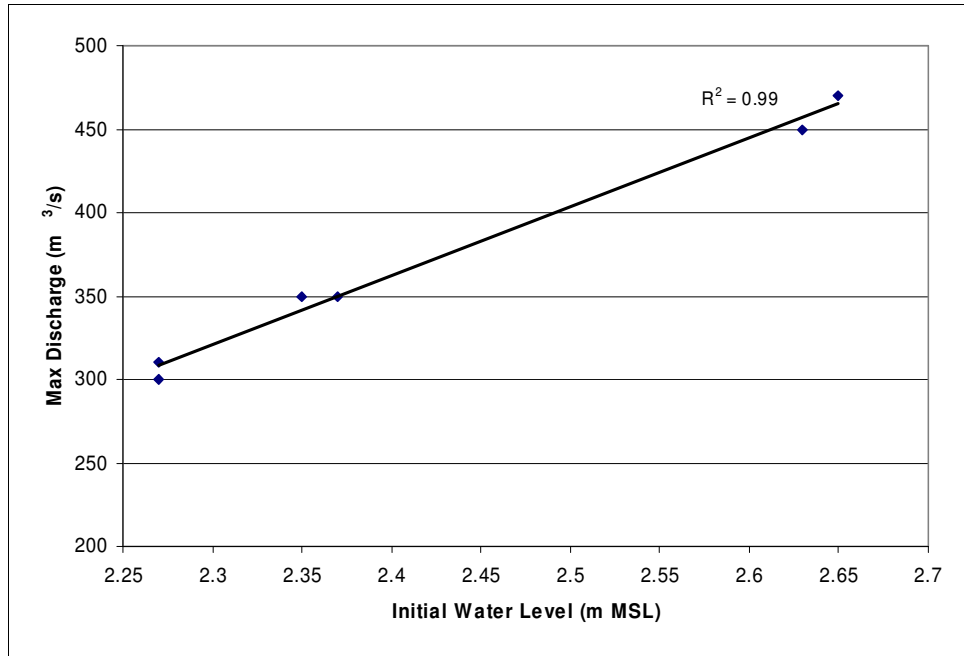


Figure 6.4-5 Relationship between observed breaching peak discharge and initial water level in the estuary at Klein River (based on data from CSIR, 1999)

6.4.3 Results and Observations

A summary of the test results is shown in Table 6.4-1 (blank spaces indicate data that could not be obtained during the experiments) with more information listed in Appendix B. The channel formed very rapidly, becoming deeper then wider, with the greatest changes taking place within five to ten minutes of the experiment (Figure 6.4-6). After the width had become stable, the hydraulic control (Figure 6.4-7) moved upstream (Figure 6.4-8) and the inlet flushing channel became longer.

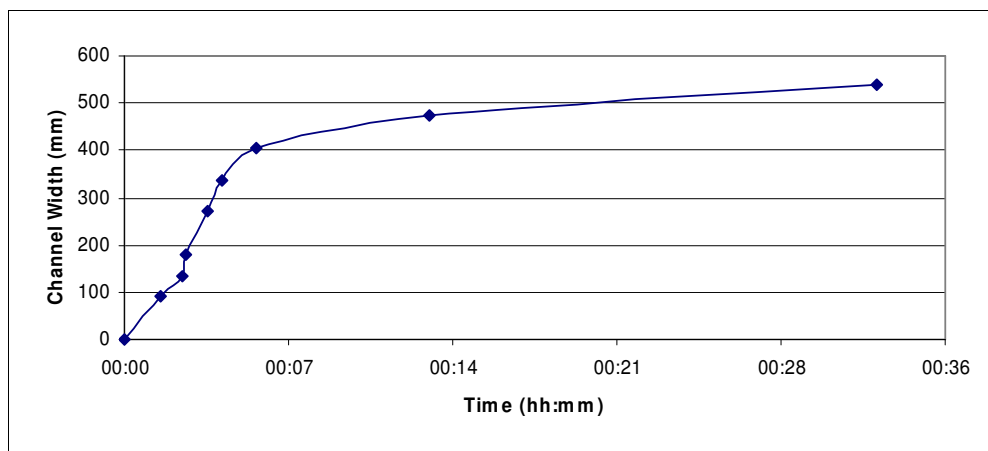


Figure 6.4-6 Progression of inlet channel width with time

Table 6.4-1 Summary of laboratory tests

Test No.	Maximum discharge [m ³ /s]	Initial berm height [m] ¹	Upstream water level [m]	dH [m] ²	Velocity [m/s]	S _r [m/m] ³	k _s [m] ⁴	Fr ₅	Volume eroded [m ³]	Final width [m]	Final depth [m]	Hydraulic control length [m]	Position of hydraulic control [m] ⁶	Flow depth at hydraulic control [m]
1	0.03	0.06	0.06	0.02	0.434	0.003	0.039	0.61	0.257	1.35	0.1		1.22	0.063
2	0.02	0.06	0.05	0.048	0.632	0.008	0.006	1.01	0.277	1.35	0.11		1.62	0.051
3	0.011	0.06	0.04	0.03	0.318	0.016	0.065	0.56	0.313	0.95	0.1	1.73	1.35	0.034
4	0.011	0.06	0.04	0.02	0.814	0.02	0.078	1.2	0.238	0.74	0.12	1.65	1.22	0.049
5	0.007	0.06	0.036	0.036						0.54	0.12	1.48	1.08	0.038
6	0.02	0.06	0.046	0.023	0.721	0.011	0.011	1.02	0.16	1.00	0.09	1.86	1.5	0.056
7	0.006	0.06	0.034	0.034	0.280	0.003	0.28	2.27	0.075	0.58	0.04	1.38	1.25	0.034
8	0.003	0.04	0.032	0.032	0.227	0.002		1.7	0.013		0.02			
9	0.002	0.02	0.032	0.032	0.268	0.002		2.36	0.007	0.4	0.01	1.00	0.92	0.028
10	0.002	0.06	0.032	0.002	0.161	0.011	0.051	0.41	0.011	0.5	0.02	0.8	0.9	0.03
11	0.004	0.04	0.034	0.011	0.131	0.019	0.088	0.3	0.026	0.5	0.02	0.94	0.72	0.041
12	0.005	0.04	0.034	0.034	0.23	0.013	0.152	0.34	0.05	0.58	0.05		1.04	0.029
13	0.005	0.02	0.034	0.034	0.364	0.003		2.08	0.072	0.65	0.05	1.45	1.16	0.019

¹ Relative to “mean sea level”

² Difference between upstream and downstream water levels as breaching started

³ Energy slope in mouth area

⁴ Bed roughness in mouth area

⁵ Froude No = $Q^2B/(gA^3)$

⁶ Relative to the berm

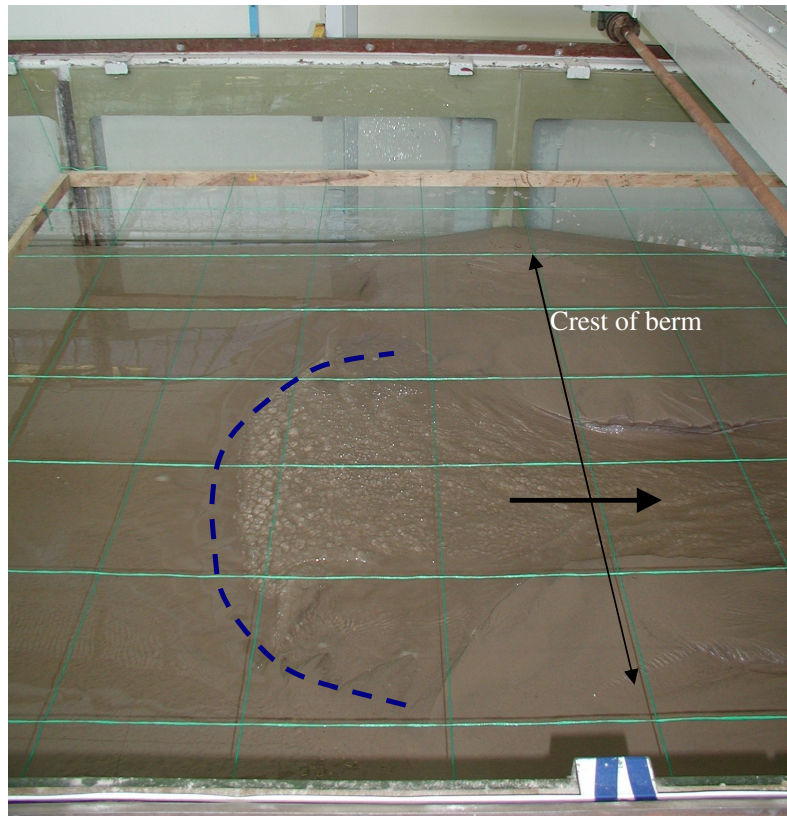


Figure 6.4-7 Hydraulic control

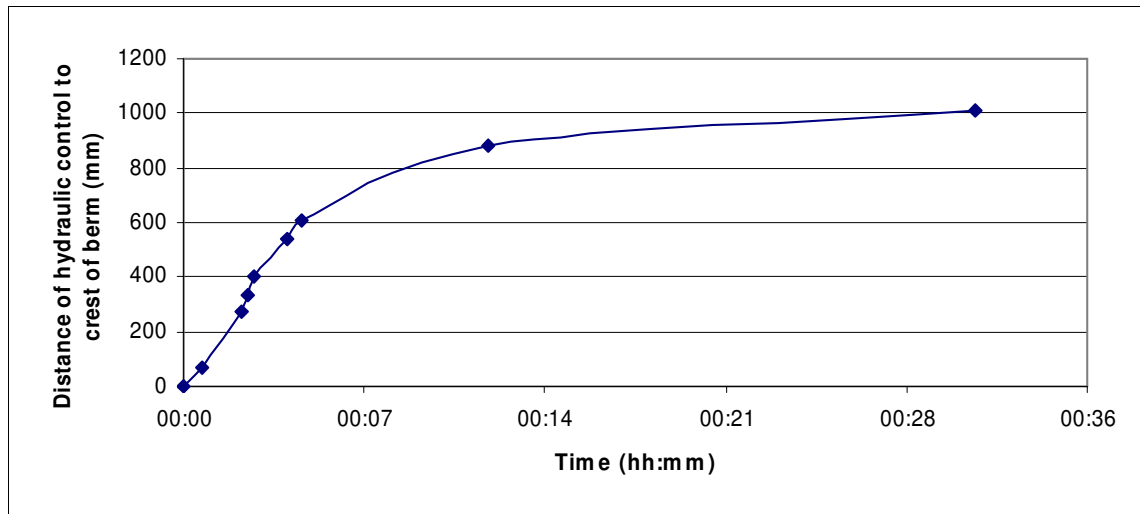


Figure 6.4-8 Position of hydraulic control in relation to the crest of the berm with time

From Figure 6.4-6 and Figure 6.4-8 it can be seen that true equilibrium was not always attained, since the curves in those two figures are still rising. During the experiments it was decided by visual inspection whether or not the inlet channel had become stable and small changes were not always picked up. However, it is believed that the true equilibrium geometry would not have been much different from that which has been recorded, since the system was very close to being stable.

The erosion potential is significant at the start, since the hydraulic gradient and velocities are high. The channel first adjusts its depth rapidly and the hydraulic gradient gradually decreases (Figure 6.4-9). As the channel deepens the banks cave in occasionally, however, the greatest width changes take place after the depth has reached some sort of equilibrium. By increasing the width and depth and reducing the hydraulic gradient the sediment transport capacity of the channel is reduced until no further erosion can take place.

From Figure 6.4-9 it can be seen that the hydraulic gradient is at first very high in the mouth area (between ch 5 and ch 7 m), with a very flat water surface upstream. With time, as the erosion progresses upstream (and with it the hydraulic control), the very steep initial hydraulic gradient decreases in the mouth area, but is now not confined only to that area, but extends a meter further upstream (between ch 4 and ch 7 m). As mentioned before, the depth and width initially changed rapidly, within 5 to 10 minutes, depending on the test conditions, and erosion is confined to the mouth area. Only then did the erosion progress upstream (retrogressive erosion), which can also be seen from Figure 6.4-9, as after 10 minutes the point where there is a definite change in the water surface slope occurs at ch 4 m, whereas it was at ch 5 m before.

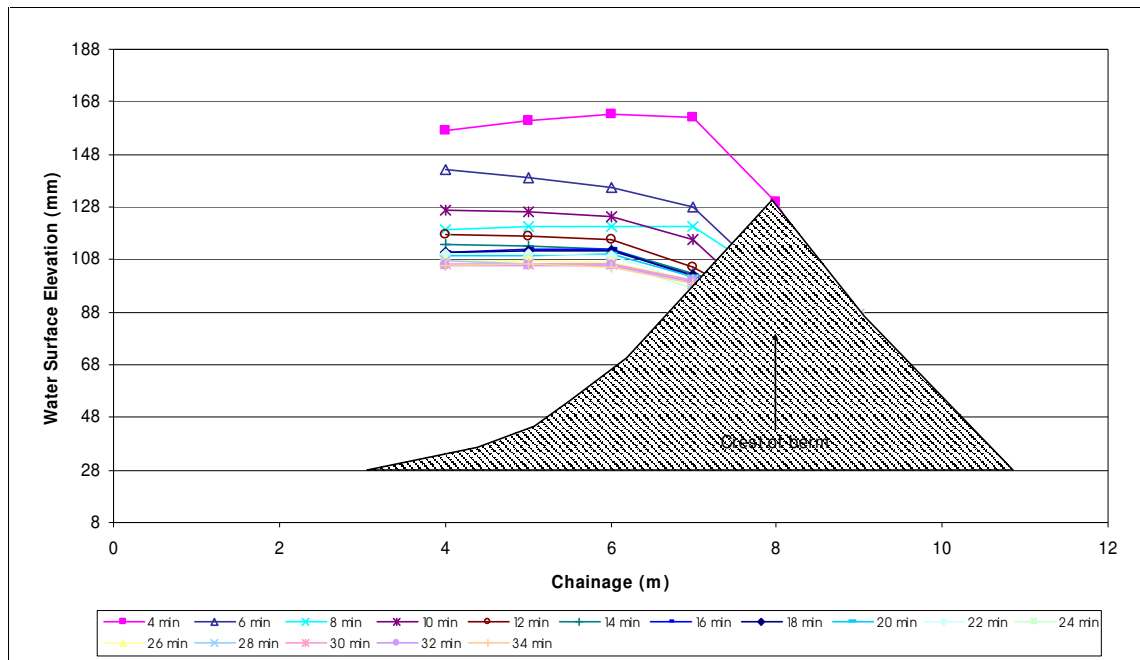


Figure 6.4-9 Water level changes with time

The initial and resulting bathymetries for experiments with initial berm levels at 0.06 m are shown in Figure 6.4-10 to Figure 6.4-14, for initial berm levels of 0.04 m in Figure 6.4-15 and Figure 6.4-16, and for 0.02 m in Figure 6.4-17 and Figure 6.4-18, respectively.

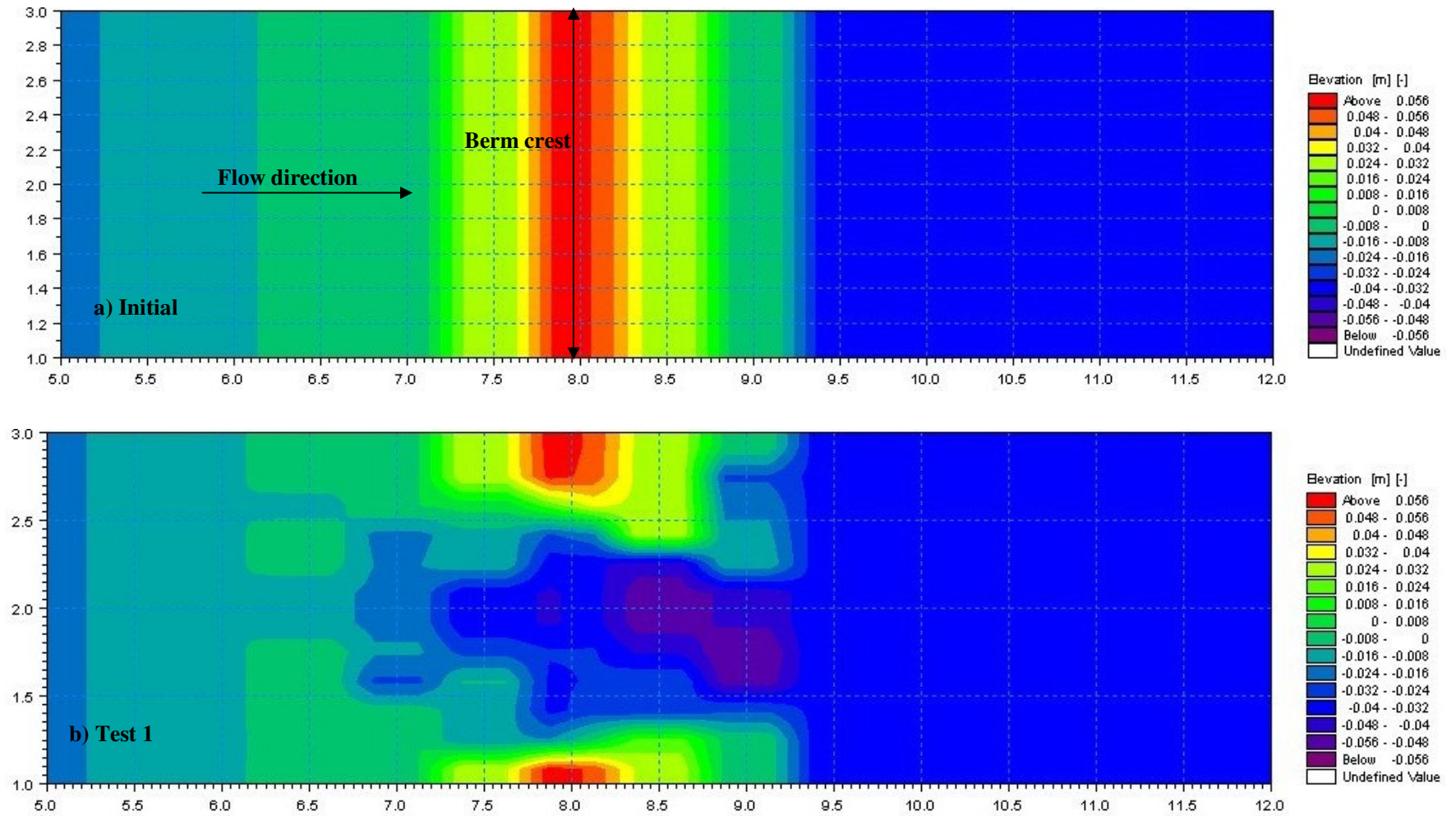


Figure 6.4-10 Initial bathymetry (a) for tests 1-7, 10, 14 (berm height 0.06 m) and final bathymetry for test 1 (b)

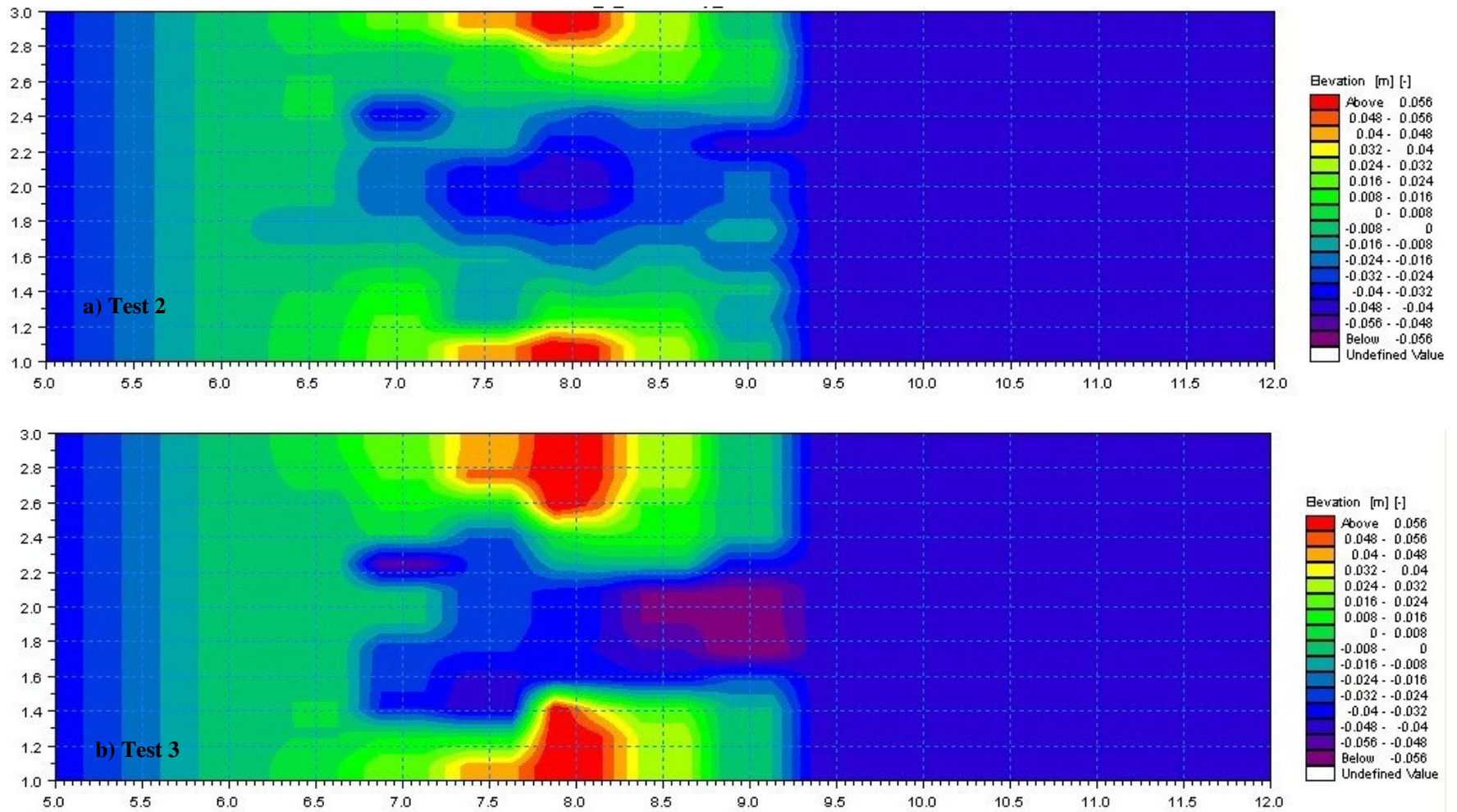


Figure 6.4-11 Final bathymetries for test 2 (a) and 3 (b)

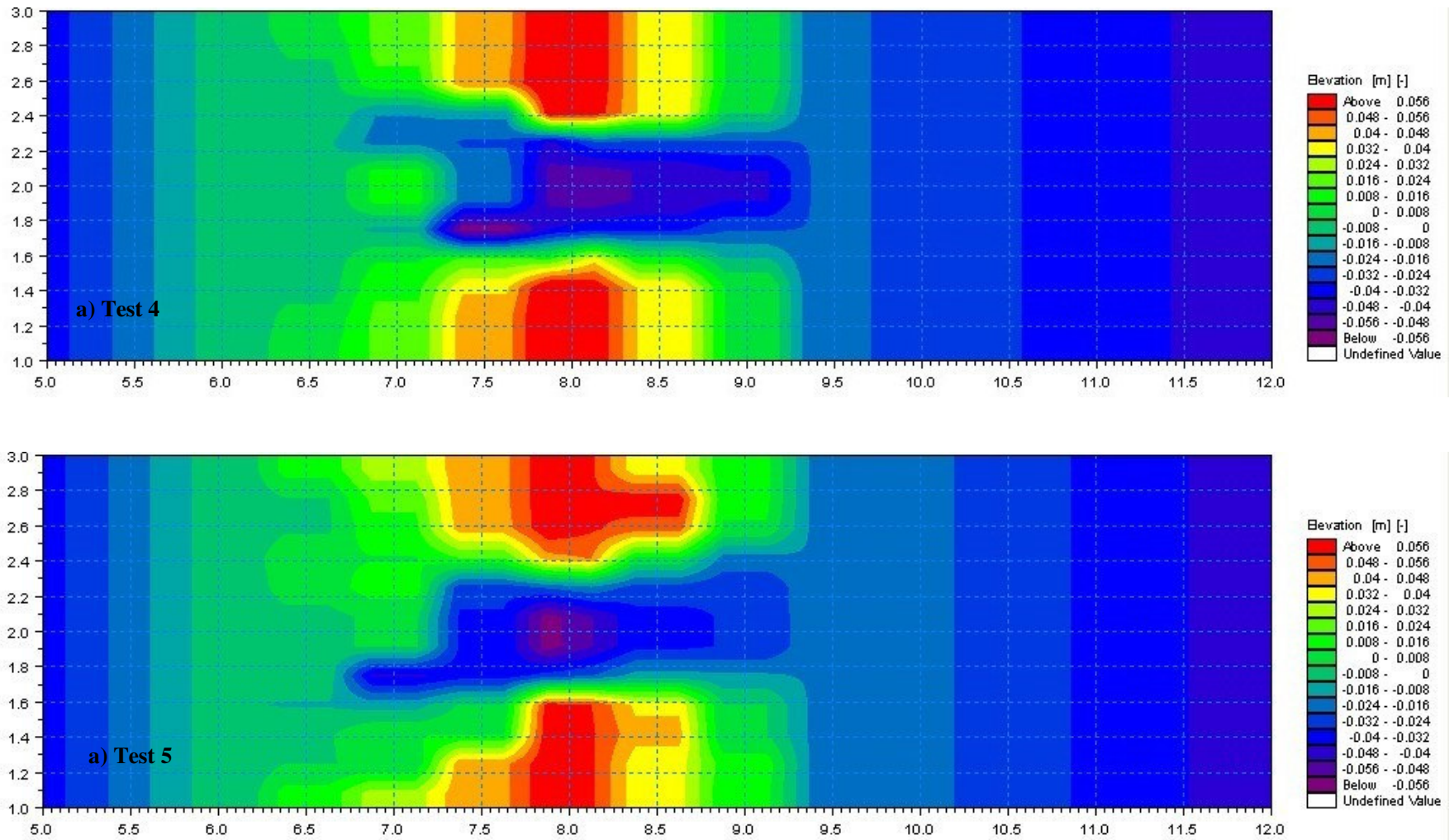


Figure 6.4-12 Final bathymetries for test 4 (a) and 5 (b)

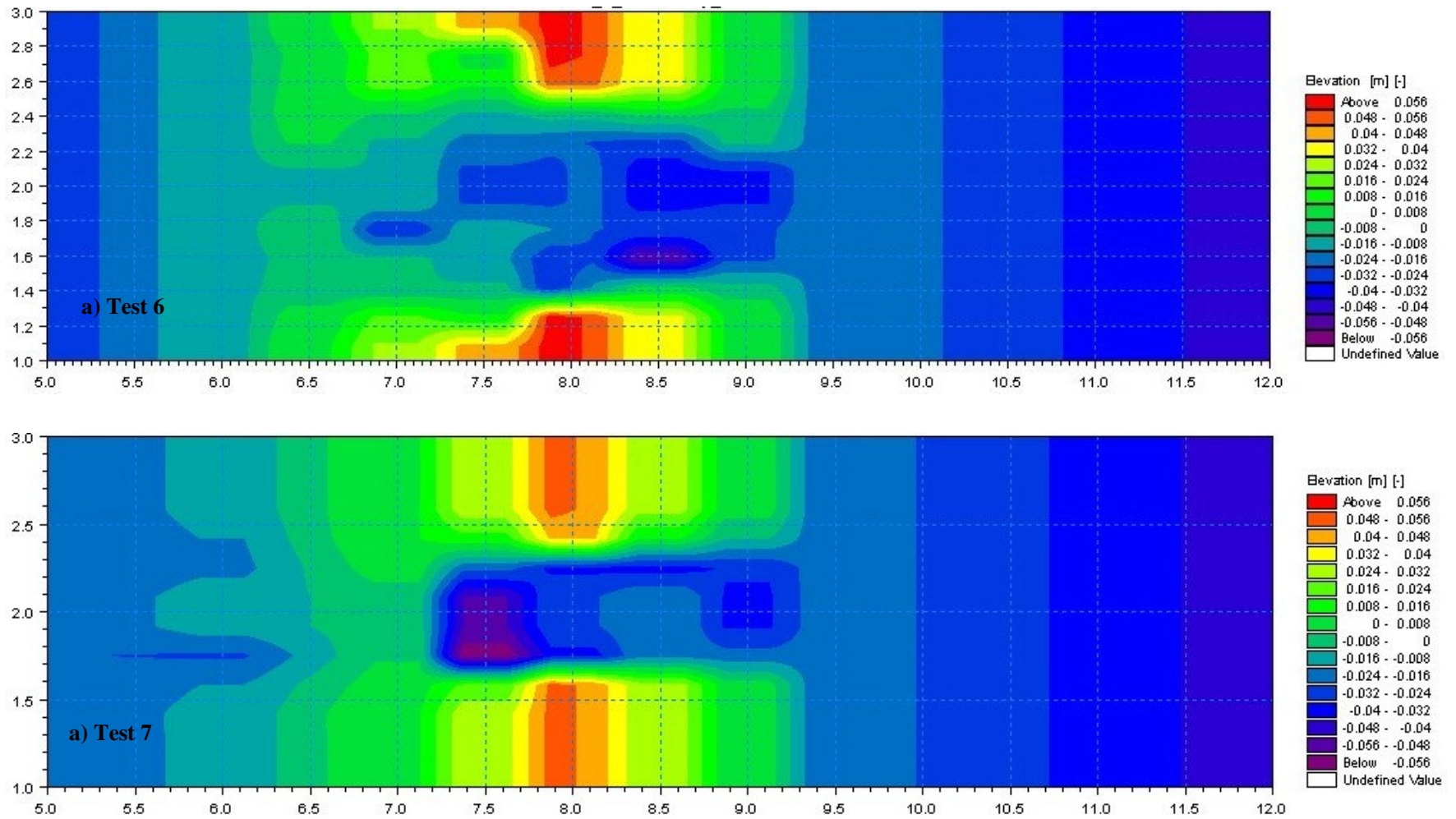


Figure 6.4-13 Final bathymetries for test 6 (a) and 7 (b)

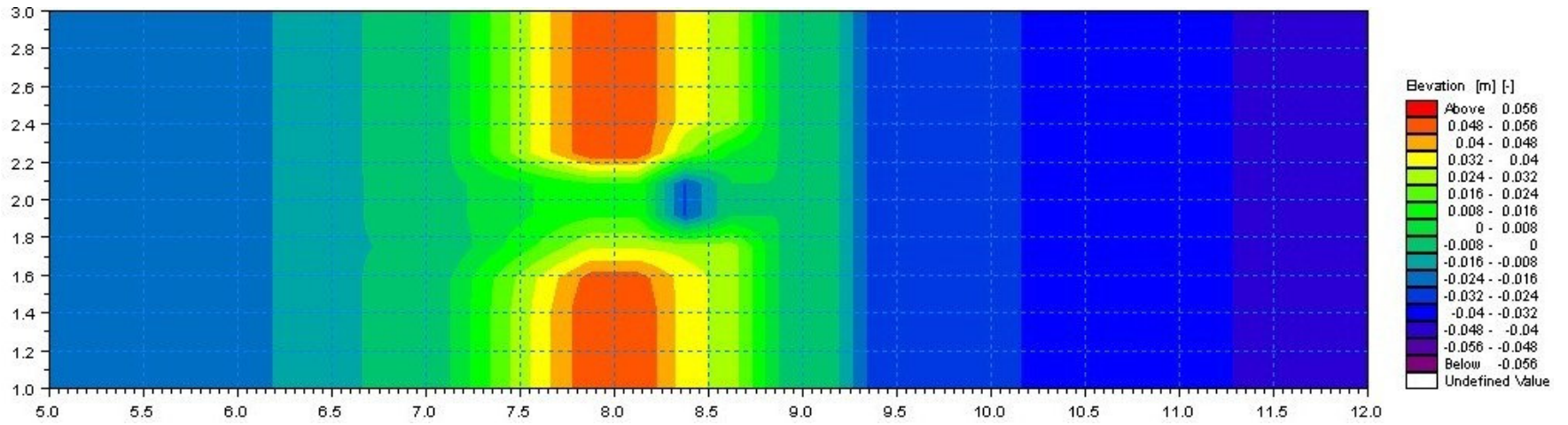


Figure 6.4-14 Final bathymetries for test 10

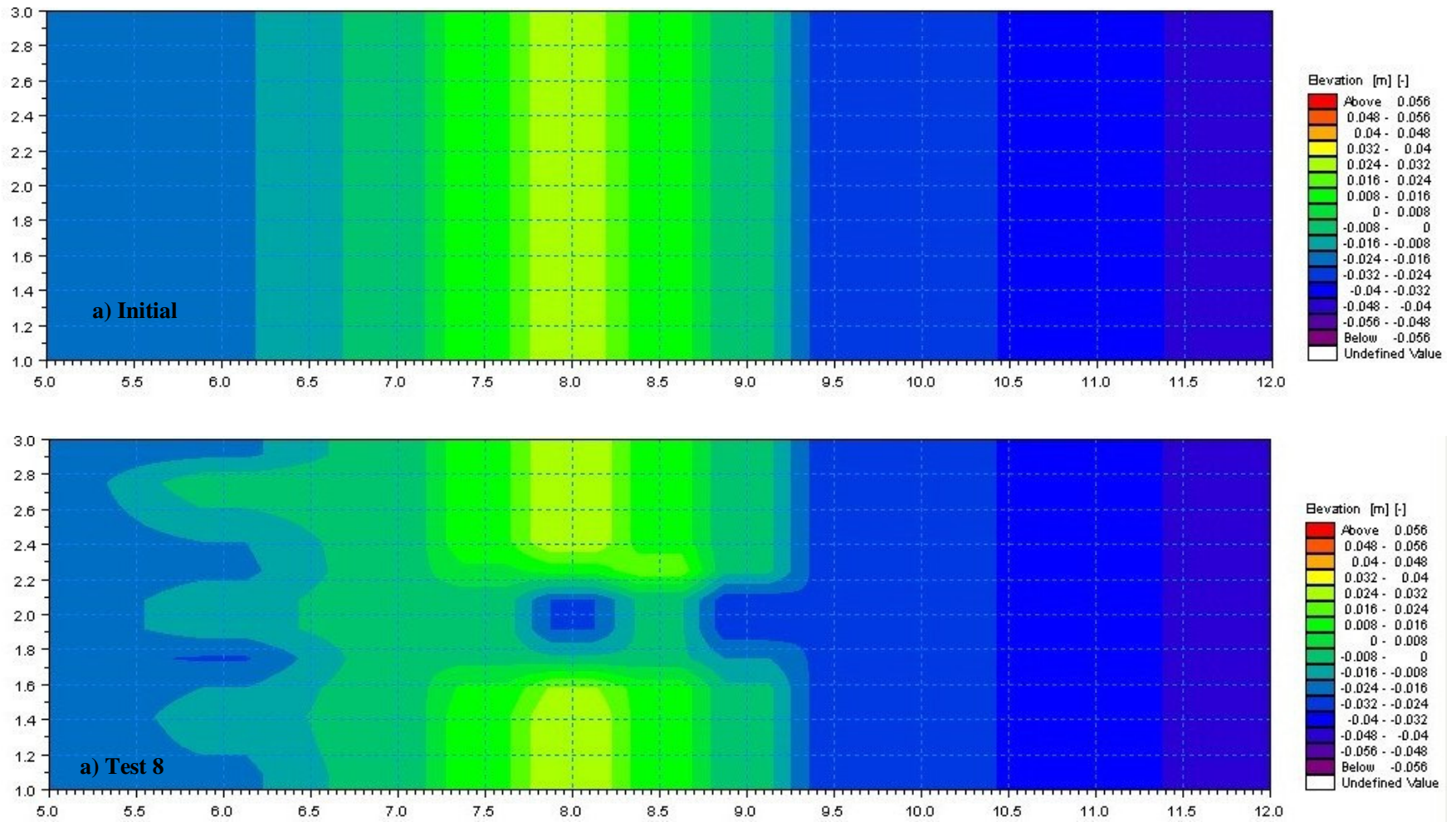


Figure 6.4-15 Initial bathymetry (a) for tests 8, 11, 12 (berm height 0.04 m) and final bathymetry for test 8 (b)

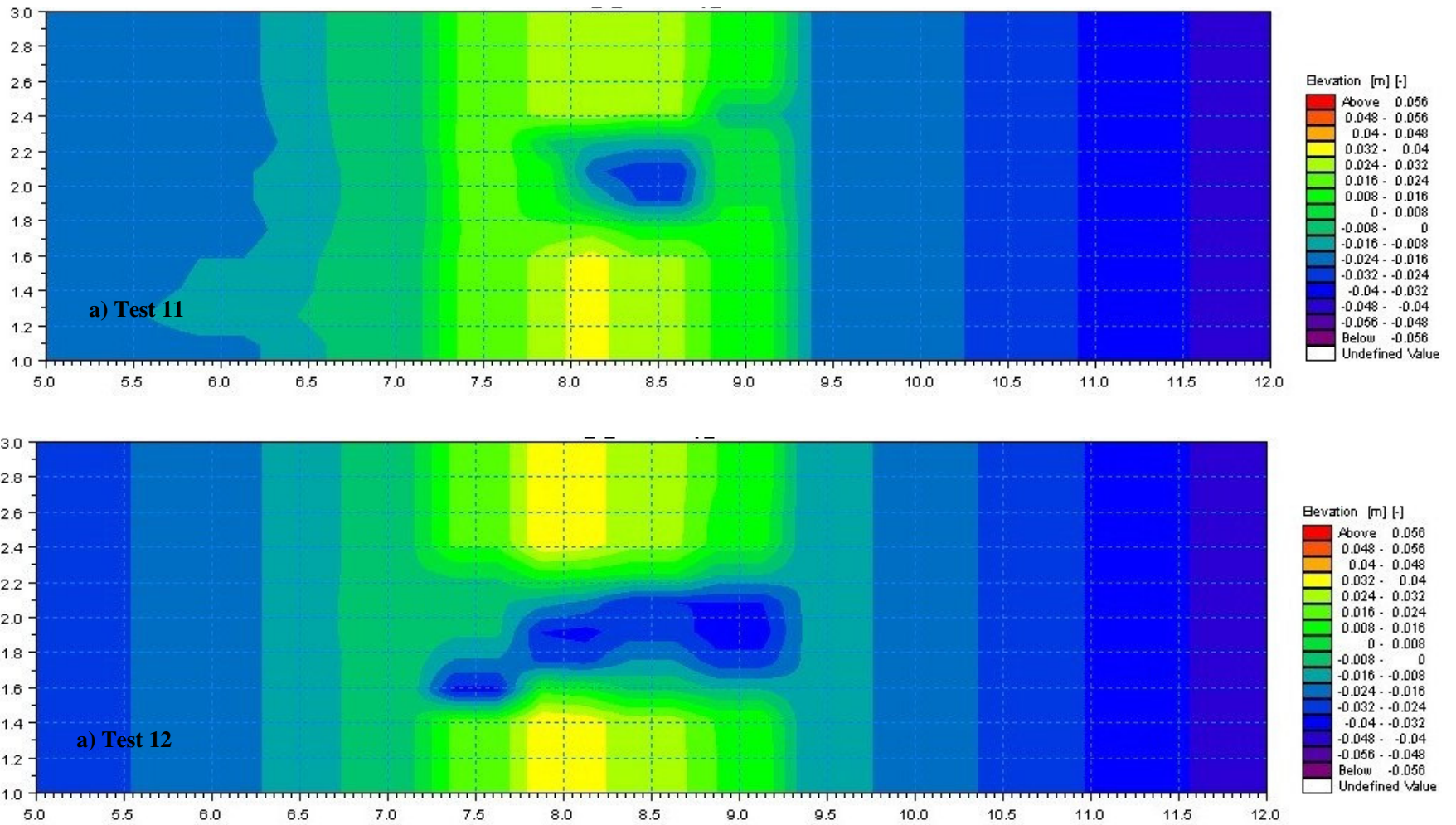


Figure 6.4-16 Final bathymetries for test 11 (a) and 12 (b)

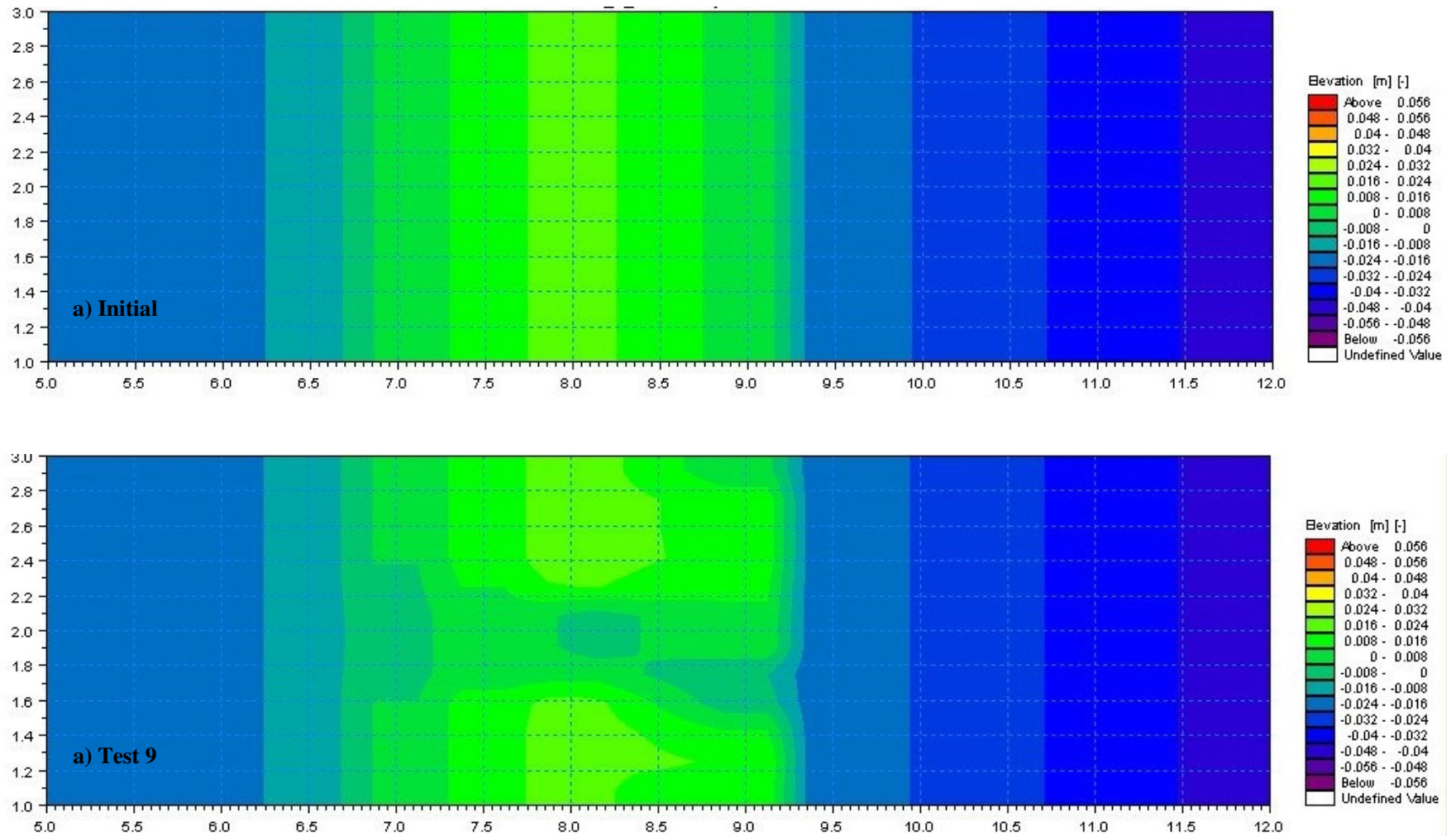


Figure 6.4-17 Initial bathymetry (a) for test 9 and 13 (berm height 0.02 m) and final bathymetry for test 9 (b)

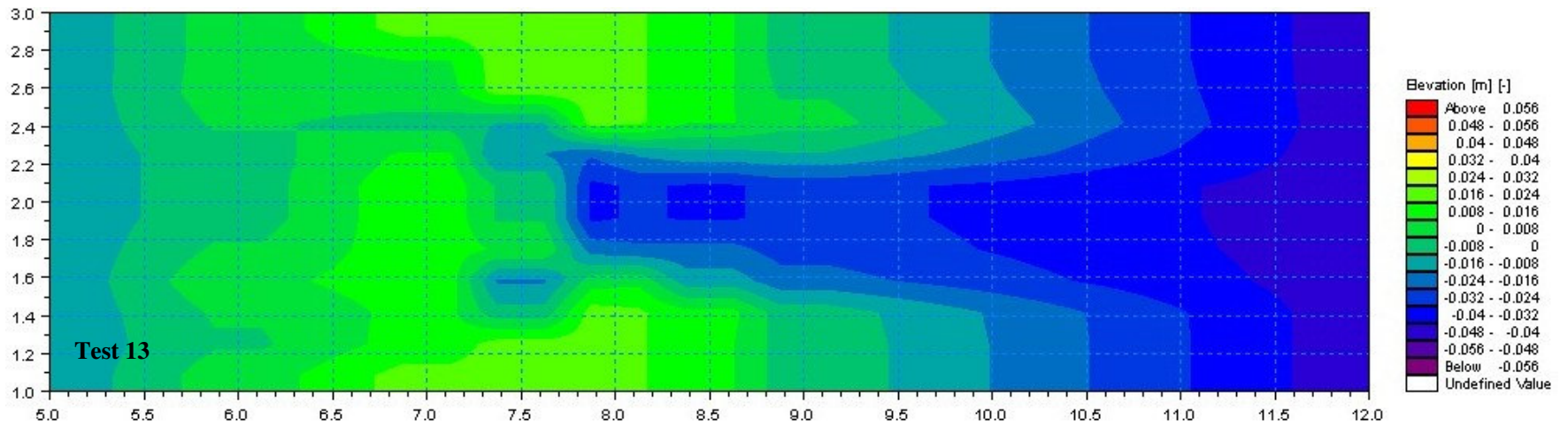


Figure 6.4-18 Final bathymetry for test 13

It became apparent during the experiments that higher discharges resulted in wider openings (see for example Figure 6.4-10(b) and Figure 6.4-11(a), although the same could not be said about the depth. The problem was that the depths were difficult to determine as the bed forms were quite substantial, and would also not remain stationary (Figure 6.4-19). The higher discharges were also associated with greater volumes of sediment eroded from the mouth and the area upstream, which was to be expected. It also became apparent that with higher downstream water levels for a fixed upstream level (i.e. fixed discharge), the mouth remained very shallow throughout the experiment, whereas the width would remain more or less the same. It thus seems that the width is mainly determined by the maximum discharge through the mouth, whereas the depth is probably dependent on both the discharge and the hydraulic gradient.

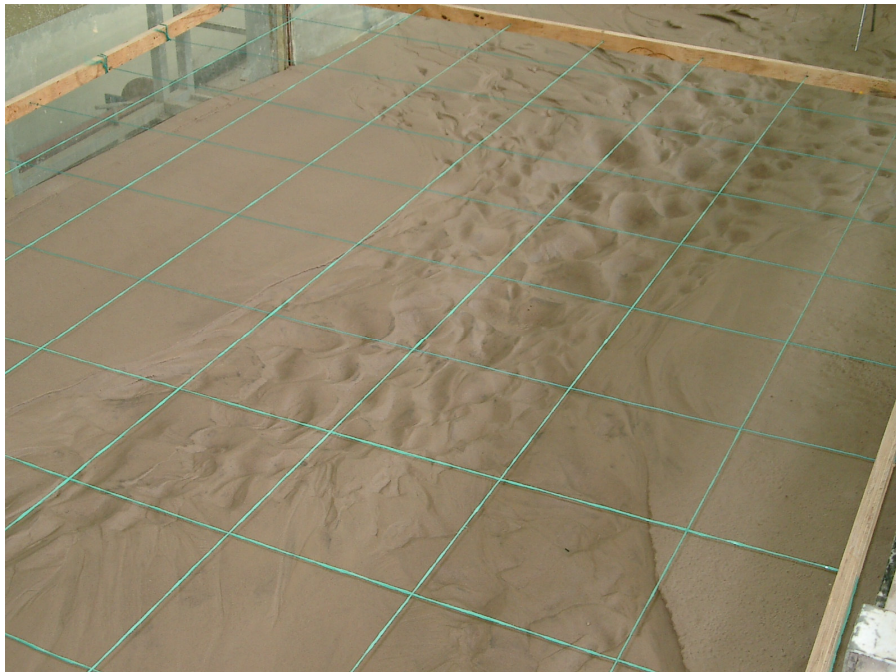


Figure 6.4-19 Bed forms

6.4.4 Analysis of Results

The results obtained from the experiments were analysed to determine whether the equilibrium mouth geometry (width and depth) and the flushing efficiency could be predicted. The approach followed was first of all to determine which factors play significant roles in the breaching process. The analysis showed that the maximum discharge Q during breaching is by far the most important parameter governing the mouth geometry as well as the erosion process. The hydraulic gradient S_f was found to be another important parameter. This is not unexpected since $\rho g Q S_f$ is the total input stream power, which has been shown to be a very important parameter in sediment transport processes. Bagnold

(1966), Yang (1972), Basson and Rooseboom (1997) and Beck and Basson (2003) to name but a few have used stream power to derive sediment transport equations. Basson and Rooseboom have also used stream power to develop an equation to determine the bed roughness. Unfortunately the maximum discharge is usually unknown, but can be estimated from volumetric calculations when field data are available as in the case of Klein River (see Figure 6.4-5) and Groot Brak (Figure 6.4-21). To be able to predict the equilibrium mouth geometry and the rate of erosion under conditions where data is limited, as is usually the case in field conditions, it was important to develop a procedure by which all the important parameters in the breaching process could be determined from known variables. There is generally only one factor that is known before breaching starts and that is the upstream water level in the estuary. In these experiments, as in the case of the Klein River, there was a definite relationship between the upstream water level in the estuary at the start of breaching H_i (relative to MSL) and the maximum discharge Q . The laboratory and field data from the Klein River could be combined (see Figure 6.4-20) to give the following relationship ($R^2 = 0.99$):

$$Q = 36.286 \cdot H_i^{2.663} \dots\dots\dots 6.4-1$$

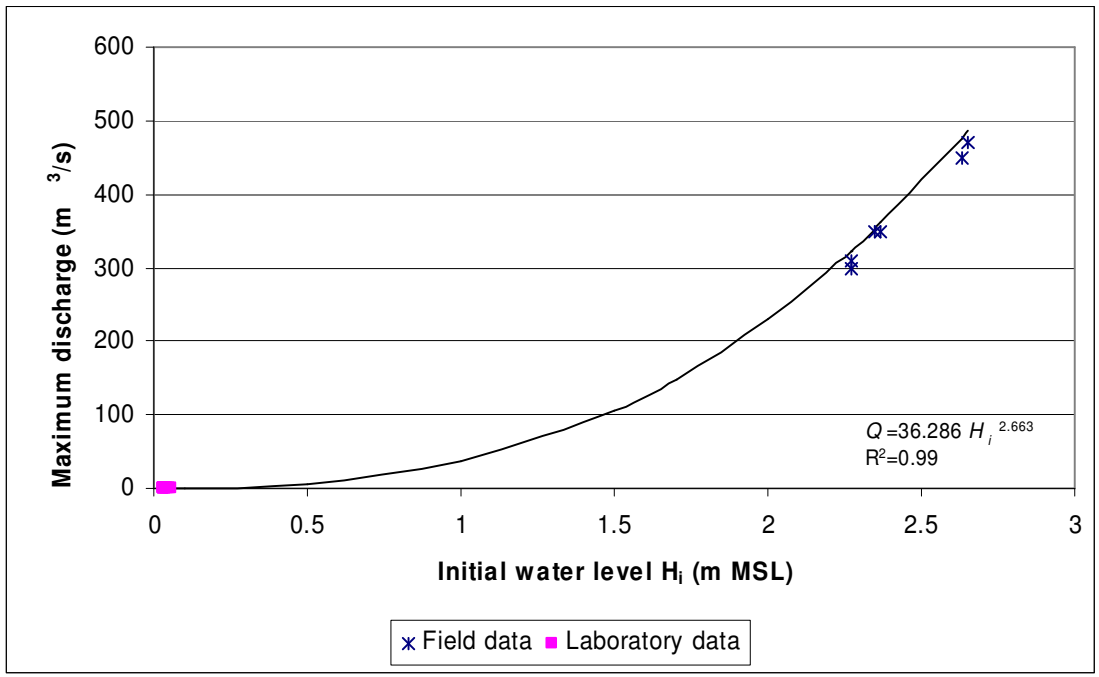


Figure 6.4-20 Relationship between initial water level and maximum discharge for both field and laboratory data

Since all the relevant parameters are based on the maximum discharge during flushing, equation 6.4-1 can be used to calculate the maximum discharge if the initial water level is known.

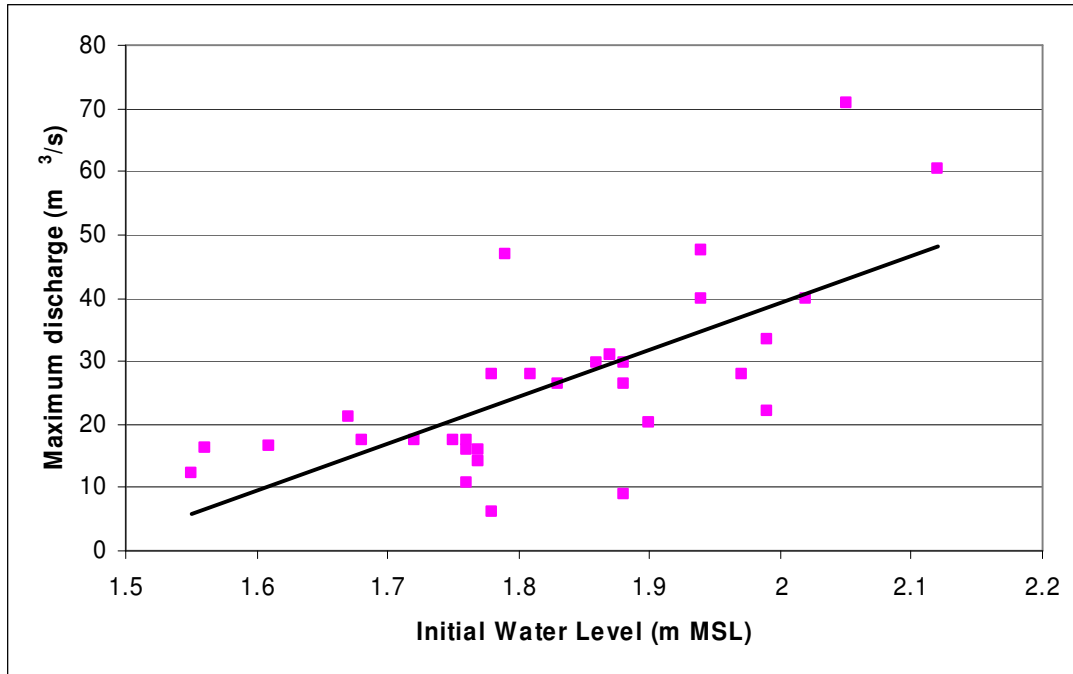


Figure 6.4-21 Relationship between observed breaching peak discharge and initial water level in the estuary at Groot Brak River (data obtained from CSIR, 2000)

6.4.4.1 Equilibrium Mouth Geometry

A definite relationship could be found between the discharge and the final breach width of the physical model channel (Figure 6.4-22 and Figure 6.4-23) in the form of:

$$B = 6.64 \cdot Q^{0.455} \dots\dots\dots 6.4-2$$

with B = equilibrium inlet channel width
 Q = maximum discharge ($r^2 = 0.88$)

This is very similar to the regime equations for rivers, found during a recent Water Research Commission project (Beck and Basson, 2003).

$$B = 4.42 \cdot Q^{0.484} \dots\dots\dots 6.4-3$$

Even when the whole berm was overtopped, as happened during one experiment due to the inflow being increased too rapidly, a smaller channel formed almost immediately.

It was also found that the difference in water levels in the estuary and the sea at the start of breaching dH was another important parameter. Combined with the maximum discharge, the equilibrium channel width can be accurately predicted ($r^2 = 0.91$).

$$B = 32.82 \cdot Q + 4.7 \cdot dH + 0.302 \dots\dots\dots 6.4-4$$

Results similar to equation 6.4-2 could be obtained for the field data from the Orange River mouth (Tromp, 2000):

$$B = 1.82 \cdot Q^{0.563} \dots\dots\dots 6.4-5$$

and the Thukela River mouth (Pollard, 2001):

$$B = 27.66 \cdot Q^{0.33} \dots\dots\dots 6.4-6$$

From the above equations it can be seen that the breach width can be fairly accurately predicted if the maximum discharge during breaching is known. However, judging from the large range of coefficients, it seems that it will be difficult to obtain a relationship that is valid for all systems.

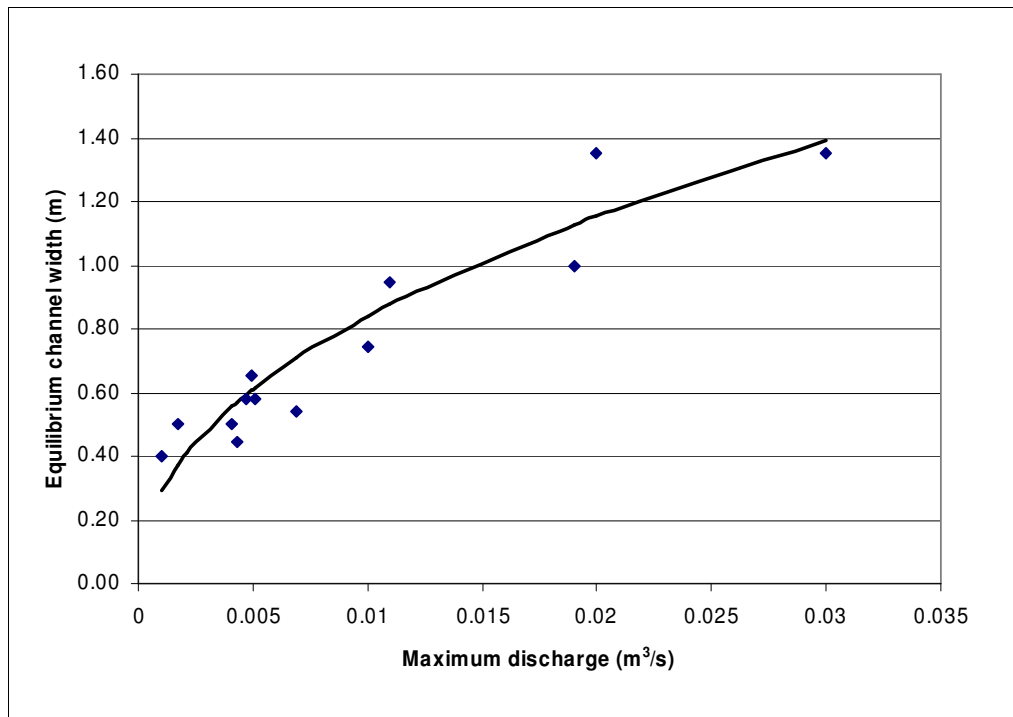


Figure 6.4-22 Relationship between the equilibrium channel width of the flushing channel and the discharge (physical model data)

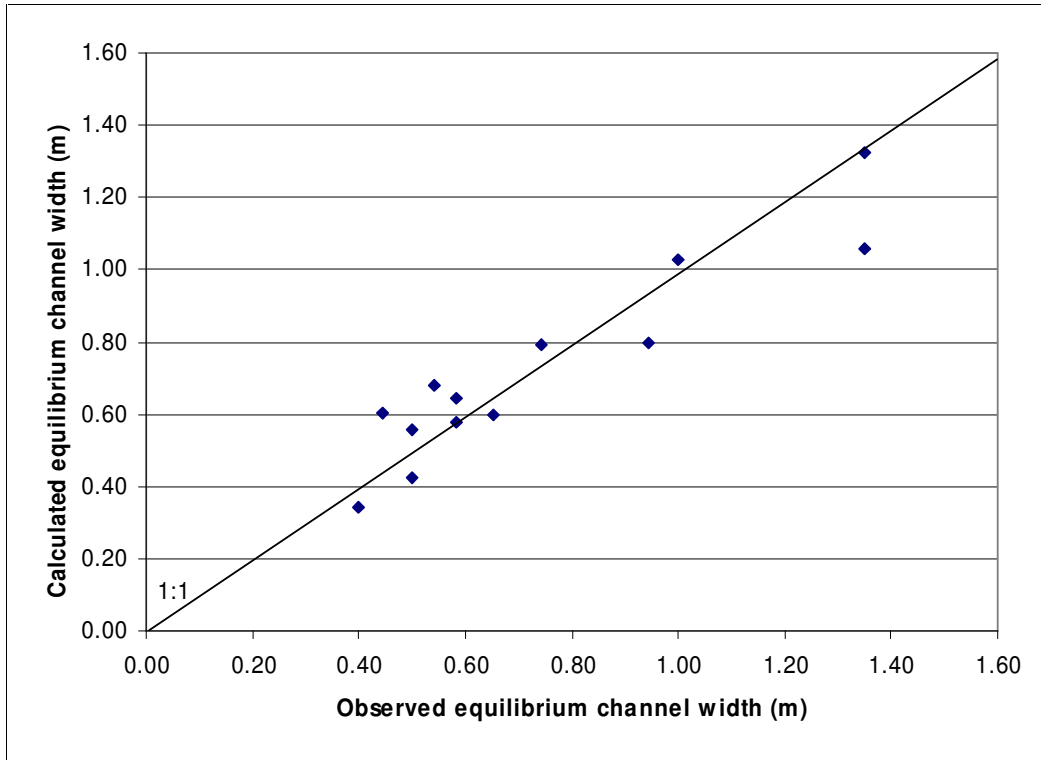


Figure 6.4-23 Comparison between observed and calculated widths (Equation 6.4-2)

The relationship between the final depth D and the discharge is not as obvious (Figure 6.4-24), mainly because it was difficult to determine the correct depth since the bed forms were fairly large and distinct (Figure 6.4-19). However, the following relationship could be obtained ($r^2 = 0.77$), as illustrated in Figure 6.4-25

$$D = 2.09 \cdot Q^{0.73} \dots\dots\dots 6.4-7$$

Somewhat better results could be obtained by including the energy slope ($r^2 = 0.8$).

$$D = 0.02 \cdot Q^{0.7} \cdot S^{0.09} \dots\dots\dots 6.4-8$$

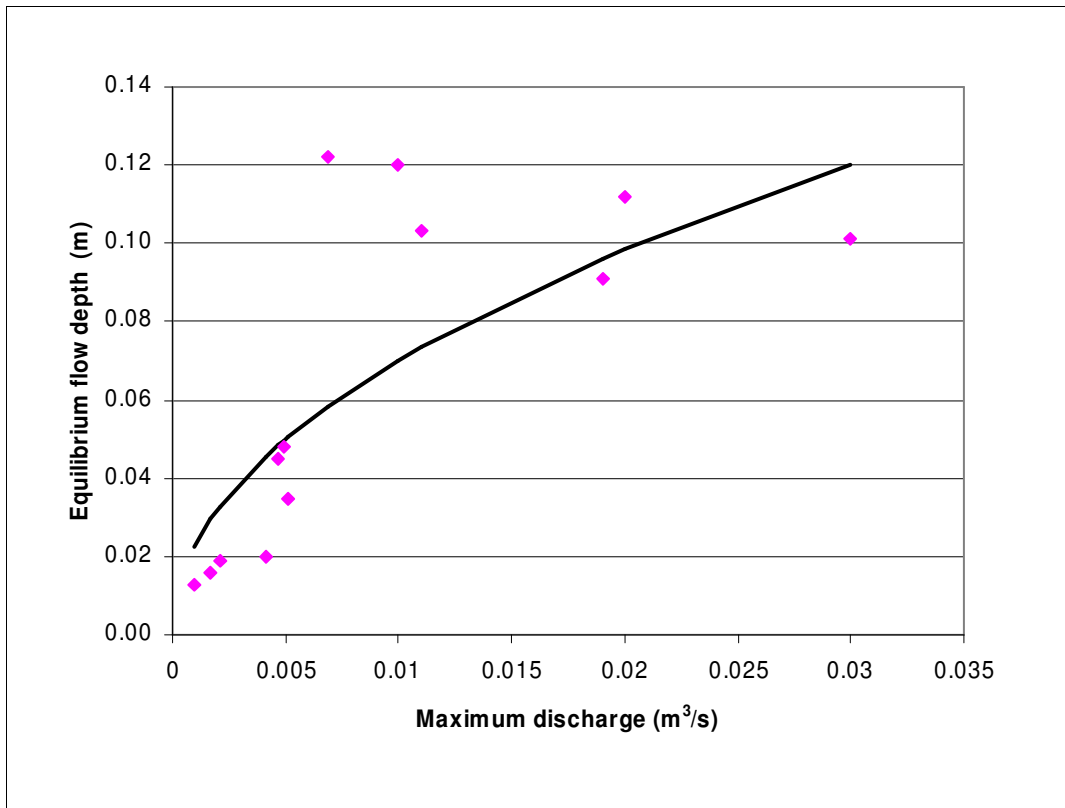


Figure 6.4-24 Relationship between the equilibrium channel depth of the flushing channel and the discharge

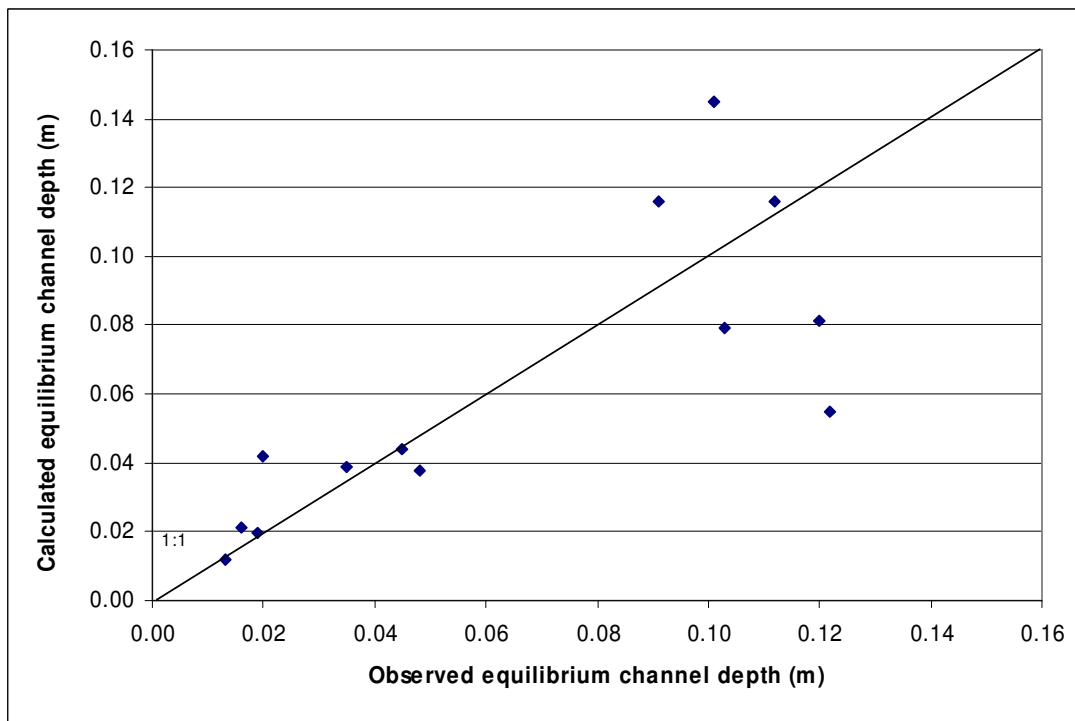


Figure 6.4-25 Comparison between observed and calculated depths (Equation 6.4-7)

The accuracy of the above equations can also be expressed in terms of their ability to predict the width and depth within certain accuracy ranges, as shown in Table 6.4-2.

Table 6.4-2 Accuracy of width and depth equations

Equation	$0.83 < \frac{X_{observed}^1}{X_{calculated}} < 1.2$	$0.67 < \frac{X_{observed}}{X_{calculated}} < 3$	$0.5 < \frac{X_{observed}}{X_{calculated}} < 2$
6.4-2	69%	100%	100%
6.4-4	69%	100%	100%
6.4-7	29%	71%	93%
6.4-8	36%	86%	86%

¹ X = either width or depth

6.4.4.2 Flushing Efficiency

To investigate the flushing efficiency it was important to not only determine how much sediment could be flushed out and at what rate, but also to see whether the sediment was flushed only from the mouth area, or from further upstream. This is important since estuaries are generally breached not only to establish a new connection with the open sea, but to remove some of the accumulated sediment in the estuary.

It was found that the position of the hydraulic control indicates the upstream limit up to where scouring takes place. In some experiments one or two smaller channels would branch off the larger flushing channel, leading to localised scouring extending further upstream than the main flushing channel (see Figure 6.4-10).

The position P_{HC} and the length L_{HC} of the hydraulic control (obtained visually from the video recordings) can be expressed as a function of the maximum discharge during breaching, with coefficients of determination of 0.59 and 0.78, respectively (see Figure 6.4-26 to Figure 6.4-29).

$$P_{HC} = 3.064 \cdot Q^{0.204} \dots\dots\dots 6.4-9$$

$$L_{HC} = 6.206 \cdot Q^{0.293} \dots\dots\dots 6.4-10$$

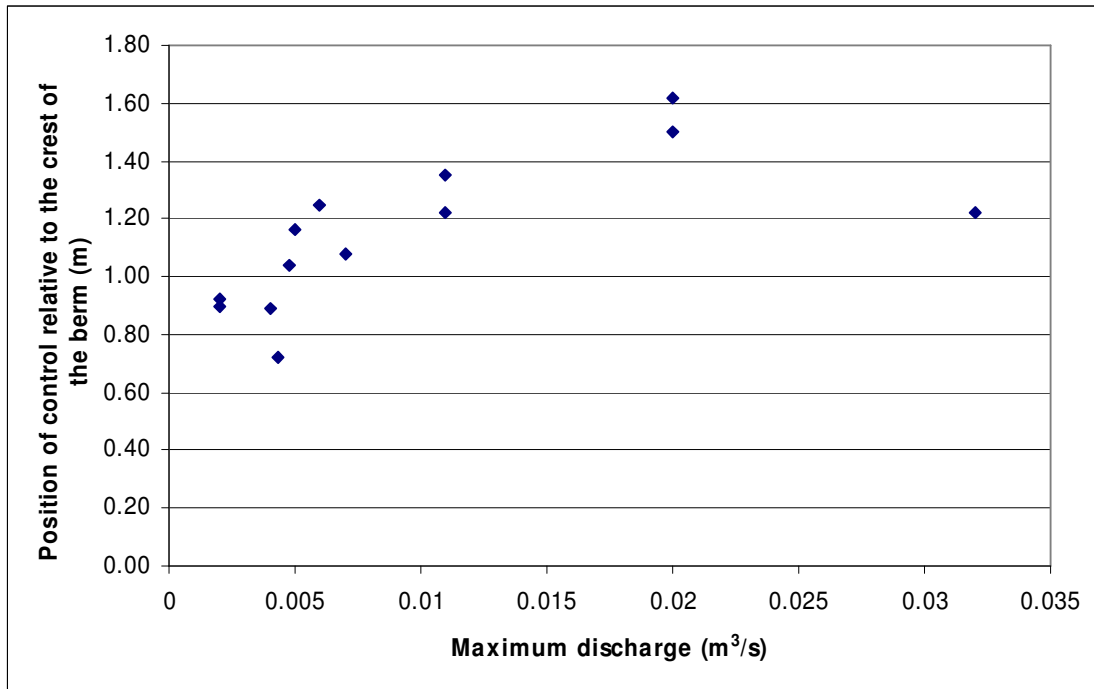


Figure 6.4-26 Relationship between the maximum discharge during flushing and the position of the control relative to the crest of the berm

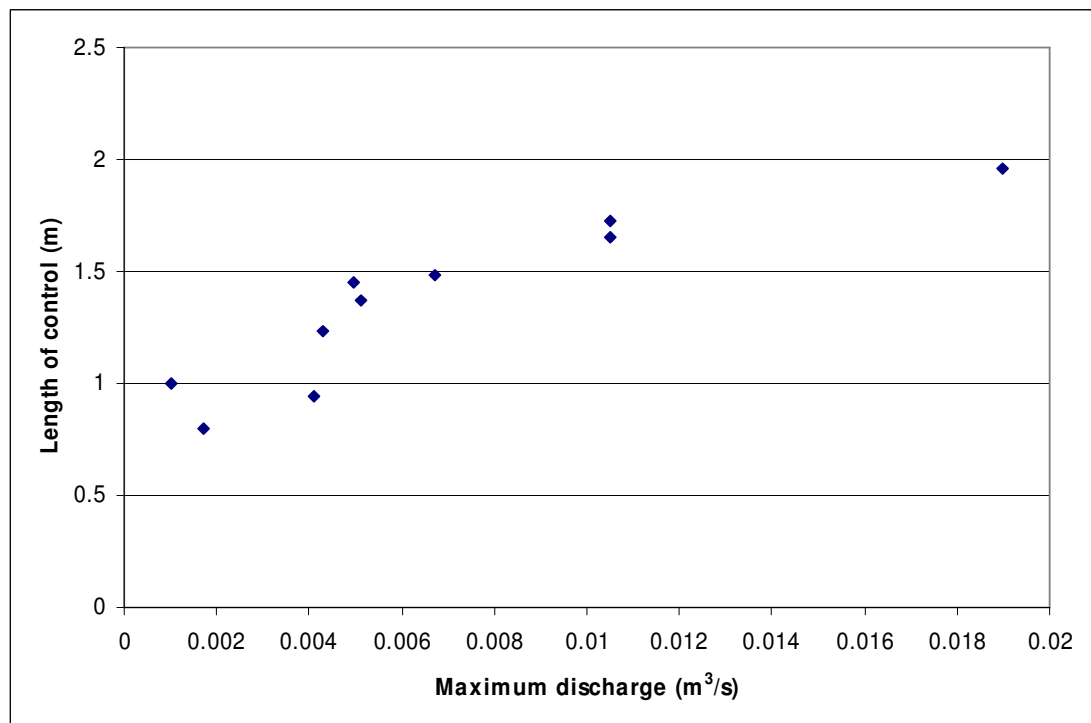


Figure 6.4-27 Relationship between the maximum discharge during flushing and the length of the control

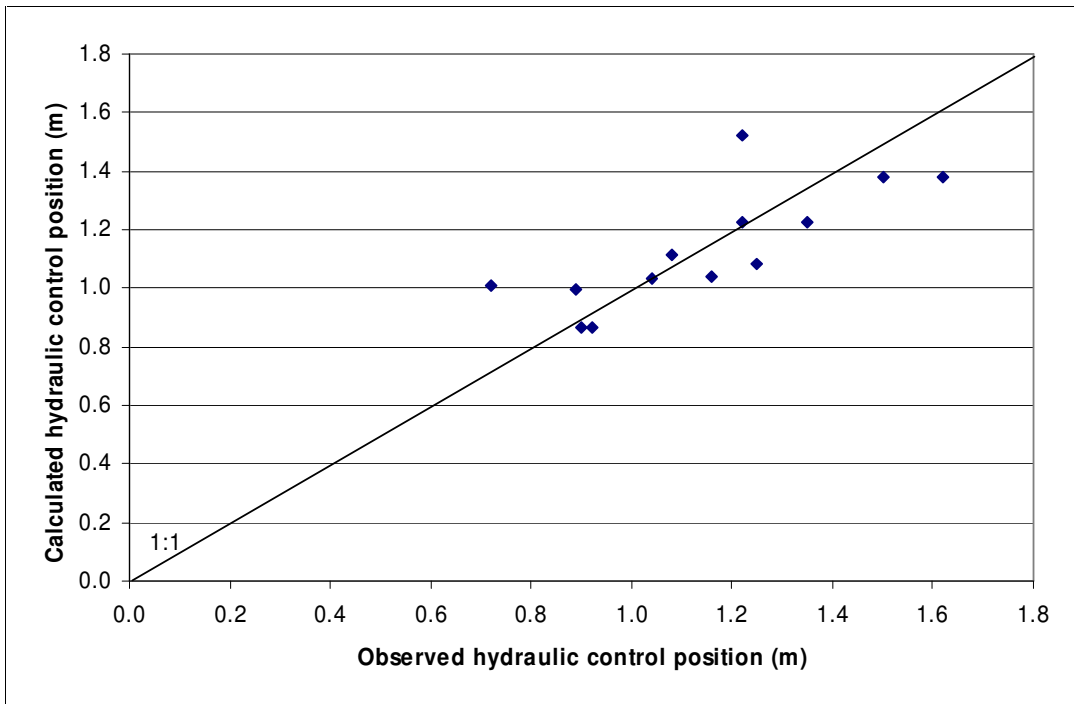


Figure 6.4-28 Comparison between observed and calculated hydraulic control position (Equation 6.4-9)

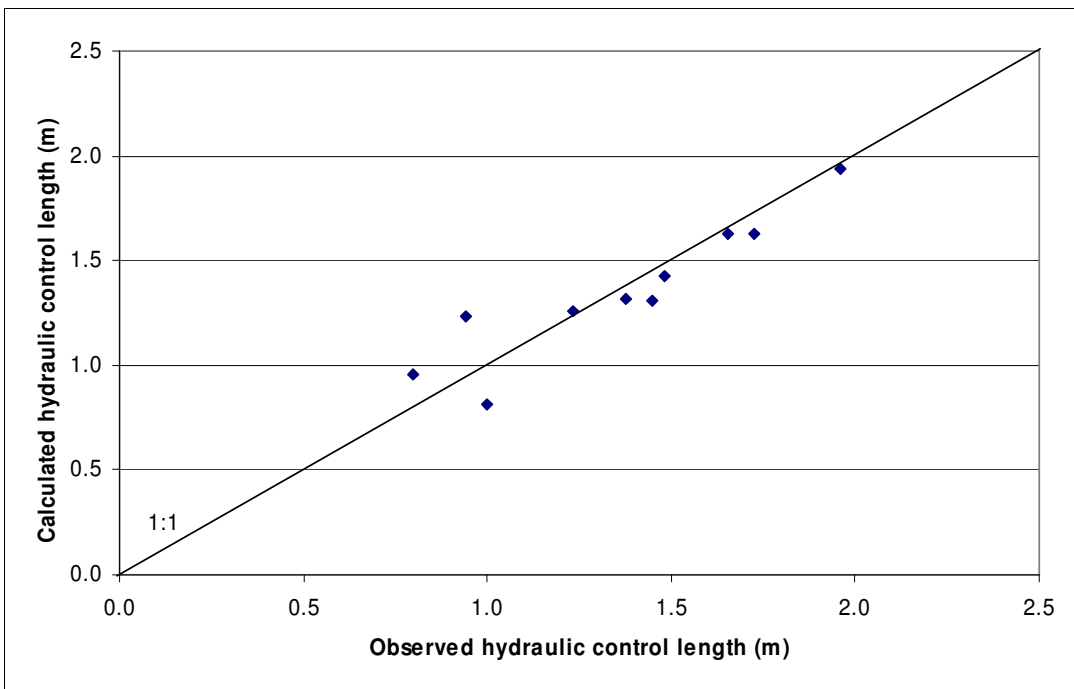


Figure 6.4-29 Comparison between observed and calculated hydraulic control length (Equation 6.4-10)

The volume of sediment flushed out during each test was also determined by surveying the area before and after the experiments. It was found that the volume of scoured sediment V could also be expressed as a function of the maximum discharge ($r^2 = 0.88$).

$$V = 31.67 \cdot Q^{1.21} \dots\dots\dots 6.4-11$$

Another factor which plays an important role is the rate of erosion and the time it takes before equilibrium is reached. The problem is that in many cases the volume of water available during breaching is limited (e.g. Groot Brak Estuary), and if the breaching process takes too long the available volume of water could be used before the mouth was properly flushed open. In South Africa it has also been found (CSIR, 1999) that breaching should ideally start at high tide or just after high tide. This is so that as the sea water level drops the hydraulic gradient in the mouth increases and there is little chance that the water will flow back into the estuary when the outflow is still small.

From the videos taken during the experiments the width of the inlet channel and the position of the hydraulic control could be determined at various time steps during the experiments, as shown in Figure 6.4-6 and Figure 6.4-8. From this the rate at which the channel widened (dB) and the hydraulic control moved upstream (dC) could be obtained. The average rate of erosion for both the width and hydraulic control could again be linked to the maximum discharge (Figure 6.4-30).

$$dB = 0.08 \cdot Q - 2.89 \cdot 10^5 \dots\dots\dots 6.4-12$$

$$dC = 0.06 \cdot Q + 4.52 \cdot 10^{-4} \dots\dots\dots 6.4-13$$

The accuracy of the above equations was expressed in terms of their ability to predict certain parameters within certain accuracy ranges, as shown in Table 6.4-3.

Table 6.4-3 Accuracy of regression equations

Equation	$0.83 < \frac{X_{observed}^1}{X_{calculated}} < 1.2$	$0.67 < \frac{X_{observed}}{X_{calculated}} < 3$	$0.5 < \frac{X_{observed}}{X_{calculated}} < 2$
6.4-9	85%	100%	100%
6.4-10	71%	100%	100%
6.4-11	25%	58%	92%
6.4-12	23%	38%	77%
6.4-13	23%	38%	77%

¹ X = Position or length of hydraulic control, or scoured sediment volume

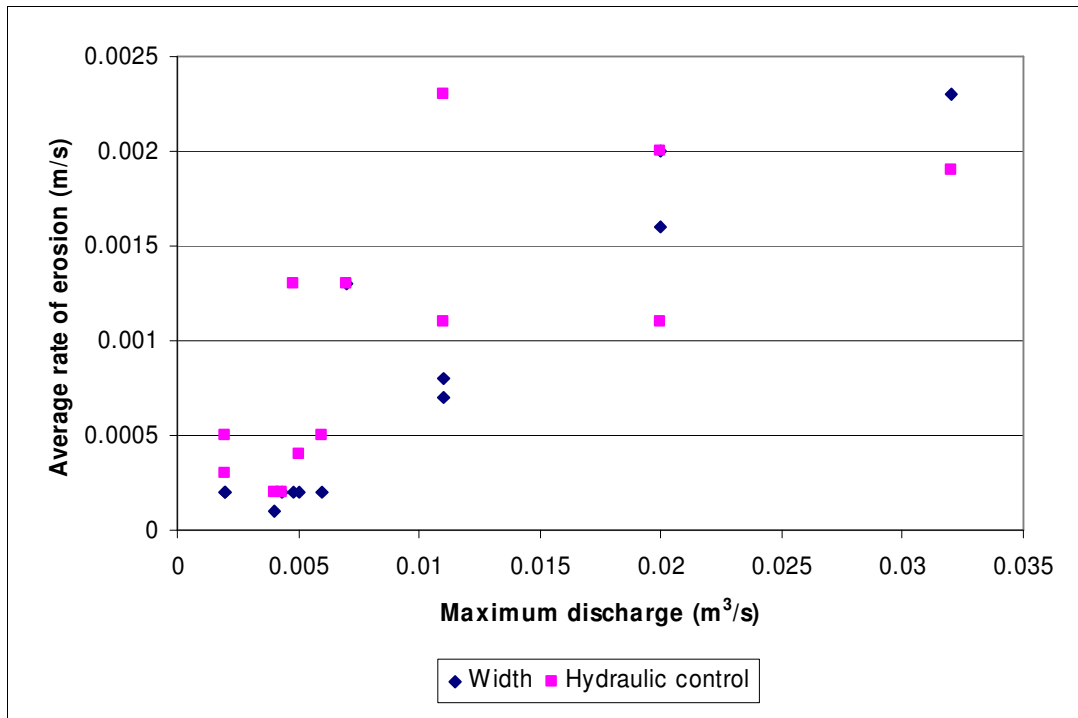


Figure 6.4-30 Relationship between the average rate of erosion and the maximum discharge during breaching

From equations 6.4-12 and 6.4-13 it can be seen that with increasing discharge the rate of erosion also increases, indicating greater flushing efficiency. However, from the experiments it could also be seen that, given enough time, some of the experiments carried out with different discharges could have had very similar results. For example, the maximum width obtained in all the experiments was 1.35 m in tests 1 and 2. The data from the other experiments were investigated and extrapolated in those cases where true equilibrium had not been obtained, to find the time at which the width would have reached 1.35 m. For the smaller discharges it was found that this would never occur, since at a certain point no further erosion would take place (see Figure 6.4-31).

The data from those experiments where it was possible to determine the time where the width would reach 1.35 m are shown in Figure 6.4-32. It can be seen that for a discharge of 0.02 m³/s it had taken about 10 minutes to reach a width of 1.35 m, whereas for a discharge of 0.01 m³/s it could take as much as two hours.

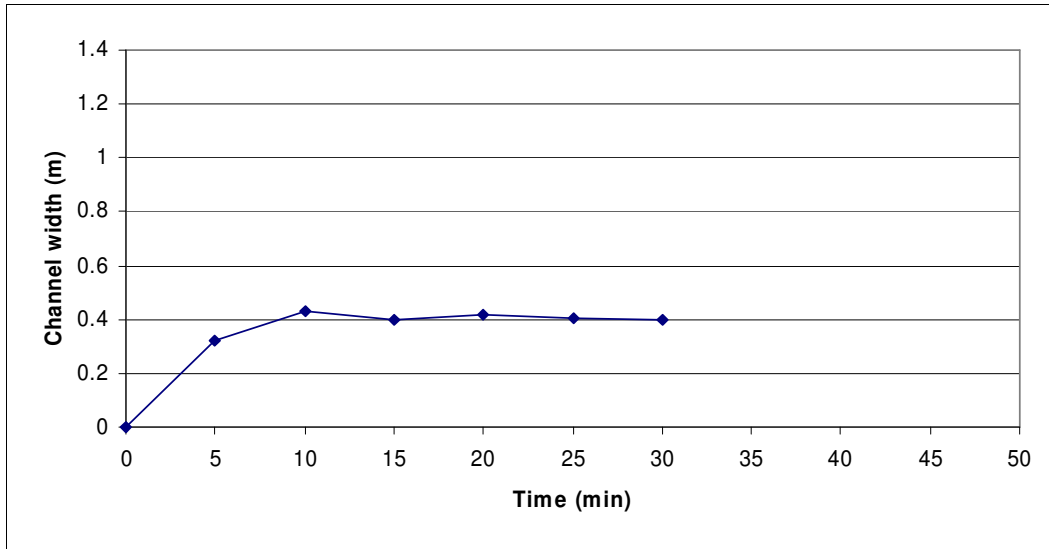


Figure 6.4-31 Width changes during test 9 with time

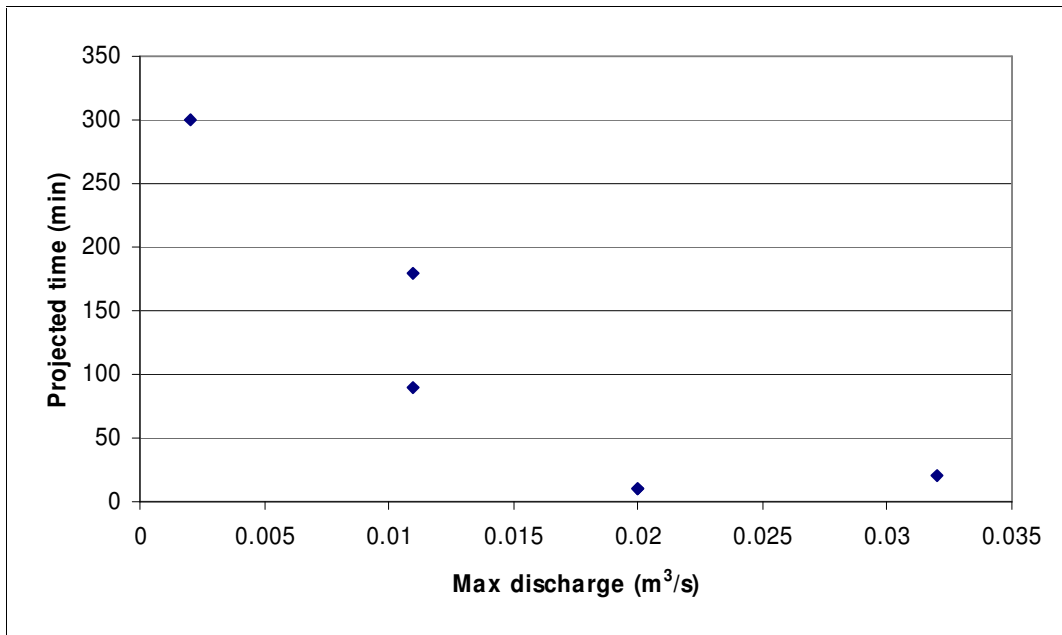


Figure 6.4-32 Projected time taken for width to reach 1.35 m in relation to the maximum discharge

6.4.5 Conclusions

From the results of the physical model experiments it can be seen that the equilibrium mouth width and depth are determined mainly by the maximum discharge during breaching, with the hydraulic gradient playing a less significant role. The same is true for the flushing efficiency. The main findings are that with increasing discharge:

- The cross-sectional inlet area increases (equation 6.4-2/4 and 6.4-7/8).

- The volume of sediment flushed out of the mouth area increases (equation 6.4-11).
- The rate of erosion increases (equation 6.4-12/13).
- Flushing progresses further upstream (equation 6.4-9/10).

The discharge on the other hand is determined mainly by the water level in the estuary when breaching starts as can be seen from Figure 6.4-5 and Figure 6.4-21. Therefore, the higher the water level in the estuary at the start of breaching, the more efficient the breaching process will be. However, many of the equations that have been derived in this section cannot be applied to field conditions directly. Therefore the data obtained from the experiments were used to calibrate and verify a mathematical model to determine whether the model could accurately simulate the breaching process. Thereafter the computational model was set up to firstly establish whether it can simulate the controlled laboratory conditions and then to verify it against observations in the field.

6.5 Computational Modelling

The decision to use a computational model was made because physical modelling can be quite time-consuming, especially if the basic setup is to be changed. Also, some factors such as tidal action could not readily be incorporated into the physical model. Another reason is that field data obtained during breaching is rare, since this is difficult and sometimes dangerous to obtain due to the high, often supercritical, flow velocities. For this reason it was thought that a computational model (MIKE 21C) could be used to investigate the breaching process in field conditions.

In order to determine whether the computational model could accurately simulate the breaching process, the first model was based on the laboratory setup. The model was calibrated and verified, and once it became evident that the computational model could indeed simulate the breaching process, another model was set up, based on field conditions at the Klein River estuary.

6.5.1 Background of Computational Model

For the computational modelling, the two-dimensional model MIKE 21, developed by *DHI Water and Environment* (DHI, 2003), was used. MIKE 21 is a software package for simulating free-surface flows, water quality, sediment transport and waves in rivers, lakes, estuaries, bays, coastal seas and other water bodies. In particular MIKE 21C, a special module developed to simulate river morphology, was used. MIKE 21C is based on a curvilinear grid, and hydrodynamics, sediment transport and river morphology can be simulated, with modules to describe:

- Flow hydrodynamics – water levels and flow velocities over a curvilinear or rectangular grid are computed.
- Helical flow (secondary currents).
- Sediment transport – based on various model types, capable of graded sediment transport computations.
- Alluvial resistance due to bed material and bed forms.
- Scour and deposition – large-scale movement of bed material is computed and the effect of supply limited sediment layers can be incorporated.
- Bank erosion and planform changes – bank lines as well as the curvilinear grid can be updated.

The effect of bed slope on the sediment transport is very important and is incorporated into MIKE 21C as a transverse and longitudinal component.

$$S_n = \left(\tan \delta_s - G \cdot \theta^{-a} \cdot \frac{\partial z^*}{\partial n} \right) S_{bl} \dots\dots\dots 6.5-1$$

where S_n = sediment transport across the streamline

G = transverse slope coefficient

a = transverse slope power

S_{bl} = bed load

$\frac{\partial z^*}{\partial n}$ = transverse bed slope

$\tan \delta_s$ = bed shear direction change due to helical flow

θ = Shields parameter

$$S_s = \left(1 - \alpha_L \frac{\partial z^*}{\partial s} \right) S_{bl} \dots\dots\dots 6.5-2$$

where S_s = sediment transport along the streamline

α_L = longitudinal slope coefficient

$\frac{\partial z^*}{\partial s}$ = longitudinal bed slope

The modules can run interactively, incorporating feedback from variations in the alluvial resistance, bed topography and bank line geometry to the hydrodynamics and sediment transport.

6.5.2 Laboratory Model

6.5.2.1 Model Setup

A rectangular grid with 100 grid cells in the flow direction and 25 grid cells across (120 mm x 80 mm) was used for the hydrodynamic and morphological simulations. Initially the bathymetry was set up in such a way that the crest of the berm was horizontal, but that led to the water flowing over the whole width of the crest. Therefore the crest of the berm was made slightly higher towards the sides than in the middle and a small channel (10 mm deep and 100 mm wide) was provided (see Figure 6.5-1).

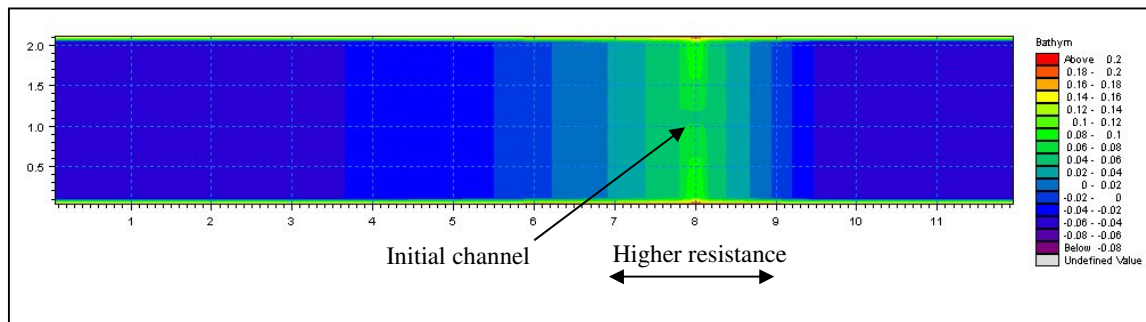


Figure 6.5-1 Laboratory bathymetry (values in m relative to “MSL”)

For the upstream boundary an inflow sequence was specified, with a steady rise in the discharge over a period of 10 minutes until the maximum discharge was reached, after which that discharge was kept constant for another hour. The downstream boundary was given as a constant water level.

6.5.2.2 Calibration and Verification

The model was calibrated on the data from Test 3 (as described in Section 6.4), because this was one of the tests which ran the longest thus providing ample data, and which also ran without problems. The erosion and deposition patterns were the main focus of the calibration process. The calibration was carried out mainly by adjusting the flow resistance in the form of the Manning number M , as well as the eddy viscosity and the bed slope effect parameters. The final parameters are listed in Table 6.5-1.

The resistance was kept constant throughout, except within an area 1 m upstream and downstream of the crest of the berm. The resistance was increased linearly from a Manning M ($=1/n$) value of $35 \text{ m}^{0.33}/\text{s}$ to $12 \text{ m}^{0.33}/\text{s}$ at the crest and then decreased again to a value of $35 \text{ m}^{0.33}/\text{s}$. A different resistance value was chosen in the berm area to account for the higher bed roughness due to the bedforms forming in that area during breaching.

Table 6.5-1 Hydrodynamic and morphological model parameters - laboratory

Parameter	Value
Hydrodynamic time step	0.2 s
Morphological time step	0.4 s
Flooding depth	0.004 m
Drying depth	0.002 m
Manning M	12 – 35 m ^{0.33} /s
Median grain diameter	0.12 mm
Sediment transport formula	Engelund and Fredsøe
Eddy viscosity	0.03 m ² /s
Mass density of sediment	2650 kg/m ³
Porosity	0.35
Transverse slope coefficient	1
Transverse slope power	0.5
Longitudinal slope coefficient	3

The model did prove to be capable of simulating the breaching process, as can be seen in Figure 6.5-2. The position and size of the breach was accurately simulated, although the point of maximum scour was further upstream than obtained during the actual laboratory tests. The most obvious difference is that the model simulated breach was very symmetrical, in contrast to the physical model results. This probably occurred because of small irregularities in the bed level and variations in bed sediment characteristics in the physical model, which were not reflected in the numerical model.

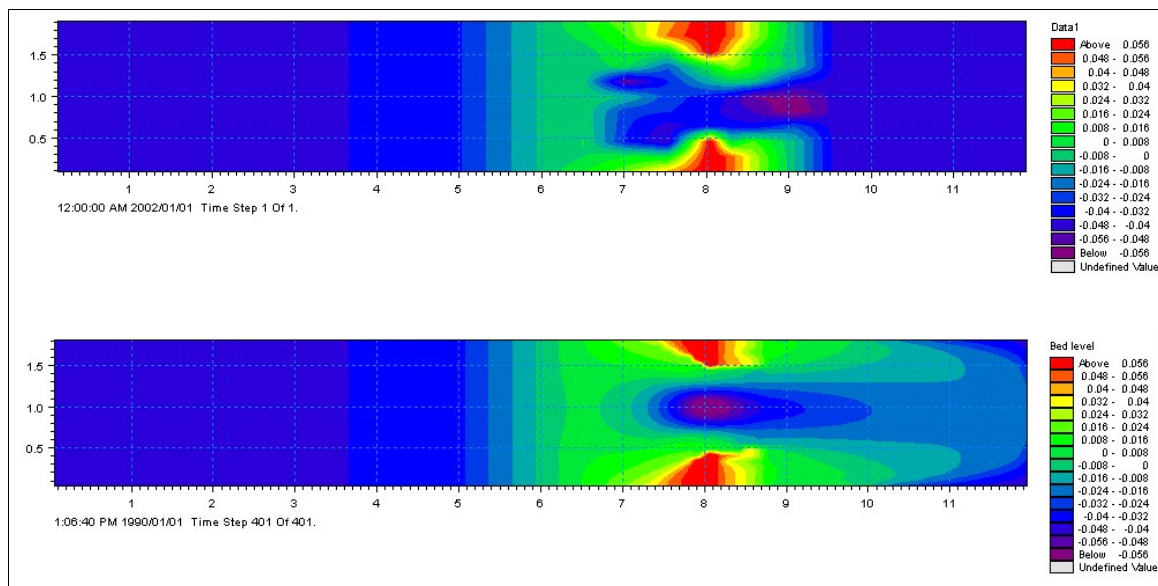


Figure 6.5-2 Actual (top) and simulated (bottom) final bed levels of Test 3

The model was then verified with data from some of the other laboratory tests with lower and higher discharges (see Figure 6.5-3), and it was found that the computational model could simulate the breaching process reasonably well. The next step was then to test the model with field data.

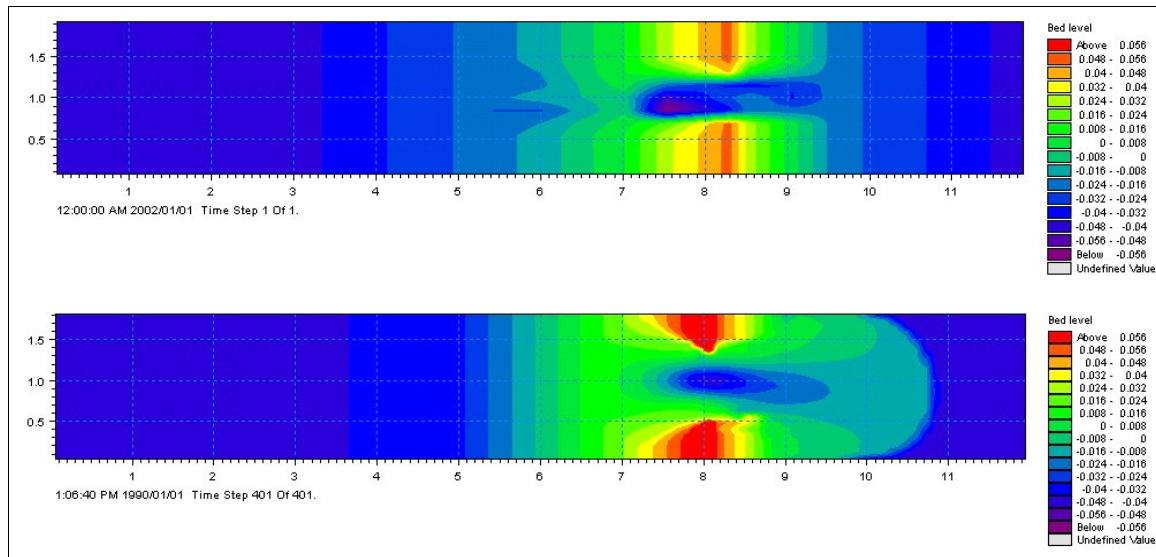


Figure 6.5-3 Actual (top) and simulated (bottom) final bed levels of Test 7

6.5.3 Klein River Estuary Model

6.5.3.1 Model Setup and Calibration

A curvilinear grid with 114 grid cells in the flow direction and 101 grid cells across (Figure 6.5-4), was used for the hydrodynamic and morphological simulations, with a cell size of approximately 28 m long by 15 m wide in the berm region. The model bathymetry was based on the June 1998 survey of the lower estuary of the Klein River (CSIR, 1998), as the area surveyed was extensive (Figure 6.5-5). The crest of the berm was around +2.8 m MSL at the time. In the region around the berm the grid spacing in the flow direction was half of that in the deeper area of the upper estuary, as it was thought that very little morphological changes would take place in the upper estuary.

At the upstream boundary a small inflow of $2 \text{ m}^3/\text{s}$ was specified. A water level time series with 10-minute time steps, representing the tidal variation in the sea, was specified at the downstream boundary (see Figure 6.5-6).

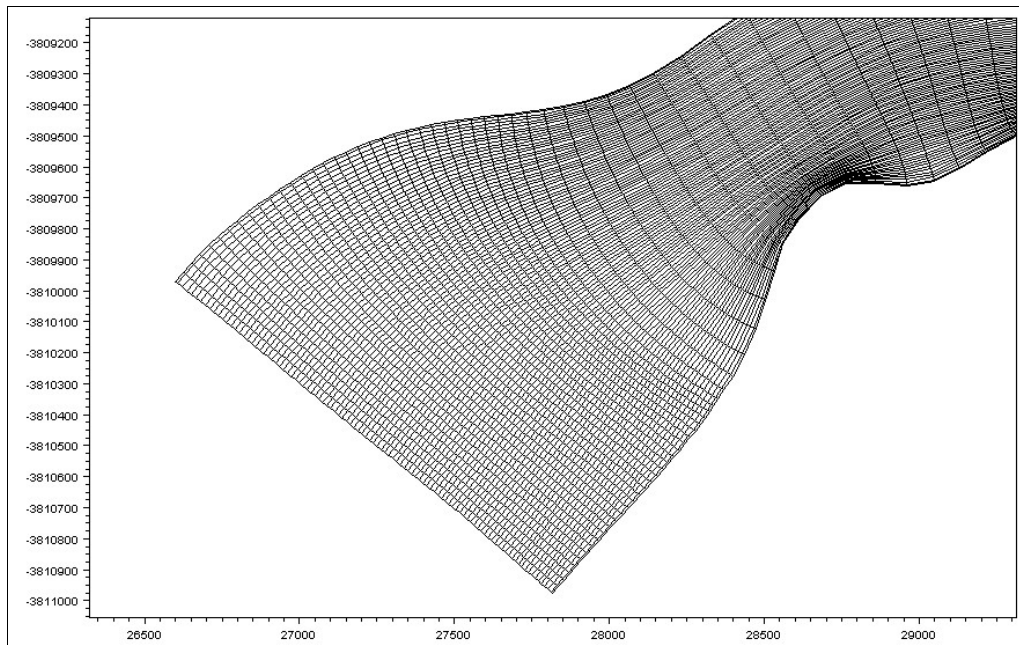


Figure 6.5-4 Klein Estuary model grid

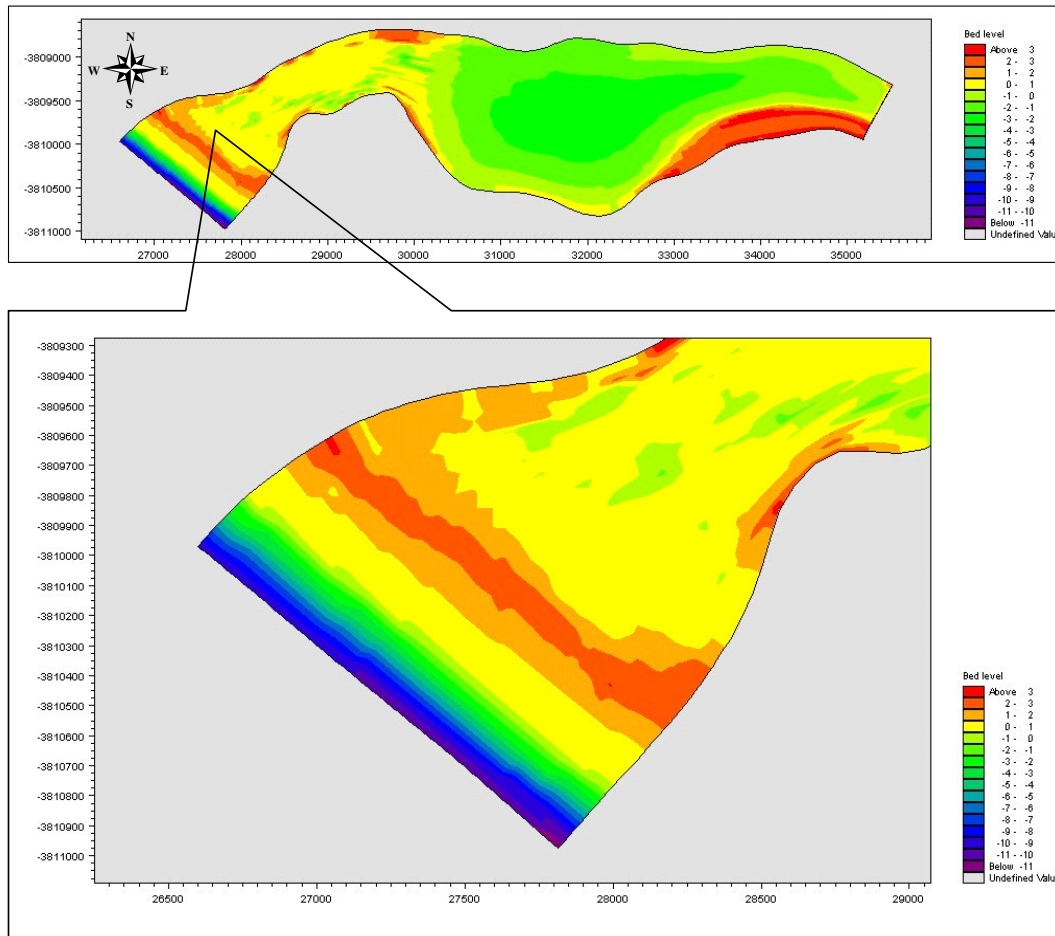


Figure 6.5-5 Klein Estuary bathymetry (relative to mean sea level)

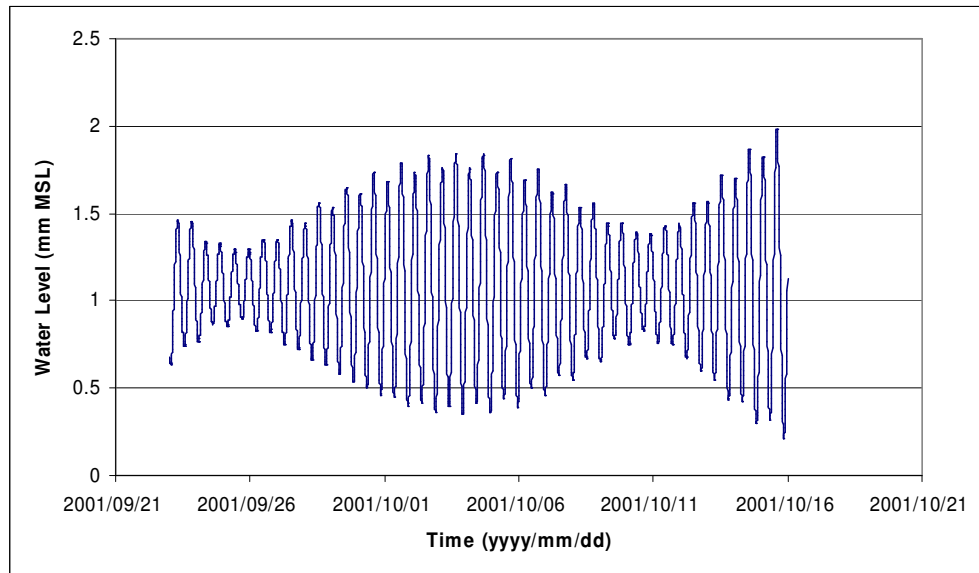


Figure 6.5-6 Tidal water levels specified at downstream boundary

A uniform sediment size of 0.21 mm was specified throughout the whole model, which was based on bed sediment samples taken in the field. The resistance was kept constant throughout. Initially it was thought to increase the resistance in the berm region as had been done for the laboratory setup. However, the resistance did not prove to affect the simulation results to a great degree, and the resistance was kept constant throughout the whole region. Other model parameters are given in Table 6.5-2.

Table 6.5-2 Hydrodynamic and morphological model parameters – Klein River

Parameter	Value
Hydrodynamic time step	4 s
Morphological time step	8 s
Flooding depth	0.02 m
Drying depth	0.01 m
Manning M	20 m ^{0.33} /s
Median grain diameter	0.21 mm
Sediment transport formula	Engelund and Fredsøe
Eddy viscosity	0.2 m ² /s
Mass density of sediment	2650 kg/m ³
Porosity	0.35
Transverse slope coefficient	0.005
Transverse slope power	0.5
Longitudinal slope coefficient	5

The model was calibrated on the field data obtained during and after the breaching of September 2001. The berm was at approximately the same height in September 2001 as in June 1998, when the data for

the bathymetry was obtained. The mouth was breached at a level of +2.8 m MSL with the initial excavated channel 15 m wide (one grid cell) and 0.5 m deep.

The model performed reasonably well, except for the fact that the breach did not develop rapidly enough. The storage volume of the estuary is quite significant and it takes a few hours for the breach to develop from the initial excavated channel and for the water level in the estuary to drop, as has been observed during actual breachings in the field (see Figure 6.3-4). However, the model responds more slowly than the field situation, which led to the result that the tide would move into the estuary again before the breach could fully develop. The solution to this problem was to provide a wide shallow initial channel width in the model. This means that breaching is started with a channel that is closer to its final form, thereby reducing the time it takes to develop a stable width. A 45 m wide initial channel was therefore specified, as part of the calibration based on field data.

The model simulated the final breach to be 75 m wide (see Figure 6.5-7), which corresponds well to the field data (see Figure 6.3-6). A survey of the area after breaching showed the bed level in the mouth to be just below -2 m MSL. During breaching the maximum scour was up to 5 m (maximum 3 m below MSL), but as the tide moves into the estuary again, some sand is deposited in the mouth, so that within a short period of time the mouth becomes somewhat shallower. Some sediment is deposited just inside the mouth, and two ebb channels form upstream of the mouth. The velocity vectors in Figure 6.5-8 clearly show that the flow is more confined in the two channels during the ebb tide, while during the flood tide the flow is initially more evenly spread out, but as sediment starts to deposit upstream of the mouth, the flow during the flood tide is diverted somewhat.

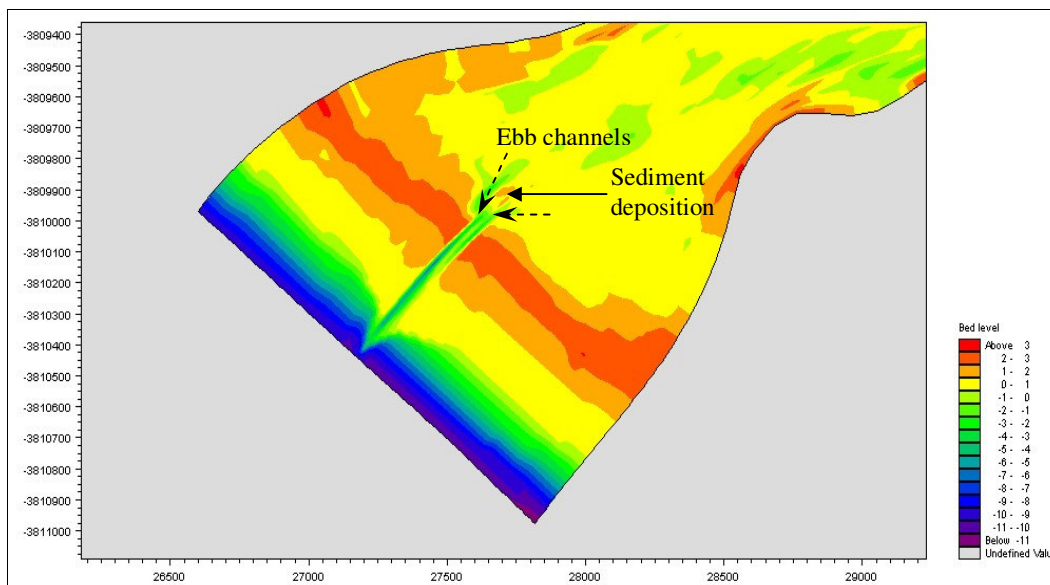


Figure 6.5-7 Simulated breach after 1 week

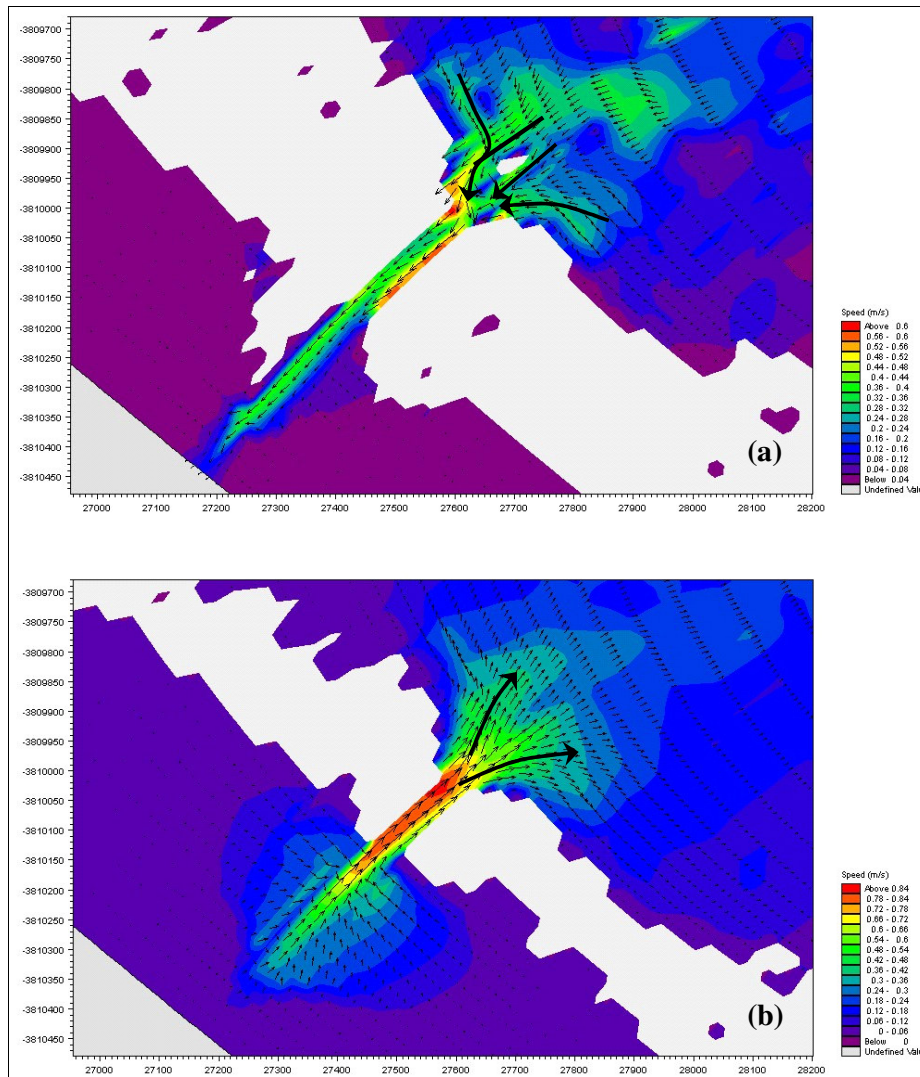


Figure 6.5-8 Velocity distribution during ebb (a) and flood (b)

6.5.3.2 Simulation Results

The scenarios were chosen mainly to investigate the effect of the initial water level at which breaching takes place, but also the location of the breach and the timing. The location of the breach has been a point of debate for many years (CSIR, 1998). Among fishermen the opinion is that breaching towards the south-eastern end of the berm would lead to improved fishing conditions. Others argue that natural breachings would occur more frequently at the north-western end of the berm, because the lowest point of the berm is frequently found towards this end. However, breachings too close to the north-western end have resulted in a combined ebb and flood channel. Ideally the ebb and flood channels should develop separately for more effective flushing. It was decided that the first choice should always be the lowest point of the berm, but the interference of the ebb and flood channels should be taken into account when deciding upon the location of the breach. The following scenarios were

investigated:

- A.** Breaching towards the south-east side of the berm
 - Scenario 1:** At spring tide, initial water level at +2 m MSL
 - Scenario 2:** At spring tide, initial water level at +2.8 m MSL
 - Scenario 3:** At neap tide, initial water level at +2 m MSL
 - Scenario 4:** At neap tide, initial water level at +2.8 m MSL
- B.** Breaching towards the north-west side of the berm
 - Scenario 5:** At spring tide, initial water level at +2 m MSL
 - Scenario 6:** At spring tide, initial water level at +2.8 m MSL
 - Scenario 7:** At neap tide, initial water level at +2 m MSL
 - Scenario 8:** At neap tide, initial water level at +2.8 m MSL

An initial shallow (0.5 m deep) breaching channel 45 m wide and 0.5 m deep was provided in all simulations. The simulations were started just before high tide in all scenarios. The simulations have shown that whether breaching takes place at spring or neap tide does not affect this particular estuary. However, the initial water level at which breaching takes place, has a very significant effect on the efficiency of the breaching.

Table 6.5-3 lists the maximum discharges that occurred during breaching, based on the drop in water level in the estuary. It shows that higher discharges occurred when breaching occurred at a higher water level, and towards the south-east side. Slightly higher discharges were also obtained during spring tide compared to neap tide, but the differences are small.

Table 6.5-3 Simulated maximum discharge

Scenario	Maximum Discharge (m ³ /s)
1. South-east side, spring tide, initial water level at 2 m MSL	125
2. South-east side, spring tide, initial water level at 2.8 m MSL	285
3. South-east side, neap tide, initial water level at 2 m MSL	102
4. South-east side, neap tide, initial water level at 2.8 m MSL	280
5. North-west side, spring tide, initial water level at 2 m MSL	85
6. North-west side, spring tide, initial water level at 2.8 m MSL	207
7. North-west side, neap tide, initial water level at 2 m MSL	50
8. North-west side, neap tide, initial water level at 2.8 m MSL	202

Figure 6.5-9 and Figure 6.5-10 show the water levels and associated discharges for scenario 3 and 4. It can be seen that the maximum discharge during breaching in the first instance is not much more than

the normal tidal discharge, whereas with a higher initial water level, the breaching discharge is more than three times the magnitude of the tidal discharge. The fact that the subsequent tidal discharges are higher for scenario 4 than for scenario 3 also indicates that flushing was more efficient during scenario 4, and that a greater tidal exchange is possible, which means that the mouth will have a better chance of staying open for longer than with scenario 3.

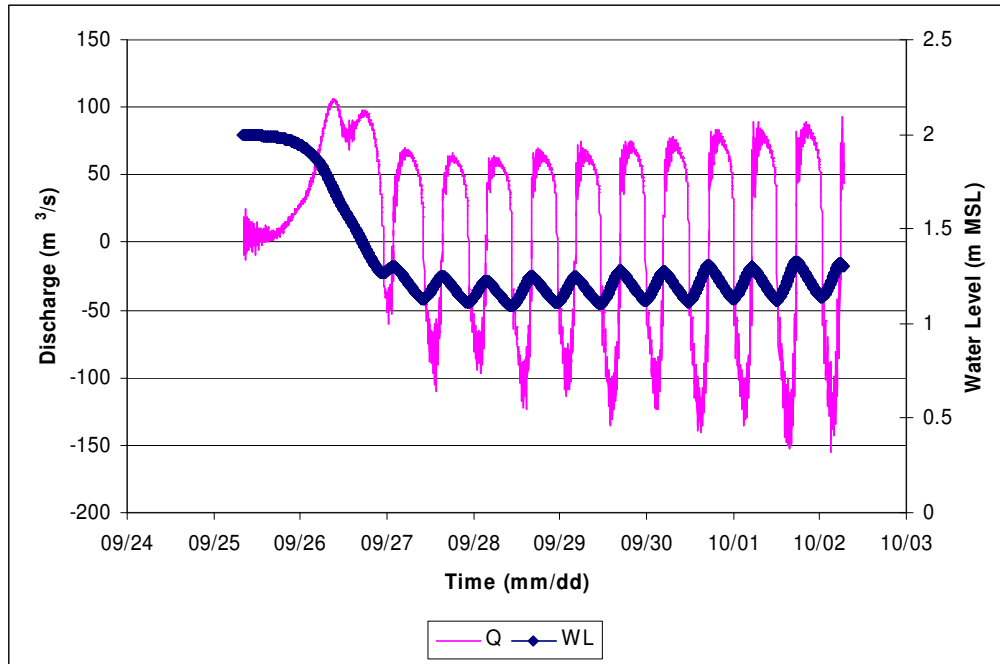


Figure 6.5-9 Scenario 3 - simulated discharge and water level

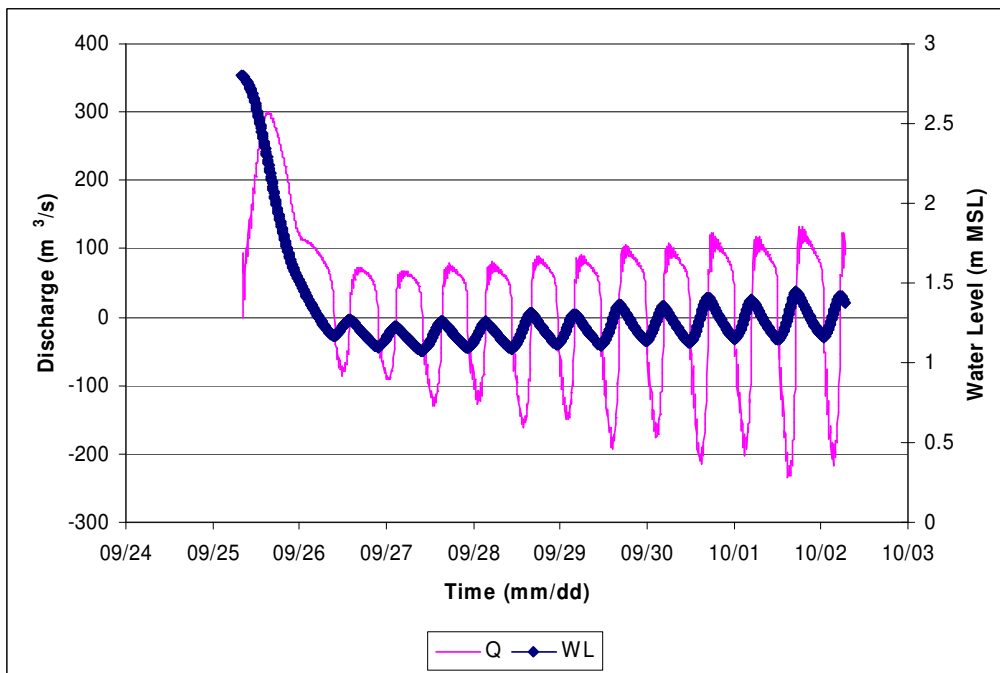


Figure 6.5-10 Scenario 4 - simulated discharge and water level

Figure 6.5-11 to Figure 6.5-14 show the final bed levels of scenarios 1, 2, 5 and 6. It can be seen that the breach width is only about 30 m when breaching takes place at +2 m MSL, while the channel is more than twice that size when breaching takes place at +2.8 m MSL. It is also interesting to note that the breaching channel on the south-east side of the berm is larger than on the north-west side, where the flow is more confined towards the left bank of the breaching channel.

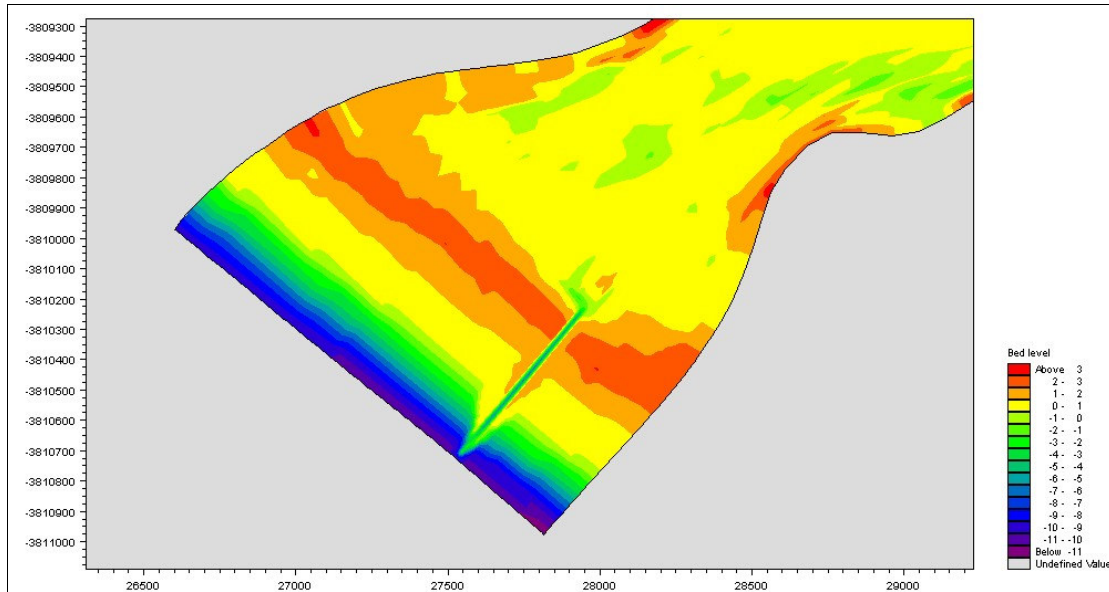


Figure 6.5-11 Scenario 1 - breaching channel towards the south-east after 7 days (+2m MSL)

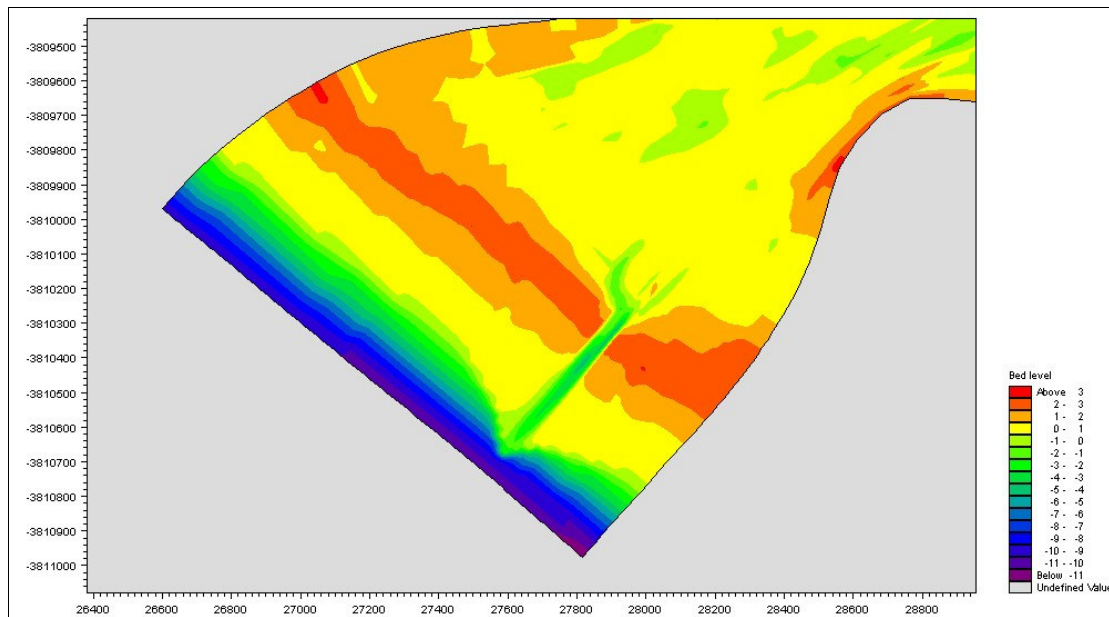


Figure 6.5-12 Scenario 2 – breaching channel towards the south-east after 7 days (+2.8 m MSL)

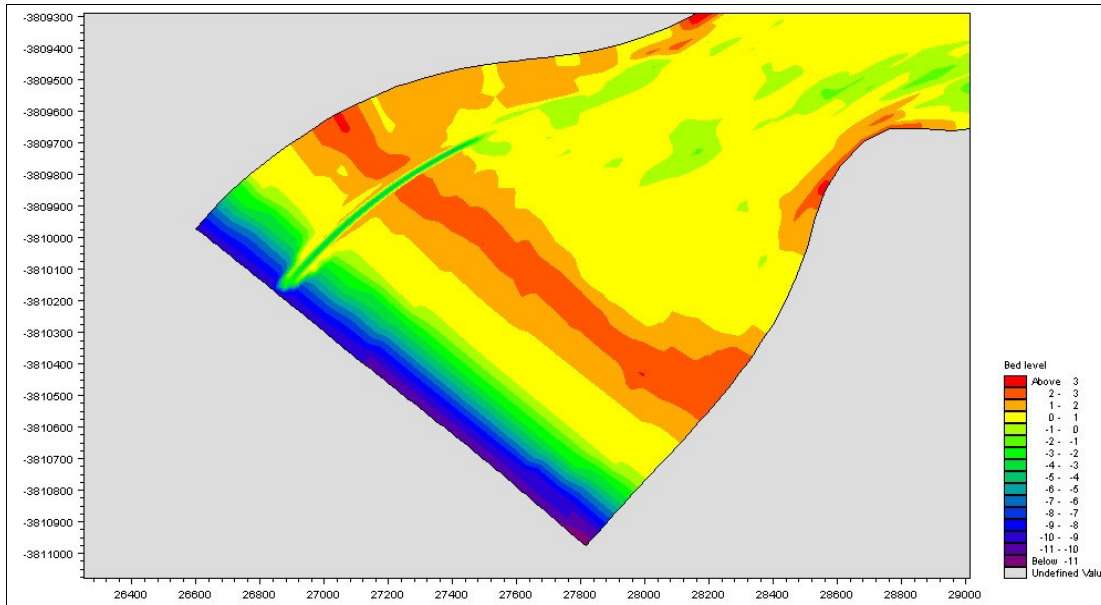


Figure 6.5-13 Scenario 5 – breaching channel towards the north-west after 7 days

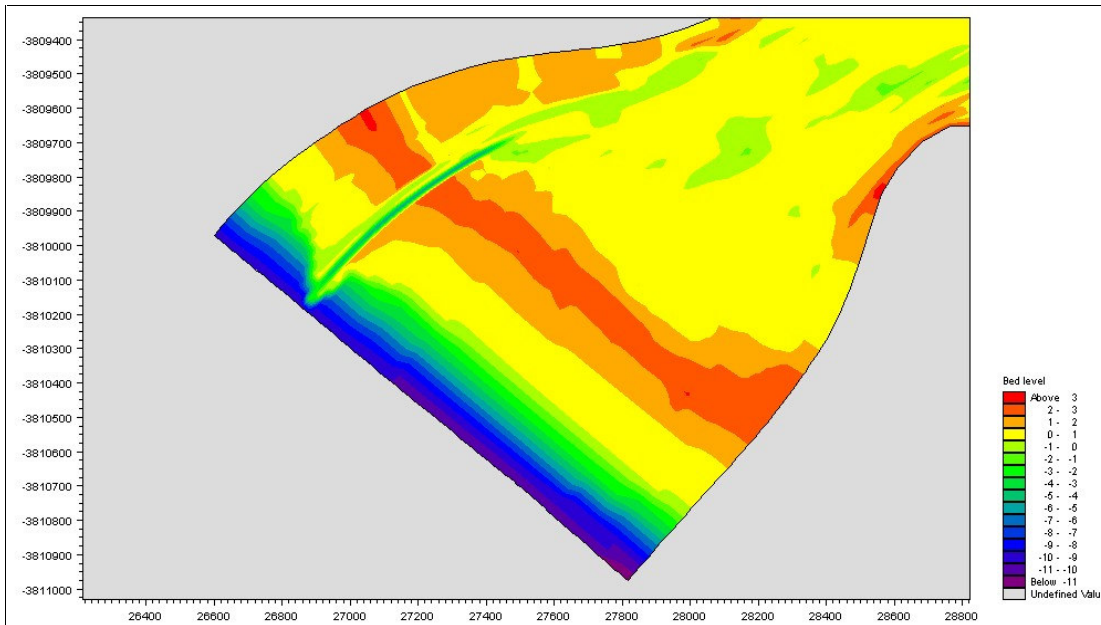


Figure 6.5-14 Scenario 6 – breaching channel towards the south-east after 7 days

It is also interesting to note that when breaching takes place towards the south-east side of the berm, the flushing channel splits into two channels upstream (see Figure 6.5-11 and Figure 6.5-12). In the field ebb and flood channels develop in much the same way, when breaching takes place more to the south-east side of the berm. The velocity vectors in Figure 6.5-15 and Figure 6.5-16 show that the ebb velocities are much stronger in the channels, whereas the flood velocities are more uniform.

On the other hand, when breaching takes place on the north-west side of the berm, the ebb and flood channels interfere (Figure 6.5-17 and Figure 6.5-18). More sediment was however flushed out on the north-western side due to the longer flushing channel associated with the wider berm in this area.

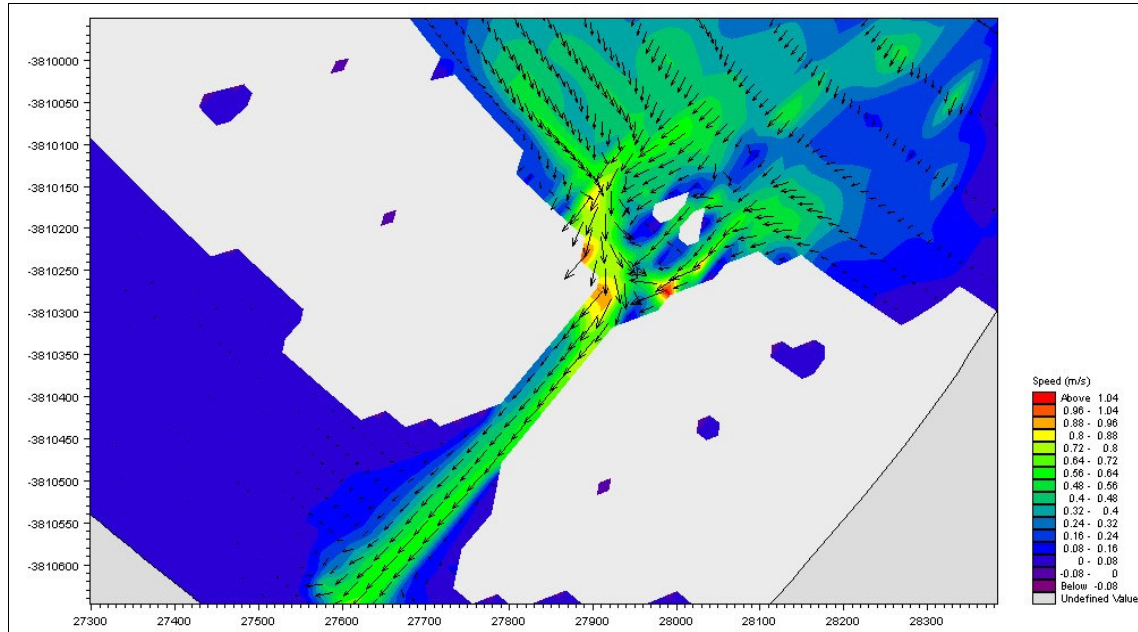


Figure 6.5-15 Scenario 2 - ebb tide velocity distribution

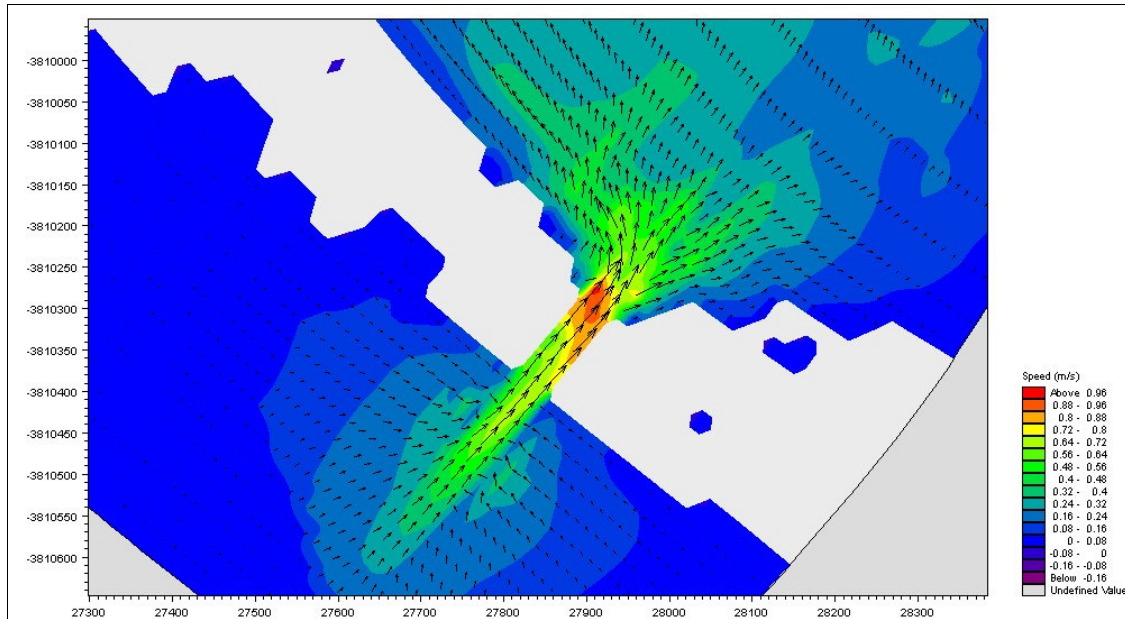


Figure 6.5-16 Scenario 2 - flood tide velocity distribution

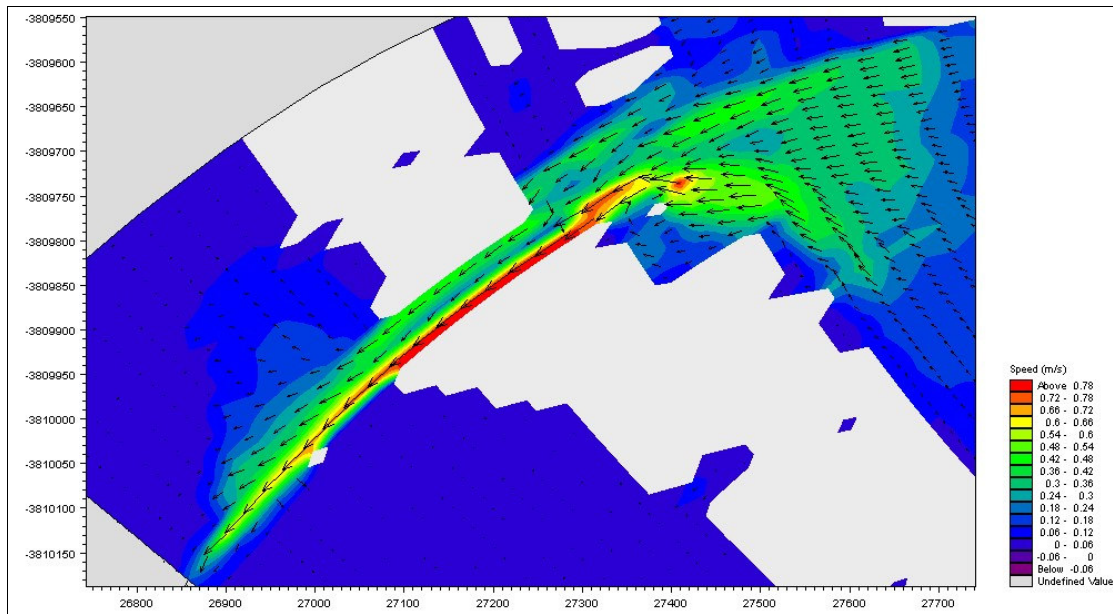


Figure 6.5-17 Scenario 6 - ebb tide velocity distribution

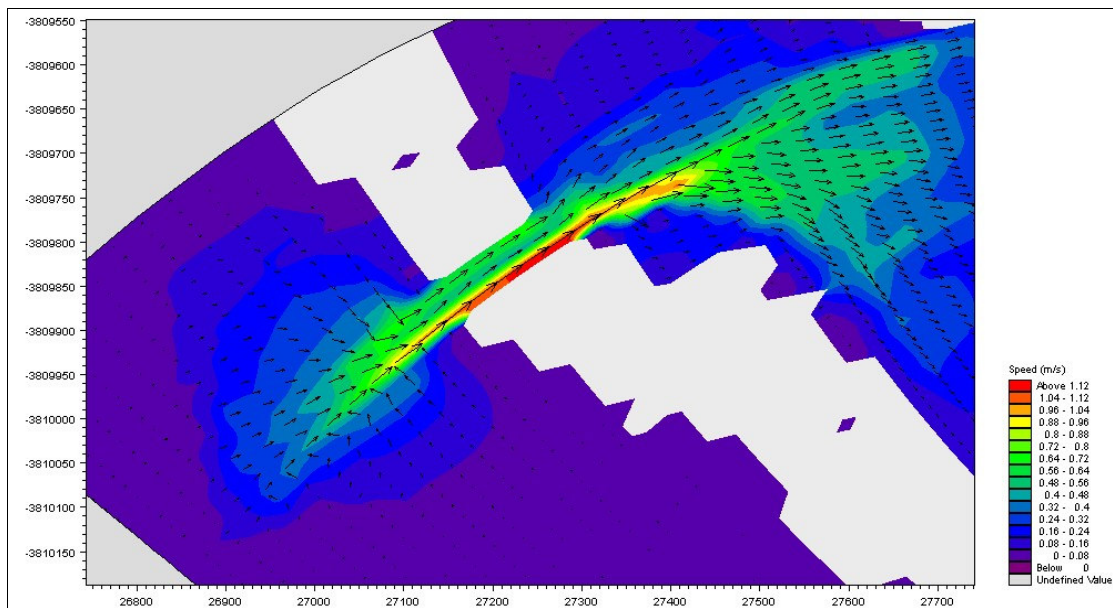


Figure 6.5-18 Scenario 6 - flood tide velocity distribution

The volume of sediment which was flushed out from upstream of the mouth during each scenario is listed in Table 6.5-4. This does not include sediment removed downstream of the crest of the berm. The volume of sediment removed at the higher water level is in some cases more than twice that which was flushed at the lower level. During breaching sediment is almost exclusively removed from upstream of the berm, but within a day or so the point where most of the sediment is removed moves downstream, so that little or no sediment transport takes place upstream, and more and more sediment is removed from downstream of the berm. It is important that the sediment is also removed or at least

dispersed downstream of the berm, because if it is allowed to accumulate in front of the mouth, it may eventually block the mouth. During spring tide it seems that this process is more efficient than during neap tide.

Table 6.5-4 Klein River - simulated volumes of sediment removed from the mouth and upstream (m³)¹

Scenario	Volume removed (m ³)
1. South-east side, spring tide, initial water level at +2 m MSL	37652
2. South-east side, spring tide, initial water level at +2.8 m MSL	58172 (55%)
3. South-east side, neap tide, initial water level at +2 m MSL	22927
4. South-east side, neap tide, initial water level at +2.8 m MSL	54577 (138%)
5. North-west side, spring tide, initial water level at +2 m MSL	38636
6. North-west side, spring tide, initial water level at +2.8 m MSL	71268 (85%)
7. North-west side, neap tide, initial water level at +2 m MSL	27770
8. North-west side, neap tide, initial water level at +2.8 m MSL	64018 (131%)

Overall it seems that breaching at a higher initial water level increases the flushing efficiency. Not only is the flushing channel wider and reaches further upstream, but a greater amount of sediment is removed from the estuary as well as downstream of the berm. Breaching further to the south-east also allows for a wider breach, although slightly less sediment is scoured than further to the north-west where the berm is wider and more sand is available because no recent breaching occurred has in the north-west.

6.6 Summary

The most important finding from both physical and mathematical modelling of the breaching process is that higher breach levels result in greater flushing efficiency, i.e. a wider breaching channel and a greater amount of sediment removed from both upstream and downstream of the berm. The physical modelling has shown that relationships can be established to describe the breach geometry and flushing efficiency. Establishing similar relationships for field conditions will be difficult, because more field data will be necessary. More field data such as those taken during this research should be obtained.

It has also been shown that the breaching process can be modelled with MIKE 21C. Some problems were encountered, such as the fact that the model had trouble determining the observed breach width,

¹ Values in parentheses indicate the extra percentage sediment removed at the higher water level

unless a wide shallow initial channel was specified. Overall, however, the model managed to simulate the breaching process at the Klein River acceptably. The mathematical modelling of the breaching process at the Klein River estuary provides much the same picture as has been observed during numerous breachings in the field, i.e. that breaching at higher water levels and towards the south-east side are more effective.

7. Conclusions and Recommendations

7.1 Conclusions

Estuaries are naturally very dynamic systems, where changes can occur within a very short period of time. This is because estuaries are driven by two powerful, variable systems – river and sea. Especially in South Africa’s semi-arid climate, large floods bring about major transformations in river morphology and thus their effect on estuaries is as significant. On the other hand, the sea with its tidal action and waves, especially during storms, affects the estuary noticeably. This is because small, microtidal estuaries, as are found in South Africa, are in a delicate balance, trying to balance the influences of both river and sea. It does not always take a major event to upset this equilibrium, be it from a natural source or due to human impacts. Understanding the delicate nature of these estuaries is the first step in better understanding and managing of estuaries.

The main focus of this dissertation was to investigate sedimentation in estuaries caused by marine sediments and by sediments being transported downstream from the catchment. To achieve this, the following aims of the project were identified:

- Identification of typical sediment related problems and probable causes.
- Improved understanding of estuarine sediment dynamics.
- Hydraulic description of sediment transport processes through the estuary during the tidal cycle.
- Hydraulic description of flushing efficiency of estuaries during breaching.

These aims were met and the following conclusions were drawn:

- Due to the interaction of various factors, such as river and tidal flows, catchment and marine sediments, as well as waves, each estuary appears to have its own unique dynamics and findings at one estuary may not be transferable to another, and as such oversimplified models cannot be used to investigate the hydro- and sediment dynamics of South African estuaries.
- Estuaries are very dynamic and not all geomorphological changes can be attributed to man-made disturbances. However, the sediment dynamics in many South African estuaries have been disrupted to some degree, which has led to many estuaries being closed off from the sea more frequently and for longer periods, adversely affecting the ecology of the estuaries.

- Sedimentation related to human impacts is mainly a result of catchment developments, such as dams, and local developments or activities such as dredging and structures built along the estuary. The human impacts have been quite substantial in some estuaries such as the Seekoei Estuary, while in others it is difficult to ascertain to what degree the perceived sedimentation problems are natural and how much is a result of human impacts. It is therefore important to understand the natural sedimentation processes first, before attempting to offer solutions to our sedimentation problems.
- In the long-term it is not affordable to do extensive field measurements on many SA estuaries. Thus, limited key field data should be collected and, using this as input, mathematical models are to be used to simulate estuarine sediment dynamics and to predict the consequences of changes in the system or impacts of management actions.
- Two-dimensional (2DH) numerical models have been found to be appropriate tools for studying hydro- and sediment dynamics in SA estuaries. The modelling shows that the sediment balance in an estuary relies on a subtle balance between dominant flood and ebb tide flows. For long-term and long reach simulations, one-dimensional (or quasi-two-dimensional) models will also be required in future.
- Mathematical modelling can be used to simulate the flushing of sediments during floods, but attempts should be made to calibrate these models when adequate field data become available in the future. The modelling has shown that floods play a very important part in estuarine sediment transport processes. However, large magnitude floods have to occur on a regular basis, or at least smaller floods are required in between large magnitude flood events, so that cohesive sediments in particular will not have time to consolidate.
- Physical and mathematical modelling, as well as field data, have shown the importance of breachings at higher water levels. The equilibrium mouth area is determined mainly by the maximum discharge during breaching. This discharge on the other hand is determined mainly by the water level in the estuary when breaching. Therefore, the higher the water level in the estuary at the start of breaching, the more efficient the breaching process will be.
- Wave-current interaction considerably complicates sediment transport predictions. That is why in many cases, existing sediment transport equations for currents have been modified to some degree to incorporate the effect of waves. A new approach, based on stream and wave power, has been followed to describe the sediment transport under both non-breaking wave and current conditions in shallow water situations.

- Experiments have shown that with increasing wave heights (i.e. wave power) and increasing current velocities (i.e. stream power), sediment transport rates would increase as well if both waves and currents travelled in the same direction. In contrast it was found that with increasing opposing waves (i.e. wave power) the sediment transport rates will actually decrease. The reason for this can be explained as follows. With increasing wave heights the sediment that is lifted from the bed through the wave action is transported a short distance upstream against the current. If the current is not strong enough the sediment is moved back only a short distance towards the point where it was first picked up. By this time another wave arrives, moving sediment upstream again. If the current is strong, the sediment will actually be carried much further downstream past the point from which it was first picked up by the wave. The distance that the sediment effectively moves, and therefore the effective transport rates are very much dependent on the strengths of the currents.
- A sediment transport equation, based on stream power, wave power, as well as sediment size was calibrated and verified, and compared to the well-known *Bijker* formula. The results show that the new sediment transport equation is straightforward to apply and gives better results than the *Bijker* formula for the data used.

7.2 Recommendations

The following recommendations are considered important for future research related to estuarine sediment dynamics:

- Many estuaries contain at least some percentage of cohesive sediments and the role of these sediments should be investigated, since it has been found that with a cohesive fraction of as low as 7%, the bed sediments will act cohesively. The effect of consolidation of cohesive sediments on the flushing efficiency of large floods should be investigated. These findings should be incorporated into mathematical models.
- The effects of man-made obstructions such as causeways, bridges, marinas, weirs, etc. on the flow in the estuaries should be investigated, since many estuaries have been affected by such obstructions, whilst the effects are not always apparent.
- Understanding of the interrelationship between abiotic and biotic components in an estuary is crucial to understanding the overall dynamics and ecology of an estuary and as such is very important, especially in Reserve determinations.

- The effect of opposing directions of currents and waves on sediment transport rates should be investigated in further detail. This aspect could, for example, be important in estuary mouths, when the currents during ebb tide oppose the direction of the waves from the sea. This interaction could play an important role in the closure mechanism of estuaries.

8. References

- Ackers, P and White, WR (1973). *Sediment Transport: New Approach and Analysis*. Proceedings ACSE, Journal of Hydraulic Engineering **99**(HY1), pp. 2041-2060.
- Bagnold, RA (1966). *An Approach to the Sediment Transport Problem from General Physics*. Geological Survey Professional Paper 422-I, U.S. Government Printing Office, Washington, D.C.
- Bailard, JA (1981). *An Energetic Total Load Sediment Transport Model for a Plane Sloping Beach*. Journal of Geophysical Research **86**(C11), pp. 10938-10954.
- Basson, GR and Rooseboom, A (1990). *Report on the Hydraulic Model Investigation of the Proposed Tugela River Bridge B351 on National Route 2 Section 27*. South African Roads Board.
- Basson, GR and Rooseboom, A (1997). *Dealing with Reservoir Sedimentation*. South African Water Research Commission, Report No. TT91/97, South Africa.
- Bayram, A; Larson, M; Miller, HC; Kraus, NC (2001). *Cross-Shore Distribution of Longshore Sediment Transport: Comparison Between Predictive Formulas and Field Measurements*. Coastal Engineering **44**, pp. 79-99. <http://www.sciencedirect.com/science/journal/03783839>
- Beck, JS and Basson, GR (2003). *The Hydraulics of the Impacts of Dam Development on the River Morphology*. Water Research Commission Report No. 1102/1/03.
- Bijker, EW (1971). *Longshore transport computations*. Journal of Waterways and Harbours Division **97**(WW4), pp.687-701.
- Bourman, RP and Barnett, EJ (1995). *Impacts of River Regulation on the Terminal Lakes and the Mouth of the River Murray*. Australian Geographical Studies **33**, pp. 101-115.
- Bruun, P (1978). *Stability of Tidal Inlets*. Elsevier. New York.
- Camenen, B and Larroude, P (2003). *Comparison of Sediment Transport Formulae for the Coastal Environment*. Coastal Engineering **48**, pp. 111-132.
- <http://www.sciencedirect.com/science/journal/03783839>
- CEM (2004). *Coastal Engineering Manual 1110-2-1100, Part III - Coastal Sediment Processes*. US Army Corps of Engineers.

- Chadwick, A and Morfett, J (1998). *Hydraulics in Civil and Environmental Engineering*. 3rd edition, E & FN Spon Publications, London.
- Cooper, JAG (2002). *The Role of Extreme Floods in Estuary-Coastal Behaviour: Contrasts Between River- and Tide-Dominated Microtidal Estuaries*. *Sedimentary Geology* **150**, pp. 123-137.
- Cooper, JAG. (1993). *Sedimentation in a River Dominated Estuary*. *Sedimentology* **40**, pp. 979-1017.
- Crowther, J (1988). *Sediment Redistribution in the Uilkraals Estuary as a Consequence of Human Disturbance*. MSc Thesis, University of Cape Town. South Africa.
- CSIR (1998). *Klein River Estuary – The Effects of Mouth Breachings in 1997*. CSIR Report No. ENV/S-C 98031. Stellenbosch.
- CSIR (1999). *Klein River Estuary – The Effects of Mouth Breachings in 1998*. CSIR Report No. ENV/S-C 99014. Stellenbosch.
- CSIR (2000). *Great Brak Estuary Management Programme – Report on the Monitoring Results for the Period November 1999 to November 2000*. CSIR Report No ENV-S-C 2000-131. Stellenbosch.
- CSIR, (2003). *Great Brak Estuary Management Programme, Review Report*. CSIR Report ENV-S-C-2003-092. March 2003. Stellenbosch.
- Dean, RG and Dalrymple, RA (1992). *Water Wave Mechanics for Engineers and Scientists*. Advanced Series on Ocean Engineering – Volume 2. World Scientific, Singapore.
- De Villiers, L (1988). *Sedimentation Changes in the Breede River Estuary*. MSc Thesis, University of Cape Town. South Africa.
- DHI (2001). *MIKE 11- A Modelling System for Rivers and Channels. User guide*. DHI Water and Environment. Denmark.
- DHI (2003). *MIKE 21C – River Hydrodynamics and Morphology – User Guide*. DHI Water and Environment. Denmark.
- Dibajnia, M and Watanabe, A (1992). *Sheet Flow under Nonlinear Waves and Currents*. Proceedings of the 23rd Coastal Engineering Conference, pp. 2015-2029.

- Dollar, ESJ (2001). *A Review of the Information Relating to the Geomorphology and Sediment Yield of the Thukela Basin with a Comment on its Implications for the Instream Flow Requirement Assessment*. University of Witwatersrand, South Africa.
- Dyer, KR (1997). *Estuaries: A Physical Introduction*. John Wiley, New York.
- Engelund, F (1966). *Hydraulic Resistance of Alluvial Streams*. Journal of the Hydraulics Division, ASCE, Vol. **92** (HY2), pp. 315-328.
- Engelund, F and Hansen, E (1967). *A Monograph on Sediment Transport in Alluvial Streams*. Teknisk Forlag, Denmark.
- Esterhuysen, K (1982). *The Seekoei Estuary: Example of Disrupted Sedimentary Ecology*. ROSIE Report No. 5, University of Port Elisabeth. South Africa.
- Fitzgerald, DM and Nummedal, D (1983). *Response Characteristics of an Ebb-Dominated Tidal Inlet Channel*. Journal of Sedimentary Petrology **47**, pp. 1171-1186.
- Fox, HR; Wilby, RL; Moore, HM (2001). *The Impact of River Regulation and Climate Change On The Barred Estuary Of The Oued Massa, Southern Morocco*. Regulated River: Research and Management **17**, pp. 235-250.
- Frijlink, HC (1952). *Discussion des Formulas de Débit Solide de Kalinske, Einstein et Meyer-Peter et Mueller Compte Tenue des Mesures Récentes de Transport Dans les Rivières Néerlandaises*. 2me Journal Hydraulique, Societe Hydraulique de France, Grenoble, France, pp. 98-103.
- Guilcher, A (1967). *Origin of Sediments in Estuaries*. In Lauff (1967), pp.149-157.
- Guillén, J and Palanques, A (1992). *Sediment Dynamics and Hydrodynamics in the Lower Course of a River Highly Regulated by Dams: the Ebro River*. Sedimentology **39**, pp. 567-579.
- Harvey, N (1996). *The Significance of Coastal Processes for the Management of the River Murray Estuary*. Australian Geographical Studies **34**, pp. 45-57.
- Hosseini, S; Eyre, B; McConchie, D (2001). *Suspended Sediment Transport Dynamics in the Sub-Tropical Microtidal Richmond River Estuary, Australia*. Estuarine, Coastal and Shelf Science **52**, pp. 529-541.
- Houwman, KT and Van Rijn, LC (1999). *Flow Resistance in the Coastal Zone*. Coastal Engineering, Vol. **38**, pp. 261-273.

- Hubbard, DK; Oertel, G; Nummedal, D (1979). *The Role of Waves and Tidal Currents in the Development of Tidal-Inlet Sedimentary Structures and Sand Body Geometry: Examples from North Carolina, South Carolina and Georgia*. *Journal of Sedimentary Petrology* **49**, pp. 1073-1092.
- Hughes, SA (1999). *Equilibrium Scour Depth at Tidal Inlets*. Coastal Engineering Technical Note CETN IV-18, U.S. Army Engineer Research and Development Centre, Vicksburg, MS. <http://bigfoot.wes.army.mil/cetn.index.html>
- Huizinga, P (1994). *Estuaries: From Midgley's Involvement in St Lucia to the Present and Challenges for the Future*. In: 50 Years of Water Engineering in South Africa, 14-15 July 1994, A Tribute to Prof Des Midgley. Water Engineering Division, South African Institution of Civil Engineers. South Africa.
- Ibáñez, C; Prat, N; Canicio, A (1996). *Changes in the Hydrology and Sediment Transport Produced by Large Dams on the Lower Ebro River And Its Estuary*. *Regulated Rivers: Research and Management* **12**, pp. 51-62.
- Karim, F (1995). *Bed Configuration and Hydraulic Resistance in Alluvial Channel Flow*. *Journal of Hydraulic Engineering*, **121**(1), pp. 15-25.
- Karim, F (1999). *Bed-Form Geometry in Sand-Bed Flows*. *Journal of Hydraulic Engineering*, Vol. **125**(12), pp. 1253-1261.
- Lauff, GH (Ed.) (1967). *Estuaries*. American Association for the Advancement of Science, Washington, US.
- O'Brien, MP (1976). *Notes on Tidal Inlets on Sandy Shores*. US Army, GITI Report 5.
- Open University (1989). *Waves, Tides and Shallow-Water Processes*. Prepared by an Open University Course Team. Pergamon Press.
- Pollard, I. (2001). *Die Effek van Damontwikkeling op die Morfologie van die Thukela Estuarium*. B.Eng. Thesis, University of Stellenbosch. South Africa.
- Ranasinghe, R; Pattiaratchi, C; Masselink, G. (1999). *A Morphodynamic Model to Simulate the Seasonal Closure of Tidal Inlets*. *Coastal Engineering*, **34**, pp. 1-36.
- Reddering, JSV (1983). *An Inlet Sequence Produced by Migration of a Small Microtidal Inlet against Longshore Drift: The Keurbooms Inlet, South Africa*. *Sedimentology*, **30**, pp. 201-218.

- Reddering, JSV (1988). *Coastal and Catchment Basin Controls on Estuary Morphology of the South-Eastern Cape Coast*. South African Journal of Science, **84**, pp. 154-157.
- Reddering, JSV and Esterhuysen, K (1981). *Sedimentation in the Bushmans Estuary*. ROSIE Report No. 2, University of Port Elisabeth. South Africa.
- Reddering, JSV and Esterhuysen, K (1983). *Sedimentation in the Kromme Estuary*. ROSIE Report No. 6, University of Port Elisabeth. South Africa.
- Reddering, JSV and Esterhuysen, K (1985). *Sedimentation in the Nahoon Estuary*. ROSIE Report No. 10, University of Port Elisabeth. South Africa.
- Rooseboom, A. (1992). *Sediment Transport in Rivers and Reservoirs - a South African Perspective*. South African Water Research Commission, Report No. 297/1/92, South Africa.
- Rooseboom, A and Mülke, FJ (1982). *Erosion Initiation*. Proceedings of the Symposium on recent developments in the explanation and prediction of erosion and sediment yield. IAHS publication No. 137.
- Rooseboom, A, and Le Grange, A du P (2000). *The Hydraulic Resistance of Sand Streambeds under Steady Flow Conditions*. Journal of Hydraulic Research, Vol. **38**(1), pp. 27-35.
- Rowntree, K.M. and Wadeson, R.A. (1999). *A Hierarchical Geomorphological Model for the Classification of Selected South African Rivers*. South African Water Research Commission, Report No.497/1/99, South Africa.
- Schumann, EH and Gray, RRW (1998). *Sedimentation in the Kowie Estuary: Feasibility of Using Ebb Tidal Flows to Remove Sediment Build-Up*. Geology Department, University of Port Elisabeth. South Africa.
- Schumann, EH, (ed) (2003). *Towards the Management of Marine Sedimentation in South African Estuaries with Special Reference to the Eastern Cape*. WRC Report No. 1109/1/03, March 2003.
- Seabergh, WC; King Jr, DB; Stephens, BE. (2001). *Tidal Inlet Equilibrium Area Experiments, Inlet Laboratory Investigations*. Coastal Inlets Research Program ERDC/CHL TR-01-20. US Army Engineer Research and Development Centre, Vicksburg.
- Sisternans, PGJ (2002). *Graded Sediment Transport by Non-Breaking Waves and a Current*. PhD Thesis. Technical University Delft. Netherlands.

- Taljaard, S; Van Niekerk, L; Huizinga, P; Basson, GR and Beck, JS (2002). *Thukela Estuary Environmental Reserve Determination – Specialist Report: Physical Dynamics and Water Quality*. CSIR, Stellenbosch, South Africa.
- Tromp, N (2000). *Sediment Dynamics of the Orange River Mouth*, Undergraduate Thesis, University of Stellenbosch. South Africa.
- USACE (2002). *Coastal Engineering Manual. Part II. Chapter 1 – Water Wave Mechanics*. EM 1110-21100. 30 April 2002.
- Van Rijn LC (1993). *Principles of Sediment Transport in Rivers, Estuaries and Coastal Seas*. Book by L C Van Rijn – Amsterdam, Aqua Publications, The Netherlands.
- Van Wyk, AC (1983). *Effect of Dredging in the Berg River Estuary*. MSc Thesis, University of Cape Town. South Africa.
- Walton, T (2002). *Tidal Velocity Asymmetry at Inlets*. ERDC/CHL CHETN IV-47. US Army Engineer Research and Development Centre, Vicksburg, MS.
- <http://chl.wes.army.mil/library/publications/chetn>
- Yang, CT (1972). *Unit Stream Power and Sediment Transport*. Journal of the Hydraulics Division, **98**(10), pp. 1805-1826.
- Zanke, U. (1977). Cited in Basson and Rooseboom.

APPENDIX A

Experimental Results – Sediment Transport under Waves and Currents

Table A1 Experimental Results: Wave – Current (Travelling in the same Direction)

Test Series	Test No	Q [l/s]	v_c [m/s]	S_f	T [s]	H [m]	L [m]	D [m]	q_s (m ² /s)	d_{50} (mm)	SP [w/m ³]	WP [w/m ³]
1	1A-1	3.4	0.128	3.47E-06	3.1	0.06	3.14	0.11	8.340E-07	0.15	0.004	142.94
2	1B-1	3.6	0.132	8.31E-05	3.4	0.04	3.90	0.13	1.211E-06	0.15	0.107	72.54
3	1C-1	4.9	0.174	2.11E-04	4.3	0.05	4.54	0.11	1.851E-06	0.15	0.360	101.64
4	2A-1	4.4	0.117	3.40E-05	3.1	0.04	3.70	0.15	9.440E-07	0.15	0.039	66.21
	2A-2	4.4	0.117	3.40E-05	2.9	0.07	3.53	0.15	9.358E-07	0.15	0.039	178.54
	2A-3	4.4	0.117	3.40E-05	3.1	0.07	3.75	0.15	1.978E-06	0.15	0.039	194.89
5	3A-1	6.4	0.174	3.01E-05	2.7	0.07	3.32	0.15	2.176E-06	0.15	0.051	178.66
	3A-2	6.4	0.176	4.50E-05	2.6	0.06	3.08	0.15	2.164E-06	0.15	0.078	128.67
	3A-3	6.4	0.178	6.00E-05	2.4	0.07	2.91	0.15	2.529E-06	0.15	0.105	220.93
6	4A-1	6.7	0.178	1.13E-05	2.7	0.05	3.28	0.15	1.228E-06	0.15	0.020	83.71
	4A-2	6.7	0.178	1.13E-05	2.2	0.05	2.72	0.15	1.439E-06	0.15	0.020	115.36
7	5A-1	8.6	0.231	5.09E-05	2.2	0.05	2.72	0.15	1.622E-06	0.15	0.115	98.45
	5A-2	8.6	0.233	4.59E-05	2.3	0.07	2.78	0.15	2.349E-06	0.15	0.105	216.78
	5A-3	8.6	0.251	4.59E-05	2.5	0.07	2.90	0.14	2.284E-06	0.15	0.113	206.46
	5A-4	8.6	0.266	4.59E-05	3.0	0.06	3.38	0.13	2.888E-06	0.15	0.120	138.01
8	6A-1	8.8	0.234	1.54E-04	3.0	0.05	3.65	0.15	2.551E-06	0.15	0.353	94.55
	6A-2	8.8	0.239	1.29E-04	2.7	0.06	3.27	0.15	3.084E-06	0.15	0.303	120.31
	6A-3	8.8	0.244	1.05E-04	2.5	0.05	2.99	0.15	3.835E-06	0.15	0.250	96.47
9	7A-1	10.8	0.283	1.50E-04	2.5	0.06	3.03	0.15	3.561E-06	0.15	0.417	132.30
	7A-2	10.8	0.289	1.26E-04	2.5	0.06	3.05	0.15	6.348E-06	0.15	0.357	165.37
	7A-3	10.8	0.294	1.02E-04	2.8	0.06	3.35	0.15	7.121E-06	0.15	0.295	163.57
10	8A-1	11.6	0.317	7.47E-05	2.7	0.06	3.20	0.15	1.259E-05	0.15	0.232	149.30
	8A-2	11.6	0.313	1.06E-04	2.5	0.06	2.98	0.15	4.839E-06	0.15	0.325	147.37
	8A-3	11.6	0.310	1.37E-04	2.3	0.06	2.83	0.15	7.181E-06	0.15	0.415	162.26
11	9A-1	12.2	0.317	1.44E-04	2.3	0.06	2.86	0.16	6.492E-06	0.15	0.449	140.12
	9A-2	12.2	0.328	1.22E-04	3.0	0.06	3.61	0.15	1.053E-05	0.15	0.391	128.32
	9A-3	12.2	0.338	9.92E-05	2.4	0.07	2.84	0.15	6.353E-06	0.15	0.329	213.68

Table A2 Experimental Results: Wave – Current (Travelling in the Opposite Direction)

Test Series	Test No	Q [l/s]	v_c [m/s]	S_f	T [s]	H [m]	L [m]	D [m]	q_s (m ² /s)	d_{50} (mm)	SP [w/m ³]	WP [w/m ³]
12	10B-1	5.7	0.148	3.26E-06	2.4	0.09	0.16	2.91	8.252E-07	0.15	0.005	308.89
	10B-2	5.7	0.148	7.81E-05	2.7	0.08	0.16	3.33	1.011E-06	0.15	0.114	261.54
	11B-1	6.9	0.186	5.35E-05	2.8	0.07	0.15	3.44	2.323E-06	0.15	0.097	176.66
	11B-2	6.9	0.186	6.84E-05	2.7	0.09	0.15	3.31	4.672E-06	0.15	0.125	291.06
13	12A-1	9.1	0.247	2.27E-05	2.7	0.07	0.15	3.21	1.090E-05	0.15	0.055	172.79
	12A-2	9.1	0.263	1.19E-04	2.7	0.08	0.14	3.20	1.348E-05	0.15	0.307	229.81
14	13A-1	10.6	0.314	3.14E-05	3.0	0.08	0.14	3.49	8.223E-06	0.15	0.097	242.75
	13A-2	10.6	0.296	7.36E-05	3.0	0.06	0.15	3.64	3.881E-06	0.15	0.213	138.54

APPENDIX B

Experimental Results - Physical Modelling of the Mouth Breaching Process

Table B-1 Experimental Data on Breaching Channel Width, Position and Length of Hydraulic Control with Time

Run	Time [mm:ss]	Width of breaching channel [mm]	Time [mm:ss]	Position of hydraulic control [mm]	Length of hydraulic control [mm]	
1	00:00	0	00:00	0		
	06:17	405	06:17	338		
	06:25	540	06:25	405		
	06:50	675	06:50	270		
	07:07	405	07:07	405		
	07:39	540	07:39	473		
	07:58	675	07:58	540		
	10:50	810	10:50	810		
	14:49	1080	14:49	1080		
	16:26	1215	16:26	1215		
	20:36	1350	20:36			
	2	00:00	0	00:00	0	
03:50		135	07:21	810		
07:21		540	09:10	945		
09:10		675	11:00	1215		
10:00		810	11:30	1215		
11:00		945	14:30	1350		
11:30		1080	18:26	1485		
14:30		1080	21:10	1620		
18:26		1215				
21:10		1350				
3		00:00	0	00:00	0	
		05:13	540	05:13	540	
	06:35	675	06:35	810		
	12:10	675	12:10	1080		
	14:10	810	14:10	1350		
	24:10	878	24:10			
	33:40	945	33:40			
	4	00:00	0	00:00	270	
03:00		203	01:00	405		
05:00		338	02:05	540		
05:45		405	03:40	675		
10:00		473	08:00	810		
11:00		540	10:00	945		
17:30		608	17:00	1080		
21:00		675	35:00	1215		
39:00		743				

Run	Time [mm:ss]	Width of breaching channel [mm]	Time [mm:ss]	Position of hydraulic control [mm]	Length of hydraulic control [mm]
5	00:00	0	00:00	0	
	04:30	270	05:00	270	
	07:10	405	06:00	405	
	08:12	540	08:20	473	
			11:10	540	
			11:50	675	
			13:10	810	
			20:20	945	
			23:00	1080	
7	00:00	0	00:00	0	0
	00:05	455	00:05	600	1170
	00:10	439	00:10	1125	1250
	00:15	492	00:15	1250	1312.5
	00:20	515	00:20	1250	1375
	00:25	523	00:25	1250	1375
	00:30	530	00:30	1250	1375
	00:35	561	00:35	1250	1375
	00:40	576	00:40	1250	1375
	00:45	583	00:45	1250	1375
8	00:00	0	00:00	0	0
	00:05	680	00:05	333	806
	00:10	383	00:10	780	1039
	00:15	437			
	00:20	461			
	00:25	485			
	00:30	524			
	00:35	534			
	00:40	558			
	00:45	558			
9	00:00	0	00:00	0	0
	00:05	319	00:05	700	500
	00:10	428	00:10	850	1000
	00:15	399	00:15	900	1000
	00:20	420	00:20	920	1000
	00:25	406	00:25	920	1000
	00:30	399	00:30	920	1000
	00:35				
	00:40				

Run	Time [mm:ss]	Width of breaching channel [mm]	Time [mm:ss]	Position of hydraulic control [mm]	Length of hydraulic control [mm]
10	00:00	0	00:00	0	0
	00:05	100	00:05	300	300
	00:10	237	00:10	650	600
	00:15	309	00:15	650	650
	00:20	355	00:20	700	750
	00:25	434	00:25	800	800
	00:30	461	00:30	900	800
	00:35	454	00:35	900	800
	00:40	461	00:40	900	800
	00:45	500	00:45	900	800
11	00:00	0	00:00	0	0
	00:05	438	00:05	306	500
	00:10	306	00:10	563	631
	00:15	356	00:15	575	700
	00:20	481	00:20	694	813
	00:25	450	00:25	694	875
	00:30	438	00:30	700	875
	00:35	438	00:35	706	906
	00:40	488	00:40	713	913
	00:45	500	00:45	719	938
13	00:00	0	00:00	0	0
	00:05	681	00:05	703	1123
	00:10	572	00:10	754	1072
	00:15	522	00:15	1159	1333
	00:20	565	00:20	1159	1268
	00:25	601	00:25	993	1196
	00:30	623	00:30	1123	1304
	00:35	623	00:35	1087	1326
	00:40	645	00:40	1051	1377
	00:45	667	00:45	1159	1377
14	00:00	0	00:00	0	0
	00:05	788	00:05	753	1370
	00:10	616	00:10	753	1096
	00:15	616	00:15	856	1370
	00:20	644	00:20	788	1267
	00:25	582	00:25	788	1336
	00:30	582	00:30	822	1336
	00:35	616	00:35	1027	1438
	00:40	514	00:40	993	1370
	00:45	548	00:45	890	1233